Master of Science Thesis

Power output of offshore wind farms
in relation to atmospheric stability

In cooperation with Vestas Wind Systems A/S

L.M. Alblas BSc

26 June 2012

Faculty of Aerospace Engineering · Delft University of Technology

Power output of offshore wind farms
in relation to atmospheric stability

In cooperation with Vestas Wind Systems A/S

Master of Science Thesis

For obtaining the degree of Master of Science in Aerospace Engineering at Delft University of Technology

L.M. Alblas BSc

26 June 2012

Faculty of Aerospace Engineering · Delft University of Technology

Delft University Of Technology
Department Of
Wind Energy

The undersigned hereby certify that they have read and recommend to the Faculty of Aerospace Engineering for acceptance a thesis entitled **"Power output of offshore wind farms"** by **L.M. Alblas BSc** in partial fulfillment of the requirements for the degree of **Master of Science**.

Dated: 26 June 2012

Head of department: _____
prof.dr. G.J.W. van Bussel

Supervisor Delft University of Technology: _____
dr.ir. W.A.A.M. Bierbooms

Supervisor Vestas Wind Systems A/S: _____
dr.ir. H.F. Veldkamp

Delft University of Technology, Aerospace Science for Sustainable Engineering and Technology: _____
dr.ing. R. Schmehl

Energy Research Centre of the Netherlands: _____
dr.ir. A.J. Brand

Summary

With more wind farms being built offshore and the size of both wind turbines and wind farms increasing, corresponding investments increase as well. Therefore location and layout of wind farms become more important, as they influence the power produced by the wind farm and hence its profitability. As a result, considerable effort is being spent to accurately predict the power output of wind farms. This leads to the wish to include more effects that influence the power output in the models. At the moment air density, wind direction and wind speed are included, while ongoing work focuses on wake effects, atmospheric stability and complex terrain.

Atmospheric stability is known to influence wind farm power output, by affecting power losses due to wakes. A stable atmosphere has a lower turbulence intensity and therefore wakes will exist longer. The opposite is true for an unstable atmosphere. Previous investigations indicate that wake losses for a wind farm can range from 5 to 15% (Barthelmie et al., 2004). The large variation in produced power of a wind farm indicates the need for more research in this field to find the causes of the variation and to improve predictions with this knowledge. This study looks at the effect of atmospheric stability on the wind farm power output.

Data from the Egmond aan Zee (OWEZ, The Netherlands) and North Hoyle (UK) wind farms are analysed. Metmast data are used to obtain the atmospheric stability distributions on each site. It is found that the dominant influence on the atmospheric stability is the temperature difference between the sea surface and the ambient temperature (it is therefore important to measure these temperatures accurately). It is observed that atmospheric stability varies with both wind speed and wind direction. Very unstable cases can be observed up to around 15-16 m/s. Very stable cases remain visible up to high wind speeds (above 20 m/s), although the number of very stable cases decreases with wind speed. The number of near-neutral (unstable, neutral and unstable) occurrences increases with wind speed. Variation of atmospheric stability with wind direction is observed and is believed to result from the warm/cold air corresponding with winds from the South/North respectively (the sea temperature shows little variation with wind direction).

Production data from the turbines are studied to establish the influence of the stability on the wake losses. It is found that in very unstable cases the production of the wind farm is higher than in near-neutral cases, and in near-neutral cases the production is higher than in very stable cases. This is as expected. For wind directions along a row of turbines the difference between very unstable and very stable cases is found to be in the order of 10-20% of normalized production. When the atmosphere gets less stable, turbulence increases and the mixing of higher energy air into the wake is increased. During the analysis it was found that wake loss data can be obtained more accurately when using the wind speed and wind direction measurements of the turbines in the first row (i.e. in the free-stream), as compared to those from the metmast.

From the Vestas mesoscale model data is obtained to compare to the metmast data. It is found that the stability distribution following from mesoscale data is similar to that of the metmast data. The mesoscale wind speed and direction can however not replace that of the metmast or turbines when investigating the wake losses as it is found that the wake losses do not closely correspond with the wake losses using metmast and/or turbines.

Simulations in WindPRO are performed with the Jensen wake model. The wake losses in the model are governed by the wake decay constant (WDC) k. At a downstream distance x, the width of the rectangular wake equals $D + 2kx$ and the wake speed is found by conservation of mass. The model does not take atmospheric stability into account. Since turbulence is related to atmospheric stability and since the WDC is related to the amount of turbulence, the WDC can be adapted to account for the effect of atmospheric stability. The WDC is adapted to achieve wake losses in a row of turbines similar to those observed in measurements. It is found that very stable cases require a WDC in the order of their turbulence intensity (TI). For the very unstable class the results vary between the two wind farms. At OWEZ the WDC value is about 1.5-1.9 times the mean TI value, whereas at North Hoyle the WDC and TI values are about equal for the larger turbine spacings. In all cases it can be said that the WDC value should be higher for the very unstable class than for the very stable class.

Simulating the wind farm efficiency shows that at North Hoyle similar WDC values can be used as those observed in the wake loss analysis in a row of turbines. For the very stable case the WDC is about 0.08 and for the very unstable case a WDC of 0.13 is obtained. For OWEZ the results are less clear which is thought to result from the small amount of data available. What is certain is that also for the wind farm efficiency very unstable cases higher WDC values should be used in WindPRO than for very stable classes.

A method to obtain the total wind farm efficiency could be to multiply the simulated wind farm efficiencies of the very stable and very unstable class with their frequency of occurrence. Summing these weighted efficiencies should give an approximate wind farm efficiency close to that of the complete wind farm for all stability classes. It is expected that the approximation improves upon including the near-neutral class. However, the most important factor is getting the WDC right, as it will influence the wind farm efficiency obtained from WindPRO.

Acknowledgements

I wish to thank the following persons. First of all I would like to thank my supervisors Wim Bierbooms (Delft University of Technology) and Dick Veldkamp (Vestas Wind Systems A/S) for guiding me in this project. Their experience and knowledge have helped me in choosing which areas to further investigate and we had good discussions about the results. Furthermore I would like to thank the people of the Wind Energy section at Delft University of Technology for having a good working environment for us students.

I would also like to thank the people at Vestas Wind Systems A/S. When starting off my thesis I had the chance to stay at the Randers (Vestas Offshore) and Aarhus (Vestas Technology R&D) offices for three weeks and I had a great time there. The knowledge and support of the people at Vestas made it possible for me to have a quick start with the programs and databases. I would like to thank everyone for their enthusiasm and willingness to help me and share their knowledge with me, both when I was in Denmark as on a further distance while I was working on my thesis after leaving Denmark.

I would especially like to thank Christian Leegaard Thomsen of Vestas Offshore, being the person searching for a student for this Master project at Vestas. I would also like to thank Christian for helping me to get to know my way around inside and outside the office and for inviting me to colleague activities (and even to the Vestas Christmas party). The same goes for the people in the Aarhus office. I enjoyed my stay, and had an efficient and useful time.

Delft, The Netherlands — L.M. Alblas BSc
26 June 2012

Contents

List of Figures

List of Tables

Nomenclature

Latin Symbols

A	Rotor disc area	m^2
a	Axial induction factor	–
B	Ambient pressure	kg/m^2
C	Constant depending on the Richardson bulk number	-
C_h	Bulk transfer coefficient for sensible heat	-
C_P	Power coefficient	-
C_p	Specific heat of air at constant pressure	$J/(kg \cdot K)$
C_T	Thrust coefficient	-
D	Rotor diameter	m
D_w	Wake diameter	m
g	Gravitational acceleration	m/s^2
I	Turbulence intensity	-
L	Monin-Obukhov length	m
$\dot{m}$	Mass flow	kg/s
P	Power	W
P_w	Vapour pressure	kg/m^2
R	Blade radius	m
R_0	Gas constant of dry air, 287.05	$J/(kg \cdot K)$
R_w	Gas constant of water vapour, 461.5	$J/(kg \cdot K)$
Ri_b	Bulk Richardson number	-
Ri_{bc}	Saturation bulk Richardson number	-

T	Ambient temperature	K
T	Thrust	N
U	Velocity	m/s
U_n	Normalized velocity	m/s
U_r	Wake velocity of air just behind the rotor	m/s
U_w	Wake velocity	m/s
u_*	Friction velocity	m/s
w	Vertical velocity	m/s
z	Measurement height	m
z_0	Roughness length	m
z_{Ch}	Charnock parameter	-
z_i	Depth of the convective boundary layer	m

Greek Symbols

α	Empirical constant	-
β	Empirical constant	-
ζ	Dimensionless stability parameter	-
η_{farm}	Wind farm efficiency	-
θ_v	Virtual potential temperature	K
κ	Von Kármán constant	-
λ	Tip speed ratio	-
ρ	Air density	kg/m^3
ρ_0	Reference air density	kg/m^3
Ω	Rotor rotational speed	rad/s

Subscripts

$_{10min}$	Mean value over 10-minute period
$_r$	Just behind the rotor
$_s$	At surface level
$_v$	Virtual
$_w$	Through wake area

Superscripts

$'$	Turbulent fluctuation
$\bar{}$	Time average

Abbreviations

ABL	Atmospheric boundary layer
ECMWF	European Centre for Medium-Range Weather Forecasts
EZ	Entrainment zone
HAWT	Horizontal Axis Wind Turbines
OWEZ	Offshore Wind farm Egmond aan Zee
SCADA	Supervisory Control And Data Acquisition system
SODAR	Sonic detection and ranging
SST	Sea surface temperature
TI	Turbulence intensity
TKE	Turbulence kinetic energy
VAWT	Vertical Axis Wind Turbines
VPDC	Vestas Performance and Diagnostic Centre
VSU	Vestas Siting Universe
WDC	Wake Decay Constant

Chapter 1

Introduction

With more wind farms being built offshore and the size of both wind turbines and wind farms increasing, corresponding investments increase as well. Therefore location and layout of wind farms become ever more important, as they influence the power that will be produced by the wind farm and hence its profitability. As a result, considerable effort is being spent to accurately predict the power output of wind farms. This leads to the wish to include more effects that influence the power output in the models. At the moment air density, wind direction and wind speed are included, while ongoing work focuses on wake effects, atmospheric stability and complex terrain (Veldkamp, 2011-2012).

Atmospheric stability is known to influence wind farm power output, by affecting power losses due to wakes. Previous investigations indicate that wake losses for a wind farm can range from 5 to 15% (Barthelmie et al., 2004), or even up to 23% (Barthelmie et al., 2010). The large variation in produced power of a wind farm indicates the need for more research in this field to find the causes of the variation and to improve predictions with this knowledge. This study looks at the effect of atmospheric stability on the wind farm power output.

The project is performed in cooperation with Vestas Wind Systems A/S. The project objectives are defined as (Vestas Wind Systems A/S, 2011a):

1. Quantify the effect of atmospheric stability on wind farm power production.
2. Compare the measurements with park/wake models with regards to predicting the effect of atmospheric stability on the production.
3. Find out if and how the used prediction models can be modified in a simple way to improve predictions.

Vestas provides data of wind farms as well as simulation tools. This enables investigating the effect of atmospheric stability on the wind turbine data and verifying the models. Results from previous measurements as found in literature and models used by industry to simulate wind farm power output are used to compare the results with.

The report starts with getting an understanding of the principles behind atmospheric stability and its influence on wind farm power production by performing a literature study. An overview of the currently available knowledge will be presented, which serves as background information for the work that is performed. After this the results are presented and discussed.

Chapter 2

Theory

This chapter explains the theory required to understand the principles and results discussed later on in the report. It also displays relevant observations found in literature.

2.1 Introduction to wind energy

This section presents a short introduction into wind energy. It is intended for readers not familiar with wind energy, and can serve as a short overview for others. It gives a short explanation of those topics in wind energy that are relevant to understand further chapters. This chapter is by no means a complete introduction to wind energy (and is not intended to be so).

2.1.1 Layout of a wind turbine

A wind turbine is a machine that can extract energy from the wind. It converts this wind power into electricity (Manwell, McGowan, & Rogers, 2009). Different layouts exist, such as vertical axis wind turbines (VAWTs) and horizontal axis wind turbines (HAWTs). Here we will focus on the HAWT, which is the conventional way of designing wind turbines. Within the group of HAWTs there are different design choices possible, but this is outside the scope of this study. In this report horizontal axis, upwind (rotor in front of the tower), pitch-regulated (the blades can be turned, or pitched to regulate the forces on them) wind turbines are considered.

A (horizontal axis) wind turbine consists of a foundation, tower, nacelle (including generator, drive train, control and yaw system) and a hub with rotor blades (Manwell et al., 2009), as can be seen in figure 2.1.

(a) Vestas V80-2.0MW wind turbine at North Hoyle (UK) wind farm (Vestas Wind Systems A/S, n.d.).

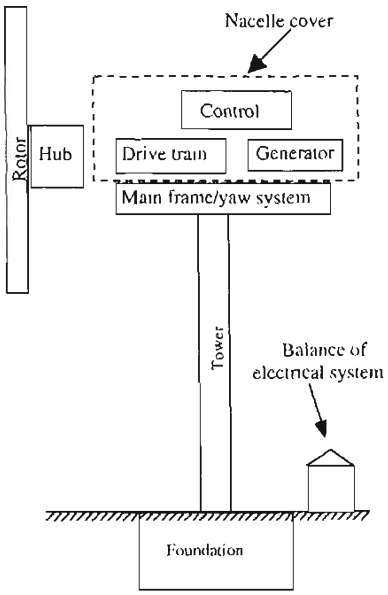

(b) Schematic wind turbine layout (Manwell et al., 2009).

Figure 2.1: Layout of a wind turbine a) in real-life and b) schematically.

2.1.2 Actuator disc theory

An overview of the power extraction from the wind by a wind turbine is the following (Manwell et al., 2009). Only the resulting equations are shown. For a derivation of the equations, see Alblas (2011).

A wind turbine can be represented by an actuator disc. When air flows through an actuator disc, it causes a pressure change on the air. The performance of a wind turbine can be explained by using a stream tube of air flowing through an actuator disc, as shown in figure 2.2.

Due to the conservation of momentum, it must hold that the force exerted on the flow by the actuator disc (i.e. the wind turbine), called the thrust, is equal to the change of momentum of the air.

The resulting fractional decrease of the wind speed at the rotor plane is called the axial induction factor. It is defined as:

$$a = \frac{U_1 - U_2}{U_1} \tag{2.1}$$

Using this definition, the U_2 can be written as follows:

$$U_2 = U_1(1 - a) \tag{2.2}$$

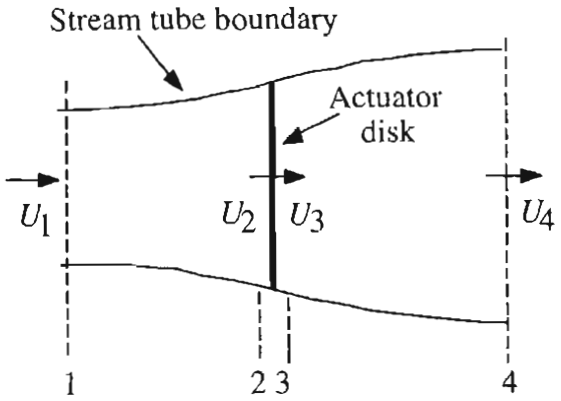

Figure 2.2: Schematic view of the velocities before, at and after an actuator disc (Manwell et al., 2009).

and U_4 as:

$$U_4 = U_1(1 - 2a) \tag{2.3}$$

Note that higher values than $a = \frac{1}{2}$ would mean that the flow would reverse and hence the theory is not valid for these values. Glauert's empirical relation is then applied.

The power P extracted from the air by the actuator disc is equal to the thrust exerted on the flow multiplied by the velocity at the actuator disc. This results in:

$$P = \frac{1}{2}\rho A U^3 4a(1 - a)^2 \tag{2.4}$$

Various assumptions are made in the actuator disc theory, such as that the static pressures at inlet and outlet of stream tube are equal to free-stream static pressure, and the air density is constant. Other assumptions include an infinite number of blades in the rotor plane, a uniform thrust over the actuator disc, no frictional drag, and a non-rotating wake. These assumptions have to be taken into account when modelling the flow using actuator disc theory.

2.1.3 Performance of a wind turbine

There are various ways of characterizing the performance of a wind turbine (Manwell et al., 2009).

One of the ways to represent the wind turbine performance is the thrust coefficient C_T. It is defined as the thrust exerted on the wind by the wind turbine made non-dimensional by the force available in the airflow:

$$C_T = \frac{T}{\frac{1}{2}\rho A U^2} \tag{2.5}$$

Using the definition of the induction factor, the thrust can be written as:

$$T = \frac{1}{2}\rho A U^2 4a(1-a) \tag{2.6}$$

Hence, the thrust coefficient can be written in terms of the induction factor:

$$C_T = 4a(1-a) \tag{2.7}$$

However, a more common measure of the wind turbine performance is the power coefficient. The power coefficient C_P of a wind turbine is defined as the power produced divided by the power available in the volume of wind that flows through the rotor area:

$$C_P = \frac{P}{\frac{1}{2}\rho A U^3} \tag{2.8}$$

The power coefficient is a non-dimensional measure of how well the wind turbine extracts the energy from the wind. Using the definition of the power as shown in equation 2.4, the power coefficient can be expressed by using the induction factor a. The expression then becomes:

$$C_P = 4a(1-a)^2 \tag{2.9}$$

Using this expression it can be found that the power coefficient has a theoretical maximum. By taking the derivative of the equation with respect to the induction factor one can find that $C_{P,max} = \frac{16}{27} = 0.593$ called the Betz limit (Manwell et al., 2009). This corresponds to an ideal induction factor of $a = \frac{1}{3}$.

The power coefficient can be plotted against tip speed ratio. The tip speed ratio is defined as:

$$\lambda = \frac{\Omega R}{U} \tag{2.10}$$

where λ is the tip speed ratio, Ω is the rotor rotational speed, R is the blade radius and U is the free-stream wind speed. Figure 2.3 shows the variation of the power coefficient against the tip speed ratio. The curve is useful in the sense that using the tip speed ratio one can find the corresponding power coefficient for any combination of wind velocity and rotor speed. Next to that the tip speed ratio corresponding to the maximum power coefficient can be found, and this can be used for optimum wind turbine performance.

A wind turbine starts operating at a certain wind speed, called the cut-in wind speed. The power generated increases when the wind speed increases from the cut-in wind speed to the rated wind speed. The rated wind speed is the wind speed at which the wind turbine reaches its rated power. From that point on, the wind turbine keeps operating at the same rated power (by pitching its blades and hence regulating the forces acting on the blades) until cut-out wind speed. The cut-out wind speed is the highest wind speed

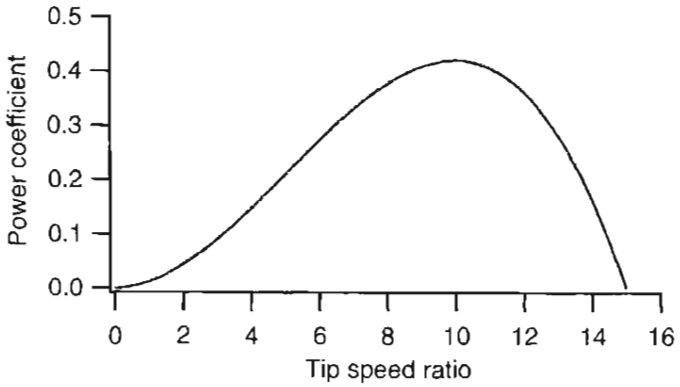

Figure 2.3: Power coefficient versus tip speed ratio (Manwell et al., 2009).

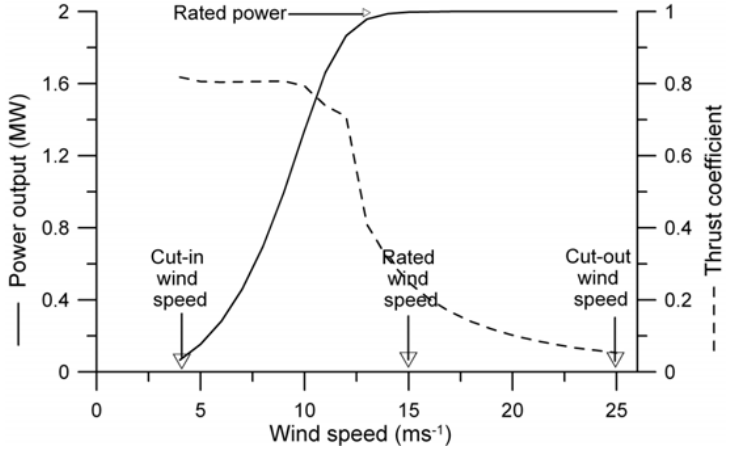

Figure 2.4: Power output and thrust coefficient versus wind speed for an example 2.0MW turbine (Barthelmie et al., 2011).

the wind turbine should be operating at. Above it the turbine is shut-down for safety (Barthelmie, Hansen, & Pryor, 2011).

The cut-in, rated and cut-out wind speed of a Vestas V80-2.0MW turbine as shown in figure 2.1a are 4, 16 and 25 m/s respectively (Vestas Wind Systems A/S, 2011c). The power output and thrust coefficient versus wind speed for an example 2.0MW turbine are shown in figure 2.4. It should be noted that a power curve is given for the wind speed at hub height and for a specific density (Barthelmie et al., 2011).

2.1.4 Wake behind a wind turbine

As the turbine extracts energy from the wind, an area of lower wind speeds results downstream of the turbine. Next to that, the turbulence intensity (being a measure for the amount of fluctuations in the wind) in this area is increased compared to the free-stream in front of the wind turbine (Barthelmie, Courtney, Højstrup, & Larsen, 1996; Barthelmie, Frandsen, Réthoré, & Jensen, 2007; Barthelmie et al., 2011; Méchali, Barthelmie, Frandsen, Jensen, & Réthoré, 2006). This area of decreased wind speed (or also: decreased

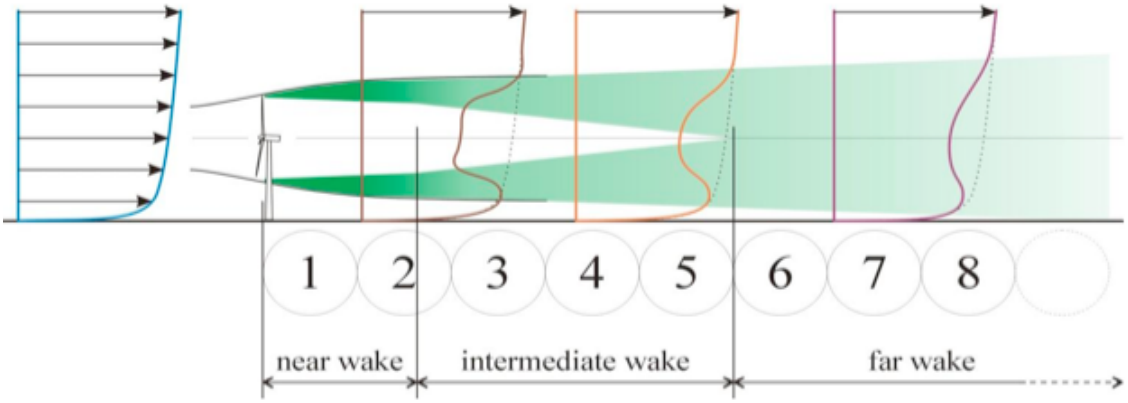

Figure 2.5: Development of the wind speed profiles in the wake of a wind turbine with downstream distance (Eecen et al., 2011).

momentum) and increased turbulence intensity is called the wake of a turbine, and is inherent to the extraction of energy from the wind by a wind turbine.

Above rated wind speed (and usually already slightly before), the blades are pitching to control (i.e. lower) the forces acting on them to make sure the wind turbine does not exceed the conditions it is designed for. The forces acting on the blades are thus highest from cut-in to rated wind speed. The forces acting on the turbine can be quantified by the thrust coefficient, being the ratio between thrust force generated by the turbine compared to the force available in the wind. At low wind speeds the thrust coefficient is thus the highest (as can also be seen in figure 2.4) and so the wake occurring behind the turbine is maximized (Barthelmie et al., 2007, 2010, 2011). The size of the wake depends on the characteristics of the wind turbine (Barthelmie et al., 2010).

Wakes expand behind the turbine, as a result of the turbulence of the wake itself and the ambient conditions (Barthelmie et al., 2010, 2011). Since the mid parts of the blades extract the most energy from the flow, directly behind the rotor the wake profile looks like a double bell wind speed profile (Barthelmie et al., 2006). This can be seen at the first wake profile downstream of the turbine in figure 2.5. The wind speed deficit at the mid part of the blades is higher than at the tips and the hub. Due to the expansion of and mixing within the wake, its shape changes. From a distance of 2-3 rotor diameters (D) behind the wind turbine the shape of the wake looks near-Gaussian (Barthelmie et al., 2011). A wake can recover by gaining energy from the surrounding (undisturbed) air (Barthelmie et al., 2007, 2011). Figure 2.5 shows the development of the wind speed profiles in the wake with downstream distance.

2.2 Observations as found in literature

Power losses can be related to the wakes occurring in wind farms and to wind shear, while turbulence can be related to wake recovery. Due to the size of a wind farm the wind will likely always vary over a wind farm, so measurement results will be scattered. Working with observations from wind farms is therefore a statistical process (Méchali et al., 2006).

Results will also vary between different wind farms. Nonetheless, it is still possible to find common influences on wind farm power output from wind farm observations.

2.2.1 Wakes in a wind farm

In a wind farm, multiple wind turbines are put together, usually in a structured layout of rows and/or columns. Here, rows will be defined as being parallel to the downstream wind direction, whereas columns are perpendicular to the wind direction. As the wind turbines are placed close together, turbines located behind one or more other turbines do not see the free-stream wind speed. Instead, they receive the wake from the turbine(s) in front of them. This means that the inflow at these turbines consists of lower wind speeds and higher turbulence intensities. This results in a reduced (and possibly more fluctuating) power output and an increase in dynamic loading (Barthelmie et al., 2011; Rohatgi & Barbezier, 1999).

A wake can recover by gaining energy from the surrounding (undisturbed) air. Higher energy flow is being mixed into the wake (Barthelmie et al., 2011). Barthelmie et al. (2010, 2011) list a few events that limit the mixing of new energy into the wake in a wind farm, as observed at the Nysted and Horns Rev wind farms. Although turbines at the two wind farms have different thrust coefficients it is expected that this is not a significant cause of differences in the wake behaviour. The order of the events depend on the movement (called meandering) and expansion of the wake, and on the layout of the wind farm. For Nysted and Horns Rev, Barthelmie et al. (2010, 2011) state that the most probable order of occurrence of the events is as follows:

1. **Wake bottom hits the ground** As the wake moves downstream and expands, the first event is likely that its bottom edge will hit the ground. This prevents further expansion at the wake bottom and it results that no more undisturbed flow is present below the wake. When this happens no more higher energy flow can be mixed in from the bottom of the wake.

2. **Next downwind turbine** The next event is likely that the wake will encounter the next downwind turbine, so again energy is extracted from its flow.

3. **Wakes merge laterally** The third event is that after some distance wakes will merge laterally with each other, see figure 2.6. In the Horns Rev and Nysted wind farms investigated by Barthelmie et al. (2010, 2011) this usually happens after 2-4 turbines in downstream direction, but it depends on the expansion and wind farm layout (like the other events).

The order of the events depends on multiple factors, such as the turbines, wind farm layout and surroundings. Events 2 and 3 (as listed in the list above) are considered most important in limiting the energy inflow into the wake (Veldkamp, 2011-2012).

When this has happened the only way for the wake to mix in higher momentum air is from above, or from the edges of the wind farm. Mixing with the higher energy flow from above the wind farm is likely the largest influence on wake recovery in the wind farm (Barthelmie et al., 2010).

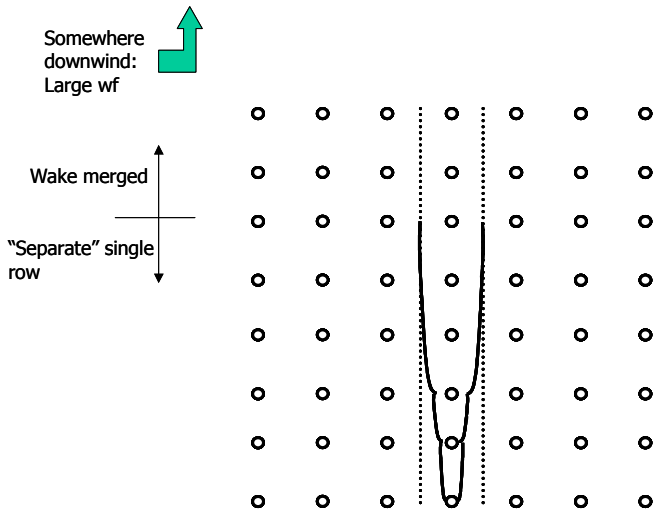

Figure 2.6: Wakes resulting from separate turbines merging laterally with each other after some downstream distance (Méchali et al., 2006).

Lateral merging of the wakes usually occurs later than downstream merging (occurring when the wake encounters the next downstream turbine), but it depends on the spacing between the turbines and the expansion of the wake. As noted by Barthelmie et al. (2011) the boundary layer influences the downstream propagation and merging of the wakes. So, the boundary layer has an influence on the power output of the wind farm.

The measurements from Horns Rev and Nysted show similar wake depth and width (see figure 2.7). This is interesting considering that the wind turbines in the two wind farms are not the same, although the turbines have a similar size and rated power (the locations of the wind farms are also significantly apart). Because the shape of the wake looks near-Gaussian, for each downstream distance behind the turbine there is a point in the wake that has the largest wake loss. Barthelmie et al. (2010) name this point the wake centre. They note that from the observations it could be seen that the wake centre remains visible for downstream movement through the wind farm. In other words, the point with the largest wake loss keeps existing in the wake when the wake moves downstream. It is not clear what causes this, but it is suspected that the wake centre either is preserved from a turbine upstream when the wake moves downstream through the wind farm, or that the wake centre in the wake of an upstream turbine is replaced by a new wake centre when the next wind turbine extracts energy from the flow.

The power losses in a wind farm are unwelcome and hence much research is put into quantifying the losses by measuring and modelling, so they can be reduced (e.g. by the design of the wind farm, or by the control strategy of the turbines in the wind farm).

2.2.2 Effects on power output of wind farms

Wakes recover by mixing in higher energy air from the surroundings. This can be from all sides when the wakes are small, but when they expand, move downstream and merge with other wakes, the only two directions from which higher energy air can be mixed into the wake are from above and from the sides of the wind farm (parallel to the downstream

movement of the wake). The outer rows (also defined parallel with the wind direction and with the downstream movement of the wake) therefore usually show lower wake losses compared to the inner rows, and so they have higher power output (Barthelmie et al., 2009). In studying the wake effects inside the wind farm it can therefore be chosen to only look at the wake losses at the inner rows.

In the literature different examples exist of the measured losses.

Barthelmie et al. (2004) have shown from investigating a number of wind farms that power losses due to wakes can range from 5 to 15% corresponding to a wind turbine spacing of 4 to 8 rotor diameters (D) in the wind farm. Barthelmie et al. (2010) lists the wake losses for the Middelgrunden, Horns Rev and Lillgrund wind farms as 10%, 12.4% and 23% respectively, corresponding to spacings of $2.4D$, $7D$ and 3.3-4.3D. The losses can thus vary significantly.

Méchali et al. (2006) found at the offshore wind farm Horns Rev that the wind direction sector used to determine the wake losses has a significant influence on the power losses observed. The highest losses occur in a narrow direction sector parallel to the direction towards the downstream turbines. At other directions, or for larger wind direction sectors, the power losses from the first to the second turbine are smaller. After a number of turbines the power losses will not change anymore from one turbine to the next. This effect should occur for an infinite wind farm where the wake recovery is in equilibrium with the energy extraction, but actually the effect occurs behind a limited number of 2-3 columns in a wind farm already. The effect depends on the spacing between the turbines in the wind farm. It might be difficult to quantify the wind direction for a whole wind farm, since the wind direction might change over the wind farm. Especially for turbines far away from the measurements location (e.g. a meteorological tower) this can be an issue. This might even lead to increasing power outputs further downstream in the wind farm, since due to different wind directions the downstream turbines might not be in a direct wake from their upstream turbine.

More recently, Barthelmie and Jensen (2010); Barthelmie et al. (2011) have found similar results for the Nysted and Horns Rev offshore wind farms, as shown in figure 2.7. Wake losses are primarily influenced by the wind speed distribution with wind direction, and at the same time with the spacing related to this wind direction. From the figure it can be seen that the highest loss in power output due to wakes can be observed when the wind direction is such that the flow is exactly aligned with the line of turbines. The second turbine then produces only 60% of power output of the first turbine. The turbines further downstream show as good as no change in power output (see also Barthelmie et al. (2010)) and also produce 60% of the first turbines power output (see also Barthelmie et al. (2009)). The biggest losses occur at low wind speeds (since the thrust coefficient is high and so the wake is strong), and the losses are higher for closer spaced turbines. The figure also shows that when the flow direction is not exactly down the row of turbines, the losses are less severe but the power output keeps decreasing for downstream turbines, so that 60% power output remains after 9-10 turbines (instead of directly at the second turbine) (see also Barthelmie et al. (2009)). This can be due to the lateral merging of wakes (Barthelmie et al., 2010), although in Barthelmie et al. (2010) it is noted too that when there is only a small difference in wind direction (e.g. $\pm 5°$), it should not make a significant change in wake expansion, merging or recovery, as the downwind distance to the end of the wind farm does not significantly change.

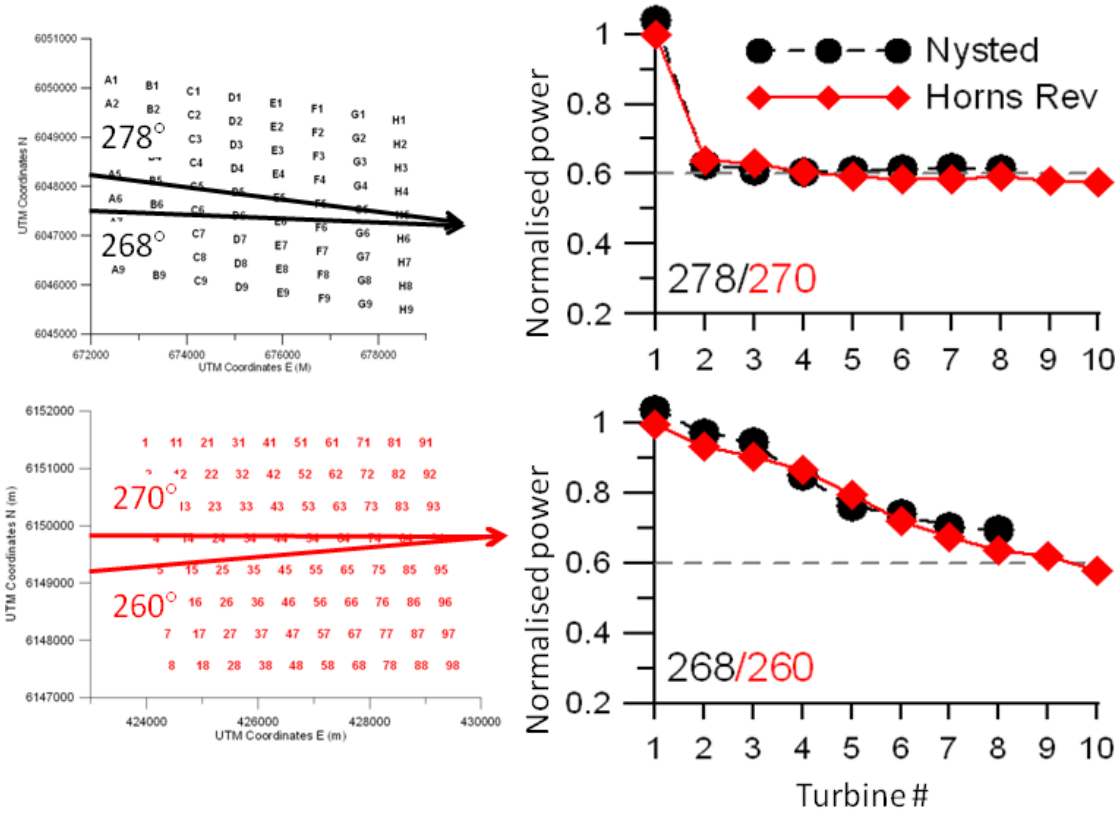

Figure 2.7: Left: wind farm layout at Nysted (top) and Horns Rev (below). Right: Wake losses at turbines at Nysted and Horns Rev for wind speeds 8.0 ± 0.5 m/s for the wind direction aligned with the row (top) and 10° off the direction aligned with the row. (Note that in both cases the wind direction has a range of $\pm 2.5^\circ$ around the shown directions.) (Barthelmie et al., 2011)

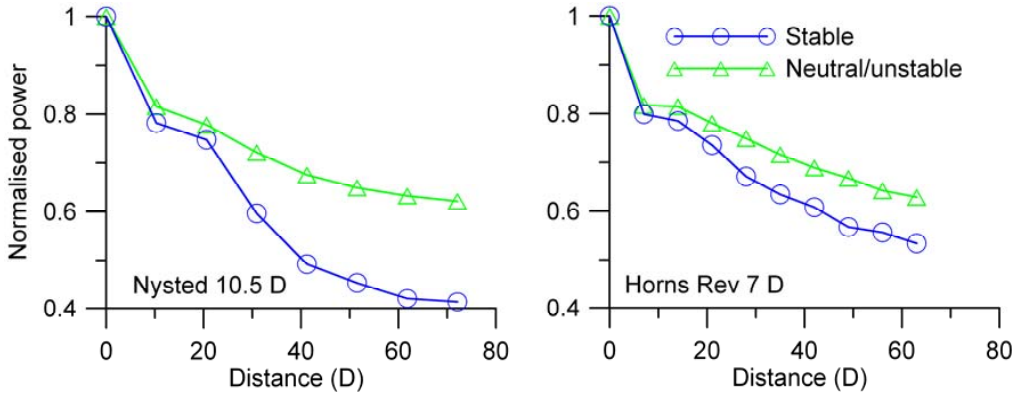

Figure 2.8: Wake losses at turbines at Nysted and Horns Rev for wind speeds 8.0 ± 0.5 m/s. Left: Nysted, wind direction $278° \pm 15°$, right: Horns Rev, wind direction $270° \pm 15°$ (Barthelmie et al., 2011).

Next to the importance of the wind direction on the variation of wake losses, the variation with atmospheric stability is shown by Barthelmie et al. (2011) for the Nysted and Horns Rev wind farms as well, see figure 2.8. The results specify two stability classes (stable and neutral/unstable) and use a wind direction sector of 30 degrees. A significant difference between the two classes exists.

At wind speeds above 15 m/s, wind farm efficiencies are above 95% in most of the directions (see also Barthelmie et al. (2007)). Below 10 m/s the efficiencies are lower in most of the directions compared to the efficiencies in the 10-15 m/s range, regardless of wind direction and hence turbine spacing. Power output at the wind farms was related to the wind turbine spacing, wind speed, ambient turbulence intensity and atmospheric stability. An increase of $1D$, in the range of 6-10D, leads to about a 1.3% increase in wind farm power output. An increase of 1 m/s, in the range 5-15 m/s, leads to about 3.7% increase in wind farm power output. A 1% increase of ambient turbulence intensity results in an increase in wind farm power output of 1% for Nysted and 2.5% for Horns Rev. The stability conditions lead to about 8% increase of wind farm power output when they change from stable to unstable, see figure 2.9. Unfortunately, these relationships are only valid for these wind farms, as conditions at other wind farms will be different (e.g. the turbine type, spacing, size of wind farm, wind climate and/or surroundings). Some of the discussed parameters are also related to each other. Even though their separate influences on the power output are quantified, they do not vary independently.

Hansen, Barthelmie, Jensen, and Sommer (2012) investigated the influence of turbulence intensity and atmospheric stability at Horns Rev. They quantified the atmospheric stability using the bulk Richardson number (see section 2.3) and used this to study the effect on the wake losses. The results are shown in figure 2.10. Note that instead of plotting the normalized power output of the turbines, the wake losses have been plotted directly. It was found that very stable and stable conditions result in large wake losses, but less difference was found between the other stability classes (the near-neutral and unstable classes).

The above examples are regarding offshore wind farms. Wharton and Lundquist (2010, 2011) analysed an onshore wind farm in the USA. They found that higher power was

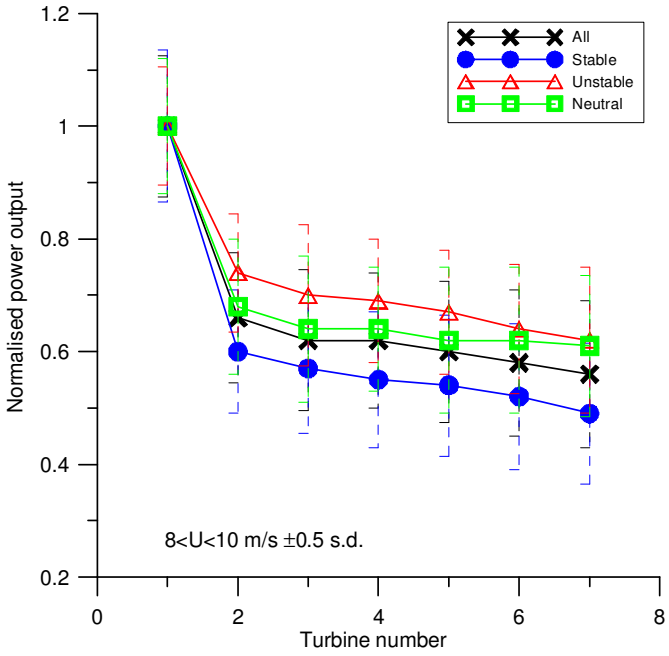

Figure 2.9: Wake losses at turbines at Nysted for wind speeds 9.0 ± 1.0 m/s for the wind direction $276° \pm 2.5°$ (Barthelmie et al., 2007).

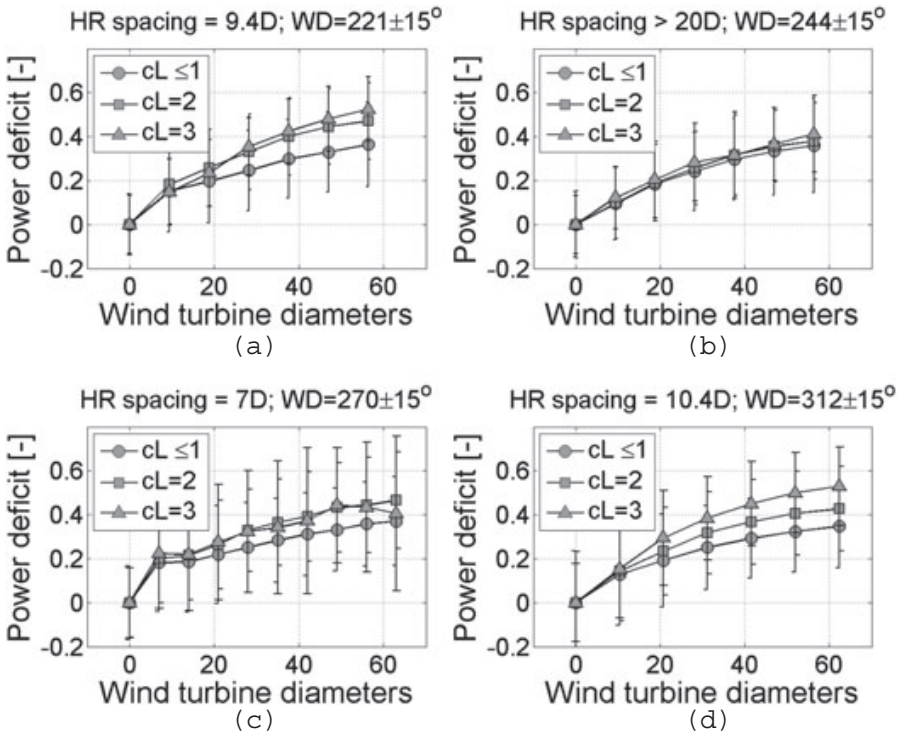

Figure 2.10: Wake losses at turbines at Horns Rev for wind speeds 8.0 ± 0.5 m/s for various row directions and spacings. The stability is grouped in very stable (indicated in the figure as class (cL) $= 3$), stable (cL $= 2$) and other (cL ≤ 1) stability classes. One standard deviation has been included as error bars (Hansen et al., 2012).

achieved when wind shear in the rotor disk increased. Increasing wind shear occurs for increasing atmospheric stability, and it also decreases the turbulence intensity (see also Barthelmie et al. (2007)). This effect of increased power output was most noticeable at moderate wind speeds (6-9 m/s). This is an interesting finding. In an offshore wind farm, the situation can be different, as Barthelmie and Jensen (2010) suggest. Higher turbulence intensities would enhance mixing the wakes with the surface boundary layer, so that energy would be transferred into the lower energy wakes. This would then result in higher wind farm efficiencies. Stable conditions inhibit turbulent mixing. Thus, for increasing stability the offshore wind farm would become less efficient, which is exactly the opposite as found by Wharton and Lundquist for their onshore wind farm. Wharton and Lundquist suggest that this might have to do with the climate and location of the wind farm they investigated.

Rados et al. (2001) on the other hand, found from measurements of the Vindeby and Bockstigen wind farms that the ambient conditions have little influence on the measurements. This is opposed to Barthelmie and Jensen (2010) who found that during summer the average wake losses are higher as a result of the lower wind speeds.

From the examples discussed above, it becomes clear that both wind shear and turbulence influence the power output of a wind farm. These influences will therefore be investigated more closely in the following sections.

2.2.3 Influence of wind shear on wind farm power output

In 2.1.3 the power curve of a wind turbine was introduced. It gives the power output as a function of hub height wind speed. Measurements indicate that other factors influence the power output as well. Ignoring wind shear and turbulence can introduce significant errors in the power curve measurements (Elliot & Cadogan, 1990), as will now be explained.

An important factor is whether the hub height wind speed is representative for the wind speed seen by the wind turbine rotor. When wind turbine rotors were small, the hub height point measurement gave a good estimate of the average wind speed over the rotor plane. However, for increasing rotor diameter the hub height wind speed becomes less representative of the disk-average wind speed. This is because of the wind shear over the rotor plane. Especially in low turbulence (often stable) conditions this is important (Elliot & Cadogan, 1990). A disk-averaged wind velocity might represent the wind flowing into the rotor area more accurately (Sumner & Masson, 2006; Wharton & Lundquist, 2010). The hub height velocity can overestimate the disk-average velocity by 1 m/s or more, and hence overestimates the available kinetic energy (Elliot & Cadogan, 1990; Sumner & Masson, 2006). When one would use a power curve measured under no shear conditions with a hub height wind speed measured under shear conditions, the power curve would indicate a too high power (corresponding to the overestimated hub height wind speed). The turbine would seem to underperform. Hence, by using hub height wind speed to plot the power curve, maximum turbine efficiency is underestimated (Sumner & Masson, 2006; Wharton & Lundquist, 2010).

Power measurements are often used to determine the hub height wind speed at the wind farm. This can be done via the power curve. It could be expected that the wind speeds resulting from the measured power would be a good representation of the wind speed

in the wind farm. An alternative is to measure the wind speed with a meteorological measurement mast, but this is usually at some distance away from the wind farm and thus measurements can significantly differ (Barthelmie & Jensen, 2010). Méchali et al. (2006) found that the hub height velocities as determined from the power measurements usually have much larger standard deviations than the metmast measurements. On the other hand, when wind speeds in the wind farm are required, for instance to study the wake losses, then metmast measurements might not be enough. The power curve is then required to obtain the wind speed from the power measurements. The wind speeds might then be subject to errors in the site-specific power curve (Barthelmie et al., 2009).

2.2.4 Influence of turbulence on wind farm power output

Stable conditions correspond generally with less turbulence and hence reduced turbulent mixing, while unstable conditions show increased energy transfer into the wake (Barthelmie et al., 2007). These atmospheric stability influences are most important in the wind speed range between cut-in and rated wind speeds (Barthelmie, 1999). At these wind speeds the wakes are strongest due to the low wind speeds and corresponding high thrust coefficients (Barthelmie & Jensen, 2010). At these moderate wind speeds lower turbulence intensities occur more frequently offshore too. Hence, there is also less recovery (Barthelmie & Jensen, 2010), and so the wakes remain stronger (Barthelmie et al., 2011).

A result of lower turbulence intensities offshore is that there is less turbulent mixing. Less mixing with the free-stream flow means that less of the more energetic free-stream flow is mixed into the wind farm wakes (Barthelmie et al., 2011). The wakes will thus recover slower, and a longer near wake structure remains (Barthelmie et al., 2006).

Barthelmie et al. (2007); Barthelmie and Jensen (2010); Barthelmie et al. (2011) found that power losses due to wakes are indeed larger during stable conditions than during neutral conditions, and larger during neutral than during unstable conditions. For the Nysted wind farm they found that the difference in power loss between stable and near-neutral conditions ($\sim 6.4\%$) is almost four times larger than for near-neutral and unstable conditions ($\sim 1.7\%$). There is thus a change of about 8% in power output over the range of atmospheric stabilities.

Note that near-neutral conditions are more common at higher wind speeds, and dominate above 15 m/s (Barthelmie, 1999; Barthelmie et al., 2007; Barthelmie & Jensen, 2010). The relationship between power loss and atmospheric stability and turbulence can therefore not be seen separately from wind speed. Even with wind speed being the main influence on the power production, the differences between stability classes occur at varying wind speeds (Barthelmie & Jensen, 2010). Also, it is noted by Barthelmie et al. (2011) that stable conditions usually have lower turbulence intensities, and unstable conditions higher intensities, but that this does not necessarily always need to be the case. For instance, turbulence is also created by the wake itself, and usually ambient turbulence is present as well (e.g. resulting from surface roughness), although the latter is less important in large wind farms (Barthelmie et al., 2007; Frandsen & Madsen, 2003).

Next to the influence of turbulence intensity on the power output of a wind farm due to wake recovery, turbulence intensity might also have a direct influence on the power output

of a single turbine. Elliot and Cadogan (1990) found that the mean power output increases substantially as turbulence intensity increases (even when the disk-averaged velocity is used). Manwell et al. (2009) on the other hand state that wind turbines usually perform better with lower turbulence intensities.

It can be seen that turbulence intensity has an influence on the power output. However, its influence is less important than that of the wind speed (Barthelmie & Jensen, 2010).

2.3 Atmospheric stability

Atmospheric stability refers to the state of the atmosphere. It indicates how stratified the atmosphere is (i.e. whether horizontal layers with different properties exist) and how likely it is that mixing occurs between the air of these different layers. Since mixing determines how much high energy flow is mixed into the wakes of a wind farm, the wake losses depend on atmospheric stability. Understanding of some other concepts is required before going into detail in how atmospheric stability works and how it can be classified. These will be explained first, after which atmospheric stability is addressed in more detail.

2.3.1 Atmospheric boundary layer

The air between the earth and space is called the atmosphere. It is separated vertically in layers with different characteristics. The layer closest to the ground is called the troposphere, and is 11 km high. It consists of the atmospheric boundary layer (ABL), being the bottom part, and the free atmosphere, being the top part. The entrainment zone (EZ) is turbulent and forms the separation between these two layers. Air can pass the entrainment zone one-way only, from the free atmosphere to the ABL. At night the turbulence in this layer ceases to exist. A non-turbulent separation layer remains which is called the capping inversion (Stull, 2000). The EZ exists at the inversion height (Rohatgi & Barbezier, 1999), which at the lowest is at an altitude of a few 100 m (Lange, Larsen, Højstrup, & Barthelmie, 2004b). At the inversion height a change in potential temperature variation with height occurs. An overview is shown in figure 2.11.

With rotor diameters nowadays being in the order of 160 m (Vestas Wind Systems A/S, 2011b), the height to which the tip of a wind turbine blade reaches up into the atmosphere can be around 200 m. The ABL is thus the part that is important for wind turbines. During turbulent conditions the ABL can also be called turbulent boundary layer or mixed layer. The first, since turbulence plays an important role in this layer, and the second because the turbulence mixes the air in this layer (Stull, 2000). Turbulence is defined as the differences in wind speed from the mean wind speed (Manwell et al., 2009; Stull, 2000).

2.3.2 Potential temperature

The bottom part of the ABL is influenced by heat conduction from the earth, friction with the earths surface, and evaporation from the surface. This results in changes in temperature, wind speed and humidity (Stull, 2000). The result is that there can be

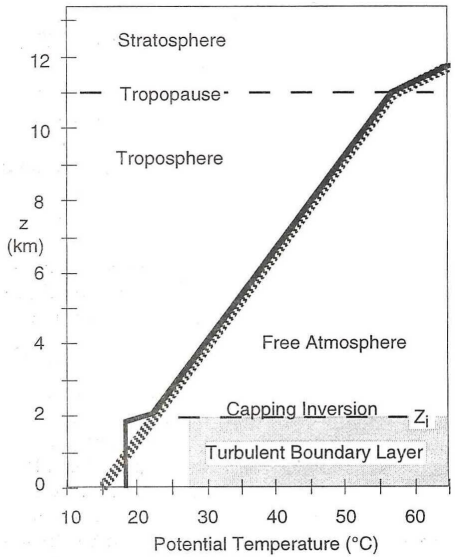

Figure 2.11: Distribution of layers in the troposphere. The hatched line is the distribution of potential temperature (explained later on) with height for the stable conditions of the standard atmosphere. The thick line shows a difference near the ground, which is the result of turbulent mixing (Stull, 2000).

differences in the way air behaves in the ABL, or in other words, whether the air in this layer shows stable behaviour.

When an air parcel moves from one pressure at one altitude to another pressure at another altitude, without any heat being exchanged with the surroundings (i.e. adiabatically), it will experience a change in temperature. A thermodynamic diagram can be used to display the relation between pressure (corresponding to height) and temperature. This diagram is shown in figure 2.12. The thin diagonal lines are representations of the relationship between pressure and temperature. The decrease in temperature with height is called the lapse rate. The dry adiabatic lapse rate corresponding to the diagonal lines is 9.8 K/km. For every kilometre increase in height, the temperature decreases with 9.8 Kelvin (Stull, 2000).

In figure 2.12 it can be seen that each diagonal adiabat is identified by looking at the temperature it has at a pressure of 100 kPa. This temperature is a constant for each line and is called the potential temperature. It is the temperature that the parcel would have if it were moved adiabatically to the ground or to a certain reference pressure (Stull, 2000).

In reality the atmosphere does not always have the same state. Moreover, changes do not occur adiabatically. For engineering purposes, an average of the atmosphere has been approximated. This is called the standard atmosphere, and is represented by the thick line in figure 2.12. The dry adiabatic lapse rate in the standard atmosphere is not 9.8 K/km, but 6.5 K/km (Stull, 2000).

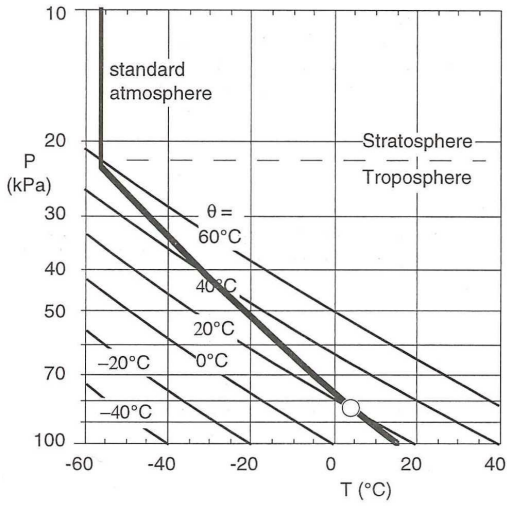

Figure 2.12: Thermodynamic diagram including the adiabats (thin diagonal lines) and variation in the standard atmosphere (thick line). The open circle represents an air parcel (Stull, 2000).

2.3.3 Movement of an air parcel

Imagine a certain air parcel, as shown by the open circle in figure 2.12. It is moved up fast enough so that no heat will be exchanged with the surroundings (i.e. adiabatically). The air parcel has a certain temperature, and a certain potential temperature. Its potential temperature will stay the same, but since its altitude is changed, its temperature will change according to the adiabat belonging to its potential temperature (in the figure $20°C$). Since the surroundings (in the figure the standard atmosphere) have a smaller decrease in temperature with increasing height, the air parcel will have a lower temperature than its surroundings at its new height. The result is that the air parcel decreases in size, so being heavier than the surrounding air and sinking back to its starting altitude. In this case the atmosphere is statically stable. In case the air parcel would have been moved downwards from its starting position in the same atmosphere, it would be warmer than its surroundings. It would then increase in size, thus being relatively lighter than its surroundings, and so it would rise back to its starting altitude (Stull, 2000).

Now, a parcel of air is moved upwards in an atmosphere that has a larger decrease in temperature with increasing height than the air parcel. The air parcel will be warmer than its surroundings at its new height, with the result that it will expand and rise up even higher. This is called the statically unstable condition (Manwell et al., 2009; Rohatgi & Barbezier, 1999; Stull, 2000), as the air parcel moves away from its initial position. In case the air parcel would have been moved downwards from its starting position in the same unstable atmosphere, it would sink further down.

When there is no difference in the change of temperature with height between the environment and the air parcel, the air parcel will have the same temperature as the surroundings at its new height, and so will not expand nor decrease in size. Hence, it will remain at its new height. This is called the statically neutral condition.

Atmospheric stability can thus be defined as the tendency to resist vertical motion

(Manwell et al., 2009; Stull, 2000). There are three types of stability conditions in the atmospheric boundary layer: stable, neutral and unstable. Stability is governed by the vertical temperature distribution. In general it can be said that when the surface is warmer than the air, an unstable (also called convective, or mixed) layer will develop, while a colder surface will result in a stable atmospheric boundary layer (Stull, 2000). When the surface temperature is similar to that of the air a neutral condition results.

Neutral conditions have been observed to exist mostly during a cloudy day with heavy cloud cover or during windy conditions, over a uniform surface (Rohatgi & Barbezier, 1999; Sathe, 2009; Stull, 2000). On a cloudy day the heavy cloud cover prevents the earth's surface from being heated while the air is not being heated either. No (large) temperature difference that could result in (un)stable conditions then exists. Windy conditions make it harder for air parcels to move back towards or away from their starting altitude since the horizontal wind speed is much greater than the vertical velocity of the air parcel. Statically stable conditions can for instance occur during evening and night time when the air has been heated up more than the surface of the earth. Due to this, no heat is convected from the surface of the earth to the air, and so no turbulence results. Since there is no turbulence due to instability there will only be very little mixing in the atmosphere (e.g. resulting from ambient turbulence), so the air will have different characteristics at different heights (Rohatgi & Barbezier, 1999). At the surface the friction and lack of mixing will result in lower wind speeds, while the lack of mixing also leads to higher wind speeds higher up in the ABL. The ABL thus tends to be more stratified. During statically unstable conditions the heat that is convected from the surface results in an unstable condition via turbulent mixing. Due to the turbulent mixing, the faster winds from higher up in the ABL are mixed with the slower winds near the surface. In this mixed layer the wind speed is vertically averaged, and so it is uniform with height. Near the surface the winds are faster than during the neutral condition, whereas higher up in the ABL they are slower than during the neutral condition. Only the bottom part of the ABL shows a change in wind speed with height, as opposed to the wind speed profiles that vary over the whole ABL in case of a stable or neutral surface layer (Stull, 2000). This condition can for instance occur during sunny days over land.

2.3.4 Monin-Obukhov length

Usually atmospheric stability is based on the Monin-Obukhov length. It can be interpreted as the height above the surface at which turbulence produced by heat conduction first starts to dominate over turbulence produced by shear (resulting from the different wind speeds with height) (Stull, 1988, 2000; Wharton & Lundquist, 2010). It is defined as (Stull, 1988):

$$L = \frac{-\overline{\theta_v} u_*^3}{\kappa g \left(\overline{w'\theta_v'}\right)_s} \tag{2.11}$$

where u_* is the friction velocity, κ the von Kármán constant and g the gravitational acceleration. $w'\theta_v'$ is the flux of virtual potential temperature (w is vertical velocity, θ_v is virtual potential temperature and the primes indicate turbulent fluctuations (Grachev

& Fairall, 1997)), and the subscript s denotes that this variable is required at surface level. The overbars indicate time averages. Virtual potential temperature θ_v is similar to the potential temperature. However, the potential temperature holds for "dry" adiabatic conditions, whereas the virtual potential temperature also includes effects of water vapour and liquid water in air (Barthelmie et al., 2011). Virtual potential temperature is the temperature that dry air would need, to have the same density as moist air at the same pressure (Stull, 1988).

A variable related to the Monin-Obukhov length is the dimensionless stability parameter ζ. It is defined as (Grachev & Fairall, 1997)

$$\zeta = \frac{z}{L} \tag{2.12}$$

where z is the height of the measurement.

Next to the Monin-Obukhov length, Wharton and Lundquist (2010) use other parameters to classify the stability parameter to see its influence on power output. They use the nacelle-based turbulence intensity, as well as SODAR-based turbulence intensity (at hub height), wind shear and turbulence kinetic energy (TKE). It is noted that nacelle-based turbulence intensity is influenced by the turbine, since the turbine extracts energy from the flow and disturbs the flow. These effects on the flow can therefore mask the actual turbulence effects, thus limiting the usability of the nacelle-based turbulence intensity as a stability parameter. The nacelle-based turbulence intensity did not agree with the other stability parameters. It underestimates the frequency of unstable conditions. TKE is the only stability parameter in the comparison that includes vertical turbulence. It compares well with the Monin-Obukhov length, as did the SODAR-based turbulence intensity.

2.3.5 Stability classes

According to Sathe (Sathe & Bierbooms, 2007) there is currently no firm criterion to define the limits of L to define the different stability classes. They are only based on previous research experience. Different stability classifications exist in literature.

The stability classifications differ in the Monin-Obukhov lengths L used as the boundaries of the stability classes. Next to that, the number of stability classes varies. As already outlined in the previous sections, atmospheric stability can be classified as unstable, neutral and stable. However, classifications as very (un)stable or near-neutral (stable/unstable) are found in literature as well. Table 2.1 summarizes some of the classifications found.

As can be seen from table 2.1 the criterion for the different stability classes is not clear. For example, some references classify a certain L-value as stable while others classify it as neutral. It is also unclear whether the stability classes should have symmetric ranges around the neutral classification (so that unstable classes would have the negative range of the corresponding stable class).

In Sathe (2009) it is noted that the values at the edges of the stability classification intervals can be an important influence on the classification. The results might be sensitive

Table 2.1: Different Monin-Obukhov length L [m] boundaries for stability classes as found in literature. VS = very stable, S = stable, NNS = near-neutrally stable, N = neutral, NNU = near-neutrally unstable, U = unstable, VU = very unstable.

Reference	Barthelmie (1999), Barthelmie et al. (2005), Motta et al. (2005), Sathe and Bierbooms (2007), Sathe (2009), Wijk et al. (1990)	Wharton and Lundquist (2010)	Wharton and Lundquist (2011)	Sathe (2009), Sathe et al. (2011), Hansen et al. (2012)
VS	$0 < L < 200$	$0 < L < 50$	$0 < L < 100$	$10 < L < 50$
S	$200 < L < 1000$	$50 < L < 200$	$100 < L < 600$	$50 < L < 200$
NNS		$L > 200$		$200 < L < 500$
N	$\|L\| > 1000$	or	$\|L\| > 600$	$\|L\| > 500$
NNU		$L < 300$		$-500 < L < -200$
U	$-1000 < L < -200$	$-300 < L < -15$	$-600 < L < -50$	$-200 < L < -100$
VU	$-200 < L < 0$	$-15 < L < 0$	$-50 < L < 0$	$-100 < L < -50$

to changes in the values at the edges, possibly significantly changing the frequency of a certain stability class at a certain site.

From the definition of L in section 2.3.4, it can be seen that high wind speeds (corresponding to higher friction velocities) result in higher absolute values of L. From table 2.1 it can be seen that high absolute values of L occur during (near-)neutral conditions. Hence, (near-)neutral conditions are more common during high wind speeds (Barthelmie et al., 2005; Sathe, 2009). Lower wind speeds correspond to lower absolute values, and can be either stable ($L > 0$) or unstable ($L < 0$), depending on the temperature gradient.

2.3.6 Determining Monin-Obukhov length from measurements

Lange, Larsen, et al. (2004b), Sathe (2009) and Grachev and Fairall (1997) describe different methods to determine the Monin-Obukhov length scale L. The following methods are described (for a more detailed description of each method, including equations of how to apply them, see Alblas (2011)):

Sonic (eddy-correlation) method This method uses sonic anemometer measurements of the friction velocity and the flux of virtual potential temperature. Using the high frequency measurements of the sonic anemometer the equation for the Monin-Obukhov length can be applied straight-away (Lange, Larsen, et al., 2004b; Sathe, 2009). In this project no high frequency measurements were available though, so this method cannot be applied.

Profile methods Strictly these methods are only valid in the surface layer. First, a Monin-Obukhov length is assumed. Using the (stability corrected) wind speed profile

and temperature profile, the friction velocity and temperature scale are obtained. These are used to determine a new Monin-Obukhov length, which can then be used as input to the procedure. This is iterated until the error between the input and output Monin-Obukhov length is less than a certain error. Different variants of this method exist, depending on the type of input data. A preliminary study (at Egmond aan Zee (OWEZ)) performed by Sathe (2009) indicates that this method tends to over-predict the wind profile significantly under stable conditions. Therefore these methods will not be applied in this project.

Gradient method The gradient method can be used by determining the temperature and wind speed difference between two heights. A high accuracy is required to measure the fluxes. The Monin-Obukhov length is determined using the Richardson number (Lange, Larsen, et al., 2004b; Sathe, 2009).

Bulk method The bulk method is exactly the same as the gradient method, with the difference that the wind speed at the sea surface is zero and hence only one wind speed measurement is required. The method uses the sea surface temperature, and the air temperature and wind speed at a certain height. The Richardson bulk number is defined as (Lange, Larsen, et al., 2004b; Sathe, 2009):

$$Ri_b = \frac{gz\Delta\overline{\theta_v}}{\overline{\theta_v}\bar{U}^2} \tag{2.13}$$

Here $\Delta\overline{\theta_v}$ is the time-average of the gradient between the two measured temperatures over the 10-minute period. Note that the temperature that is being measured is the virtual temperature (as it already includes the effects of humidity on the temperature). The virtual potential temperature can then be found using the following relation (Stull, 1988):

$$\theta \cong T + \left(\frac{g}{C_p}\right) z \tag{2.14}$$

where C_p is the specific heat of air at constant pressure. The ratio g/C_p can be approximated by 0.0098 K/m (Stull, 1988).

The basic relation between the Monin-Obukhov length and the Richardson bulk number was defined by Deardorff (Grachev & Fairall, 1997):

$$\frac{z}{L} = \zeta = CRi_b \tag{2.15}$$

where C is a constant depending on the Richardson bulk number, and for which various values for different ranges have been proposed. Grachev and Fairall (1997) and Sathe (2009) use a value of $C = 10$ in their comparisons. However, the relation does not include stability.

Stability can explicitly be included into the equation by adding a correction factor depending on the Monin-Obukhov length. The drawback of this is that it requires iterative solution methods. Functions without this drawback have been derived.

For stable conditions Businger et al. (Grachev & Fairall, 1997) found the following relation:

$$\zeta = \frac{CRi_b}{1 - \alpha Ri_b} \tag{2.16}$$

where $\alpha \approx 5$ is an empirical constant. The relation has been verified up to ζ about 0.5. Next to that there is a critical bulk Richardson number of about 0.2-0.25, resulting in a singularity.

Grachev and Fairall (1997) derived a function of ζ depending on the Richardson bulk number for unstable conditions. It is defined as:

$$\zeta = \frac{CRi_b}{1 + Ri_b/Ri_{bc}} \tag{2.17}$$

where Ri_{bc} is the saturation bulk Richardson number (Grachev & Fairall, 1997):

$$Ri_{bc} = -\frac{z}{z_i C_h \beta^3} \tag{2.18}$$

Here z is the measurement height, z_i is the depth of the convective boundary layer, $\beta = 1.25$ is an empirical constant and C_h is the bulk transfer coefficient for sensible heat. C_h is a function of stability. It is found for Ri_{bc} using a fixed value ζ_m for ζ, resulting when the bulk Richardson number goes to minus infinity (Grachev & Fairall, 1997). As the relation for Ri_{bc}, required for the function of ζ for unstable conditions, involves parameters that are hard to determine, the simple linear relation for ζ derived by Deardorff as shown in equation 2.15 can be used for practical purposes (Sathe, 2009).

Using the above relations, the Monin-Obukhov length can be found as (Sathe, 2009):

$$L = \begin{cases} \frac{z}{10Ri_b} & Ri_b < 0 \\ \frac{z(1-5Ri_b)}{10Ri_b} & 0 < Ri_b < 0.2 \end{cases} \tag{2.19}$$

In neutral conditions the air and sea surface temperatures are close together. This increases the uncertainty of the method. This drawback should be taken into account when using the method. During stable and unstable conditions the uncertainty in L reduces (Lange, Larsen, et al., 2004b; Sathe, 2009).

Sathe (2009) states that the bulk method is considered to be the most accurate method. The higher accuracy of the method compared to the other stability methods is also confirmed by (Nielsen Nissen, 2008, 2012). The explanation for the higher accuracy of the method is that it uses the sea surface temperature (SST) instead of another ambient temperature (as in the gradient method). The SST varies more slowly than the ambient temperature. It therefore adds a certain damping to the stability determination, which makes the bulk method more robust than the gradient method. The bulk method is therefore the selected method that is applied in this study.

Table 2.2: Frequency of stability classes in percent for various wind farms as found in literature. VS: very stable, S: stable, NNS: near-neutral stable, N: neutral, NNU: near-neutral unstable, U: unstable, VU: unstable.

Location	VS	S	NNS	N	NNU	U	VU	Reference
Western North America (USA)[a]	42			18-30		28-40		Wharton and Lundquist (2010, 2011)
Tystofte (DK)[b]	29	21		20		10	20	Motta et al. (2005)
Vindeby (DK)[c]	21	21		48		9	1	Motta et al. (2005)
Rødsand (DK)	20	11		33		29	7	Motta et al. (2005)
Omø Stålgrunde (DK)	19	10		28		34	9	Motta et al. (2005)
Horns Rev (DK)[d]	2	18	10	18	19	19	14	Sathe et al. (2011)
OWEZ (NL)[d]	<1	9	11	23	15	23	18	Sathe et al. (2011)

[a] This concerns an onshore wind farm. The stability distribution depends on the used Monin-Obukhov stability classification. See also table 2.1.

[b] This concerns an onshore measurement mast. It is surrounded by land for at least 3 km in each direction (Motta et al., 2005).

[c] This concerns an offshore measurement mast. However, it is located at only 2 km from the shoreline and hence coastal influences are present (Motta et al., 2005).

[d] Sathe et al. (2011) investigated the stability conditions at the offshore wind farms OWEZ and Horns Rev. They only looked at inflow from the sea (North Sea), to avoid any coastal effects.

2.3.7 Observed distributions of atmospheric stability

In literature distributions of atmospheric stability at various wind farms can be found. These are shown in table 2.2. Differences in the variation of stability can be seen between onshore, offshore and coastal zones.

The stability distributions shown depend on the definition of the stability classes used (see also table 2.1). This is illustrated by the two different stability classifications used for the North American wind farm, resulting in a 12% difference in neutral or unstable conditions. Furthermore, the stability frequencies discussed in the table are averaged values. Hence, the daily and/or seasonal variations are not visible in these values. Looking at only a certain time of the day or time of the year would thus show different values.

The tables represent locations onshore and offshore. The wind farm in the USA is located onshore, Tystofte refers to a measurement mast onshore (in a coastal zone, surrounded by at least 3 km land in each direction (Motta et al., 2005)) and Vindeby refers to a mast offshore (in a coastal zone, at only 2 km from the coast (Motta et al., 2005)). The other locations are offshore. However, only in the analyses of Horns Rev and OWEZ the coastal effects have been excluded by only looking at inflow from sea. In that sense, these two locations are the only ones represented which are truly offshore, while the others could be classified as coastal. The biggest difference between the offshore and other sites seems to be that the offshore measurements show a significant decrease in stable conditions and an increase in neutral conditions.

Barthelmie et al. (2005) investigated ten years of meteorological measurements from offshore wind farms and found that stability conditions at offshore wind farms around Denmark have a similar variation of stability conditions with wind direction. They note that this can be at least partly connected to similar occurrences of average air temperatures (at 50 m) and air temperature differences (between 10 and 50 m) with wind direction.

2.4 Offshore environment

The wind farms considered in this study are all located offshore. Some differences between offshore and onshore sites will therefore be explained.

2.4.1 Differences between onshore and offshore

There are some differences in the behaviour of the atmospheric boundary layer onshore and offshore. The differences can for example lead to differences in wind speed profiles (Barthelmie, 1999). The European Wind Atlas (Barthelmie et al., 2009; Troen & Petersen, 1989) defines an offshore site as being located at open sea and at least 10 km from the coast. An onshore site should be 10 km from the coast inland.

It has been shown that mesoscale wind features can result in similar stability distributions at separate sites, even when a significant distance separates these sites. However, local effects due to the surroundings or the presence of a coastline can alter the stability distributions. Compared to an offshore site, another offshore site further away might have

a more similar stability distribution than an onshore site that is located close by (Motta et al., 2005).

Some differences in characteristics between onshore and offshore sites as found in the literature are described next. They originate from the differences in surface roughness and thermal surface properties (Barthelmie et al., 2005; Troen & Petersen, 1989).

- The wind speed at offshore sites is usually higher than that at onshore sites (Barthelmie, Courtney, Lange, Nielsen, & Sempreviva, 1999; Manwell et al., 2009) and therefore there is also a higher occurrence of the wind speeds that are used for extracting energy from the wind by the turbine (Barthelmie et al., 2005). The higher wind speed results from the lower surface roughness of the water. The sea surface is much smoother than normal land (Manwell et al., 2009), so less friction exists between the surface and air. As a result of the higher wind speeds the power production of wind turbines offshore is higher than onshore. However, this comes at an increased cost (related to installation, operation and maintenance).

- Ambient turbulence intensity is usually lower at offshore sites (Barthelmie et al., 1999, 2006, 2009; Manwell et al., 2009). This is due to lower surface roughness offshore as compared to on land (Barthelmie et al., 1999; Lange, Larsen, et al., 2004b; Manwell et al., 2009). Offshore, the turbulence generated by the turbines will likely be of higher importance than the ambient turbulence resulting from terrain surface roughness (Barthelmie et al., 2006; Frandsen & Madsen, 2003; Manwell et al., 2009).

- Ambient turbulence intensity varies differently offshore. The surface roughness is constant onshore, but the situation is different offshore (Lange, Larsen, et al., 2004b). The situation offshore can be described by three different wind speed regimes. At low wind speeds, the turbulence intensity is high, since thermal generation results in vertical mixing. When the wind speed increases to moderate wind speeds (8-12 m/s), a minimum in turbulence intensity exists. At higher wind speeds, the surface friction between air and water generates waves. The increasing wave height increases the surface roughness of the water, and so turbulence intensity increases again (Barthelmie et al., 1999, 2006, 2007; Barthelmie & Jensen, 2010). This is visualized in figure 2.13. Note that in the figure the turbulence intensity scale is stretched, and so the variation seems more extreme.

- On land the surface roughness can be taken constant. The variation of sea surface roughness with wind speed offshore can be described by the Charnock equation (Barthelmie, 1999; Lange, Larsen, et al., 2004b; Sathe, 2009):

$$z_0 = z_{Ch}\frac{u_*^2}{g} \tag{2.20}$$

  where z_0 is the roughness length, u_* is the friction velocity, g is the gravitational acceleration and z_{Ch} is the Charnock parameter (0.0144 (Wijk et al., 1990), 0.015 (Barthelmie, 1999) or 0.0185 (Lange, Larsen, et al., 2004b)).

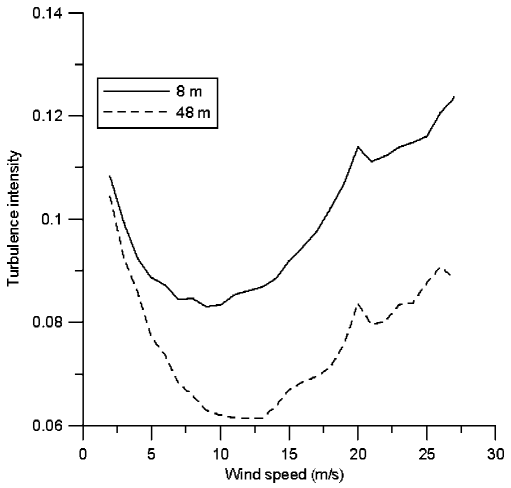

Figure 2.13: Variation of turbulence intensity with wind speed offshore (Barthelmie et al., 2005).

- Atmospheric stability is more important offshore than on land (Barthelmie et al., 2006). Since there is less turbulent mixing, the temperature differences that govern atmospheric stability will remain stronger and will have a higher impact (Barthelmie, 1999; Barthelmie et al., 2009).

- Another difference in atmospheric stability between onshore and offshore is the difference in timescales. Onshore, the land gets heated during the day, while during the night the land will cool down again. This is called a diurnal (daily) cycle. The result is that there is a larger number of unstable conditions during the day than during the night, and a larger number of stable conditions during the night than during the day (Barthelmie, 1999). The same heating and cooling occurs offshore. However, the sea has such a large heat capacity that the temperature difference of the sea between day and night is not as large as that of the land onshore (Barthelmie et al., 2005; Elliot & Cadogan, 1990; Sathe, 2009). Offshore the sea temperature will therefore vary slowly. The temperature difference between the sea and air varies on a monthly scale, rather than a daily one (Barthelmie, 1999). As mentioned earlier, stability is related to the temperature difference between the air and surface. Hence, atmospheric stability offshore will vary on a monthly scale too, rather than the daily one observed onshore. The effect occurs on a seasonal scale (Sathe, 2009). During winter the seawater cools down. When the air gets warmer again during spring, the seawater is therefore still cold. The result is that the stable and very stable conditions are most frequent during winter and spring. On the other hand, in summer and autumn the seawater has been able to heat up. As a result the unstable conditions exist more frequently (Barthelmie, 1999; Barthelmie et al., 2005; Sathe, 2009). Note that the seasonal variation of wind speed means that there also is a seasonal effect on roughness (Barthelmie et al., 1996), as the sea surface changes with wind speed.

  Offshore there is thus a seasonal cycle in temperature/stability variation, whereas onshore there is a daily and a seasonal cycle. It should be noted that the seasonal cycles onshore and offshore have the same general pattern (Barthelmie et al., 2005).

The highest wind speeds occur during winter and the lowest wind speeds occur in summer. With increasing wind speeds, neutral conditions get more frequent (Sathe, 2009).

At higher altitudes, the differences between onshore and offshore disappear. This indicates that the differences are mainly caused by changes in the surface characteristics (Barthelmie, 1999). According to (Rohatgi & Barbezier, 1999), surface friction has an influence on the lower 100-150 m of the atmosphere.

Summarizing, offshore the wind speeds are generally higher, the turbulence intensities are lower and vary with wind speed. These phenomena are all related with the surface roughness of the sea. Next to that, atmospheric stability behaves differently offshore. Its effect is stronger than onshore and varies on a monthly, rather than on a daily scale.

2.4.2 Coastal zone

In between sites that are surrounded by land (onshore) or completely at sea (offshore) there is a coastal zone. According to the European Wind Atlas this zone occurs at 10 km on either side of the coast, but also varies with climate and landscape (Troen & Petersen, 1989). The zone experiences influences from both the onshore and the offshore regimes. Next to that, the influences likely depend on the direction from which the wind is coming. It is therefore not so easy to characterize the behaviour of the atmosphere in these kinds of regions (Barthelmie, 1999; Barthelmie et al., 2005).

An example is a site that is located on sea, but close to the shore. When air flows from land to water it experiences a discontinuity (Barthelmie, 1999). It is clear that two changes occur. The first is a change in roughness, with the water having a lower roughness than the land. The second is a change in the temperature difference between surface and air, since the sea has a larger heat capacity. The temperature difference is of influence to the atmospheric stability.

As air flows from land to sea a change in surface roughness occurs. As a result of the lower surface roughness, the wind speed and energy density in the wind will increase. The biggest increase occurs in the first 3-5 km from the shore (Barthelmie et al., 1996).

The offshore variation of surface roughness with wind speed is described by the Charnock equation in the previous section. The Charnock equation only includes the effect of wind speed. For coastal zones, the fetch (the distance that the wind is blowing over the sea before it reaches the measurement location) and the wave age become important factors that influence the surface roughness as well (Lange, Johnson, et al., 2004; Lange, Larsen, et al., 2004b; Sathe, 2009). A wave age dependent model, incorporating a varying Charnock parameter, can be applied for coastal zones (Lange, Larsen, et al., 2004b).

Due to the proximity of the land to a coastal site, warm air from land can be blown to the site. The result of this is that the air at the site will vary more in temperature than what would occur at a site far offshore. Hence, the seasonal temperature variations are larger closer to the coast (Barthelmie, 1999). Next to that, for wind farms in shallow water the diurnal temperature variation might also be noticed (Barthelmie et al., 1996), while that is not the case at other offshore sites. When the wind direction is from land, in the

early afternoon the air blowing from land has been heated up already while the seawater is still cold. The surface is thus colder than the air. As a result, the number of stable and very stable conditions with higher wind speeds increases, and is highest during the early afternoon (Barthelmie et al., 1996; Barthelmie, 1999; Barthelmie et al., 2005). A true offshore fetch (over sea) has more near-neutral and unstable conditions (Barthelmie, 1999). At the end of the day the seawater has been warmed up a little bit and gradually cools down again during the night. In the beginning of the morning the seawater is still warmer than the air, which has cooled down faster during the night. The surface is then warmer than the air and unstable conditions will be present (Barthelmie et al., 2005). In coastal regions the diurnal cycles can thus be inverted from that occurring onshore, due to the difference in the temperature of the air advected from land compared to the temperature of the sea (Barthelmie et al., 1996, 2005). The higher wind speeds coming from land and the breeze coming from sea likely have an effect on this inverted diurnal cycle too (Barthelmie et al., 1999). A seasonal cycle is also still visible next to the daily one. Barthelmie et al. (1996) found that the largest diurnal cycles for Vindeby occurred in spring and summer.

According to Lange, Larsen, Højstrup, and Barthelmie (2004a) (for Rødsand) wind shear varies more with varying atmospheric stability than with varying wind speed. Since atmospheric stability varies differently in the coastal zone than onshore or far offshore, it follows that wind shear will be varying differently as well.

Due to the presence of the coast the wind speed over a wind farm might not be uniform. This can occur due to variations in stability due to the coast (Barthelmie et al., 2007), but also because the coast is closer to a certain part of the wind farm (Barthelmie et al., 1996). The result is that the wind speed gradients might not be consistent over the wind farm, both horizontally and vertically. Certain parts of the wind farm can then experience a different free-stream wind speed, or there might be an influence on the wake behaviour at certain parts of the wind farm (Barthelmie et al., 2007, 2010).

In 1999 Barthelmie concluded that 1-2 km offshore the influence of the land could still be measured. Lange, Johnson, et al. (in 2004) state that air from land influences air at sea for 100-200 km(!). In 2005 Barthelmie et al., using ten years of meteorological measurements, stated that in 0-15 km from the coast the influence of land is most important. It can still be noted at 40 km, but after 20 km no significant change in turbulence intensity can be noticed anymore.

It is clear that it is difficult to characterize a coastal zone, since it is not clear when the influence of land does not impact a site on sea anymore, or when the effects become so small that they can be ignored. As mentioned before, the European Wind Atlas (Barthelmie et al., 2009; Troen & Petersen, 1989) defines an offshore site as being located at open sea and at least 10 km from the coast. According to the mentioned research, the distance might need to be (much) larger in order not to observe effects originating from land. The distance also depends on the atmospheric stability situation, as a stable atmosphere transfers the effects from land much further (Barthelmie et al., 1999).

Currently, most offshore wind farms are located close to the coast (Barthelmie et al., 2007). This, together with the uncertainty of the influence of the coast on an offshore wind farm, indicates that one needs to take possible coastal effects into account.

Coastal zones are thus difficult to characterize, because of the different influences on

them. Even though a site may appear to be located offshore, the land might still have an influence on the atmospheric characteristics observed at the site. The stability climate will be influenced, and hence there will be an influence on the mean wind profile, turbulence intensity and possibly the wake effects within the wind farm.

2.5 Wind speed normalization

Due to the variation in air temperature, humidity and pressure the air density on a site can change. The produced power is a function of the air density. Hence, when comparing the power measurements at the different time instants a normalization has to be applied to account for the difference in ambient conditions.

According to the IEC-61400-12-1 regulations for power performance of electricity producing wind turbines ("Wind turbines – Part 12-1: Power performance measurements of electricity producing wind turbines", 2011) the air density should be corrected using the following equation:

$$\rho_{10min} = \frac{1}{T_{10min}} \left(\frac{B_{10min}}{R_0} - \phi P_w \left(\frac{1}{R_0} - \frac{1}{R_w} \right) \right) \tag{2.21}$$

where T takes into account the effect of ambient temperature, B the ambient pressure and ϕ the relative humidity. When the relative humidity is not available (which is for instance the case at North Hoyle), a value of 0.50 can be assumed. R_0 and R_w are the gas constants of dry air and water vapour respectively. P_w is the vapour pressure.

The reference air density to which the data will be normalized can be a pre-defined value, or the average of the valid measurements at the site. If the average of the valid site measurements is taken, the average shall be rounded to 0.01 kg/m^3.

The standard also states that for wind turbines with active power control (i.e. not stall turbines), such as the wind turbines at the sites under investigation here, one should normalize the wind speed and not the power. The power depends on the wind speed to the power of three. Hence, the wind speed is normalized using:

$$U_n = U_{10min} \left(\frac{\rho_{10min}}{\rho_0} \right)^{\frac{1}{3}} \tag{2.22}$$

2.6 Jensen wake model

In this study one of the most parameterized and well-known wake models is used. It is based on the model by Jensen (1983) and further developed by Katic and Højstrup (1986). The wake is assumed symmetric in both horizontal and vertical direction, and has a "top hat" vertical wind speed deficit profile instead of the "double bell" or Gaussian shape discussed in section 2.1.4. It is visualized in figure 2.14. The theory is shortly explained

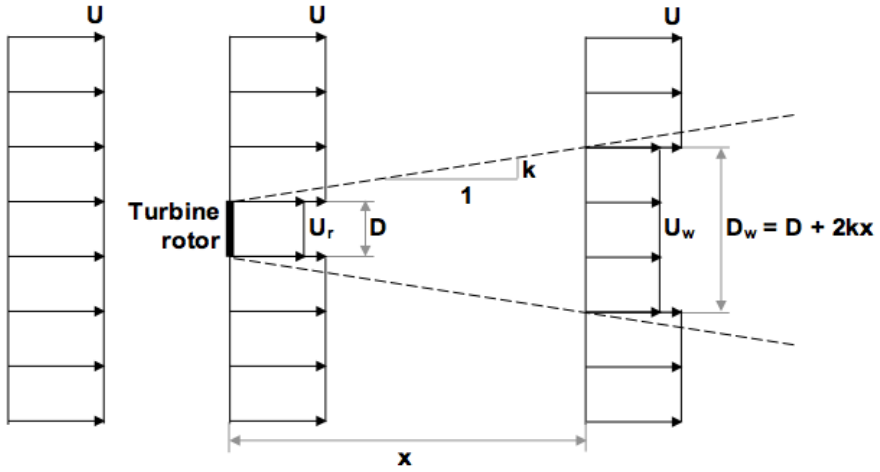

Figure 2.14: Visualization of the "top hat" wake wind speed profile applied in the model by Jensen (after Thøgersen, 2011).

here. A more detailed description, including a derivation of the equations used by the model, can be found in appendix A.

The wake diameter D_w has a linear expansion modelled with downstream distance x:

$$D_w = D + 2kx \tag{2.23}$$

where D is the rotor diameter and k is the wake decay constant (also called wake expansion factor), with suggested values 0.04-0.05 offshore and 0.075 onshore (Barthelmie et al., 2006, 2009). The wake decay constant determines the linear expansion of the wake, and depends amongst others on the ambient and wake-induced turbulence (Katic & Højstrup, 1986). Roughness is taken into account, but atmospheric stability is not (Barthelmie & Jensen, 2010), although the wake decay constant could be modified (Barthelmie et al., 2010; Katic & Højstrup, 1986).

As the wake decay constant (WDC) determines how fast the wake expands, it determines at the same time how fast the wind speed deficit recovers. It can be seen that it has some similarities with the effect that turbulence has on the wake. A higher WDC gives a larger wake expansion and therefore a higher wind speed deficit recovery, analogous to the effect of a higher turbulence intensity. In literature this relationship is described as (Thomsen & Sørensen, 1999):

$$k = \frac{A}{ln\,(z/z_0)} \tag{2.24}$$

where A is a constant of about 0.5, z is the height of interest (e.g. hub height) and z_0 is the roughness length. Turbulence intensity can be estimated by the following equation (Thomsen & Sørensen, 1999):

$$I = \frac{1}{ln\,(z/z_0)} \tag{2.25}$$

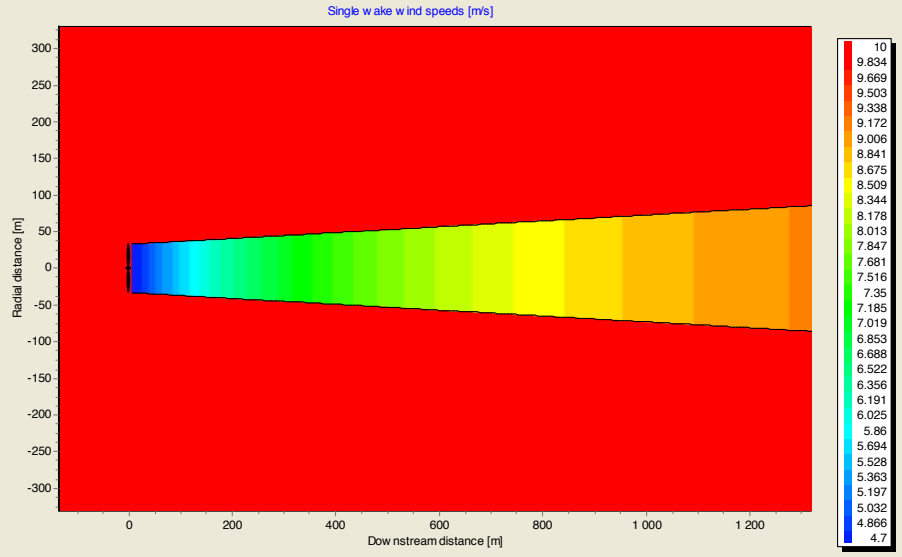

Figure 2.15: Single wake deficit according to the Jensen wake model (Thøgersen, 2011).

Hence, the wake decay constant k can be related to the turbulence intensity by (Thomsen & Sørensen, 1999):

$$k \approx 0.5I \tag{2.26}$$

With the wake shape defined, a velocity deficit can be determined:

$$U_w = U\left[1 - \left(1 - \sqrt{1 - C_T}\right)\left(\frac{D}{D + 2kx}\right)^2\right] \tag{2.27}$$

where U is the free-stream wind speed, U_w is the wind speed in the wake and C_T is the wind turbine thrust coefficient. Since the model determines the wake velocity and the wake diameter according to a linear wake expansion, the wake deficit at a certain downstream position is uniform (Katic & Højstrup, 1986). This is illustrated in figure 2.15. Other models use for instance a near-Gaussian profile instead of a uniform distribution, but these models are not discussed nor used here. For more information on models implemented in WindPRO, see for example Thøgersen (2011).

It is assumed that for interacting wakes the momentum deficits of the wakes are conserved. To determine the wake velocity $U_{w,mixed}$ at a downstream turbine resulting from $n-1$ wakes interacting at that location, the wakes are added together by taking the square root of the sum of squares of the separate velocity deficits caused by the upstream turbines (Thøgersen, 2011; Katic & Højstrup, 1986):

$$U_{w,mixed} = U - \sqrt{\sum_{i=1}^{n-1} \left(U - U_{w,i}\right)^2} \tag{2.28}$$

where $U_{w,i}$ is the wake velocity at turbine n due to turbine number i. The resulting mixed wake velocity and all the wake velocities as dictated by their corresponding turbine are determined at the same downstream location.

The simplicity of the model means that it can be executed in the order of minutes (Barthelmie et al., 2010). However, due to the same reason it is limited in its modelling.

Chapter 3

Data

In this project two types of data are compared, being data measured by a meteorological tower (metmast) on the wind farm site and data retrieved from a mesoscale model based on long-term measurements.

Metmast data is usually, as in the cases considered in this project, stored in 10-minute periods. Metmast data may however not always be available at a certain (possibly future) site. Therefore one may use mesoscale data. Mesoscale data is meteo data recreated by a computer model on a grid covering the earth using long-term meteorological measurements, most probably not on-site.

For this project the mesoscale data was obtained as hourly data from Vestas' internal mesoscale model called Vestas Siting Universe (VSU). The grid used in VSU is 3 by 3 km in the horizontal plane. The time-step of the model is in the order of a few minutes. The data is extracted at each hour as the mean over those few minutes (Zagar, 2011-2012). The data is obtained from the grid point closest to the respective metmast.

Sea surface temperature is not yet available from VSU. Therefore, the ambient temperature at 2 metres above sea surface was used instead. Air has a smaller heat capacity than the sea, resulting in a faster fluctuation of the temperature. To recreate the slow fluctuation of the sea surface temperature a running average was taken of the ambient temperature. The running average is taken backwards in time, since the sea surface temperature responds slower to temperature changes than the air. For example, at time i, the average is taken over times i, $i-1$, $i-2$, ..., depending on the length of the running average.

Mesoscale data is available from the year 2000 onwards. To give a fair comparison with the metmast data, only those (hourly) mesoscale timestamps are used that occur in the metmast data.

Figure 3.1: Locations of the offshore wind farms used in the project (*Google Earth*, 2012).

3.1 Site description

Two offshore wind farms have been investigated in this project, being Egmond aan Zee (OWEZ) in The Netherlands and North Hoyle in the United Kingdom. The locations of these wind farms are indicated in figure 3.1. General information about the wind farms is shown in table 3.1.

3.1.1 OWEZ

Offshore wind farm Egmond aan Zee (OWEZ) is located in the North Sea, close to the Dutch coast. It consists of 36 Vestas V90-3.0MW turbines. A meteorological mast (metmast) is located at the site for measurements of the atmosphere and sea, with measurements at 21, 70 and 116 metres height, where 70 m corresponds to hub height. Detailed information about the metmast can be found in Kouwenhoven (2007). The layout of the park and the location of the metmast are shown in figure 3.2.

Measurements of the metmast are available via `NoordzeeWind.nl` from 1 July 2005 to 31 December 2010, although unfortunately the sea water temperature sensor data is invalid from 30 November 2008 onwards and so the data cannot be used after that. The available sensors are as shown in Kouwenhoven (2007). Turbine data is available via the Vestas Performance and Diagnostic Centre (VPDC) database, originating from the turbine Supervisory Control And Data Acquisition system (SCADA) data. Turbine data is available from September 2006, although not all turbines are operative before the end

Table 3.1: General information regarding the offshore wind farms used in the project.

Wind farm	OWEZ	North Hoyle
Number of turbines	36	30
Turbine	Vestas V90-3.0MW	Vestas V80-2.0MW
Control type	Pitch, variable speed	Pitch, variable speed
Rotor diameter (D)	90 m	80 m
Hub height (above MSL)	70 m	70 m
Rated capacity	108 MW	60 MW
Year commissioned	2006	2003-2004
Distance to shore	About 10 km	About 7.5 km

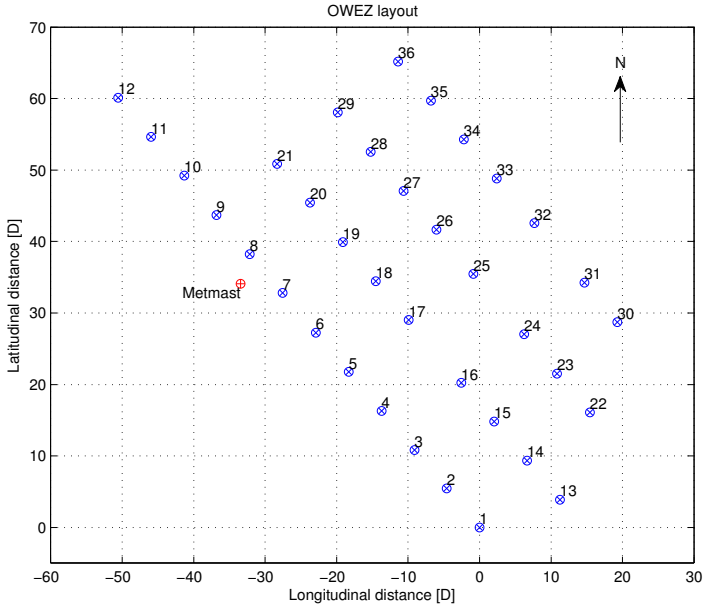

Figure 3.2: Layout of park and location of metmast at OWEZ. Numbers indicate the turbine number (North is up).

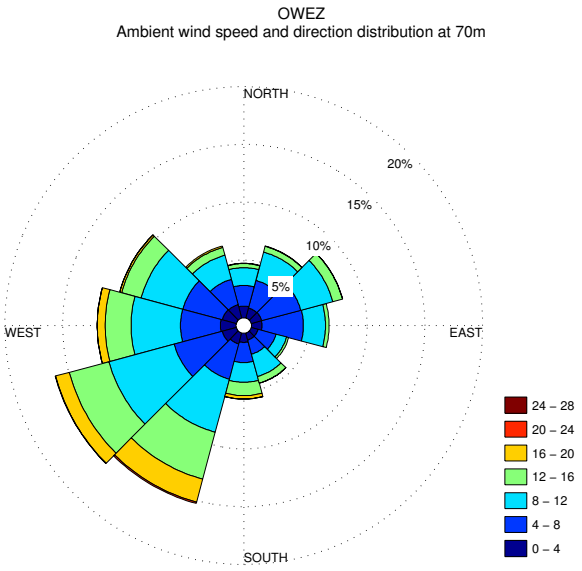

Figure 3.3: Wind rose at OWEZ. Colours indicate wind speed in m/s, while the percentages on the circles represent the frequency of occurrence. Note that part of the data in this plot is disturbed as it results from measurements where the metmast is in the wake of the wind farm. Data is taken from the metmast over the period of 1 July 2005 to 30 November 2008.

of December 2006. Both the metmast and the turbine data is averaged over 10-minute periods. It should be noted that the timestamp of the OWEZ 10-minute period is taken at the start of the measurement period, while the turbine SCADA system puts the timestamp at the end of the 10-minute period. This should be taken into account when matching the two datasets. Another thing that should be taken into account is the timezone that OWEZ is in. Some data have been stored with UTC timestamps, whereas others have been stored with timestamps corresponding to the local timezone UTC+1. Since the data is matched according to their timestamps and since some of the results are referring to times, all data has been shifted to the local timezone of the wind farm.

The wind rose over the period 1 July 2005 to 30 November 2008 is shown in figure 3.3, using the wind speed and wind direction at hub height (70 m). From the site layout it can be seen that the row direction of turbines 1 to 12 is about along the line 140° / 320°. Along the same line the distance between the turbines is about $7.1D$. The turbulence intensity versus the wind direction is shown in figure 3.4. It can be seen that when the wind direction is such that the flow passes the wind farm before hitting the metmast, a higher turbulence intensity results (as expected). Interestingly, a higher turbulence intensity also exists for flow from the West, where there is no disturbance from the wind farm. The increase in turbulence intensity might be due to the waves that result from the long sea fetch. Since it is hard to determine the boundaries of the sector that is not disturbed by the wind farm, a 10° safety offset is taken from the 140° to 320° direction, to make sure the expanding wakes of the wind turbines do not disturb the metmast measurements. The sector with undisturbed measurements that is used in the analysis then becomes 150° to 310°.

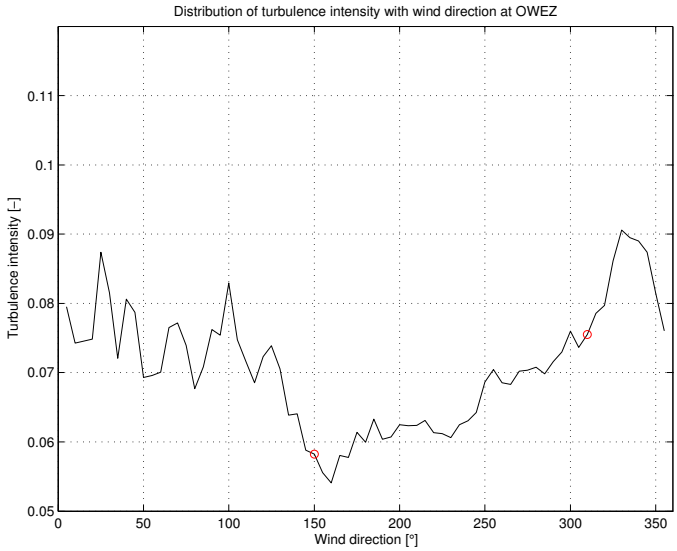

Figure 3.4: Turbulence intensity versus wind direction at OWEZ. The metmast measurements are disturbed due to the wind farm wake from 310° to 150°, as indicated in the figure by the red circles. Data is taken from the metmast over the period of 1 July 2005 to 30 November 2008.

The sea surface temperature at OWEZ is measured at 3.8 metres below sea level. Ideally one would like to measure the true sea surface temperature, but in reality this proves to be difficult when using a fixed metmast. An alternative for the metmast sea surface temperature measurement may therefore be considered for future projects, for instance a floating buoy measuring the temperature at the air-sea interface. Sathe et al. (2011) compared the sea surface temperature at OWEZ with the sea surface temperature as determined by a re-analysis obtained from the European Centre for Medium-Range Weather Forecasts (ECMWF). A similar analysis has been performed here, with different results. However, based on the fact that the sea surface temperature sensor at OWEZ is 3.8 metres below mean sea level and that the difference between the sea temperature below one metre depth and that at the sea surface can vary between -1.0 and 1.0 K (Schluessel, Emery, Grassl, & Mammen, 1990) with a mean difference in the order of tenths of degrees, it is proposed that a correction should be applied. A correction of -0.8 K is applied here to the sea surface temperature measured at OWEZ. See appendix C for a more detailed explanation.

3.1.2 North Hoyle

Offshore wind farm North Hoyle is located in the Irish Sea, about 30 km West of Liverpool. It consists of 30 Vestas V80-2.0MW turbines, located in a 6 by 5 grid of parallel rows and columns as shown in figure 3.5. The rows parallel to turbines 1-5 is about along the direction 79° / 259°, whereas the rows parallel to turbines 1-26 are about along the direction 169° / 349°. The corresponding spacing of the turbines in the rows is about $9.9D$ and $4.4D$ respectively. A metmast is located at the site, with measurements at 10, 35, 52 and 70 metres height, where 70 m corresponds to hub height.

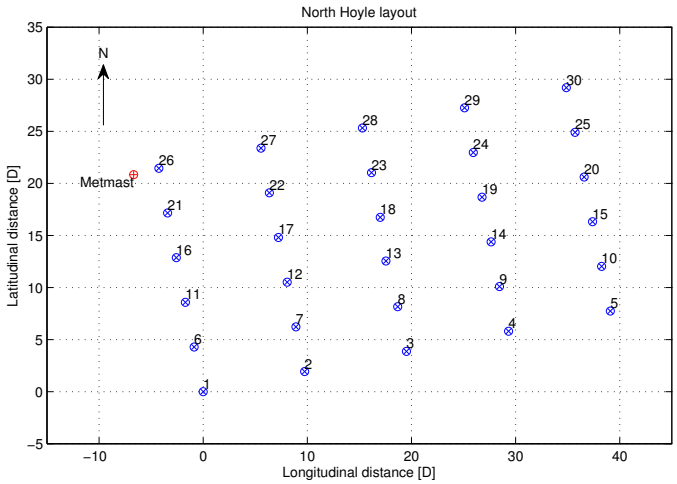

Figure 3.5: Layout of park and location of metmast at North Hoyle. Numbers indicate the turbine number (North is up).

Metmast data is available through the SCADA database, while turbine data is available through the Vestas VPDC database, also originating from the SCADA data. Both metmast and turbine data are available in 10-minute periods. The metmast data is available from 14 September 2007, while the turbine data is available from 11 June 2008. The data is extracted up to 31 December 2011. The local timezone at North Hoyle is UTC, and both metmast and turbine data have been stored corresponding to this timezone. However, in the metmast data summertime is applied, which is not applied in the turbine data. The metmast data has therefore been corrected for this.

The wind rose over the period 14 September 2007 to 31 December 2011 is shown in figure 3.6, using the measurements at 70 m. This is the period of interest as no production data is available before this date. Part of the data in this graph is disturbed due to the wake of the wind farm, and that data should not be used in the stability analysis. From the layout of the wind farm as shown in figure 3.5 it can be expected that the metmast measurements are disturbed when the wind comes from the Southeast. Figure 3.7 shows the turbulence intensity as measured by the metmast over all wind directions for the corresponding period. The turbulence intensity is significantly higher from 40° to 170° (indicated in the figure by the red circles). The metmast data between these two wind directions is therefore said to be disturbed by the wind turbines and not taken into account during the analysis.

From January 2008 to December 2009 the ambient pressure measurements at North Hoyle indicate a zero value. The ambient pressure is required to normalize the wind speed. To avoid loosing two years of data and since the ambient pressure does not vary too much, the ambient pressure value over this period is replaced by the mean value over the other measurements.

Only one wind speed sensor is present at North Hoyle at 70 m and this sensor is placed Northwest of the metmast. This means that when wind comes from the Southeast, the sensor will be disturbed. This is not a problem to the analysis, since the wind farm itself is also located on the Southeast and so these wind directions will be excluded from the

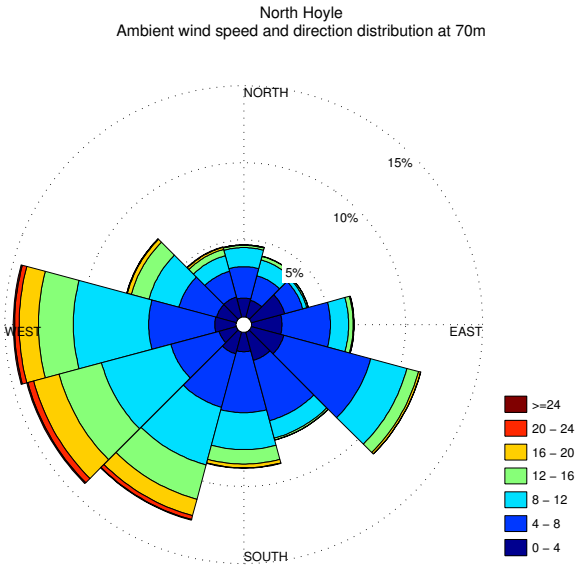

Figure 3.6: Wind rose at North Hoyle. Colours indicate wind speed in m/s, while the percentages on the circles represent the frequency of occurrence. Note that part of the data in this plot is disturbed as it results from measurements where the metmast is in the wake of the wind farm. Data is taken from the metmast over the period of 14 September 2007 to 31 December 2011.

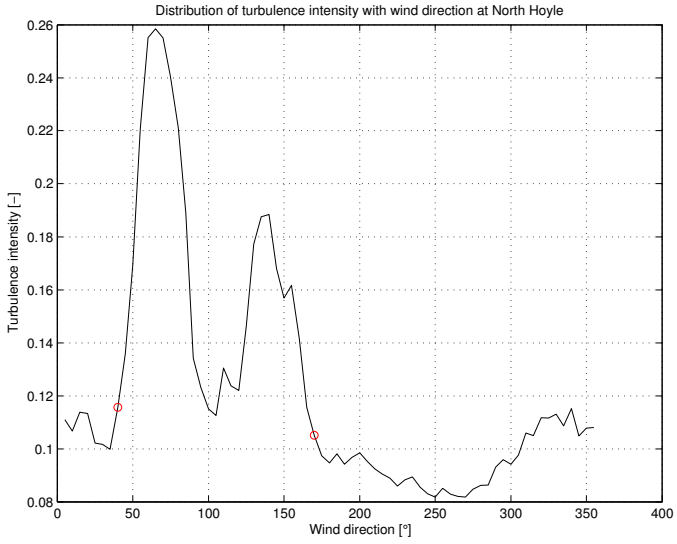

Figure 3.7: Turbulence intensity versus wind direction at North Hoyle. The metmast measurements are disturbed due to the wind farm wake from $40°$ to $170°$, as indicated in the figure by the red circles. Data is taken from the metmast over the period of 14 September 2007 to 31 December 2011.

analysis.

The sea surface temperature measurements at North Hoyle have not been corrected for a possible temperature offset, but a temperature correction might still need to be applied. For North Hoyle no information was provided about the metmast. Except from the brands and types of installed sensors and the installed heights and directions for some of these as derived from the SCADA database no information is available. It is therefore unknown whether there might be offsets due to calibration or for instance due to the (unknown) water depth of the sea surface temperature measurements. Hence, no correction of the sea surface temperature is applied. See appendix C for a more detailed explanation.

3.2 Data selection

In this section the data selection is explained. Accuracy of the sensors, the applied filters and checks and statistics of the remaining data are shown.

3.2.1 Accuracy of measurements

In section 2.2.3 it was noted that wind turbine power curves might not be accurate at all times, for instance due to the presence of wind shear over the rotor disk. However, another inaccuracy stemming from measurements can result from insufficient filtering of data or from the measurement equipment itself.

Wind turbines are usually equipped with a SCADA system. This stands for Supervisory Control And Data Acquisition system (Barthelmie et al., 2009). It measures performance related variables such as the power output, yaw direction and nacelle wind speed, but also status signals of the turbine. In this way it can be seen whether a turbine is operating normally, or if it has some problems and/or is undergoing maintenance. This is especially helpful in data processing. One can filter out all cases that do not conform to normal operation. Another possibility is to only use those time series at which certain turbines were operating (e.g. one or multiple rows, columns or the whole wind farm), or with none of the turbines being de-rated. It should be noted though that the measurement equipment itself could be inaccurate.

Lange, Larsen, et al. (2004b) estimated the calibration accuracy of the Risø P2546a cup anemometer to be about 1%, resulting in an overall uncertainty of the wind speed measurements to be about 2% and additionally 0.1 m/s. The cup anemometers used at North Hoyle have, at a wind speed of 8 m/s, an accuracy of 0.1 m/s (Vector Instruments, n.d.). Cup anemometers have the tendency to respond faster to speed up than to speed down effects. This might overestimate the true mean wind speed, and it makes the cup anemometers not suitable for turbulence measurements (Wharton & Lundquist, 2010). Lange, Larsen, et al. (2004b) note that the overspeeding effect depends on the measurement height, so that the effect might become small. SODAR might be an alternative to cup anemometers, but measurements can be noisy and profiles are often distorted. Its sampling variability introduces an additional statistical uncertainty. Measured wind speed and turbulence intensity can therefore show fundamental differences between measurements made with cup anemometers and SODAR (Wharton & Lundquist, 2010).

Lange, Larsen, et al. (2004b) also state that the inaccuracy of the Risø Aa 3590 wind vane they use is likely to come from the adjustment of the orientation of the wind vane, and not from the instrument itself. The result is an accuracy of about 5 degrees.

Temperature measurements required to determine the atmospheric stability can be inaccurate too. Those used at OWEZ have an accuracy of $\pm 0.1°C$ (Sathe et al., 2011). The temperature sensors at North Hoyle have, in the applicable operating range, an accuracy of $\pm 0.1°C$ too (Campbell Scientific, 1999). Barthelmie et al. (2009) note that temperature measurements are often not accurate enough. This is for instance the case for purposes of wake recovery prediction, which depends primarily on turbulence, and so on atmospheric stability.

The height of the measurements matters as well. The sea surface temperature is required for determining the stability condition. However, temperature measurements might not be available at the sea surface. Motta et al. (2005) say that ideally the sea surface temperature should be measured by remote sensing (e.g. satellites), but that this is not so common. They state that often the measured sea "surface" temperature does not represent the actual surface temperature of the sea, but one at the top layer of the sea. At OWEZ for instance, no mean sea surface temperature is available. The seawater temperature is measured 3.8 metres below the mean sea level. This temperature is used to represent the sea surface temperature (Sathe et al., 2011).

The sea and air temperature are usually measured separately. When they are not calibrated together, this can lead to large errors when calculating the difference between them. The difference between the air temperatures at two different heights is thought to be more accurate, as it can be measured directly using one sensor. Hence, in that case it should be more representative in determining the stability condition of the atmosphere (Motta et al., 2005).

The instruments mentioned can be installed at special meteorological towers (metmasts), or at the turbine itself. The wind speed and wind direction at a turbine are measured at the nacelle. These might therefore be influenced by the wake resulting from the wind turbine's rotor. In regard of the inaccuracies connected to these measurements, it can be assumed that the measurements of rotor power and rotor rotational speed are exact (Veldkamp, 2011-2012).

3.2.2 Filters and checks applied to data

Ideally, measurement data is available at all time periods for all sensors. However, at some periods some sensors might be unavailable or show incorrect values (e.g. due to freezing of sensors or calibration errors). Incorrect or missing values are indicated in the metmast and turbine data by an error code, and hence can be recognized and discarded. The values are also checked to be in a certain validity range (i.e. a negative wind speed naturally does not make sense, neither does an extremely high temperature). Filters are applied to make sure the metmast and turbine data that is used does not contain any of these values. For the metmast, the applied validity ranges are as shown in table 3.2, while table 3.3 shows similar information for the turbines.

When analysing the data for a certain 10-minute period all required signals should be available. This means that in case one of the required signals is missing due to an

Table 3.2: Parameters to which filters are applied, with their corresponding validity ranges, as applied to the metmast data.

Parameter	Minimum	Maximum
Wind speed	0.1 m/s	80 m/s
Wind direction	0°	360°
Ambient temperature	$-50°C$	$80°C$
Ambient pressure[a]	950 mbar	1050 mbar
Sea water temperature	$-50°C$	$80°C$

[a] At North Hoyle about 2 years of data has an erroneous pressure of 0 mbar. To avoid excluding this large amount of data from the analysis the ambient pressure of these 10-minute periods is set equal to the average of the other 10-minute periods.

Table 3.3: Parameters to which filters are applied, with their corresponding validity ranges, and other checks, as applied to the turbine data.

Parameter	Minimum	Maximum
Wind speed	0.1 m/s	80 m/s
Wind direction[a]	0°	360°
Ambient temperature	$-50°C$	$80°C$
Power output	0.1 kW	6000 kW
Check if turbine was running the full 10-minute period		
Check if generator was running the full 10-minute period		
Check if no alarm was on		
Check if no servicing was going on		
Check if turbine is not de-rated (e.g. due to wind sector management)		
Check if turbine does not produce 10 kW or more under its expected value		

[a] At OWEZ the wind direction indicated in SCADA does not correspond to that of the metmast, and is known to be incorrect, or is missing completely for some turbines. Therefore this filter has not been applied for the OWEZ turbines.

Table 3.4: Percentage of data remaining for the different wind farms, including how much data remains after each step in the filtering process.

Step	OWEZ	North Hoyle
After discarding erroneous data[a]	54.5%	59.9%
∟ Of this, not disturbed by wakes	76.1%	68.9%
∟ Of this, not discarded in stability analysis	96.0%	93.4%
∟ Of this, with corresponding turbine data[b]	53.1% (96.0%)	71.7% (85.0%)
Filtered data remaining [%]	38.8%	45.9%
Filtered data remaining [10-min measurements]	26865 cases	62206 cases

[a] The values in the first line of the table indicate how much of the 10-minute period measurements can actually be used in the analysis. This value is regarded as the 100% value in the analysis, as only this data is without errors and has passed the filters.

[b] The first value reflects the amount of metmast data that can be used from the still available filtered data and has corresponding turbine data. The second value reflects the same, but taking into account the period for which turbine data is available only, since the metmast data covers a longer period.

incorrect or error value, the whole 10-minute period has to be discarded. This has the unfortunate effect that a lot of 10-minute periods can be lost due to an invalid value of just one sensor, while all the other sensors might be working completely fine. One should therefore take care to only filter the signals of those sensors that are required for the analysis.

3.2.3 Statistics of filtered data

The percentages of data remaining after applying the filters and after the steps in the analysis where data is discarded are as shown in table 3.4.

First the erroneous data is discarded, by applying the filters as shown in table 3.2. The values in the first line of the table indicate how much of the 10-minute period measurements can actually be used in the analysis. This value is regarded as the 100% value in the analysis, as only this data is without errors and has passed the filters.

Once the data has been filtered, the next step is to see what data is possibly disturbed by the wake of the wind farm, or because the sensors might be in the wake of the metmast. Next, the remaining data is analysed further and a stability analysis is performed on it. From equation 2.19 it can be seen that only for Richardson numbers up to 0.2 a Monin-Obukhov length can be found. Therefore, a small part of the data has to be discarded here, since the theory is not valid for these measurements. The remaining data is compared to the production data of the turbines. Only those timestamps that occur in both the metmast and the turbine data are maintained. The percentages indicate the percentages of data that passed each step, where the percentage is taken as the number of 10-minute periods remaining with respect to those remaining in the previous step.

The percentage and number of 10-minute measurements remaining to determine the wake losses is shown in the last part of the table. The percentage indicates the amount of data remaining with respect to the amount of data that was initially imported and had no errors in them.

Chapter 4

Results

In this chapter the results for the atmospheric stability distributions, wake losses and wind farm efficiency are shown and discussed.

4.1 Atmospheric stability

Metmast data and mesoscale data are two sources of meteorological data which can be used to classify the atmospheric stability. Metmast data is measured on-site by a meteorological tower (metmast) and usually (as in the cases considered in this project) stored in 10-minute periods. Mesoscale data on the other hand is created by a computer model on a grid covering the earth using long-term meteorological measurements, most probably not on-site. For this project the mesoscale data was obtained as hourly data from VSU, from the grid point closest to the respective metmast. See chapter 3 for more information.

The atmospheric stability classification used in this study is the one used by Barthelmie (1999); Barthelmie et al. (2005); Motta et al. (2005); Sathe and Bierbooms (2007); Sathe (2009); Wijk et al. (1990) as shown in the left column in table 2.1, and shown again here in table 4.1. This is the most common distribution found in literature. Another classification was tried as well, being the 7-bin classification by (Sathe, 2009; Sathe et al., 2011), but to have more data per bin this method was discarded. Verification of the results obtained by the bulk method as implemented in the analysis is done in appendix D.

4.1.1 OWEZ

The stability distribution at OWEZ is shown in figures 4.1a. It can be seen that there are more (very) unstable cases than (very) stable cases. The distribution versus hub height wind speed is shown in figure 4.1b. From the figure it can be seen that at low wind speeds the very (un)stable cases are most common, while for increasing wind speeds the neutral and stable cases occur more often and the amount of very (un)stable cases decreases.

Table 4.1: Monin-Obukhov length L [m] boundaries for stability classes as used in the analysis

Stability class	Boundaries
Very stable	$0 < L < 200$
Stable	$200 < L < 1000$
Neutral	$\|L\| > 1000$
Unstable	$-1000 < L < -200$
Very unstable	$-200 < L < 0$

Wind speeds above 20 m/s have been excluded due to low data availability (i.e. less than 0.1% of total amount of data per bin). The results are similar to those observed at OWEZ in Sathe et al. (2011).

Figure 4.1c shows the distribution with wind direction (where the wind directions where the metmast is in the wake of the wind farm have been excluded). It can be seen that there is a lower amount of very unstable cases present for wind directions of about 200° to 245°, which corresponds to the wind direction coming from the English Channel and hence corresponds to a long sea fetch. The long sea fetch might result in higher wind speeds and the higher amount of neutral cases. Furthermore it can be seen that the amount of very stable cases is higher for winds coming from the South compared to winds coming from the Northwest. A similar, but reverse effect can be seen on the very unstable cases, for which a higher amount is present for winds coming from the Northwest than for winds coming from the South, although the higher wind speeds corresponding to the wind direction coming from the English Channel reduce the occurrence of instability. The observation that more very stable cases occur for winds from the South (warm air) and more very unstable cases occur for winds from the Northwest (cold air) corresponds to the theory that when the air is colder (/warmer) than the sea more very unstable (/very stable) conditions occur. The results are similar to those observed at OWEZ in Sathe et al. (2011).

The variation of atmospheric stability with time is shown in figure 4.2 on a monthly and on a hourly scale. Even though each month has a significant amount of data, the monthly distribution is not as smooth as expected. Theoretically the thermal inertia effect of the sea is such that during summer and autumn there are more (very) unstable cases, while during winter and spring there are more (very) stable cases. Looking at the figure, it can be seen that this can be observed, although some months (January, August and December) seem to agree less with the months surrounding them. No clear explanation can be given for this.

The hourly distribution of atmospheric stability, shown in figure 4.2b, shows a smoother variation. The effect of the heat capacity of the sea on the atmospheric stability can clearly be observed. During the night and early morning the air cools while the water is still warm, resulting in a higher percentage (very) unstable cases. During the afternoon and early evening the air has warmed more than the sea water, which results in a higher amount of (very) stable cases. Plotting the hourly variation of atmospheric stability per season, as shown in figure 4.3, the differences between each season become visible. During autumn it is clear that the sea has a large thermal inertia. The sea is still warm after

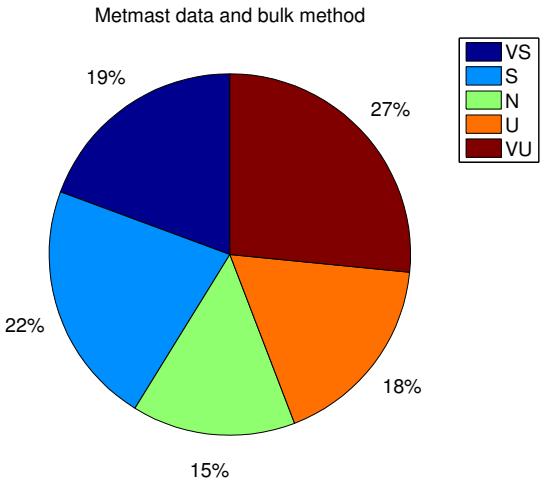

(a) In percentage

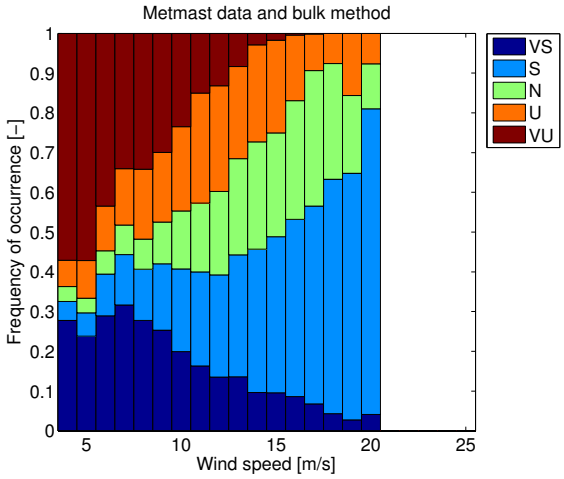

(b) Versus wind speed

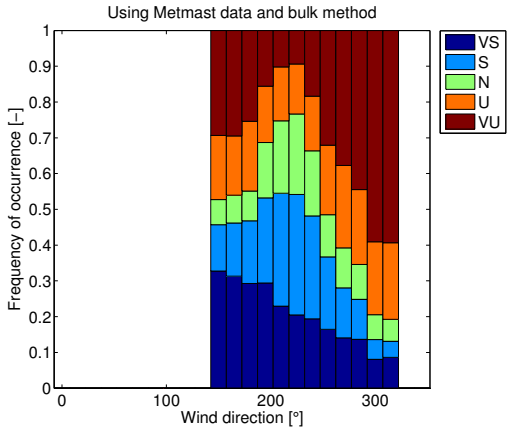

(c) Versus wind direction

Figure 4.1: Distribution of stability classes at OWEZ, using metmast data. VS = very stable, S = stable, N = neutral, U = unstable, VU = very unstable. Data is taken over the period from 1 July 2005 to 30 November 2008. Wind directions $310°$ to $150°$ are excluded.

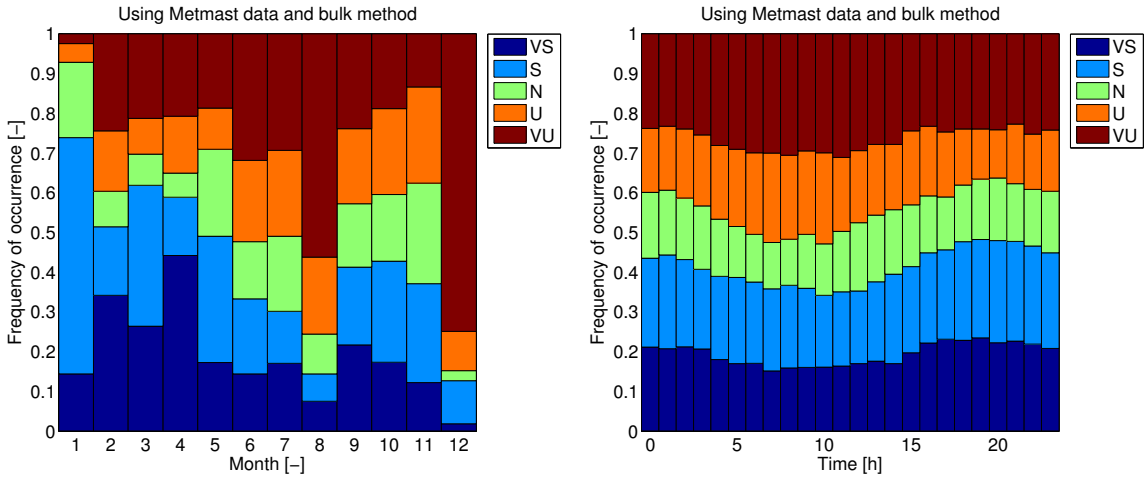

(a) Monthly (b) Hourly

Figure 4.2: Monthly and hourly distribution of stability classes at OWEZ, using metmast data. VS = very stable, S = stable, N = neutral, U = unstable, VU = very unstable. Data is taken over the period from 1 July 2005 to 30 November 2008. Wind directions 310° to 150° are excluded.

summer and because of the large heat capacity it does not cool down so much during the night. However, the air has a much smaller heat capacity and hence cools down more during the night (see the variation of the air and sea surface temperature in figure 4.4). This results in a more unstable atmosphere in the night/early morning. The same effect can be observed during the other seasons. Other observations that can be made are the higher amount of (very) unstable cases during summer and autumn, corresponding to a larger temperature difference between the air and sea surface (the sea surface is warmer), while there is a higher amount of (very) stable cases during winter and spring.

In appendix E.4 it is found that the temperature gradient between air and sea surface causes the largest errors in the atmospheric stability measurement. Next to that it also causes the errors that are on average the worst (i.e. the stability lies away the furthest from where it is supposed to be). Therefore an analysis is performed to see the sensitivity of the atmospheric stability to the size of the temperature gradient in appendix F. From the analysis it can be understood that a small measurement error or offset in one of the temperatures can have a significant impact on the atmospheric stability found from the measurements.

A distribution of atmospheric stability similar to those shown in figures 4.1a and 4.1b can be made using mesoscale data. The results are shown in figure 4.6. Note that (as mentioned in chapter 3) no mesoscale sea surface temperature is available from VSU. Instead, the air temperature at 2 m is used and a backwards running average is taken of this data to recreate the slow variation of the sea surface temperature. For OWEZ, the running average is taken over 144h (i.e. 6 days), as this is found to give the closest correspondence to the metmast stability distribution.

The stability distribution for the mesocale data with only those hourly timestamps that also occur in the metmast data is shown in figure 4.5. The results are close to that obtained

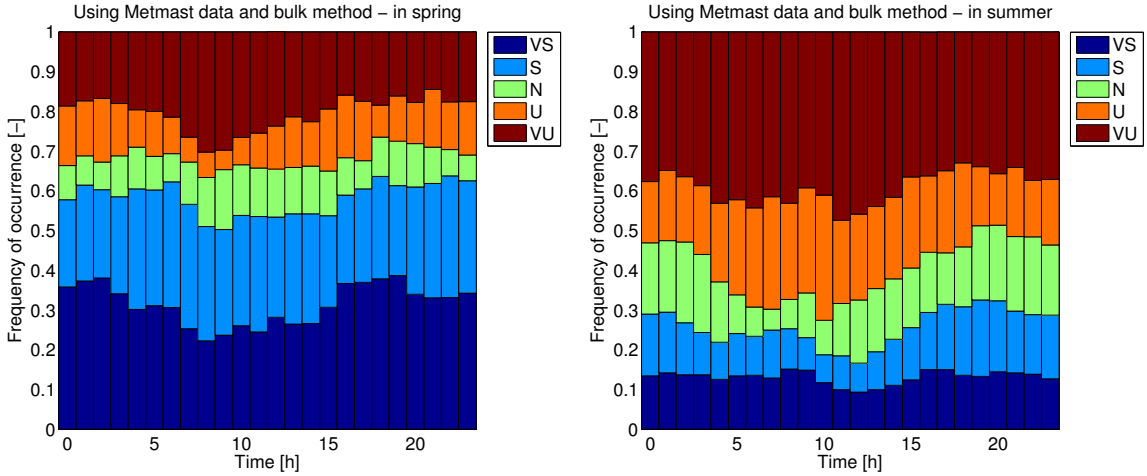

(a) Spring

(b) Summer

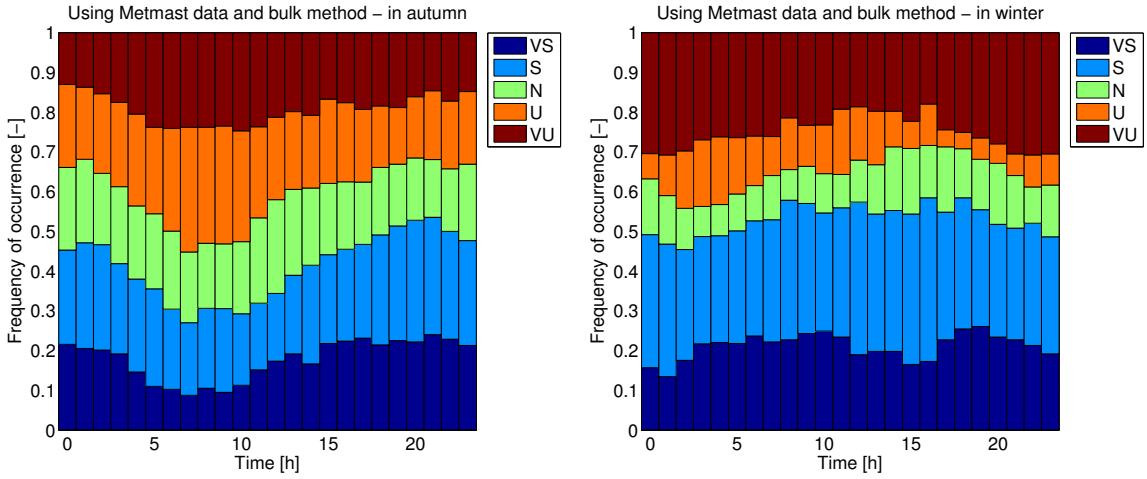

(c) Autumn

(d) Winter

Figure 4.3: Hourly distribution of stability classes per season at OWEZ, using metmast data. VS = very stable, S = stable, N = neutral, U = unstable, VU = very unstable. Data is taken over the period from 1 July 2005 to 30 November 2008. Wind directions $310°$ to $150°$ are excluded.

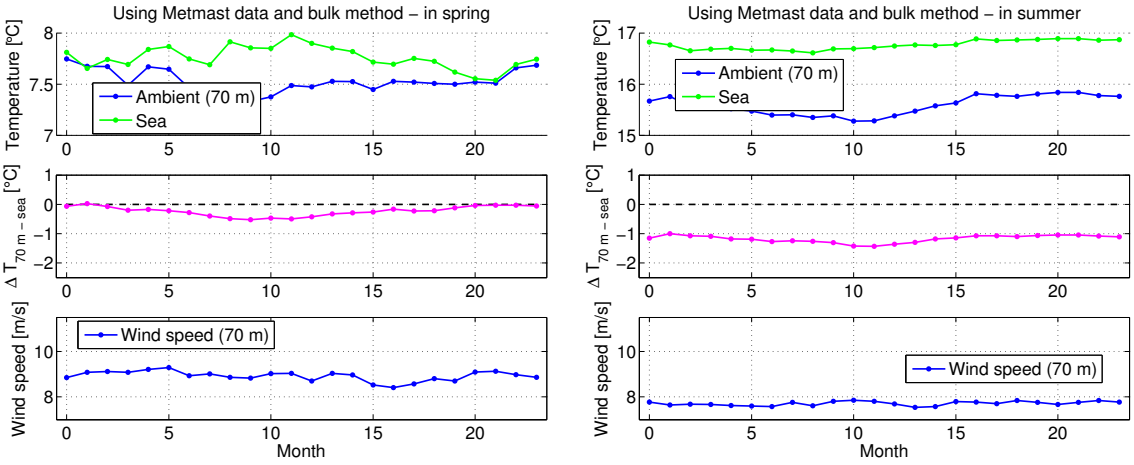

(a) Spring

(b) Summer

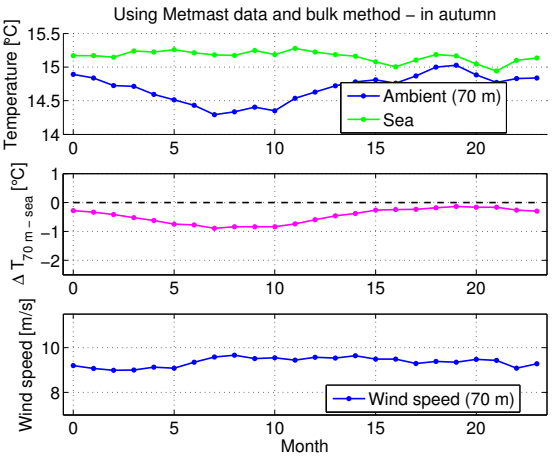

(c) Autumn

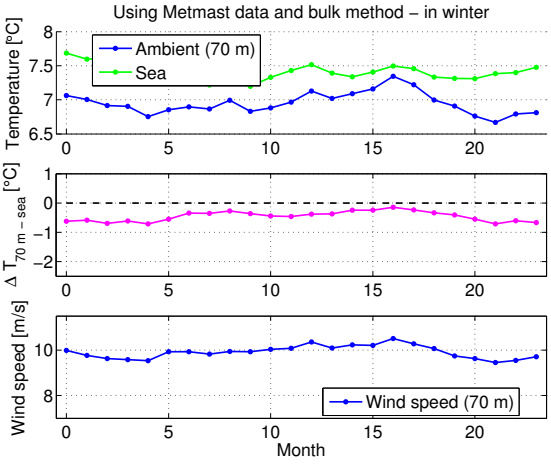

(d) Winter

Figure 4.4: Temperature and wind speed variation per season at OWEZ, using metmast data. VS = very stable, S = stable, N = neutral, U = unstable, VU = very unstable. Data is taken over the period from 1 July 2005 to 30 November 2008. Wind directions $310°$ to $150°$ are excluded.

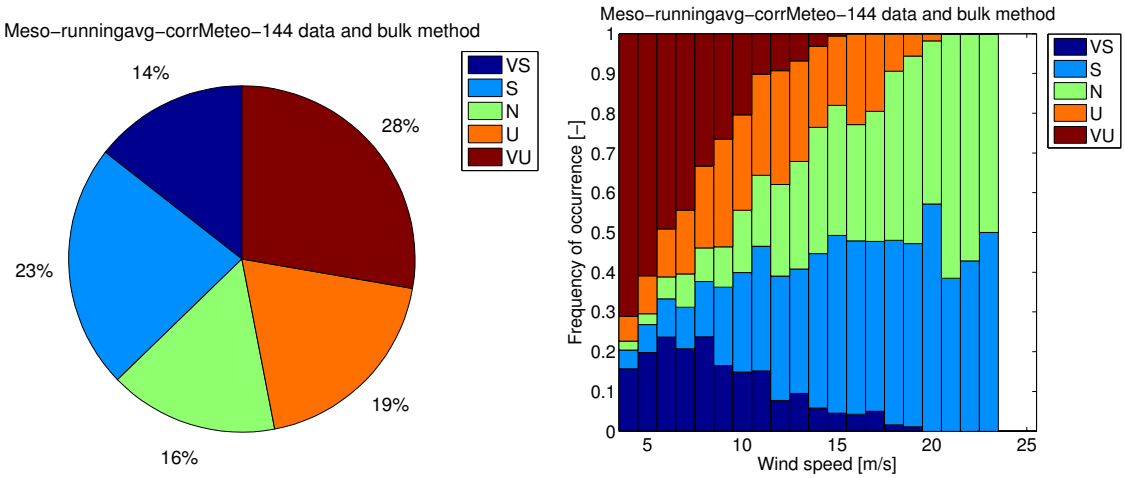

(a) In percentage

(b) Versus wind speed

Figure 4.5: Distribution of stability classes at OWEZ, only using hourly mesoscale timestamps also occurring in the metmast data. VS = very stable, S = stable, N = neutral, U = unstable, VU = very unstable. Data is taken over the period from 1 July 2005 to 30 November 2008. Wind directions 310° to 150° are excluded.

by the metmast (compare with figure 4.1). The very stable bin is 5% off, while all other bins are only 1% off. The distribution of stability versus wind speed looks similar to that of the metmast as well. Hence, when looking at similar timestamps the two datasets seem to have similar properties according to the statistics. When using all hourly mesoscale timestamps, as shown in figure 4.6, a change in the mesoscale stability distribution can be seen. It might be assumed that if metmast data would have been available over the complete measurement period the stability distribution would be similar to the one shown by the mesoscale data in figure 4.6.

The variation with atmospheric stability for various parameters is shown in figure 4.7. It can be seen that the temperature gradient (figure 4.7a) is clearly different for the various stability classes. As expected the (very) unstable classes have a negative temperature gradient (the sea surface temperature is larger than the ambient temperature), whereas the (very) stable classes correspond to a positive gradient. The neutral bin also has a negative gradient. The wind speed gradient (figure 4.7b) on the other hand does not show so much variation for the various stability bins. Larger wind speed gradients correspond to the near-neutral bins (neutral, stable and unstable), as expected. The smaller wind speed gradients correspond to the very stable and very unstable classes. Note that since the wind speed gradient is taken between hub height and sea surface, and since the wind speed at sea surface is zero, the plot actually just shows the hub height wind speed. It should also be noted that it is the combined effect of wind speed gradient, ambient temperature and temperature gradient that influences the atmospheric stability. It is therefore possible that the parameters vary with wind direction within one stability class. For instance an increase in temperature gradient (e.g. for the very stable class for winds coming from the South) can also have an increase in wind speed gradient, still resulting in the same stability class. Figure 4.7c shows the turbulence intensity variation. As expected the turbulence intensity is the largest in the very unstable case and the smallest in the

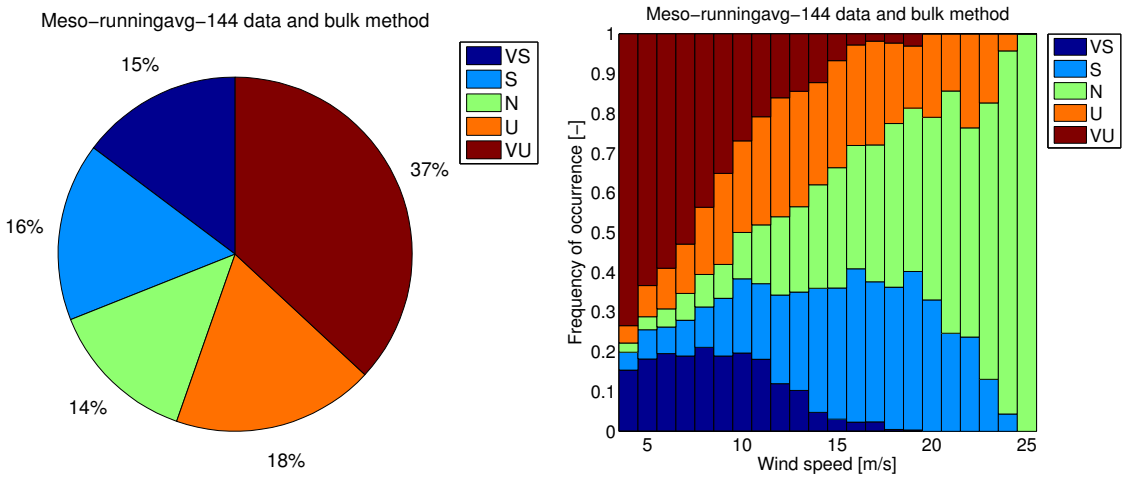

(a) In percentage

(b) Versus wind speed

Figure 4.6: Distribution of stability classes at OWEZ, using all hourly mesoscale timestamps in the data period. VS = very stable, S = stable, N = neutral, U = unstable, VU = very unstable. Data is taken over the period from 1 July 2005 to 30 November 2008. Wind directions 310° to 150° are excluded.

very stable case. The near-neutral classes all show a turbulence intensity in between these two and are close together. The variation in turbulence intensity suggests that there will be a difference in wake losses in the wind farm between the very stable, near-neutral and very unstable classes.

4.1.2 North Hoyle

The stability distribution at North Hoyle is shown in figure 4.8a. From the figure it can be seen that there is a large number of (very) stable cases occurring compared to the number of (very) unstable cases. The distribution of stability versus hub height wind speed, shown in figure 4.8b, shows that the very unstable cases occur mostly at low and medium wind speeds (up to about 16 m/s). With increasing wind speed the number of very (un)stable cases decreases and the number of neutral, stable and unstable cases increases. For the highest wind speeds only the number of neutral cases increases while the number of stable and unstable cases decreases. This is as expected. Comparing to the results from OWEZ (figure 4.1), it can be seen that at North Hoyle a larger number of very stable cases exists and that these occur up to higher wind speeds. It can also be seen that North Hoyle has a larger number of (very) unstable cases than OWEZ, which should be beneficial for the power production at North Hoyle.

The distribution of atmospheric stability with wind direction at North Hoyle is shown in figure 4.8c. The wind directions for which the metmast is in the wake of the wind farm have been excluded. From the plot it can be seen that there is a clear variation of the stability with wind direction. For winds coming from the North, the number of very unstable cases increases significantly, which can be explained by the cold air corresponding to winds coming from the North whereas the high heat capacity of the sea prevents the sea

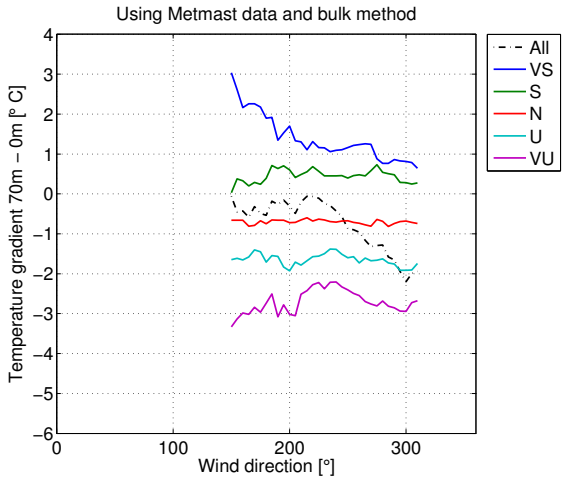

(a) Temperature gradient

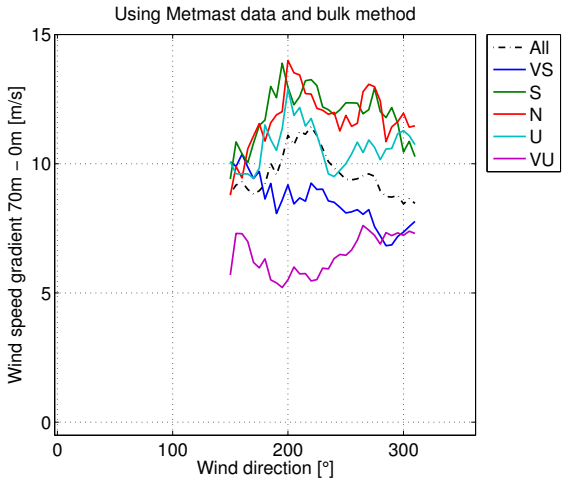

(b) Wind speed gradient

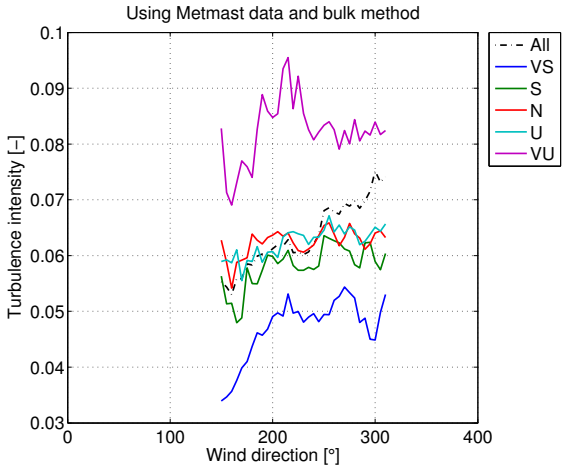

(c) Turbulence intensity

Figure 4.7: Sensitivity of atmospheric stability for various input parameters at OWEZ over the investigated wind directions. VS = very stable, S = stable, N = neutral, U = unstable, VU = very unstable. Data is taken from 1 July 2005 to 30 November 2008.

surface temperature from showing large fluctuations in temperature with wind direction. For winds from the South the opposite effect can be observed: a larger number of very stable cases occurs for these wind directions. It should be noted that North Hoyle is surrounded by land more closely and on more sides than OWEZ, and no similar long sea fetches occur at North Hoyle. A simultaneous significant decrease of very unstable cases and increase of (near-)neutral cases at a certain wind direction as is visible at OWEZ is therefore not visible at North Hoyle.

The monthly distribution of atmospheric stability at North Hoyle, shown in figure 4.9a, indicates that there is a clear difference between the winter and spring months compared to the summer and autumn months. The winter and spring months have a higher occurrence of (very) stable conditions, whereas the summer and autumn months show a higher occurrence of (very) unstable cases. This is the same as at OWEZ and according to theory.

The distribution of atmospheric stability per hour is shown in figure 4.9b. It is very similar to the distribution at OWEZ, although the variation of very (un)stable cases seems to be a bit larger at North Hoyle. This might be caused by the closer proximity of the land surrounding the waters where North Hoyle is located and since the land is surrounding the wind farm on more sides than at OWEZ. The daily cycle of atmospheric stability is larger on land than on sea, and hence the hourly distribution at North Hoyle might be influenced by this when the wind is coming from land. When looking at the daily variation per season (see figure 4.10) it can be seen that the differences per season are much larger than what was visible at OWEZ. As at OWEZ, during winter and spring there is a high amount of (very) stable cases, whereas there is a high amount of (very) unstable cases during summer and autumn. The variation of stability is larger during spring and summer, while it is less pronounced during autumn and winter. This is related to the variation of the difference in temperature between the air and sea surface shown in figure 4.11. The daily and seasonal variation of stability are according to theory.

A distribution of atmospheric stability similar to those shown in figures 4.8a and 4.8b can be made using mesoscale data as well. The results are shown in figure 4.13. Note that (as mentioned in chapter 3) no sea surface temperature is available from VSU. Instead the air temperature at 2 m is used and a backwards running average is taken of this data to recreate the slow variation of the sea surface temperature. For North Hoyle, the running average is taken over 144h (i.e. 6 days), as this is found to give the closest correspondence to the metmast stability distribution. This is the same as at OWEZ.

The metmast stability distribution in figure 4.8 can be compared with that of the mesoscale data using only the time stamps that also occur in the metmast data in figure 4.12. It can be seen that the results are mostly a few percent off at each bin compared to the results of the metmast data although the very unstable case is off the most by 8%. When all mesoscale data timestamps are used as shown in figure 4.13 the comparison with the metmast data is slightly better. In both cases the distribution of stability with the wind speed looks similar. As at OWEZ, the metmast and mesoscale datasets seem to have similar properties regarding atmospheric stability. This is positive, considering that the metmast consists of measurements of the atmosphere whereas the mesoscale data results from a meteorological model which is supposed to approximate the atmospheric conditions using different measurements.

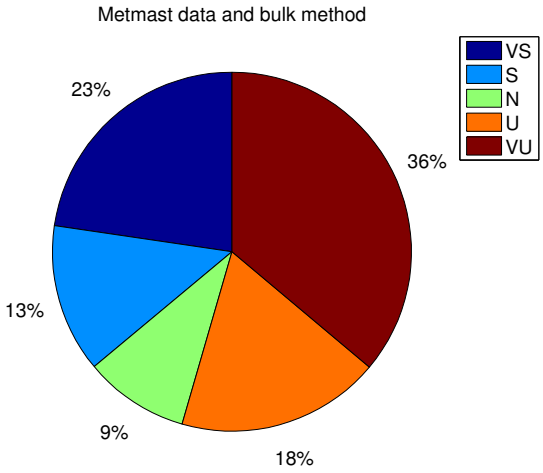

(a) In percentage

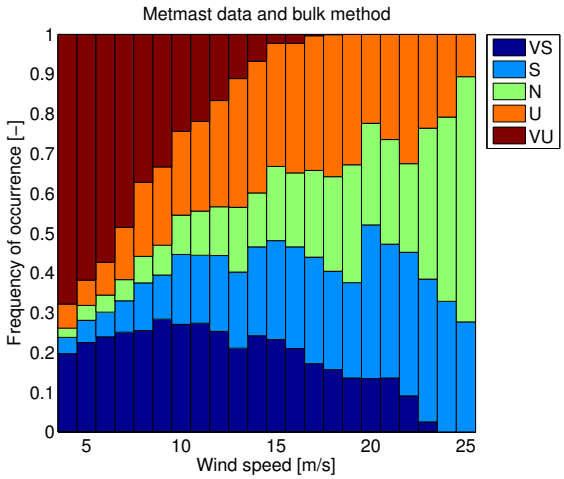

(b) Versus wind speed

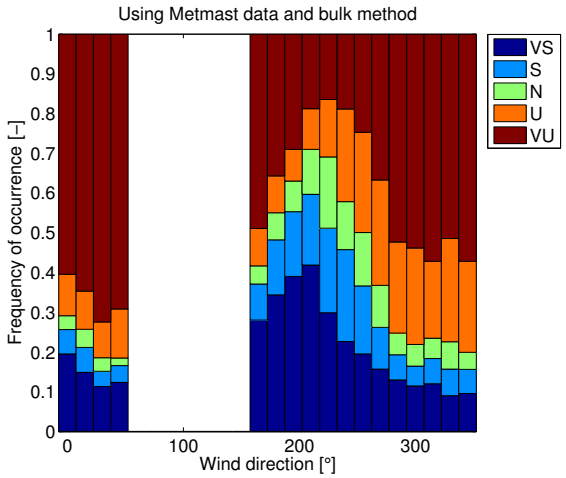

(c) Versus wind direction

Figure 4.8: Distribution of stability classes at North Hoyle, using metmast data. VS = very stable, S = stable, N = neutral, U = unstable, VU = very unstable. Data is taken over the period from 14 September 2007 to 31 December 2011. Wind directions $40°$ to $170°$ are excluded.

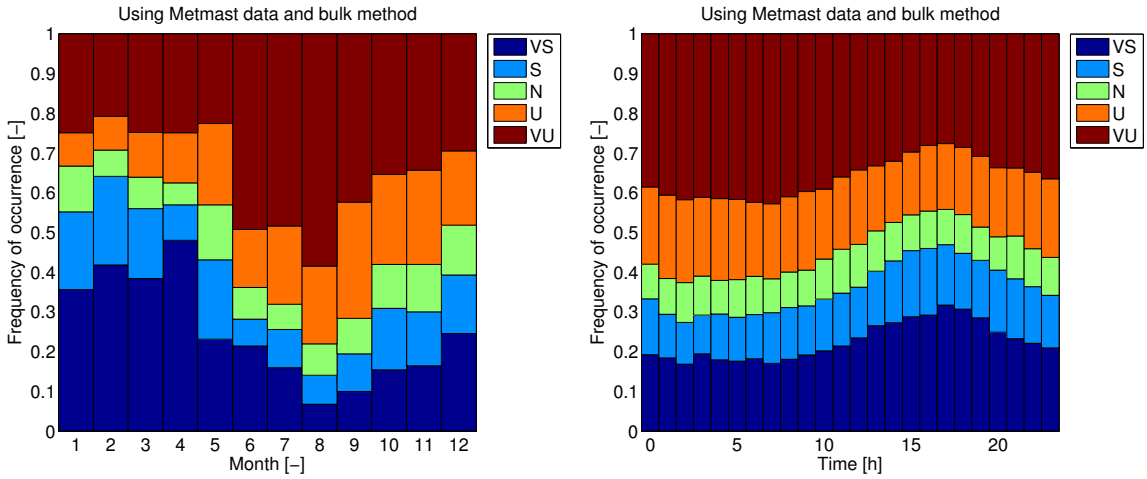

(a) Monthly (b) Hourly

Figure 4.9: Monthly and hourly distribution of stability classes at North Hoyle, using metmast data. VS = very stable, S = stable, N = neutral, U = unstable, VU = very unstable. Data is taken over the period from 14 September 2007 to 31 December 2011. Wind directions 40° to 170° are excluded.

Similarly as for OWEZ, the variation of various parameters with atmospheric stability is shown in figure 4.14. Figure 4.14a shows the temperature gradient variation. As at OWEZ, the temperature gradient increases (from negative to positive) when going from very unstable to very stable classes. The wind speed gradients for the near-neutral classes are similar to each other, as is the case at OWEZ. The very stable class and (in a more significant amount) the very unstable classes have smaller wind speed gradients. The turbulence intensity is largest for the very unstable class and it is smaller for the near-neutral classes. This is as expected. The very stable class partially has a similar turbulence intensity as the near-neutral classes and partially has a turbulence intensity which is higher than that of the near-neutral classes. This is against what is expected. An explanation might be that there is a certain offset in one or more of the measurements and that the calculated atmospheric stability therefore does not exactly match the real one that occurred when the measurements were taken. Another explanation might be that the turbulence intensity only shows the turbulence that is present in the horizontal direction as measured by the cup anemometer, whereas temperature differences create turbulence in the vertical direction as well. The turbulence intensity plot thus does not show all turbulence effects that influence the wake losses. However, like at OWEZ, the turbulence intensity plot does suggest that there will be differences in wake losses and thus in power output of the wind farm between the stability classes.

Appendix E investigates what happens when the mesoscale data is adapted by comparing it to the metmast data. When the mesoscale wind speed, ambient temperature and sea surface temperature are adapted using the explained method, the stability distribution becomes closer to that using the metmast data. The stability distribution using the adapted mesoscale data is shown in figure E.6.

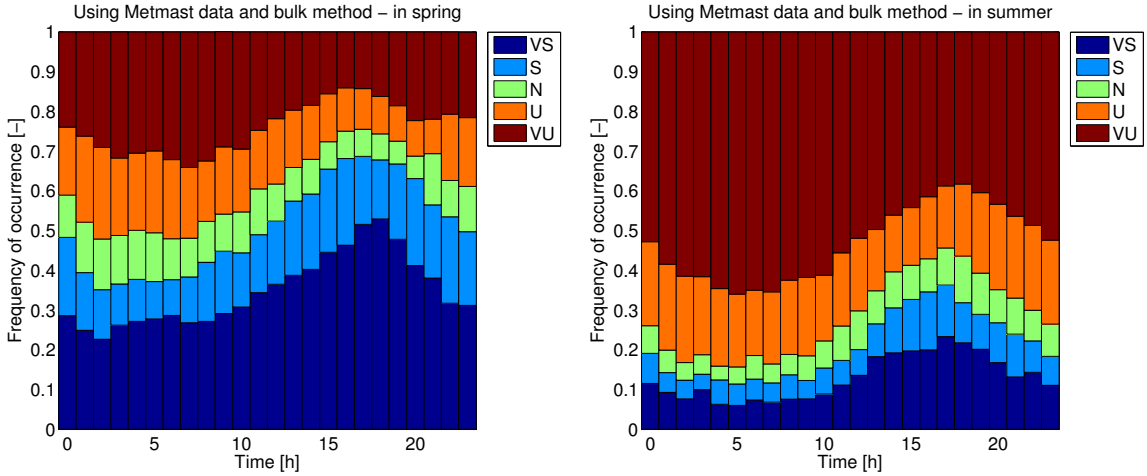

(a) Spring

(b) Summer

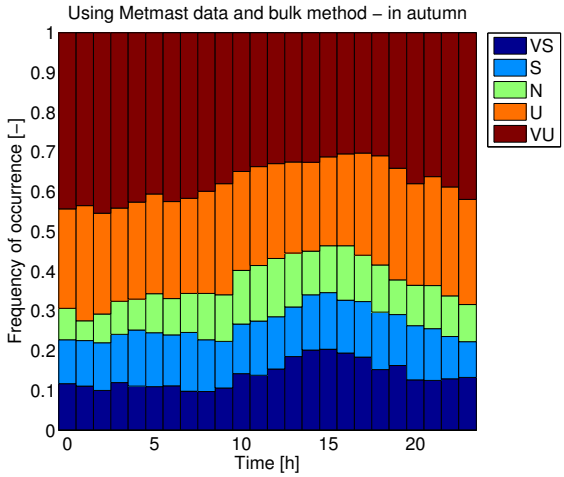

(c) Autumn

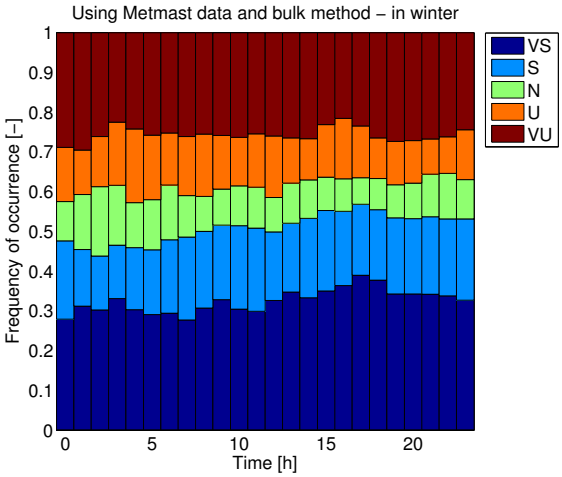

(d) Winter

Figure 4.10: Hourly distribution of stability classes per season at North Hoyle, using metmast data. VS = very stable, S = stable, N = neutral, U = unstable, VU = very unstable. Data is taken over the period from 14 September 2007 to 31 December 2011. Wind directions $40°$ to $170°$ are excluded.

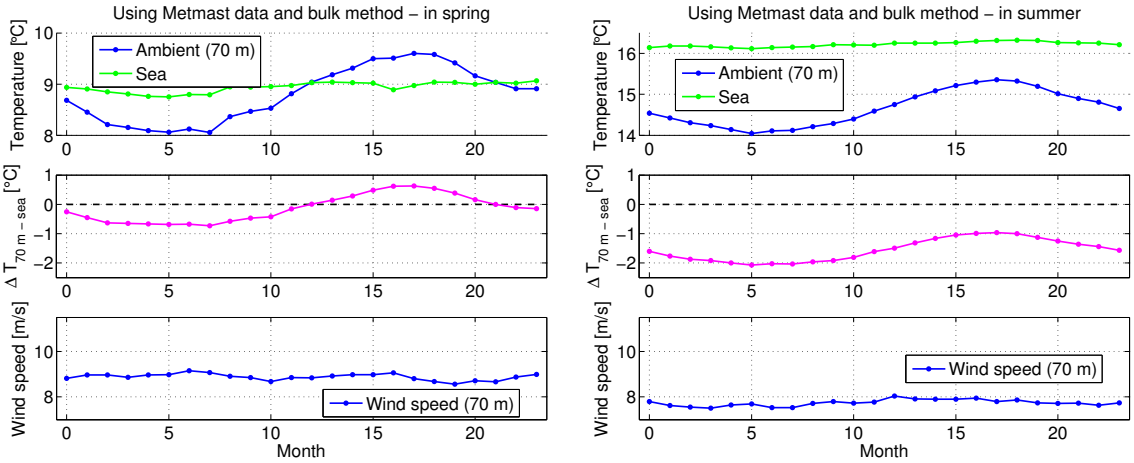

(a) Spring

(b) Summer

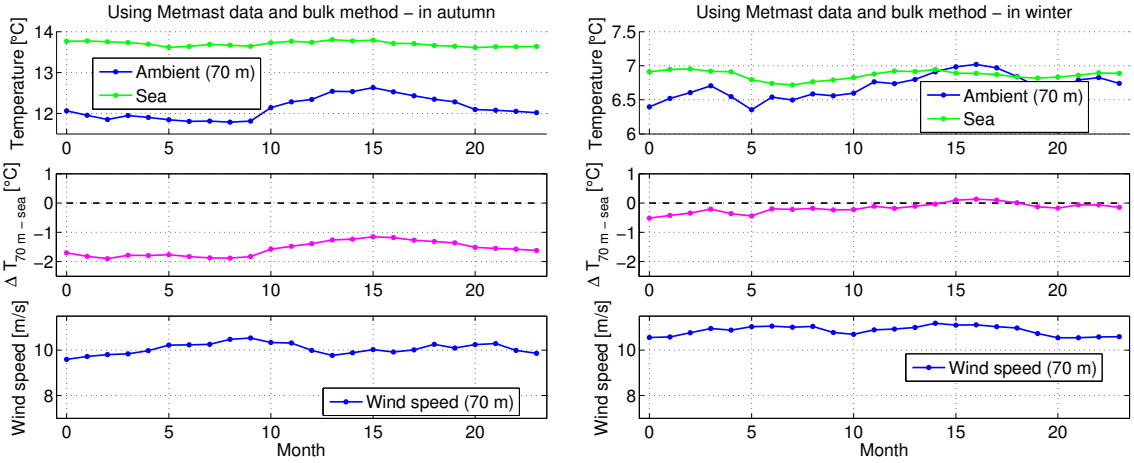

(c) Autumn

(d) Winter

Figure 4.11: Temperature and wind speed variation per season at North Hoyle, using metmast data. VS = very stable, S = stable, N = neutral, U = unstable, VU = very unstable. Data is taken over the period from 14 September 2007 to 31 December 2011. Wind directions $40°$ to $170°$ are excluded.

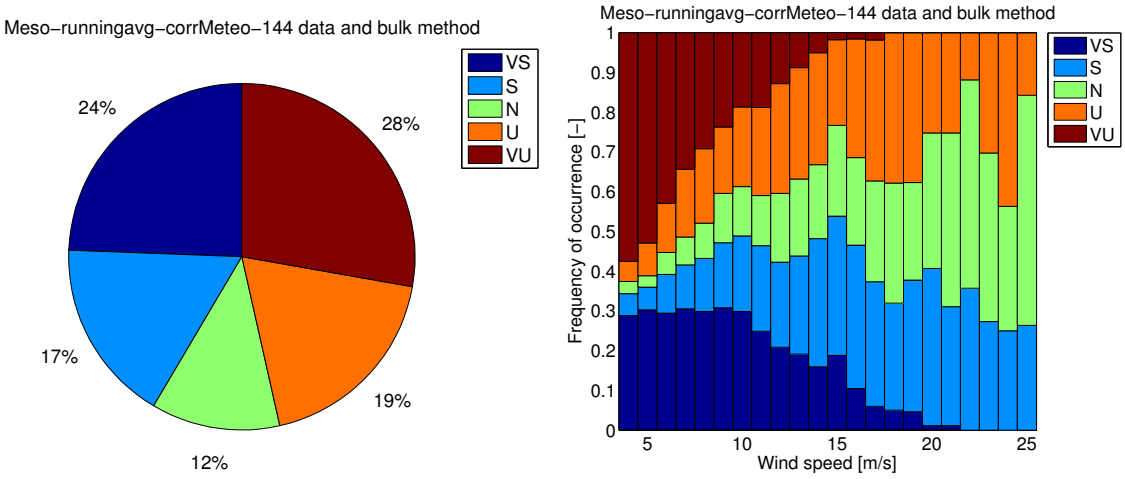

(a) In percentage (b) Versus wind speed

Figure 4.12: Distribution of stability classes at North Hoyle, only using hourly mesoscale timestamps also occurring in the metmast data. VS = very stable, S = stable, N = neutral, U = unstable, VU = very unstable. Data is taken over the period from 14 September 2007 to 31 December 2011. Wind directions $40°$ to $170°$ are excluded.

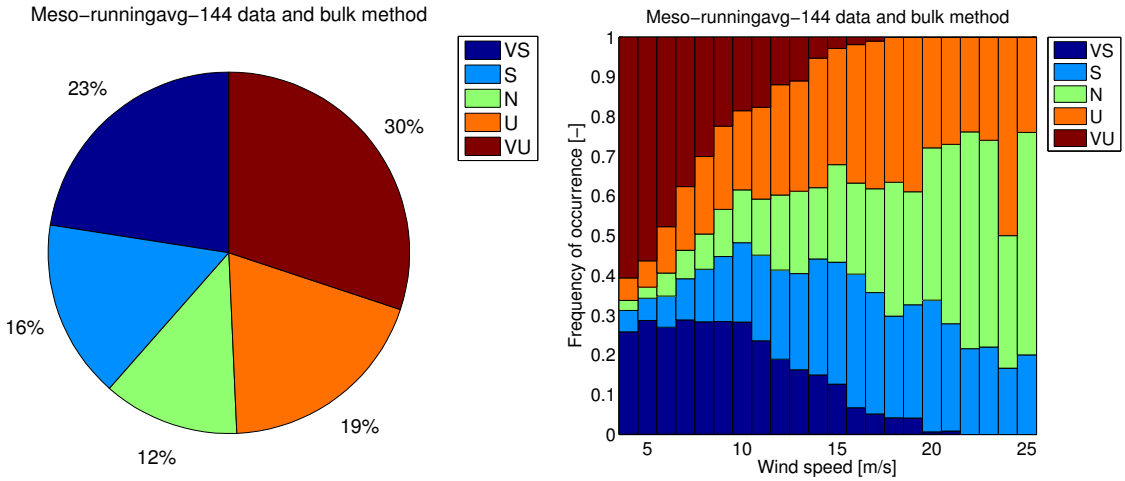

(a) In percentage (b) Versus wind speed

Figure 4.13: Distribution of stability classes at North Hoyle, using all hourly mesoscale timestamps in the data period. VS = very stable, S = stable, N = neutral, U = unstable, VU = very unstable. Data is taken over the period from 14 September 2007 to 31 December 2011. Wind directions $40°$ to $170°$ are excluded.

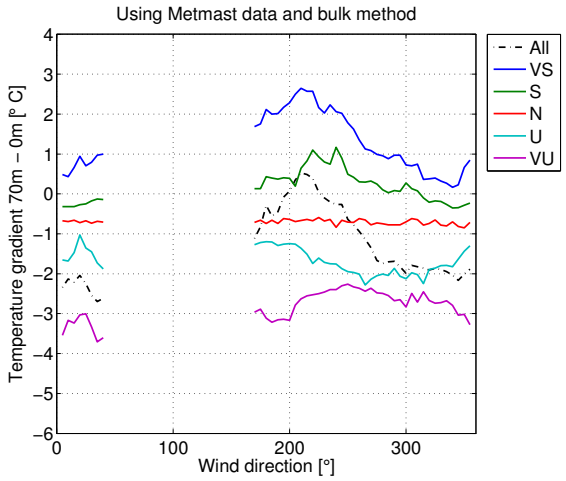

(a) Temperature gradient

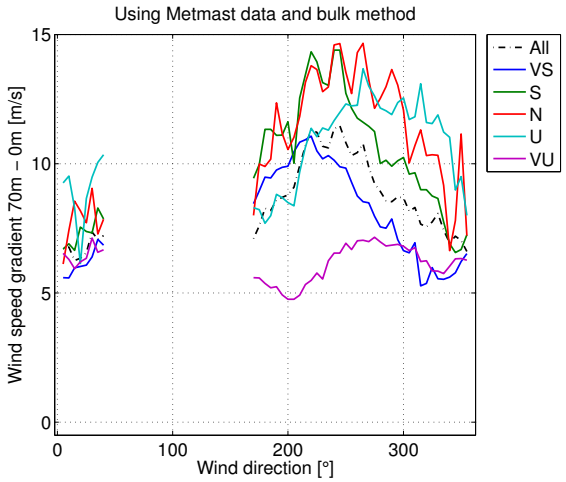

(b) Wind speed gradient

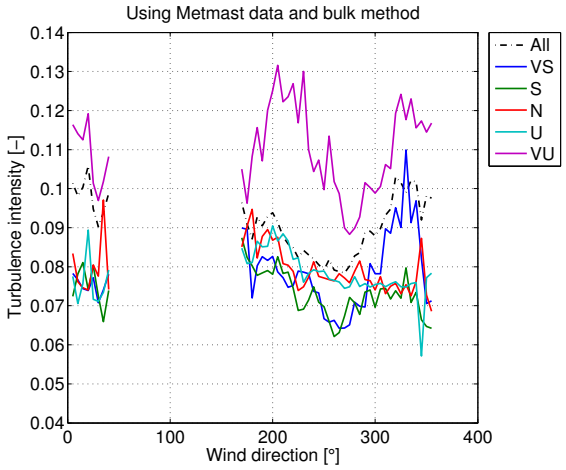

(c) Turbulence intensity

Figure 4.14: Sensitivity of atmospheric stability for various input parameters at North Hoyle over the investigated wind directions. VS = very stable, S = stable, N = neutral, U = unstable, VU = very unstable. Data is taken from 14 September 2007 to 31 December 2011.

4.2 Wake losses

With the stability distribution known, the effect of the atmospheric stability on the power output of the wind farm can now be investigated. The power production of rows of downstream turbines is investigated, where the data is filtered for those 10-minute periods where all turbines of a row are operating at the same time. This is done for various row directions (and hence downstream distances between the turbines). Using the stability classification of each 10-minute period the wake losses can be investigated per stability class.

From literature it is known that the wake losses in a wind farm are the largest for wind directions parallel to the downstream direction of the row of turbines. Therefore a narrow wind direction sector of ±2.5° around each row direction is used. The wind speed that is used is 8.0 m/s. This wind speed is used because it is not too far from average wind speeds at sea, while also ensuring that the turbines are not controlling their power output by pitching their blades as happens at higher wind speeds. Note that since the wake losses are largest inside the wind farm (since at the outer rows the flow has more energy mixing in from the sides of the wind farm), only the inner rows are investigated for their wake losses.

Since only cases are selected for which the whole row of downstream turbines is operating at the same time, and only for a narrow wind direction and wind speed sector, the number of cases available for the wake loss investigation is limited. Therefore, only 3 stability bins are used in the investigation: very stable, near-neutral and very unstable. The very stable and very unstable classes correspond with the respective class of the 5-bin classification as used in section 4.1, whereas the near-neutral class combines the cases from the stable, neutral and unstable classes into one bin.

The data in the wake loss analysis has been normalized according to the standards, as explained in section 2.5. The reference air density used at each site is the measured average air density, rounded to the nearest 0.01 kg/m^3 as indicated by the standards.

4.2.1 OWEZ

OWEZ consists of 4 rows of turbines, varying from 7 to 12 turbines per row. The wake losses are investigated for three wind directions corresponding to row directions of turbines as found from the turbine coordinates, being: 229.7°, 262.8° and 196.8°. These correspond to downstream spacings of $11D$, $13D$ and $13D$ respectively. The directions are shown in 4.15. To be able to compare the results using metmast data with the results using mesoscale data, only directions for which the metmast is not in the wake of the wind farm are considered. The average air density measured at OWEZ, rounded to the nearest 0.01 kg/m^3, is 1.23 kg/m^3. This is used to normalize the wind speeds.

Before discussing the wake losses at OWEZ, the following should be noted. During the investigation of North Hoyle it was found that the wake losses in a row of turbines are more clear when plotted versus the wind speed and wind direction as measured by the turbines (see section 4.2.2). It is therefore investigated if the same is the case at OWEZ. Unfortunately though, the wind direction measured by the turbines at OWEZ is incorrect. The nacelle direction measured by the turbines has not been reset properly during the

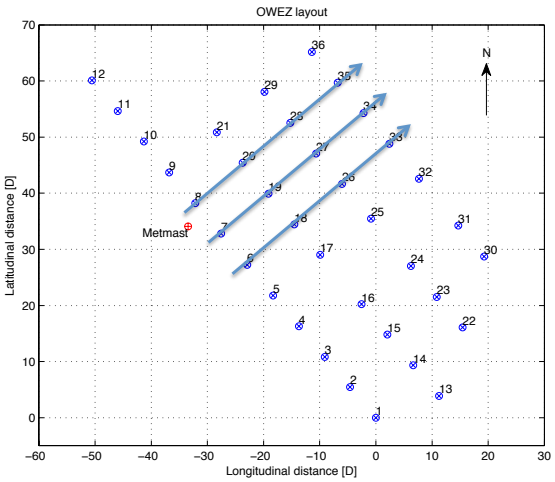

(a) 229.7°, downstream distance $11D$

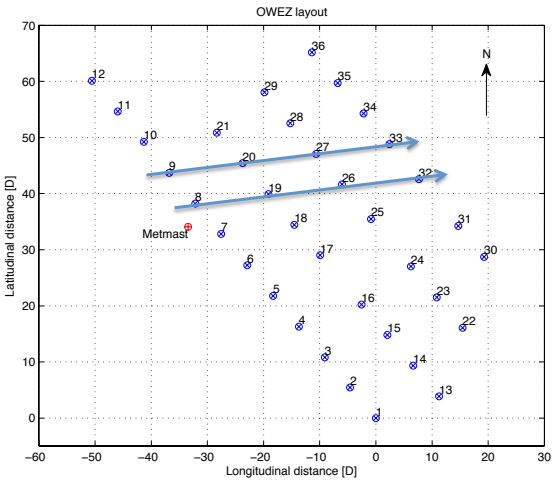

(b) 262.8°, downstream distance $13D$

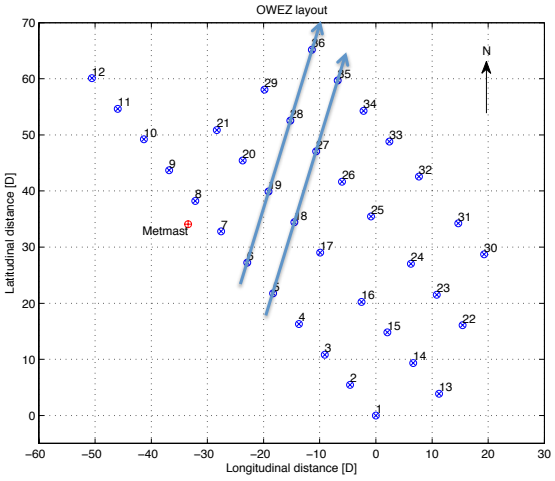

(c) 196.8°, downstream distance $13D$

Figure 4.15: Wind directions and the corresponding rows of turbines used to investigate wake losses at OWEZ.

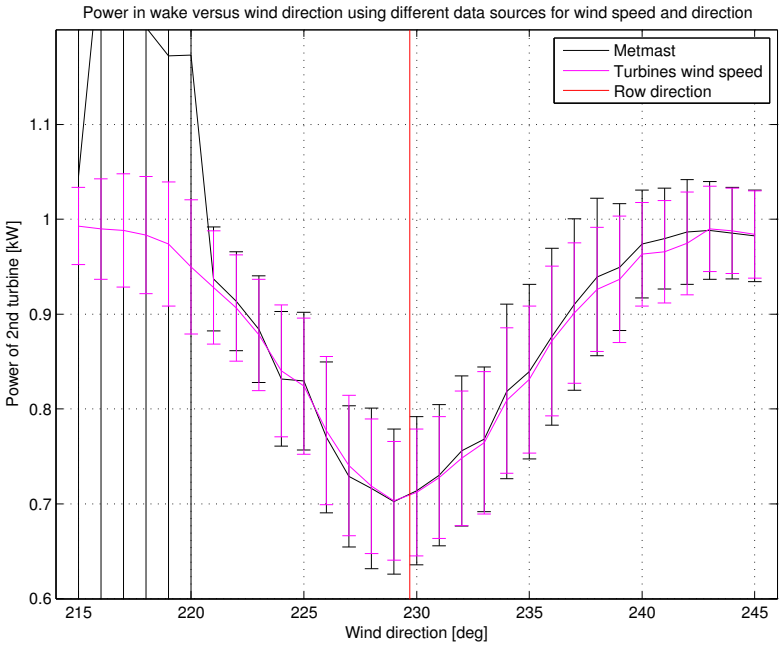

Figure 4.16: Wake losses for varying wind directions at OWEZ for winds coming from the Southwest. Comparison using wind speed and direction from either metmast or wind speed average of first turbine in the rows with metmast wind direction. Row direction is 229.7°. The error bars represent one standard deviation (half above and half below the mean value).

rotation of the nacelle (Veldkamp, 2011-2012), resulting in wind directions that can not be used. As a result the method applied at North Hoyle can not be applied for OWEZ. However, the wind speed measured by the turbines is correct. The wake loss is therefore plotted using either the wind speed and wind direction as obtained from the metmast or with the wind direction obtained from the metmast and the wind speed obtained from the first turbine in the rows (which is in free, undisturbed flow). How these wind speeds and directions can be obtained is explained in appendix B.

A plot of the power of the second turbine in the row with respect to the power produced by the first turbine is made for a range of wind directions around the expected row wind direction. This is shown in figures 4.16, 4.17 and 4.18. The plots show data for wind speeds in the range 8.0 ± 0.5 m/s in wind directions sectors of ±2.5° around each degree.

From the figures it can be seen that in general the largest wake loss occurs close to the expected wind direction (i.e. the row direction of the turbines, indicated by the red line in each figure). It can also be seen that when the wake loss is plotted using the wind speed as measured by the wind turbines the variation of the wake losses with wind direction is not very different compared to the wake losses plotted using metmast wind speed. The standard deviation of the wake losses using the wind speed as measured by the wind turbines is quite similar to that using the metmast wind speed and direction. Since the metmast is quite close to the first turbines in the rows for the three wind directions investigated this could have been expected. Therefore the metmast wind speed and direction will be used to plot the wake losses below.

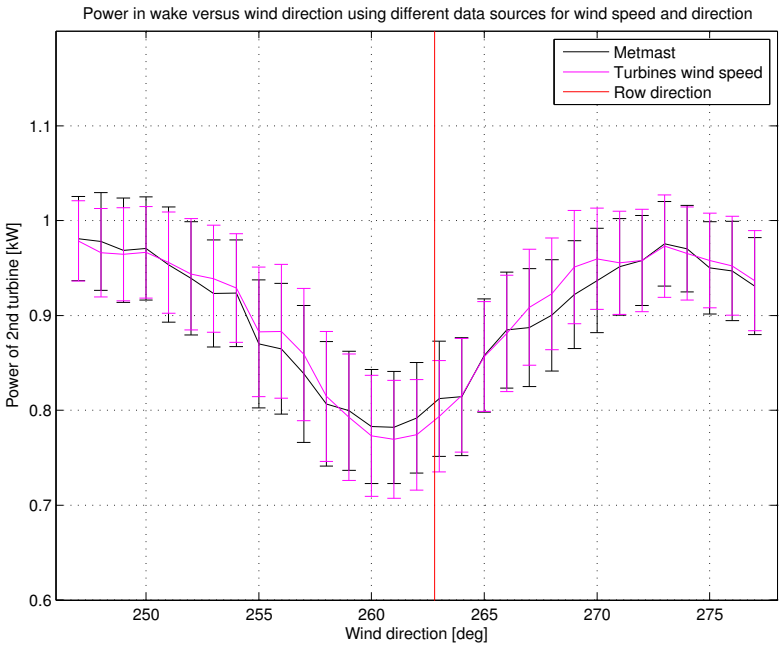

Figure 4.17: Wake losses for varying wind directions at OWEZ for winds coming from the West. Comparison using wind speed and direction from either metmast or wind speed average of first turbine in the rows with metmast wind direction. Row direction is $262.8°$. The error bars represent one standard deviation (half above and half below the mean value).

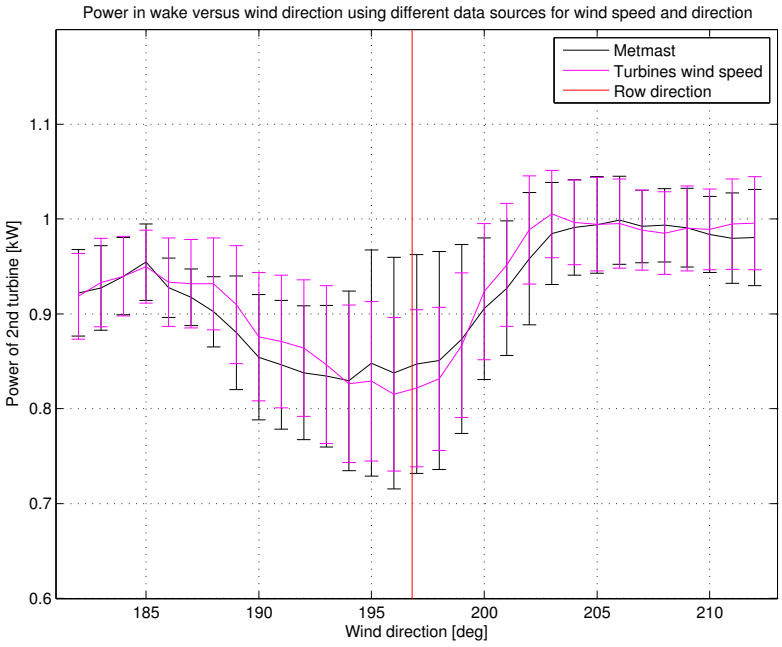

Figure 4.18: Wake losses for varying wind directions at OWEZ for winds coming from the South. Comparison using wind speed and direction from either metmast or wind speed average of first turbine in the rows with metmast wind direction. Row direction is $196.8°$. The error bars represent one standard deviation (half above and half below the mean value).

From the wake loss variation with wind direction as shown in figure 4.16 with winds from the Southwest it can be seen that the line using the metmast wind speed gives a clear dip in the power output around the row direction. At wind direction 215° to 220° it can be seen that the power output and the standard deviation using metmast data suddenly are very high. Upon further investigation this is found to come from two measurements that appear to have a different power output than what would be expected from the wind speed indicated by the metmast. Since the plot looks at the power output over ±2.5° of the wind direction these measurements appear in 6 wind direction bins in the plot. No similar problems arise in the rest of the data and since these measurements are not in the wind direction sector that will be investigated no problems are expected due to these.

In the figures of the other two cases the wake loss variation can clearly be observed too. Comparing the directions of the largest wake loss with the expected downstream direction as obtained from the turbine coordinates for the three cases, it is found that the wind direction measured by the metmast is about 2° too low. This can indicate a slight measurement and/or calibration error in the metmast wind direction measurement. The measurements are therefore corrected for this offset.

Using a narrow wind speed (8.0±0.5 m/s) and wind direction sector (downstream direction ±2.5°), to avoid any large fluctuations in power output of the turbines, the wake losses in downstream direction are plotted for the different directions. Different lines have been plotted for very stable, near-neutral and very unstable conditions, as well as the average of all cases. Figures 4.19, 4.20 and 4.21 show the results, using metmast or mesoscale data.

Figures 4.19a, 4.20a and 4.21 show the wake losses when using metmast data. For wind around 229.7° the difference between each stability class is clear. The very unstable case has higher power output than the near-neutral case, which has a higher power output than the very stable case. The power decreases for further downstream turbines, although the largest wake loss occurs when going from the first to the second turbine in the row. The fourth turbine in the row shows an increase in power output, meaning that the turbines have a higher energy inflow. This is expected to come from the use of the wind direction from the metmast instead of from the turbines. The wind might therefore not be exactly down the row of turbines. The power output of the downstream turbines is about 80%, 70% and 60% for the very unstable, near-neutral and very stable stability bins respectively, corresponding to a 20%, 30% and 40% wake loss.

For winds coming from 262.8° the results are similar. The three stability bins are clearly separated. Again the fourth turbines seem to have a small increase in the power output. The power output of the downstream turbines now converges to about 80%, 75% and 70% for the very unstable, near-neutral and very stable stability bins respectively, corresponding to a 20%, 25% and 30% wake loss. It can be seen that for the very stable and near-neutral classes the wake losses are smaller than for the 229.7° wind direction, as can be expected from the increase in spacing between the turbines as compared to the first case. The very unstable class has a similar power output as at the 229.7° wind direction though. This suggests that the very unstable has enough turbulence resulting from the atmospheric instability to mix in higher energy flow from above the wind farm. As such it is independent of the spacing between the turbines. It should be noted though that only two specific cases are considered here.

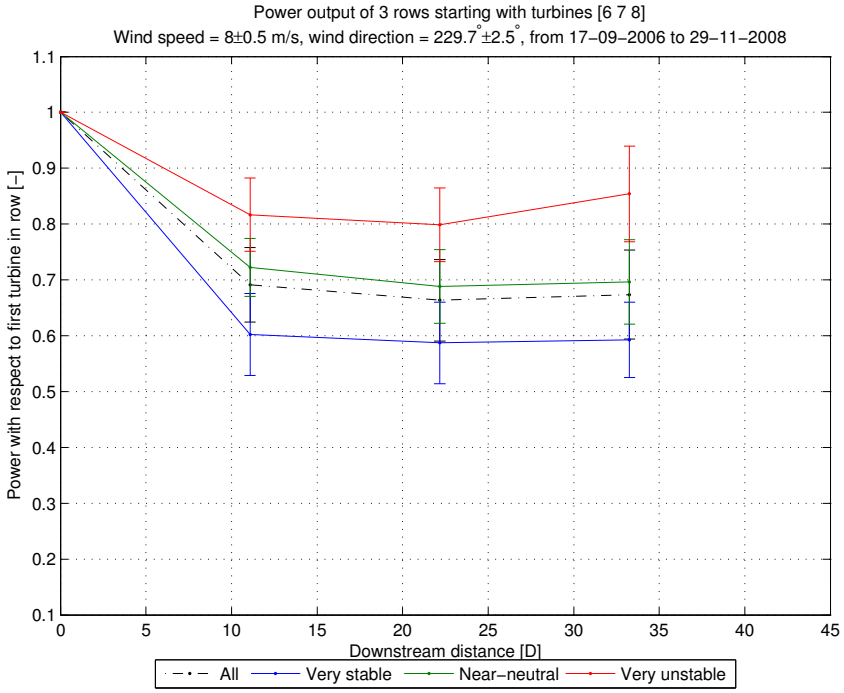

(a) Using metmast data

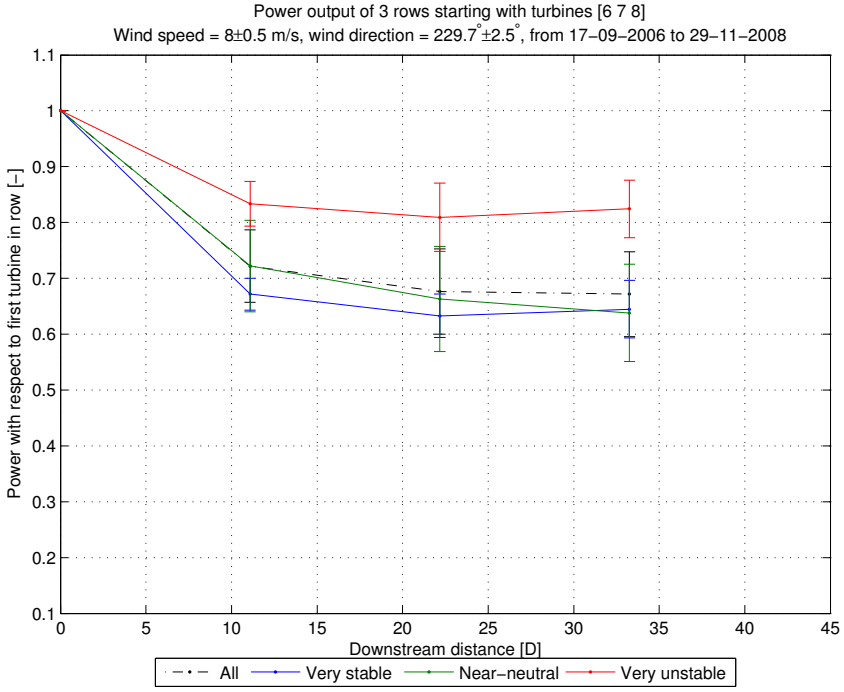

(b) Using mesoscale data

Figure 4.19: Wake losses at OWEZ for winds coming from the $229.7° \pm 2.5°$ and wind speeds at 8.0 ± 0.5 m/s for various stability classes. Atmospheric stability a) using metmast data, b) using mesoscale data. Wind speed and direction are taken from the metmast. Data is taken over the period from 1 September 2006 to 30 November 2008. The error bars represent one standard deviation (half above and half below the mean value).

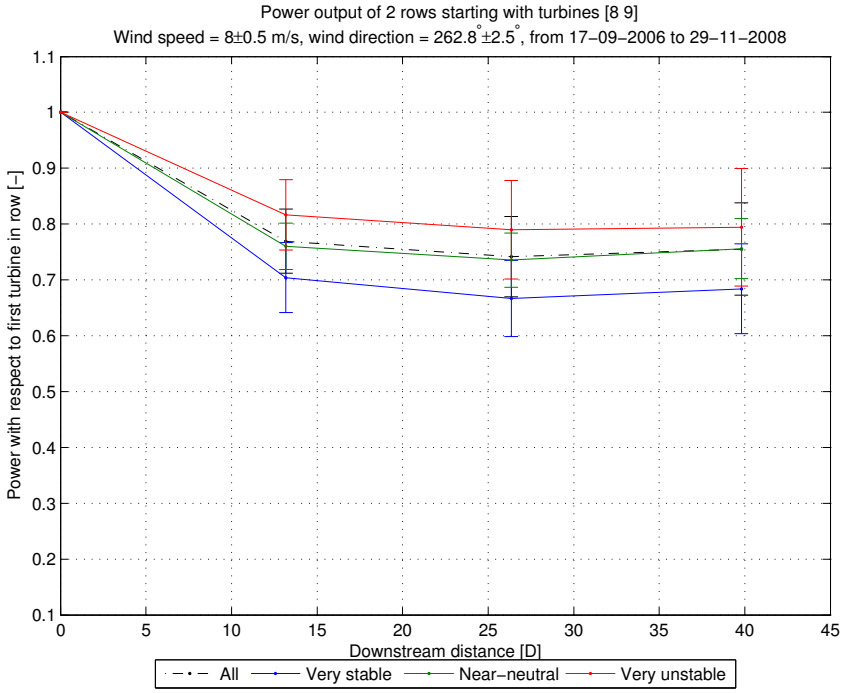

(a) Using metmast data

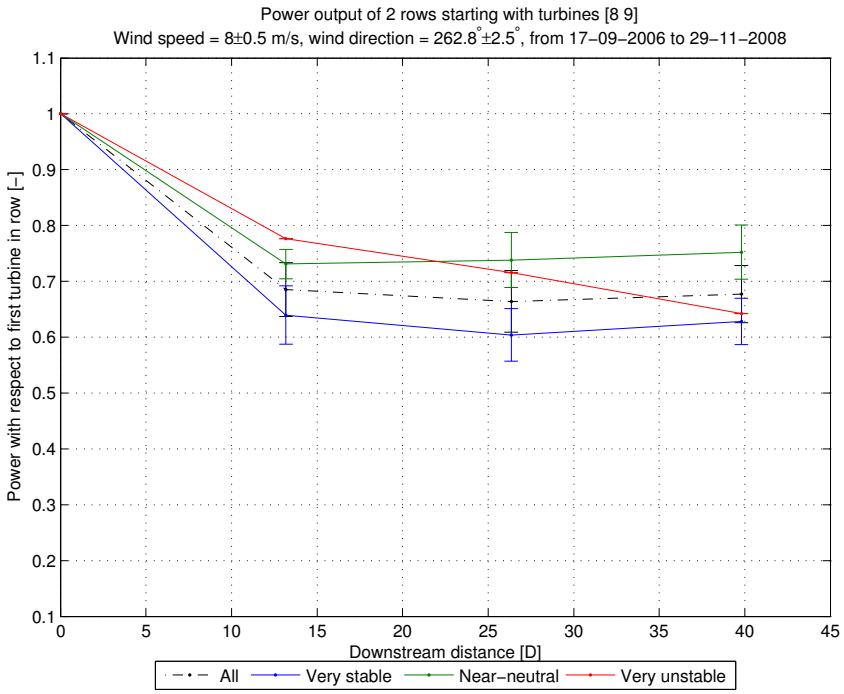

(b) Using mesoscale data

Figure 4.20: Wake losses at OWEZ for winds coming from the $262.8° \pm 2.5°$ and wind speeds at 8.0 ± 0.5 m/s for various stability classes. Atmospheric stability a) using metmast data, b) using mesoscale data. Wind speed and direction are taken from the metmast. Data is taken over the period from 1 September 2006 to 30 November 2008. The error bars represent one standard deviation (half above and half below the mean value).

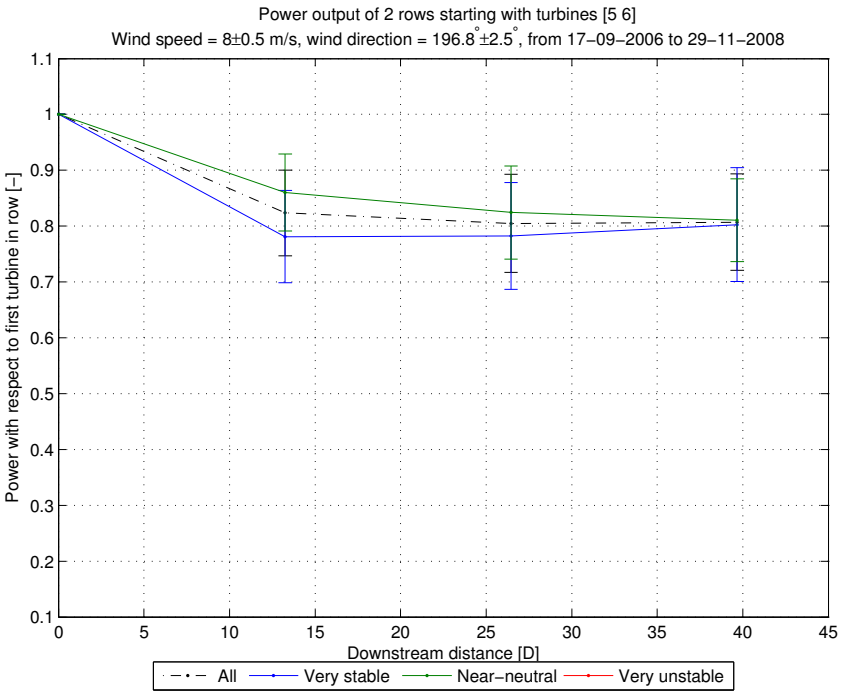

Figure 4.21: Wake losses at OWEZ for wind coming from $196.8° \pm 2.5°$ and wind speeds at 8.0 ± 0.5 m/s for various stability classes. Atmospheric stability, wind speed and direction are taken from the metmast. Data is taken over the period from 1 September 2006 to 30 November 2008. The error bars represent one standard deviation (half above and half below the mean value).

Table 4.2: Relative production of the second turbine (i.e. first turbine in the wake) with respect to free-stream turbine as obtained from measurements.

Wind farm	OWEZ	North Hoyle	North Hoyle
Distance	11-13D	4.4D	10-11D
Very unstable ($-200 < L < 0$)	80%[a]	50%[a]	75-80%[c]
Very stable ($0 < L < 200$)	60-70%[a]	25%[b]	70%[c]

[a] Similar production for turbines further downstream.
[b] The third turbine has 35% while the turbines further downstream all have around 30% relative production.
[c] The turbines further downstream lose 5% normalized production to the next turbine. The decrease in production becomes less for turbines further downstream and is about 1-2% at the last turbine.

For a wind direction of 196.8° there are no very unstable cases for this particular wind speed and wind direction selection in the investigated and filtered data. Although the spacing is similar as for the case when winds are coming from 262.8°, the wake losses appear to be smaller here. Due to lack of data this case will not be looked into further. No mesoscale data is remaining corresponding to the metmast data either, hence no wake loss plot is shown for the mesoscale data.

The results of the wake losses using metmast data are summarized in table 4.2.

During the investigation it was found that mesoscale data can, up to a certain extent but not completely, replace the metmast data to plot the wake losses. When the mesoscale wind direction, wind speed and atmospheric stability are used it is found that the wake losses do not correspond very well with those observed using metmast data. This is shown for a wind direction of 229.7° in figure 4.22. The wake losses do not show the clear variation per stability bin as is apparent when using metmast data. The main reason for this is the following. Turbine power output is sensitive to changes in wind speed and wind direction, as well as to other parameters such as turbulence intensity and wind shear (hence this study). Even in a certain wind speed bin, wind direction sector and atmospheric stability class the power output can vary, as can be seen from the standard deviations in the wake loss plots using metmast data. The VSU mesoscale data is a simulation of the atmosphere, and the mesoscale data will always be deviating from the real world. If the turbine power output would have been simulated as well (e.g. using WindPRO), this would not have been a problem. The turbine power output would then vary according to the input data, e.g. the mesoscale data. However, the power output used here is measured in the real world and the mesoscale wind data does not match the wind data of the real world close enough to replace the metmast data. This leads to the conclusion that the mesoscale wind speed and wind direction can be used to simulate the turbine production, but the mesoscale wind speed and wind direction can not replace the metmast data when investigating the measured wake losses.

Atmospheric stability on the other hand changes less fast, as it is binned into three stability classes. It therefore appears to be quite comparable to that measured by the metmast (compare figures 4.1 and 4.5). The following is therefore proposed. The wake losses will be plotted using either metmast or mesoscale atmospheric stability. The metmast wake

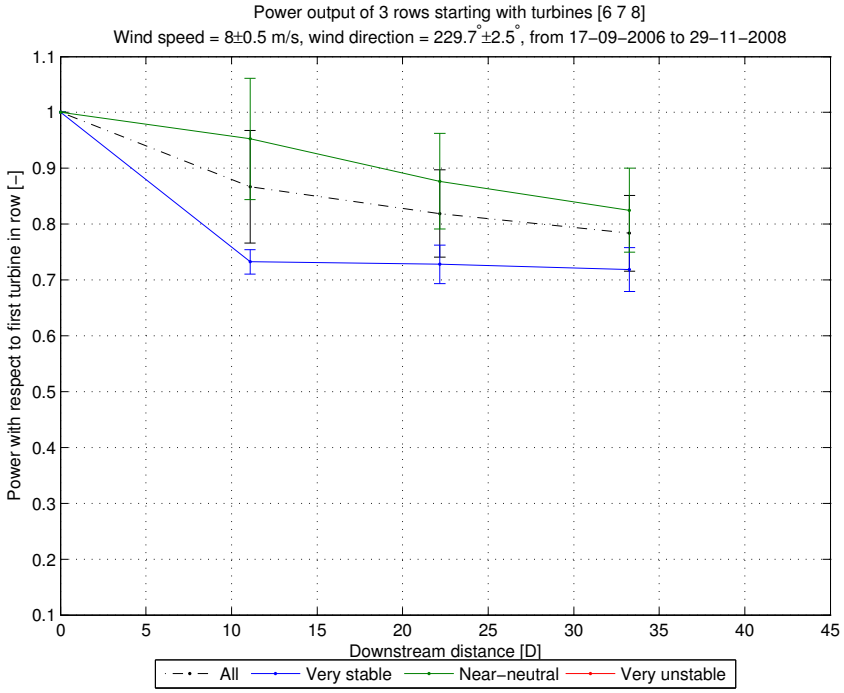

Figure 4.22: Wake losses at OWEZ for winds coming from the $229.7° \pm 2.5°$ and wind speeds at 8.0 ± 0.5 m/s for various stability classes. Atmospheric stability, wind speed and wind direction are taken from the mesoscale data. Data is taken over the period from 1 September 2006 to 30 November 2008. The error bars represent one standard deviation (half above and half below the mean value).

losses use the metmast atmospheric stability, whereas the mesoscale wake losses use the mesoscale atmospheric stability. Since the turbine wind direction is not available, the wind speed and wind direction are taken from the metmast to select the measurements that will be plotted in both the metmast and mesoscale wake losses. This is a similar approach as applied at North Hoyle, where the atmospheric stability is taken from either the metmast or mesoscale data and the turbine wind speed and direction are used to plot the wake losses. Therefore, also at North Hoyle the only thing that changes in going from metmast to mesoscale wake losses is the atmospheric stability (and the amount of measurements, as mesoscale only has hourly timestamps instead of one every 10 minutes). A similar approach is therefore applied here.

Figures 4.19b and 4.20b show the wake losses when using mesoscale atmospheric stability for row directions 229.7° and 262.8° respectively. For 229.7° the very unstable class in the mesoscale wake loss plot is very similar to that in the metmast wake loss plot. The near-neutral and very stable bin in the mesoscale plot are close to the metmast wake losses, but have respectively a lower and a higher power output in the mesoscale data. For wind direction 262.8° the near-neutral case in the mesoscale plot is similar to that in the metmast wake loss plot, but the very stable and very unstable case have a lower power output. The differences must be due to the differences between metmast and mesoscale atmospheric stability. An additional difference might result due to the fact that the mesoscale data only has hourly timestamps whereas the metmast data has a measurement every 10 minutes, and only those hourly timestamps are shown that also occurred in the metmast wake loss plot. Less data is therefore available to plot the mesoscale wake losses, which is also the reason that the average over all stability classes is not exactly the same for the metmast and mesoscale wake losses. In general it can be said that the mesoscale atmospheric stability can reasonably well be applied to separate the different stability classes of the wake losses although obviously improvements are possible.

4.2.2 North Hoyle

The wind farm layout at North Hoyle is a grid of 6 by 5 turbines. The row directions of the turbines are found using the turbine coordinates. The following wind directions, corresponding to row directions of turbines as found from the turbine coordinates, are investigated: 348.9°, 258.8° and 282.5°. These correspond to downstream spacings of $4.4D$, $10D$ and $11D$ respectively. The directions are shown in 4.23. To be able to compare the results using metmast data with the results using mesoscale data, only directions for which the metmast is not in the wake of the wind farm are considered. The average air density measured at North Hoyle, rounded to the nearest 0.01 kg/m^3, is 1.23 kg/m^3. This is used to normalize the wind speeds.

During the investigation of North Hoyle it was found that the wake losses were not as expected when they were plotted using the wind speed and direction as measured by the metmast. Therefore, a plot of the power of the second turbine in the row with respect to the power produced by the first turbine was made for a range of wind directions around the expected row wind direction. This is shown in figures 4.24, 4.25 and 4.26. The plots show data for wind speeds in the range 8.0 ± 0.5 m/s in wind direction sectors of ±2.5° around each degree.

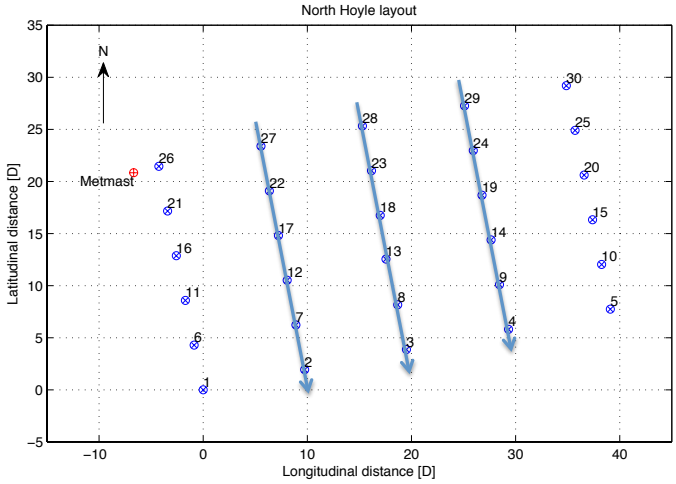

(a) 348.9°, downstream distance $4.4D$

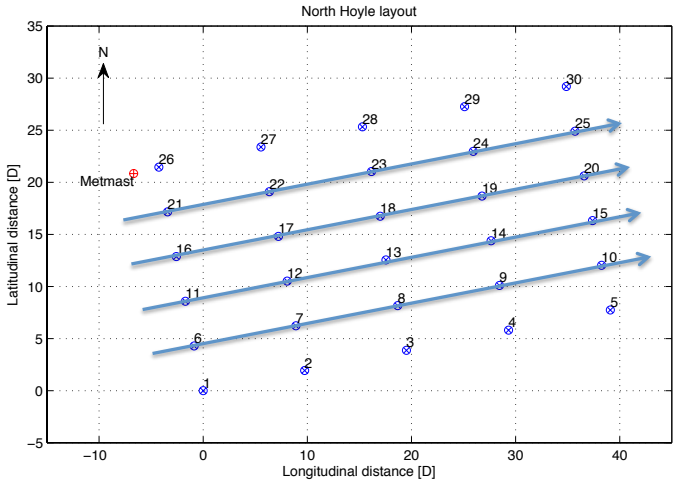

(b) 258.8°, downstream distance $10D$

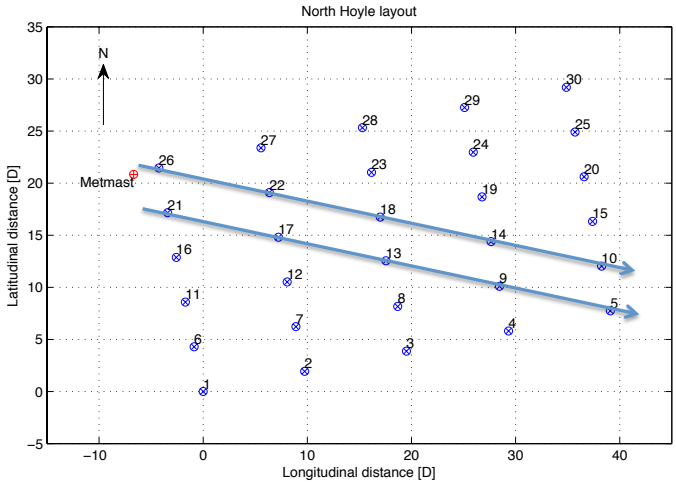

(c) 282.5°, downstream distance $11D$

Figure 4.23: Wind directions and the corresponding rows of turbines used to investigate wake losses at North Hoyle.

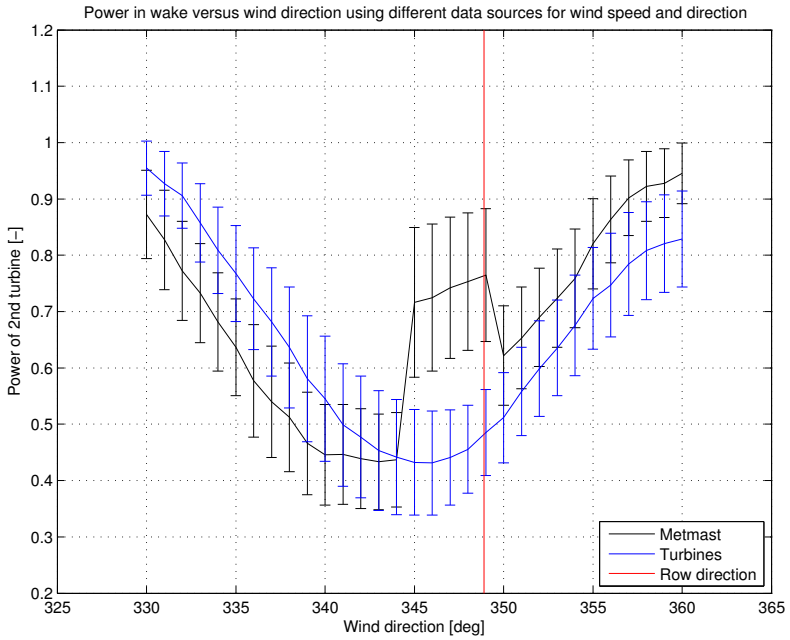

Figure 4.24: Wake losses for varying wind directions at North Hoyle for winds coming from the North. Comparison using wind speed and direction from either metmast or average of first turbine in the rows. Row direction is $348.9°$. The error bars represent one standard deviation (half above and half below the mean value).

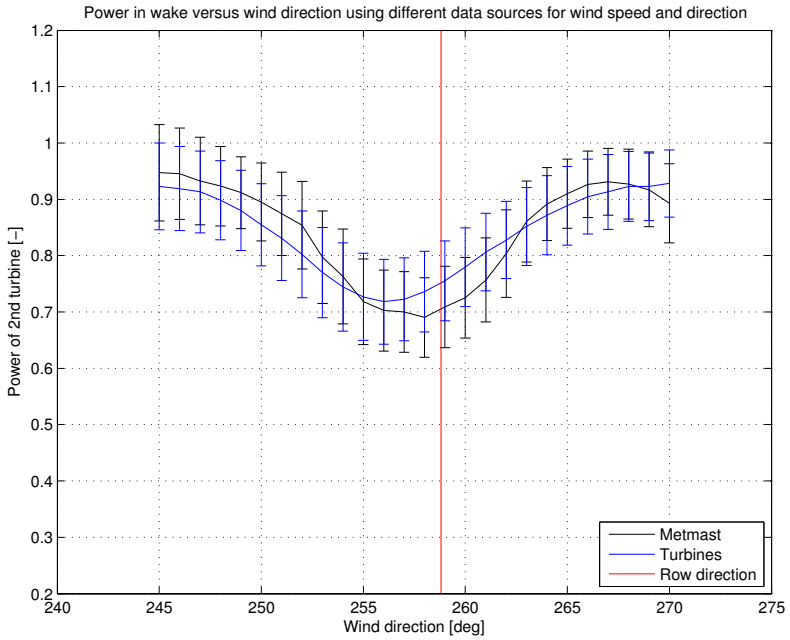

Figure 4.25: Wake losses for varying wind directions at North Hoyle for winds coming from the West. Comparison using wind speed and direction from either metmast or average of first turbine in the rows. Row direction is $258.8°$. The error bars represent one standard deviation (half above and half below the mean value).

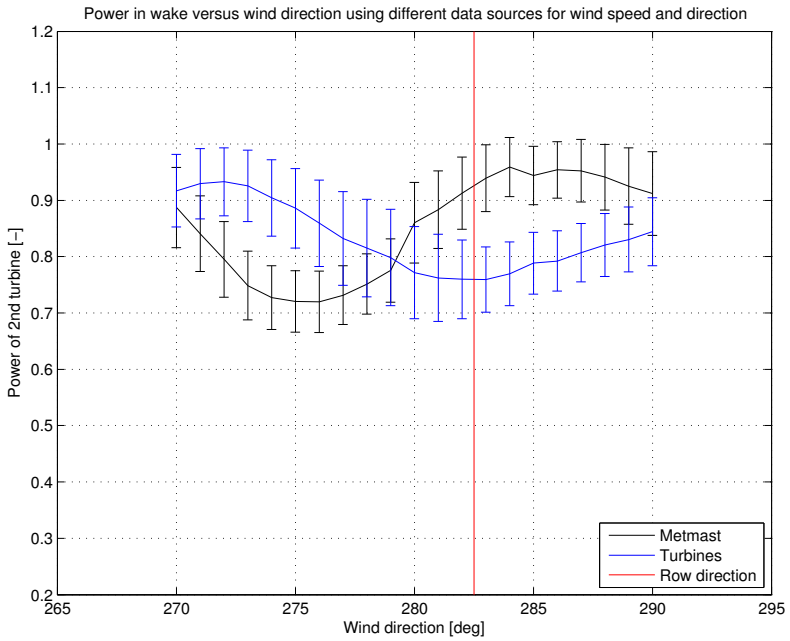

Figure 4.26: Wake losses for varying wind directions at North Hoyle for winds coming from the Northwest. Comparison using wind speed and direction from either metmast or average of first turbine in the rows. Row direction is 282.5°. The error bars represent one standard deviation (half above and half below the mean value).

The wake loss is plotted using either the wind speed and wind direction as obtained from the metmast or as obtained from the first turbine in the rows (which is in free, undisturbed flow). How these wind speeds and directions can be obtained is explained in appendix B. Looking at the plots it can be seen that for the case with winds from the North (figure 4.24) a jump in the metmast wake losses is visible for 5 directions. Upon further investigation this is caused by a significant amount of measurements where the second turbine in the row has a larger power output than the first turbine in the row. Since each wind direction bin in the plot averages the measurements over ±2.5° the deviation is visible in 5 direction bins. The deviation might indicate that the metmast is inaccurate for inflow to the turbines at this wind direction. Otherwise, for winds coming from the North the wake losses based on metmast and turbine seem to agree, although an offset in wind direction is visible. The same two observations can be made for winds coming from the West (figure 4.25). For winds coming from the Northwest (figure 4.26) a significant difference between the two lines can be seen. This might indicate that the metmast is inaccurate for this wind direction as well, even though the metmast is located at the Northwest corner of the wind farm.

From the figures it can be seen that the largest wake loss does not occur at the expected wind direction (i.e. the row direction of the turbines, indicated by the red line in each figure). The standard deviation of the wake losses using the wind speed and direction as measured by the wind turbines is similar compared to that using the metmast wind speed and direction, but when the wake losses are plotted using the wind speed and direction as measured by the wind turbines the variation of the wake losses with wind direction can be

significantly different than when plotted using the metmast data. These are reasonable observations. It might be difficult to quantify the wind direction for a whole wind farm using a measurement at a single location (such as a metmast), since the wind direction might change over the wind farm, as also mentioned by Barthelmie and Jensen (2010) and Méchali et al. (2006). Especially for turbines far away from the measurement location this can be an issue. This might even lead to increasing power outputs further downstream in the wind farm, since due to different wind directions the downstream turbines might not be in a direct wake from their upstream turbine. To avoid the inaccuracy of using a point measurement for the whole wind farm, it should therefore be recommended that data from the first turbine in the rows is used to put the power in a wind speed and direction bin for the wake loss investigation. When possible this is done in this study as well (e.g. for OWEZ it is not possible due to incorrect wind direction measurements by the turbines).

Although the wind speed and wind direction as measured by the turbines is used to plot the wake losses, the atmospheric stability is still used as measured by the metmast to classify the state of the atmosphere and to see its influence on the wake losses. The temperature measured by the turbines is stored in the SCADA database using integers and hence is not precise enough to determine the atmospheric stability.

Comparing the directions of the largest wake loss with the expected downstream direction as obtained from the turbine coordinates, it is found that the wind direction measured by the turbines is about 3° too low. This can indicate a slight measurement and/or calibration error in the turbine wind direction measurement. The measurements are therefore corrected for this offset.

Using a narrow wind speed (8.0±0.5 m/s) and wind direction sector (downstream direction ±2.5°), to avoid any large fluctuations in power output of the turbines, the wake losses in downstream direction are plotted for the different directions. Different lines have been plotted for very stable, near-neutral and very unstable conditions, as well as the average of all cases. Figures 4.27, 4.28 and 4.29 show the results, using metmast or mesoscale data.

Figures 4.27a, 4.28a and 4.29a show the wake losses using the atmospheric stability obtained from the metmast data and using the wind speed and direction as measured by the turbines. The wake loss is larger for very stable cases than for very unstable cases, which is as expected. The influence of wind turbine spacing can clearly be seen. For a row direction of 348.9° the spacing is small ($4.4D$), resulting in a high wake loss from the first to the second turbine and a small recovery towards the third turbine, after which the wake loss converges. On average this results in a wake loss of about 60%. For the very stable case this is 70%, whereas the very unstable case converges to a wake loss around 50%. For wind directions of 258.8° and 282.5° the turbine spacing is larger ($10-11D$), which results in wake losses that converge to about 40% as the average of all measurements for both cases. It is hard to make a general statement about the standard deviation, which may be due to the limited amount of measurements for each class and for each wind direction case.

For all three row directions the very unstable class has the smallest wake losses, whereas the very stable case has the highest wake losses. This is as expected, since the very unstable cases have more turbulence and hence more high energy flow is mixed into the

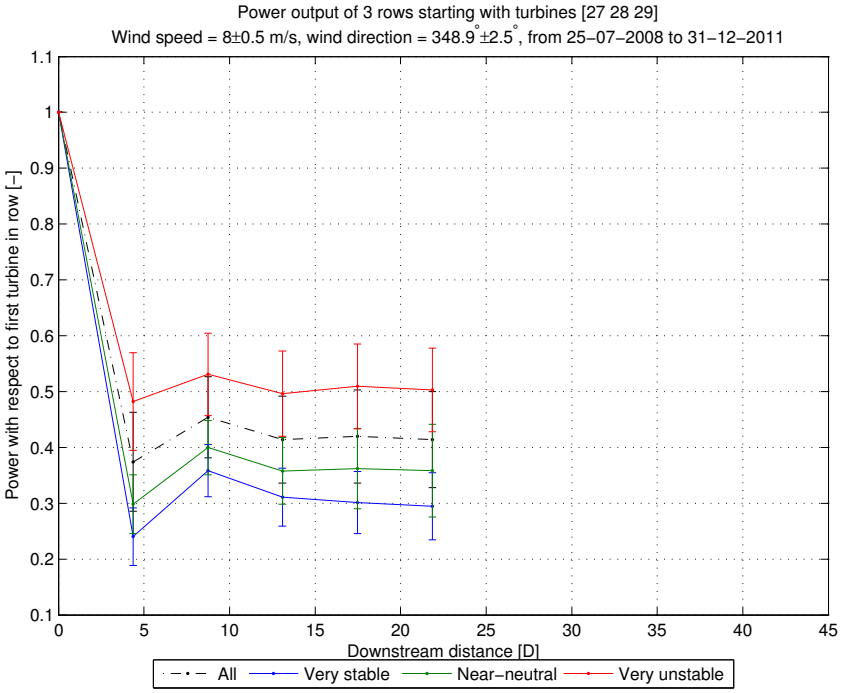

(a) Using metmast data

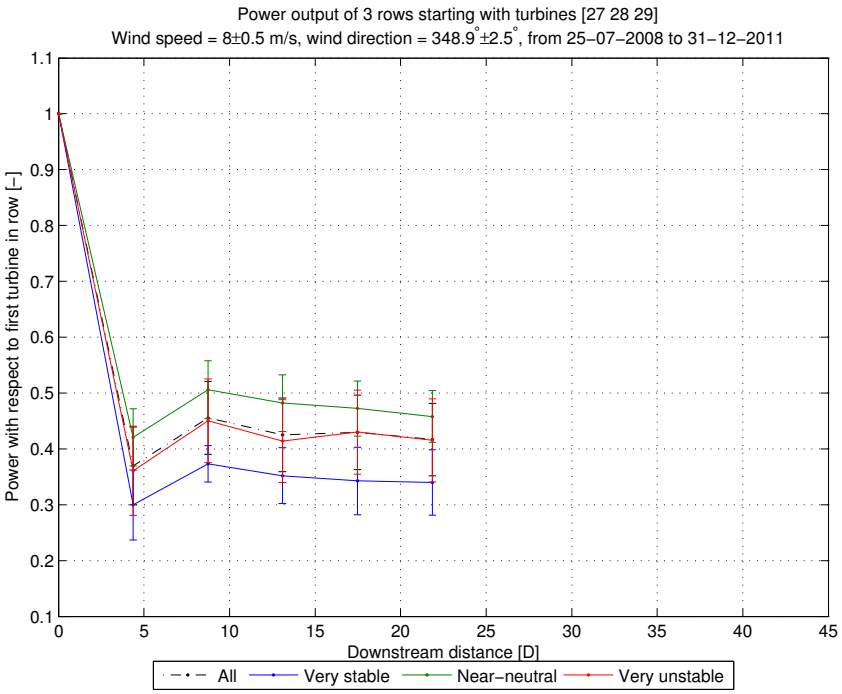

(b) Using mesoscale data

Figure 4.27: Wake losses at North Hoyle for winds coming from the $348.9° \pm 2.5°$ and wind speeds at 8.0 ± 0.5 m/s for various stability classes. Atmospheric stability a) using metmast data, b) using mesoscale data. Wind speed and direction are taken from the first turbine in the rows. Data is taken over the period from 11 June 2008 to 31 December 2011. The error bars represent one standard deviation (half above and half below the mean value).

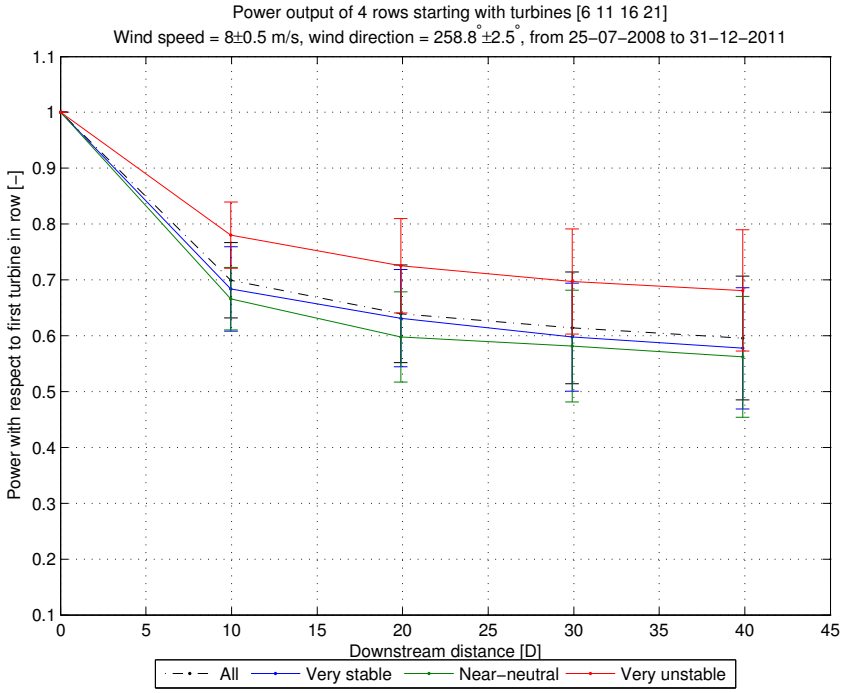

(a) Using metmast data

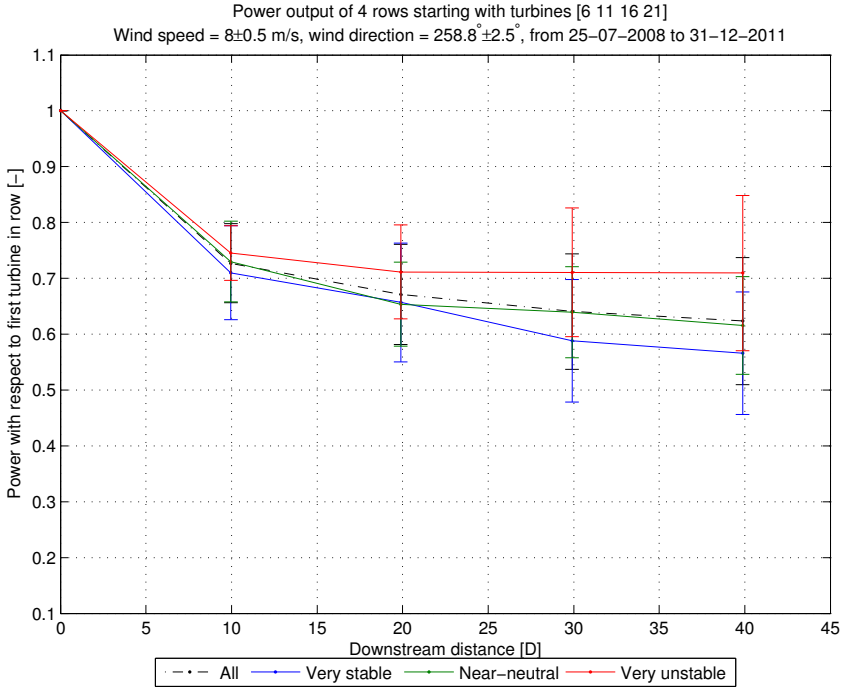

(b) Using mesoscale data

Figure 4.28: Wake losses at North Hoyle for winds coming from the $258.8° \pm 2.5°$ and wind speeds at 8.0 ± 0.5 m/s for various stability classes. Atmospheric stability a) using metmast data, b) using mesoscale data. Wind speed and direction are taken from the first turbine in the rows. Data is taken over the period from 11 June 2008 to 31 December 2011. The error bars represent one standard deviation (half above and half below the mean value).

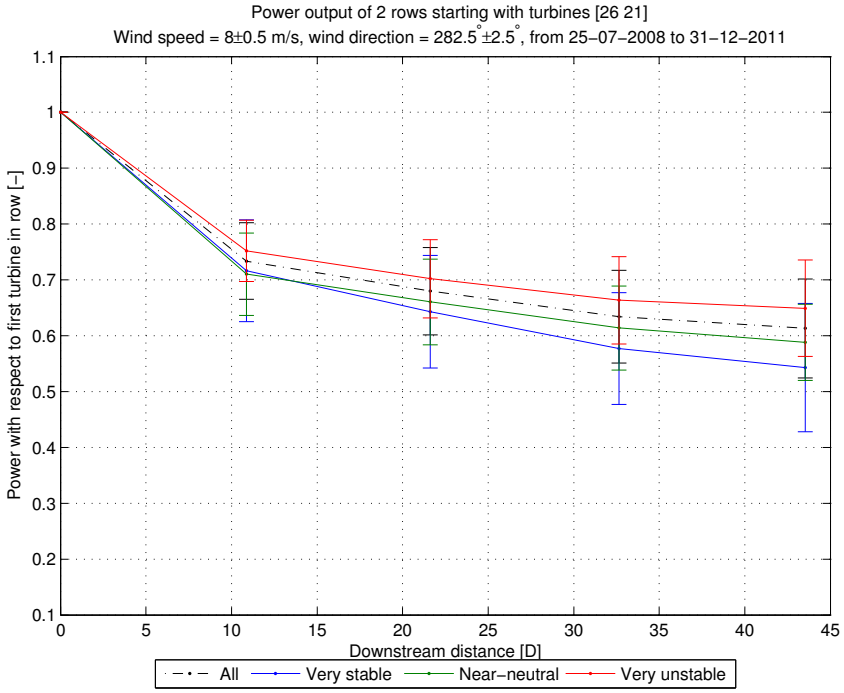

(a) Using metmast data

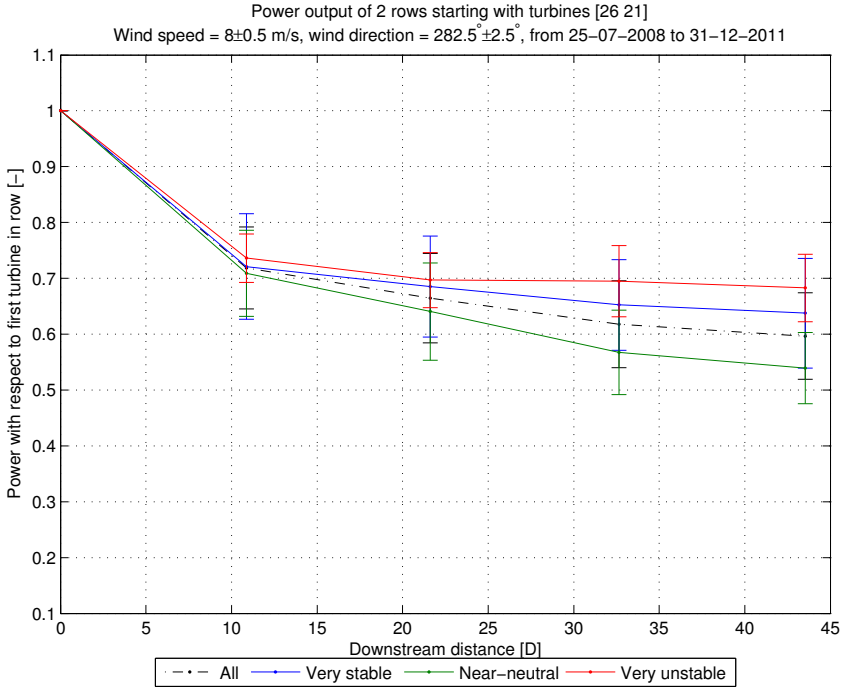

(b) Using mesoscale data

Figure 4.29: Wake losses at North Hoyle for wind coming from $282.5° \pm 2.5°$ and wind speeds at 8.0 ± 0.5 m/s for various stability classes. Atmospheric stability a) using metmast data, b) using mesoscale data. Wind speed and direction are taken from the first turbine in the rows. Data is taken over the period from 11 June 2008 to 31 December 2011. The error bars represent one standard deviation (half above and half below the mean value).

wake. The near-neutral case is expected to be located somewhere in between the very stable and very unstable case. This is not the case for a wind direction of 258.8°. For the other two cases the near-neutral line does not always have the same location. In near-neutral conditions the air and sea surface temperatures are close together. From literature it is known that this increases the uncertainty of the bulk method (Lange, Larsen, et al., 2004b; Sathe, 2009). This can be a reason for the inconsistent placement of the line indicating the near-neutral wake losses. During stable and unstable conditions the uncertainty in L reduces.

The results of the wake losses using metmast data are summarized in table 4.2. The results agree with those found by Barthelmie et al. (2011); Hansen et al. (2012) at the Horns Rev wind farm and by Barthelmie et al. (2007, 2011) at the Nysted wind farm (see also section 2.2). For both OWEZ and North Hoyle the difference in relative production between the very stable and very unstable classes is 10-20%. As opposed to what is stated in Barthelmie et al. (2011); Hansen et al. (2012) a difference between the unstable and near-neutral classes is observed in the current study. It should be noted that the atmospheric stability classes, wind speed and/or wind direction bins are not agreed upon in the different research projects and vary between the different projects and from the one used in this project.

Figures 4.27b, 4.28b and 4.29b show the wake losses where mesoscale data is used to determine the atmospheric stability. In general it can be seen that the graphs are not the same as those using the metmast data. For 348.9° it seems that the very stable cases of metmast and mesoscale data are quite similar, whereas the very unstable class shows a larger difference and the near-neutral case shows an even bigger deviation with the metmast data. For 258.8° the mesoscale data results are within about 5 percent off from the metmast data, although the variation in downstream direction is somewhat different. For 282.5° the mesoscale near-neutral line seems to be closer to the very stable line in the metmast data than to the near-neutral line. The very stable and near-neutral line are off the most compared to their metmast counterpart and the difference seems to increase for further downstream movement. The very unstable classes are quite similar to each other and differ within about 5 percent.

It is suggested that the comparison of metmast and mesoscale data might improve by adapting the mesoscale data according to its correlation with the measured metmast data. This is performed in appendix E. The results are varying regarding how well the comparison has improved.

Although the wake losses using the (unadapted) mesoscale data shown above are not exactly the same in detail as the wake losses of the metmast data, it can be said that in general the wake losses using mesoscale data compare reasonably well with those using metmast data. For all three wind direction cases, the power output of the very unstable cases is larger than that of the very stable cases. The fact that the near-neutral line is not always placed in between the very unstable and very stable cases (as would be expected) can be explained by the reduced accuracy of the bulk method for near-neutral conditions.

In appendix F the effect of some measurement errors on the wake losses is investigated. It is found that the wake losses corresponding to the very unstable and very stable cases show almost no sensitivity to an offset in the measurement of wind speed, ambient temperature or sea surface temperature. The wake loss corresponding to the near-neutral case on

the other hand is sensitive to these measurement errors, especially for the temperature difference. This is another reason for only taking into account the wake losses of the very stable and very unstable cases and not those of the near-neutral case.

4.3 Wake losses simulated using WindPRO

In the previous section the wake losses were shown as measured in the real wind farms. One of the questions of the study is how well the current wake models predict the effect of atmospheric stability on the production. For this the software package WindPRO is used, which is widely used in the wind energy industry, as also by Vestas Wind Systems A/S.

Various wake models are implemented in WindPRO, but this study focuses on using one of the most parameterized and well-known wake models, which is the one by Jensen. The theory behind the model is shortly explained in section 2.6. A more detailed explanation, including a derivation of the equations, is shown in appendix A.

Since the WDC is related to the turbulence intensity, and since turbulence is linked to the atmospheric stability, the wake model might be able to predict the wake losses corresponding to the various atmospheric stabilities by adjusting the WDC.

Each wind farm is recreated in WindPRO and the wake losses are modelled for various values of the WDC. The power curves of the modelled turbines have been corrected such that they take the average measured air density at the site into account. The measurements used in the wake loss plots in section 4.2 are imported into WindPRO, to recreate the wind speed and direction as measured. The wind speed is subsequently put into a bin of 1 m/s, whereas the wind direction is put into bins of 1°. Modelling the wind direction in small steps (as opposed to the 12 standard 30° wide sectors) ensures that the modelled wind will be as good as parallel to the row direction, which is important to obtain the wake losses associated with the downstream direction of the row of turbines.

Since in section 4.2 it was found that the near-neutral cases have a reduced accuracy, which is caused by the small difference between the air and sea surface temperatures, only the very stable and very unstable cases are investigated here. These are also the two cases with the largest difference in wake losses.

4.3.1 OWEZ

Two of the three wind direction cases discussed in section 4.2.1 are simulated separately in WindPRO, being wind direction 229.7° and 262.8°. Wind direction 196.8° has no very unstable cases for the selected wind speed and wind direction sector and is not modelled.

The results for 229.7° are shown in figure 4.30. For the very unstable class it can be seen that the line corresponding to the measurements lies close the line for k = 0.14, where k is the wake decay constant (WDC). The measurement of the fourth turbine is higher, which is expected to come from the use of the wind direction from the metmast instead of from the turbines. As the simulated wind in WindPRO is exactly along a certain direction over the whole wind farm, this increase in power output of the fourth turbine

is not seen in the simulation and hence confirms the expected cause of the increase. The lines for the different WDCs seem to converge to a power output of 80% for WDC values of $k = 0.09 - 0.14$. It is unknown what causes this, but it might be caused by the layout of the wind farm. For a higher WDC value of $k = 0.15$ the wake losses are considerably smaller again compared to the differences between the different WDC values near the convergence. The adjustment in WDC value together with the layout of OWEZ, which consists of 4 lines of turbines which do not have the same amount of turbines in each line and of which the turbines do not all have the same spacing, might therefore cause a difference in power output because the wakes hitting the turbines under investigation change.

The very stable class corresponds best to a WDC value of $k = 0.05$. The measurements do not have the same downstream variation of the wake loss as is found from the simulations. The measurements show a larger wake loss at the second turbine and this wake loss stays about the same for the next two turbines.

For 262.8° the results are shown in figure 4.31. For the very unstable case there are again a few lines for different WDC that are close together, this time for WDC values of $k = 0.08 - 0.11$. The measurement of the very unstable class is close to the line with WDC value $k = 0.11$. The very stable class is close to $k = 0.05$, as is the case for wind direction 229.7°. Note that in the case of the very stable line the last turbine in the row shows a higher power output, which is also shown by the WindPRO simulations. Upon further investigation the increase of power output of the fourth turbine in this case stems from the row of turbines starting with turbine 8 (see the wind farm layout in figure 4.15b). In this row the fourth turbine has a higher power output than the third turbine. The row of turbines starting with turbine 9 does not show this behaviour. From the wind farm layout it can be seen that turbine 32, which is the last turbine in the row starting with turbine 8, has a larger spacing to the turbines on its Southwest side than what turbine 33 has, which is the last turbine in the row starting with turbine 9. This explains the reason why only the row starting with turbine 8 shows the increased power output behaviour. It is caused by the wind farm layout of OWEZ.

Comparing the WDC values of both wind direction cases it can be seen that the very unstable cases have a high WDC value of 0.14 and 0.11 respectively whereas the very stable cases have a lower WDC value which is 0.05 for both cases. These values are higher than expected. WindPRO suggests the WDC values as shown in table 4.4, based on the terrain type. It can be seen that even though the wind farm is located offshore (or in a coastal zone) the very unstable case has a higher WDC value than suggested for large build-up areas. The increase may result from the increase in turbulence due to the temperature difference between sea surface and air. For the recommended offshore WDC the relative production is summarized in table 4.3. The recommended WDC $k = 0.04$ underpredicts the production.

The WDC values can also be compared with the turbulence intensity (TI) occurring at the corresponding 10-minute periods. The mean values of the measured turbulence intensities are shown in table 4.5. The values are consistent per stability class for the different wind directions. According to equation 2.26, found from previous wake measurements, the WDC value can be approximated as half of the TI. This is also shown in the values in WindPRO, as can be seen in table 4.4. In the case of the very stable and very unstable

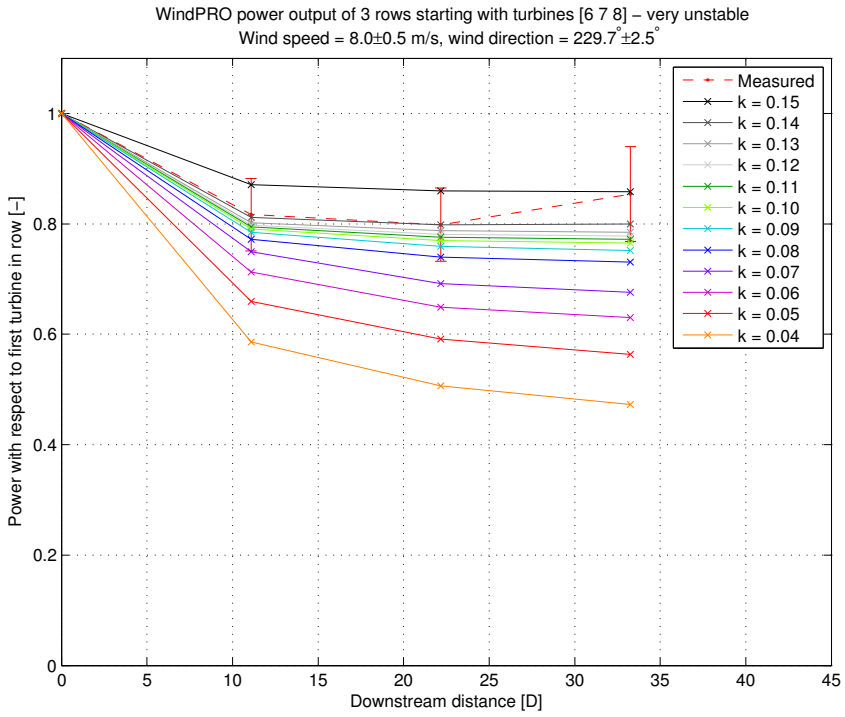

(a) Very unstable

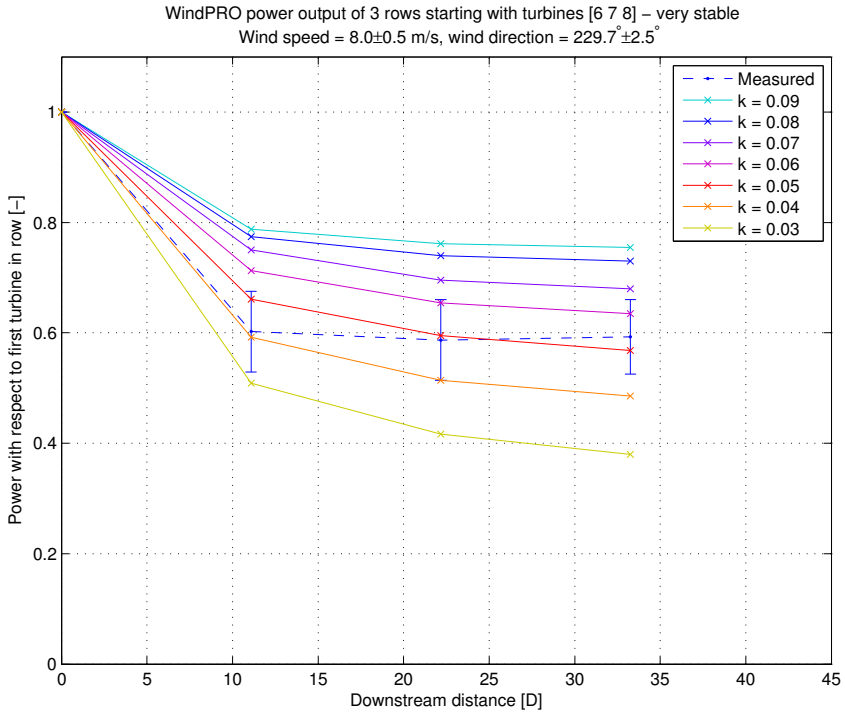

(b) Very stable

Figure 4.30: Simulated wake losses at OWEZ for winds coming from the $229.7° \pm 2.5°$ and wind speeds at 8.0 ± 0.5 m/s for various stability classes. a) very unstable, b) very stable. The error bars represent one standard deviation (half above and half below the mean value).

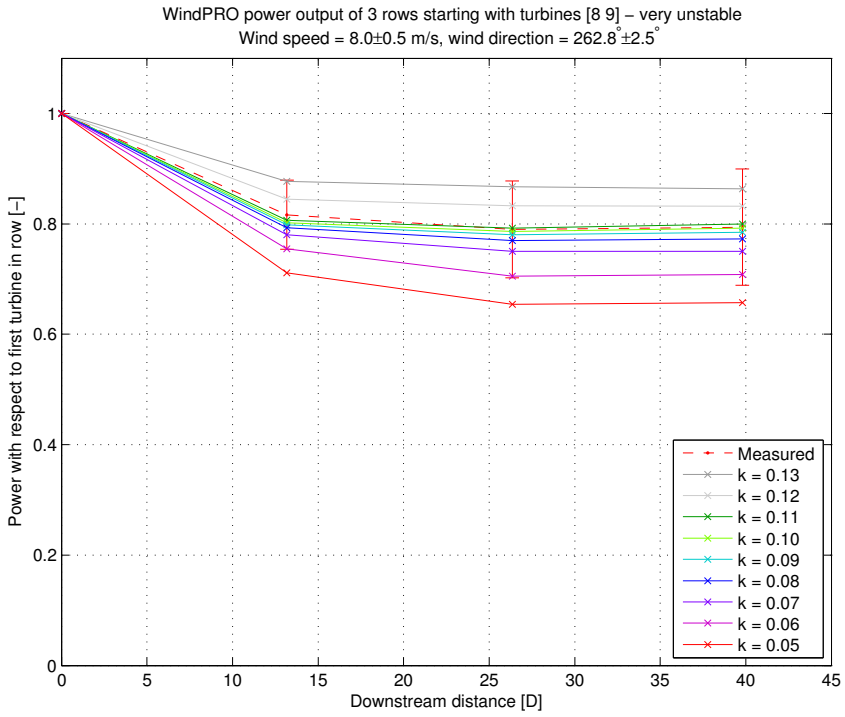

(a) Very unstable

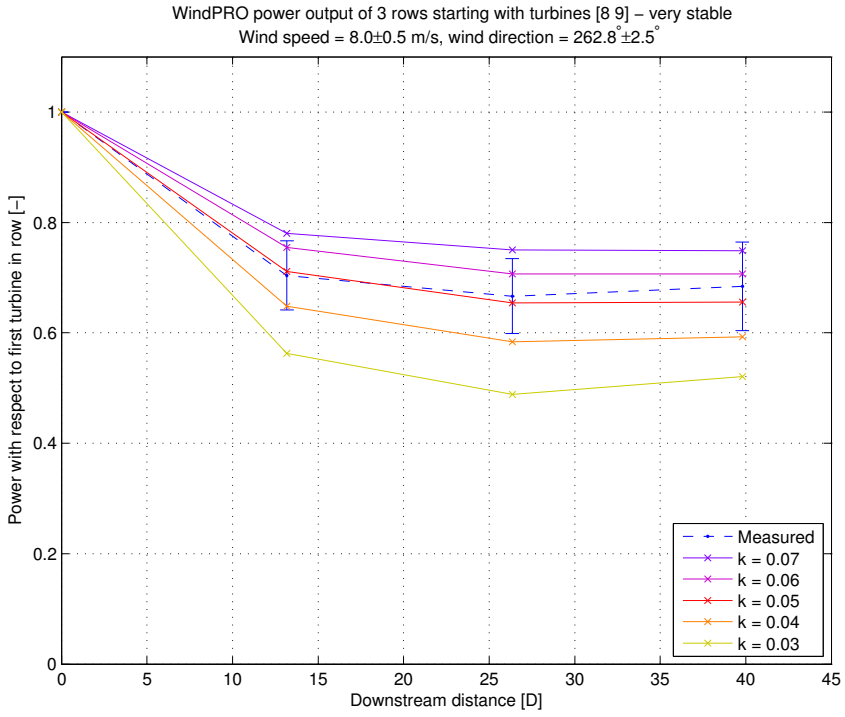

(b) Very stable

Figure 4.31: Simulated wake losses at OWEZ for winds coming from the $262.8° \pm 2.5°$ and wind speeds at 8.0 ± 0.5 m/s for various stability classes. a) very unstable, b) very stable. The error bars represent one standard deviation (half above and half below the mean value).

Table 4.3: Relative production of the second turbine (i.e. first turbine in the wake) with respect to free-stream turbine as obtained from WindPRO simulations using a conventional WDC ($k = 0.04$).

Wind farm	OWEZ	North Hoyle	North Hoyle
Distance	11-13D	4.4D	10-11D
Very unstable ($-200 < L < 0$)	60-65%[a b]	25-30%[c]	50-55%[a]
Very stable ($0 < L < 200$)	60-65%[a b]	25-30%[c]	50-55%[a]

[a] The turbines further downstream lose about 10% normalized production to the next turbine. The decrease in production becomes less for turbines further downstream and is about 1-2% at the last turbine.
[b] For row direction 262.8° a increase in production was observed at the last turbine.
[c] The turbines further downstream lose about 15% normalized production to the next turbine. The decrease in production becomes less for turbines further downstream and is about 1-2% at the last turbine.

Table 4.4: Wake decay constant and turbulence intensity [-] based on terrain type in WindPRO (Thøgersen, 2011).

Terrain classification	WDC	TI
Offshore and water areas	0.040	0.08
Mixed water and land	0.052	0.10
Very open farmland	0.063	0.13
Open farmland	0.075	0.15
Mixed farmland	0.083	0.16
Closed farmland	0.092	0.18
Very closed farmland	0.100	0.21
Large towns and cities	0.108	0.24
Large build-up cities	0.117	0.29

Table 4.5: Mean turbulence intensity values [-] measured at OWEZ per wind direction and stability class, corresponding to the 10-minute periods used in the wake loss plots.

	229.7° (11D)		262.8° (13D)	
	TI	WDC	TI	WDC
Very unstable	0.075	0.14	0.077	0.11
Very stable	0.048	0.05	0.049	0.05

atmosphere the equation does not correspond with that found from the WDC value found from the WindPRO simulations and the TI found from the measurements. The WDC value for the very stable class is about equal to the mean TI value of the 10-minute periods when looking at the same amount of significant digits. The WDC value of the very unstable class is about 1.5-1.9 times the corresponding TI. A reason for the observed differences between WDC and TI between the very stable and very unstable cases might be that in reality there will be more turbulence in the very unstable cases than indicated by the measurements. The cup anemometers only measure horizontal turbulence. In the very unstable case the temperature differences between sea surface and air most probably also cause vertical turbulence though.

4.3.2 North Hoyle

The three wind direction cases discussed in section 4.2.2 are simulated separately in WindPRO.

The results for 348.9° are shown in figure 4.32. It can be seen that the lines for $k = 0.11$ and $k = 0.12$ are close to the very unstable case, whereas the lines for $k = 0.07$ and $k = 0.08$ are close to that for the stable case. In both cases however, the large wake loss at the second turbine in the row is not captured by the model (which is closer to the lines of $k = 0.08$ and $k = 0.03 - 0.04$ respectively). This seems to be a general constraint of the method.

For 258.8° the results are shown in figure 4.33. Again there are lines with WDC values that are close to the measurement. The very unstable case seems to change from $k = 0.09$ towards $k = 0.08$ when moving downstream the row. The very stable line on the other hand is in between the lines with WDC of $k = 0.07$ and $k = 0.06$ and changes towards the line with a WDC value of $k = 0.06$ when moving downstream.

The results for 282.5° are shown in figure 4.34. For the very stable case the results are similar for those at 258.8° in figure 4.33 for the first few turbines. After the third turbine the wake losses for 282.5° are larger, such that the measurements are closer to a k-value 0.01 lower than those found at a wind direction of 258.8°. The very stable line lies between $k = 0.07$ and $k = 0.06$ for the first three turbines, but lies closer to $k = 0.05$ for the last two turbines. The very unstable line lies between WDC values of $k = 0.08$ and $k = 0.07$ for the first three turbines but below $k = 0.07$ for the last two turbines.

Especially for the wind direction of 348.9° and 258.8° WindPRO seems to be able to come quite close to the measured wake losses. As expected, the very unstable cases always need a higher k-value than the very stable cases. For the recommended offshore WDC

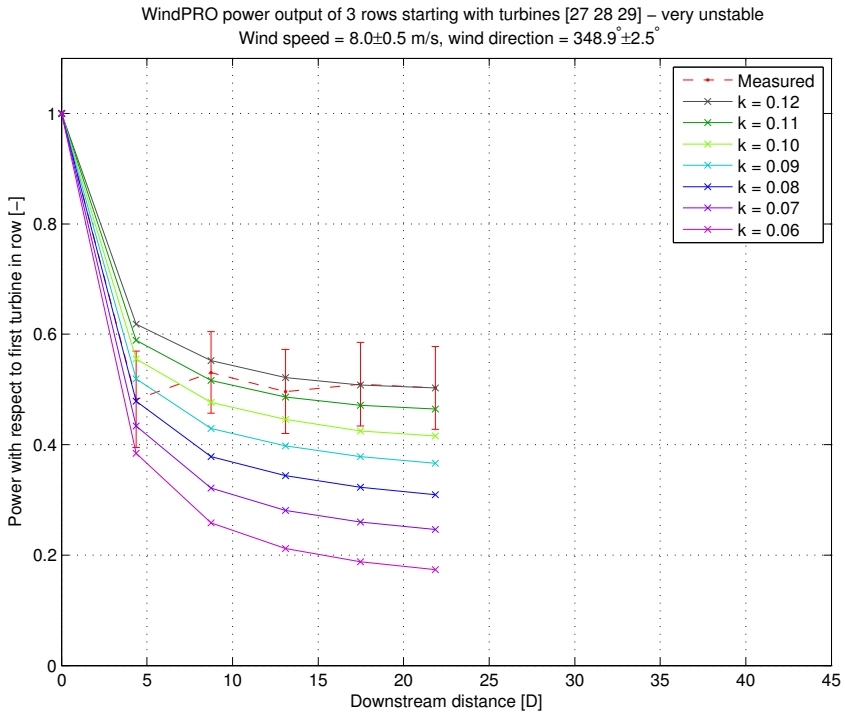

(a) Very unstable

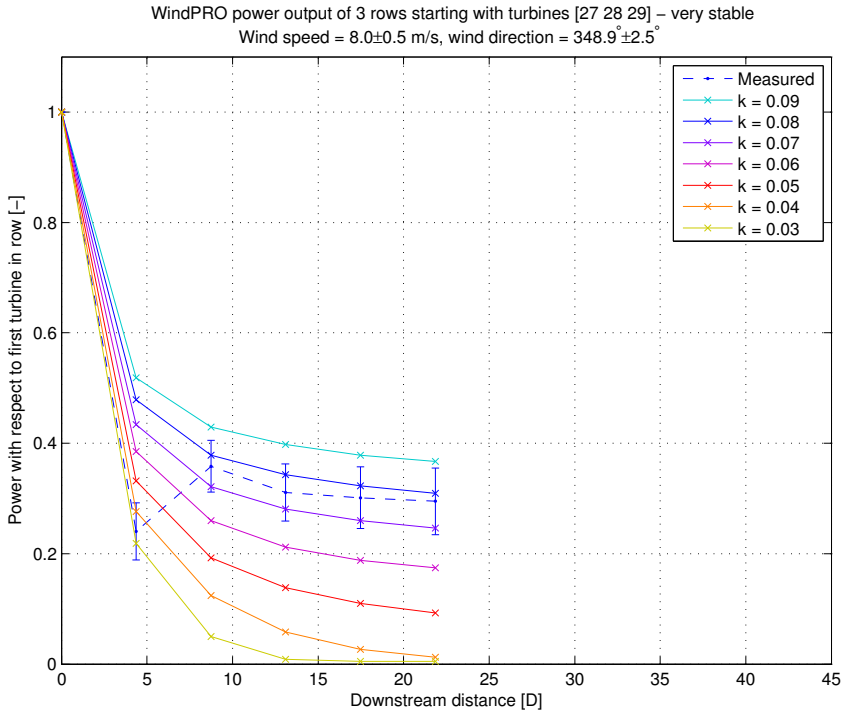

(b) Very stable

Figure 4.32: Simulated wake losses at North Hoyle for winds coming from the $348.9° \pm 2.5°$ and wind speeds at 8.0 ± 0.5 m/s for various stability classes. a) very unstable, b) very stable. The error bars represent one standard deviation (half above and half below the mean value).

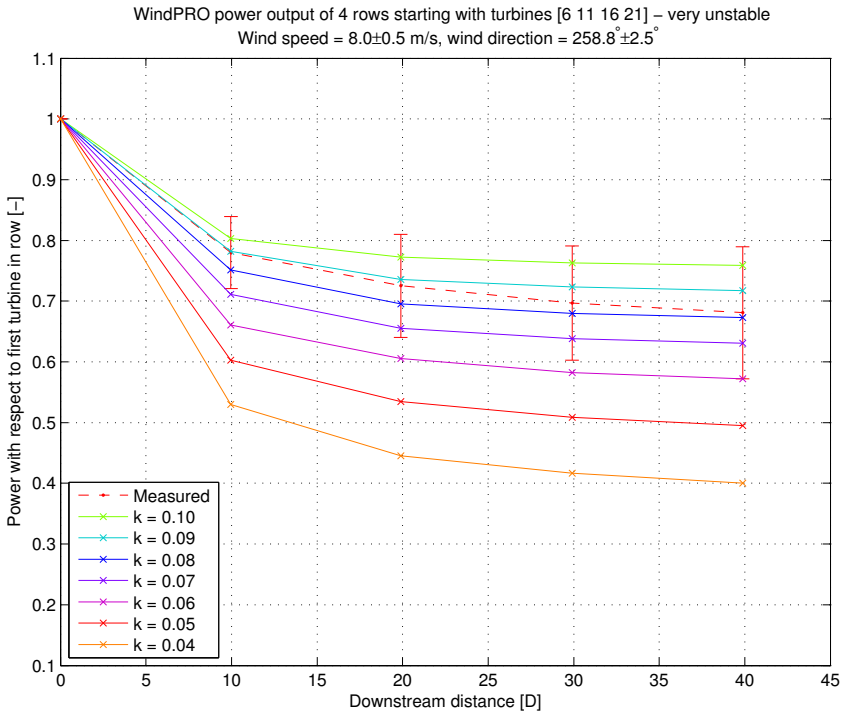

(a) Very unstable

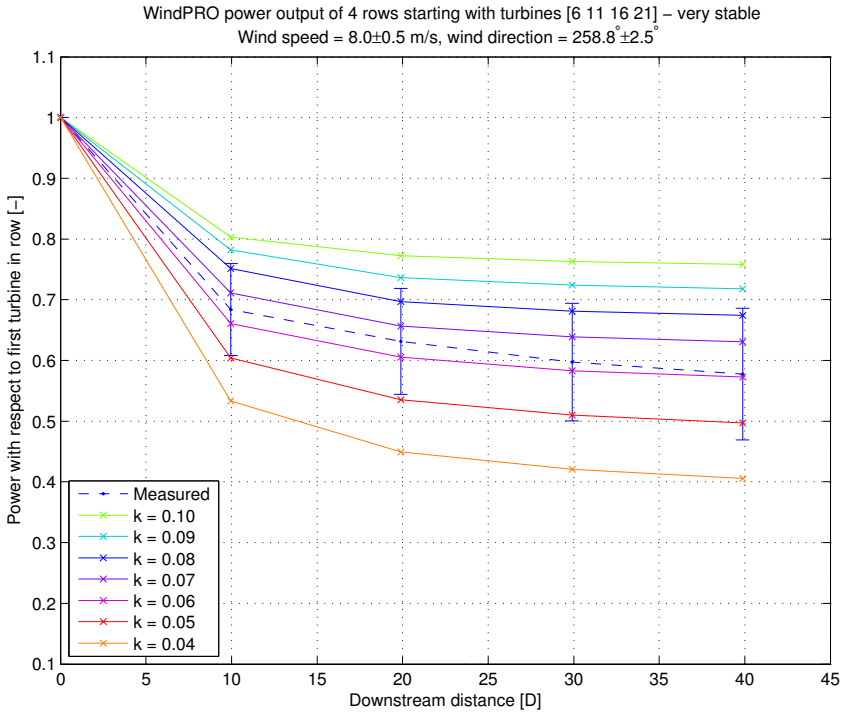

(b) Very stable

Figure 4.33: Simulated wake losses at North Hoyle for winds coming from the $258.8° \pm 2.5°$ and wind speeds at 8.0 ± 0.5 m/s for various stability classes. a) very unstable, b) very stable. The error bars represent one standard deviation (half above and half below the mean value).

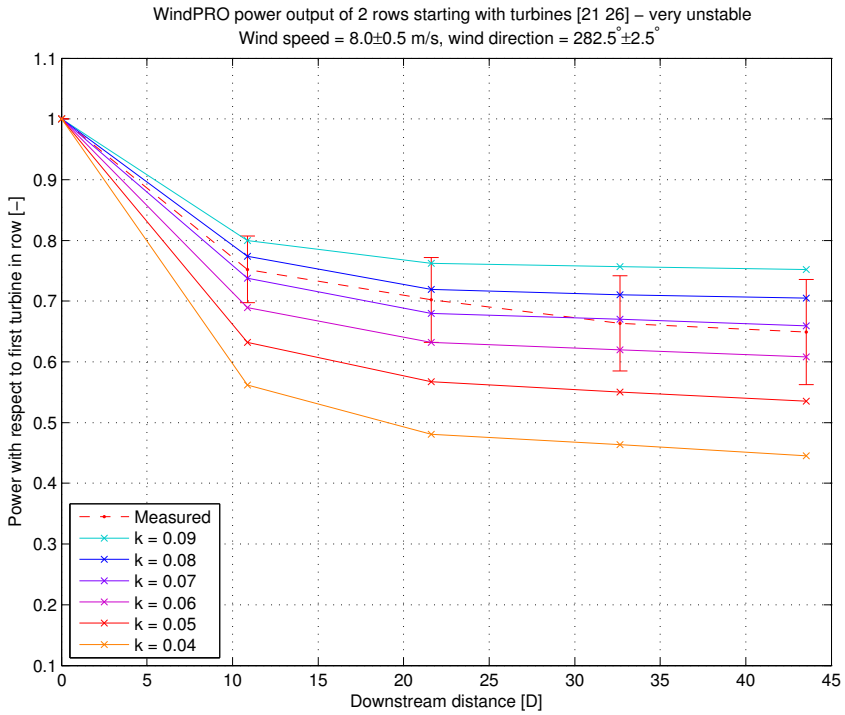

(a) Very unstable

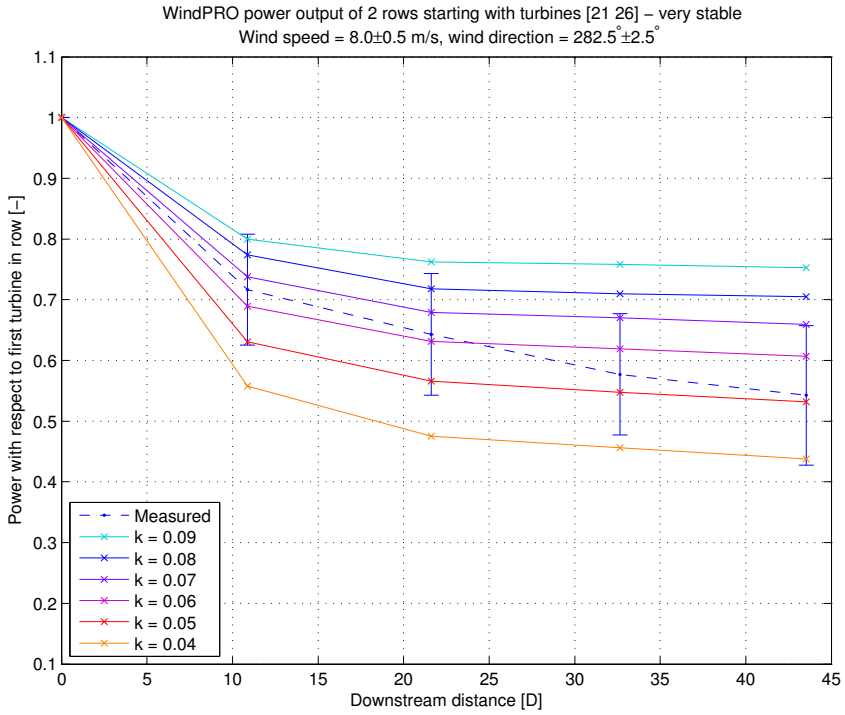

(b) Very stable

Figure 4.34: Simulated wake losses at North Hoyle for winds coming from the $282.5° \pm 2.5°$ and wind speeds at 8.0 ± 0.5 m/s for various stability classes. a) very unstable, b) very stable. The error bars represent one standard deviation (half above and half below the mean value).

Table 4.6: Mean turbulence intensity values [-] measured at North Hoyle per wind direction and stability class, corresponding to the 10-minute periods used in the wake loss plots.

	348.9° (4.4D)		258.8° (10D)		282.5° (11D)	
	TI	WDC	TI	WDC	TI	WDC
Very unstable	0.085	0.11-0.12	0.083	0.08-0.09	0.070	0.07
Very stable	0.062	0.07-0.08	0.067	0.06-0.07	0.056	0.05-0.07

the relative production is summarized in table 4.3. The recommended WDC k = 0.04 underpredicts the production. The turbulence intensity and WDC values are shown in table 4.6. As at OWEZ it can be seen that the TI and WDC values are about equal for the very stable class when looking at the same amount of significant digits. As opposed to OWEZ the TI and WDC values are also about equal for the very unstable class. An exception for both the very stable and the very unstable class is the case with wind direction 348.9° and a spacing of 4.4D. For this case the WDC value seems to be about 1.3-1.4 times the TI value. This might be due to the small turbine spacing, but further investigation would be required to confirm that.

From the results at OWEZ and North Hoyle it can be concluded that the WDC value is about equal to the turbulence intensity for the very stable class. For the very unstable class the results vary between the two wind farms. At OWEZ the WDC value is about 1.5-1.9 times the mean TI value, whereas at North Hoyle the WDC and TI values are about equal for the larger turbine spacings. In all cases it can be said that the WDC value must be higher for the very unstable class than for the very stable class.

4.4 Wind farm power output

In the previous section the WDC values were found per atmospheric stability class for a row of turbines operating simultaneously for various wind direction cases. The WDC values were higher than expected. Here it is investigated whether the WDC values should be similar when investigating the efficiency (normalized power output) of the complete wind farm, when all turbines are operating.

Note that, as explained in chapter 3, data has been filtered out for wind directions for which the metmast is in the wake of the wind farm. Therefore the indicated wind farm efficiencies are not those of the complete wind farm, but only for the investigated sector.

There is a limited number of 10-minute periods available for which the whole wind farm was operating. This number is even smaller when splitting up the data into different stability classes. Using all available measurements in the range of 6-10 m/s (8.0 ± 2.0 m/s) and for all available wind directions the wind farm efficiency is investigated when all turbines are operating. The wind speed range is larger than that is used to investigate the wake losses in section 4.2, but still makes sure that the wakes in the wind farm can be observed (which would not be the case at high wind speeds when all turbines are operating at their rated power) and that the turbines are not pitching their blades yet. The wind direction range is larger as well, and not ±2.5° around the row direction anymore.

The increased wind speed and wind direction sector give a higher number of measurements to base the wind farm efficiency on. At the same time it can be investigated whether the WDC values found for the narrow wind speed and wind direction bins in section 4.2 are also applicable for the full wind farm. This is important since the efficiency of the wind farm is usually required for a range of wind speeds and wind directions and not just for the narrow bins used in section 4.2.

4.4.1 OWEZ

Using all available measurements in the range of 6-10 m/s (8.0 ± 2.0 m/s) and for all available wind directions ($150° - 310°$) the wind farm efficiency of OWEZ is investigated when all turbines are operating. Table 4.7 shows the wind farm efficiency according to the measurements. The wind farm efficiency is determined as the average of the normalized power output of the turbines in the farm, where the power has been normalized with respect to the power of the turbines in the free-stream.

To compare the efficiency of the wind farm according to the WindPRO simulations first a conventional WindPRO simulation is executed. The conventional method is set up using an offshore WDC of 0.04 and the resulting wind farm efficiency is shown in table 4.7. It can be seen that for the very unstable class the conventional result is 3.1% of normalized production lower than the actual production, whereas the conventional simulation of the very stable class indicates a 4.2% higher wind farm efficiency than what is measured. The WindPRO simulations overestimate the very stable case and underestimate the very unstable case.

The conventional method uses 12 30° wind direction bins. WindPRO integrates larger wind directions bins using 1° bins internally. Despite this, the result is a little different and the simulation time varies significantly when only using 12 instead of 360 bins. When only using 12 bins the wind farm efficiency can be some tenths of percent normalized production off (see also appendix F). The results shown here all use 360 1° wind direction bins, even for the conventional calculations.

From table 4.7 it can be seen that as expected the very unstable case needs a higher WDC value than the very stable case. These are however not the same as those observed for the wake losses investigated in section 4.3, see table 4.5. Both the very stable and the very unstable class have a lower WDC value than was found in section 4.3. Moreover, even using a WDC of 0.01 WindPRO still predicts a higher wind farm efficiency for the very stable case than what the measurements indicate.

A reason for the differences between the WDC values found in section 4.3 and those observed here might be due to the small number of wind farm measurements available. Only 50 measurements are available for the very stable class and 44 for the very unstable class. From Sørensen, Thøgersen, and Nielsen (2008) it is known that the total wind farm efficiency using the Jensen wake model (which is used here) is the closest to the measurements, but also that for individual wind directions the simulations might deviate from measurements. Although the WindPRO simulations use the same inflow as that from which the measured wind farm efficiency is obtained, the small amount of data in combination with the deviation for individual wind directions might be a reason for the

Table 4.7: Wind farm efficiency at 8.0 ± 2.0 m/s for wind directions $150° - 310°$ at OWEZ. Only measurements for which all turbines in the wind farm are active are included. It is of interest to see how well the WindPRO simulations model the wind farm efficiency.

Data	Measured	Simulated	Simulated (conventional)
Very unstable	91.0%	91.2%, WDC = 0.08	87.9%, WDC = 0.04
Very stable	87.9%	89.1%, WDC = 0.01	92.1%, WDC = 0.04

different WDC values resulting from the WindPRO simulations as compared to those found in section 4.3.

4.4.2 North Hoyle

Using all available measurements in the range of 6-10 m/s (8.0 ± 2.0 m/s) and for all available wind directions ($170° - 40°$) the wind farm efficiency of North Hoyle is investigated when all turbines are operating. For North Hoyle a higher number of measurements is available, being 396 for the very stable class and 608 for the very unstable class. Table 4.8 shows the wind farm efficiency according to the measurements. The wind farm efficiency is determined as the average of the normalized power output of the turbines in the farm, where the power has been normalized with respect to the power of the turbines in the free-stream.

The first thing that attracts the attention is that the efficiency of the wind farm seems to be higher during the very stable class than during the very unstable class. From the previous sections of this study it can be understood that this is not expected. However, there is a simple explanation to this apparent inadequacy: the wind speeds, wind directions and atmospheric stabilities are not represented equally in the shown result, as the result is based on the available measurements only. This means that in the very stable class there might for instance be more occurrences of wind not being aligned with the row direction, resulting in lower wake losses and thus an apparent higher wind farm efficiency, whereas the very unstable class might have more occurrences of wind along the rows of turbines, resulting in higher wake losses and thus a lower wind farm efficiency. This is exactly the reason why in section 4.2 a small wind speed bin and a narrow wind direction sector where chosen to investigate the wake losses, and when this was done the results were indeed as expected (i.e. very unstable has higher power output/lower wake losses than very stable cases). In this section it is only of interest to see how well the WindPRO simulations model the efficiency (i.e. total power output/wake losses) of the wind farm.

The simulated wind farm efficiencies using the conventional offshore WDC value of 0.04 are shown in the table. As expected these efficiencies are lower than for the higher WDC values and than for the measurements. The wind farm efficiency using the conventional WDC of 0.04 is respectively 7.0% and 5.6% normalized production lower for the very unstable and very stable case. This indicates that the very unstable class is underestimated using the conventional WDC value, but also that the very stable case is underestimated. The very unstable case is underestimated more than the very stable case.

From the table it can be seen that the very unstable case still needs a higher WDC value

Table 4.8: Wind farm efficiency at 8.0 ± 0.5 m/s for wind directions $170° - 40°$ at North Hoyle. Only measurements for which all turbines in the wind farm are active are included. It is of interest to see how well the WindPRO simulations model the wind farm efficiency.

Data	Measured	Simulated	Simulated (conventional)
Very unstable	87.4%	87.5%, WDC = 0.13	80.4%, WDC = 0.04
Very stable	88.3%	88.4%, WDC = 0.08	82.7%, WDC = 0.04

than the very stable case. It can also be seen that these are close to the ones observed for the wake losses investigated in section 4.2, see table 4.6. It is interesting that the WDC value is closest to those for the 348.9° ($4.4D$) case.

With the simulated wind farm efficiency being close to the observed efficiency a method to obtain the total wind farm efficiency could be to multiply the wind farm efficiencies of the very stable and very unstable class with their frequency of occurrence in the total dataset. Summing the weighted wind farm efficiencies of the very stable and very unstable classes should give an approximate wind farm efficiency close to the wind farm efficiency of the complete wind farm for all stability classes. For North Hoyle this would result in:

$$\eta_{farm} = \frac{608}{608+396} \cdot 87.5\% + \frac{398}{608+396} \cdot 88.4\% = 87.9\% \tag{4.1}$$

This is close to the measured total wind farm efficiency of 86.8% considering only the two most extreme stability classes have been used for this calculation. It is expected that the approximation improves upon including the near-neutral class. However, the most important factor is getting the WDC right, as it will influence the wind farm efficiency obtained from WindPRO.

Concluding, it can be said that the WDC values as found in section 4.3 seem to be close to the ones that could be used to find the wind farm efficiency. For the complete wind farm similar WDC values give wind farm efficiencies close to those indicated by the measurements. Deviations can be explained by low amount of data. What is certain is that for very unstable classes higher WDC values should be used in WindPRO than for very stable classes.

Chapter 5

Conclusions and recommendations

The conclusions of the study are reported in this chapter. Recommendations found during the study are also reported.

5.1 Primary conclusions

In the introduction of the report the project objectives were defined. The conclusions regarding each point are described here.

Quantify the effect of atmospheric stability on wind farm power production

At OWEZ, for the 5 class stability distribution, each stability bin occurs roughly 20% of the time. At North Hoyle, the very unstable class is apparent to occur about twice as much as all other bins. The results at OWEZ are similar to those found by Sathe (2009). North Hoyle has not been reported in literature yet.

Atmospheric stability varies with both wind speed and wind direction. Very unstable cases can be observed up to around 15-16 m/s. Very stable cases remain visible up to high wind speeds (above 20 m/s), although the number of very stable cases decreases with wind speed. The number of near-neutral (unstable, neutral and unstable) occurrences increases with wind speed. Variation of atmospheric stability with wind direction is observed and is believed to result from the warm/cold air corresponding with winds from the South/North respectively (the sea temperature shows little variation with wind direction). Variation of turbulence intensity with atmospheric stability can be observed, although the difference between the classes is less clear as for the temperature difference. The very unstable class shows the highest turbulence intensity.

Production data from the turbines are studied to establish the influence of the stability on the wake losses. The data is investigated for the row direction of the turbines ±2.5°,

resulting in the largest wake losses, and for a wind speed of 8.0 ± 0.5 m/s to make sure the turbines are not pitching their blades yet. It is found that in very unstable cases the production of the wind farm is higher than in near-neutral cases, and in near-neutral cases the production is higher than in very stable cases. This is as expected. When the atmosphere gets less stable, turbulence increases and the mixing of higher energy air into the wake is increased. Power output for neutral cases is in between those of very stable and very unstable, but the precise level cannot be determined due to difficulties in sorting on stability class.

The results agree with those found by Barthelmie et al. (2011); Hansen et al. (2012) at the Horns Rev wind farm and by Barthelmie et al. (2007, 2011) at the Nysted wind farm. The difference in relative production between the very stable and very unstable classes is 10-20%. As opposed to what is stated in Barthelmie et al. (2011); Hansen et al. (2012) a difference between the unstable and near-neutral classes is observed in the current study. It should be noted that the atmospheric stability classes, wind speed and/or wind direction bins are not agreed upon in the different research projects and vary between the different projects and from the one used in this project.

Compare the measurements with park/wake models with regards to predicting the effect of atmospheric stability on the production

The wind farms have been modelled in WindPRO and power output has been simulated using the Jensen wake model. The wake losses in the model are governed by the wake decay constant (WDC) k. At a downstream distance x, the width of the rectangular wake equals $D + 2kx$ and the wake speed is found by conservation of mass. The recommended WDC value is $k \approx 0.5I$. For offshore the recommended WDC is $k = 0.04$. The recommended WDC underpredicts the production.

The model does not take into account the effect of atmospheric stability on the production by default. Since turbulence in a wind farm is related to the atmospheric stability and since the WDC is related to the amount of turbulence, the effect of the atmospheric stability on the predicted production can be taken into account by adapting the WDC. Comparing the measurements with the model is therefore done by adapting the WDC and investigating for which WDC the measured and predicted wake losses agree best. See the next item.

Find out if and how the used prediction models can be modified in a simple way to improve predictions

The wake losses in the model are governed by the wake decay constant (WDC). Since turbulence in a wind farm is related to the atmospheric stability and since the WDC is related to the amount of turbulence, the effect of the atmospheric stability on the predicted production can be taken into account by adapting the WDC.

It is found that the WDC should be equal to or greater than the turbulence intensity (TI). The very stable cases require a WDC in the order of their turbulence intensity (TI). For the very unstable class the results vary between the two wind farms. At OWEZ the WDC value is about 1.5-1.9 times the mean TI value, whereas at North Hoyle the WDC

and TI values are about equal for the larger turbine spacings. For the small spacing at North Hoyle ($4.4D$) the WDC values are higher. In all cases the WDC value should be higher for the very unstable class than for the very stable class.

Simulating the wind farm efficiency shows that at North Hoyle similar WDC values can be used as those observed in the wake loss analysis in a row of turbines. For the very stable case the WDC is about 0.08 and for the very unstable case a WDC of 0.13 is obtained. For OWEZ the results are less clear which is thought to result from the small amount of data available.

A method to obtain the total wind farm efficiency could be to multiply the simulated wind farm efficiencies of the very stable and very unstable class with their frequency of occurrence. Summing these weighted efficiencies should give an approximate wind farm efficiency close to that of the complete wind farm for all stability classes. It is expected that the approximation improves upon including the near-neutral class. However, the most important factor is getting the WDC right, as it will influence the wind farm efficiency obtained from WindPRO.

5.2 Secondary conclusions

Other conclusions obtained during the study that are not directly related to the objectives are reported in this section:

1a. The dominant parameter influencing the stability parameter and thus the stability classification is the temperature difference between the sea surface and the ambient temperature. For example, the temperature interval for neutral stability is only 0.2 K. Therefore it is important to measure this temperature difference accurately.

1b. The temperature gradient causes the largest errors in the atmospheric stability measurement. Next to that it also causes the errors that are on average the worst (i.e. the stability lies away the furthest from where it is supposed to be).

1c. The near-neutral classes are most sensitive to measurement errors in the temperature gradient, resulting in an offset in the bulk Richardson number and hence in stability classification.

1d. Ideally one would like to measure the true sea surface temperature, but in reality this proves to be difficult when using a fixed metmast. Based on the fact that the sea surface temperature sensor at OWEZ is 3.8 metres below mean sea level and that the difference between the sea temperature below one metre depth and that at the sea surface can vary between -1.0 and 1.0 K (Schluessel et al., 1990) with a mean difference in the order of tenths of degrees, it is proposed that a correction should be applied. Re-analysis data from ECMWF is available, but is concluded to have a too coarse grid for this purpose.

2. During the analysis it was found that wake loss data can be obtained more accurately when using the wind speed and wind direction measurements of the turbines in the first column (i.e. in the free-stream), as compared to those from the metmast. The

metmast is a point measurement, and the wind speed and wind direction are most probably not the same over the whole wind farm.

3a. From the Vestas mesoscale model (VSU) data is obtained to compare to the metmast data. It is found that the stability distribution following from mesoscale data is similar to that of the metmast data. The mesoscale wind speed and direction can however not replace that of the metmast or turbines when investigating the wake losses as it is found that the wake losses do not closely correspond with the wake losses using metmast and/or turbines.

3b. When the mesoscale wind speed, ambient temperature and sea surface temperature are adapted using the correlation with the metmast data, the distribution of atmospheric stability becomes closer to that using the metmast data. However, results are varying regarding how well the comparison between the metmast and mesoscale wake losses has improved.

4a. For the cases investigated it is found that the park efficiency obtained from WindPRO varies by a few tenths of percent when either taking 12 30° sectors or 360 1° sectors. However, the simulation time is about 8 times larger when 360 bins are modelled instead of 12.

4b. At North Hoyle the largest wake loss in WindPRO is 1° off from the row direction. Secondly, the power output increases faster (i.e. the wake losses decrease faster) when increasing the wind direction as compared to decreasing the wind direction. These observations are unexpected and correspondence with EMD/WindPRO has not resulted in an explanation for this.

5.3 Recommendations

The recommendations resulting from the study are reported here.

5.3.1 Best practices

The following recommendations of best practices result from the study:

1. Although maybe trivial, timestamps of datasets should be checked before using them. In the current study not all datasets were stored in the same timezone, even when looking at a single wind farm. Next to that it is recommended to not use summertime for storing data as had been done in some of the datasets that are used in this project. It should also be checked whether the timestamp of the 10-minute period data is taken at the start or at the end of the period.

2. During the analysis it was found that wake loss data can be obtained more accurately when using the wind speed and wind direction measurements of the turbines in the first column (i.e. in the free-stream), as compared to those from the metmast. The metmast is a point measurement, and the wind speed and wind direction are most probably not the same over the whole wind farm. It is therefore recommended to use the first turbines when studying wake losses in a row of turbines.

3. Regarding the wake losses, it is recommended to only look at three stability classes so that there will be enough data per class. It could even be recommended to only look at the wake losses of the very stable and very unstable class, as these classes are least sensitive to measurement errors to determine the atmospheric stability and since they show the highest and lowest wake losses (i.e. lowest and highest production) respectively. Furthermore, it is recommended to investigate the data for the row direction of the turbines ±2.5°, resulting in the largest wake losses, and for a wind speed of 8 m/s ± 0.5 m/s to make sure the turbines are not pitching their blades yet.

5.3.2 Further research

Further research is suggested in the following areas:

1. It is recommended to look further into possible temperature offsets in the SST measurement. The sea surface temperature is required, but since the water temperature sensor on a metmast is fixed at a certain depth it measures the water temperature below the sea surface. It is known that this gives a temperature difference with the real SST and this again influences the atmospheric stability. It is also recommended to look for alternative ways of measuring the SST on-site that do not have the problem that they measure the SST at the wrong depth, e.g. a floating buoy. It could also be investigated whether it is possible to measure the temperature difference directly, as then only one sensor's accuracy is involved in the temperature gradient (as opposed to both that of the sea surface and ambient temperature now).

2. It is recommended to model the sea surface temperature in Vestas' mesoscale model VSU. In this study the sea surface temperature from the mesoscale data was approximated using the ambient temperature at 2 m, but the comparison with the measurements could become better when using the sea surface temperature and/or temperature difference directly from the mesoscale model.

3. It is recommended to do similar research as in this study but at different wind speeds.

4. It should be investigated how well WindPRO simulates wind farm efficiency over all wind speeds and wind directions and whether errors are cancelled against each other when the average is taken (e.g. by partly underpredicting and partly overpredicting production).

5. There are differences between the two investigated wind farms regarding wake losses and regarding choice of WDC in WindPRO and with those suggested by EMD/WindPRO. It is recommended to further investigate measurements and simulations of other wind farms and the relation between WDC and TI.

6. It is recommended to look at including the influence of vertical turbulence (e.g. using turbulent kinetic energy as done by (Wharton & Lundquist, 2010, 2011)). Cup anemometers only measure horizontal (i.e. two-dimensional) turbulence intensity. However, the temperature differences between sea surface and air most probably also

cause vertical turbulence. The WDC values obtained for the wake losses are close to the measured turbulence intensities for the very stable class. For the very unstable class the WDC values are higher than the turbulence intensities. It is interesting to see how the WDC and TI compare when the vertical turbulence would also be included in the TI. For the very stable class not much difference in TI is expected, as turbulent movements are suppressed. For the very unstable class the TI is expected to increase upon including the vertical turbulence. They may therefore compare better with the WDC values found for the very unstable class, which would mean that the WDC value to be chosen for a certain stability class should be close to the (three-dimensional) turbulence intensity corresponding to that class. Further research is necessary to look into this hypothesis. In case a relationship between WDC and TI is found (and since TI varies with atmospheric stability), the WDC can be based on (three-dimensional) TI and the classification of atmospheric stability is not necessary anymore.

References

Alblas, L. (2011, November). *Literature research - Comparison of available park/wake models and the effect of atmospheric stability on the energy production.*

Barthelmie, R. (1999, March). The effects of atmospheric stability on coastal wind climates. *Meteorological Applications*, *6*(1), 39-47.

Barthelmie, R., Courtney, M., Højstrup, J., & Larsen, S. (1996, September). Meteorological aspects of offshore wind energy: Observations from the Vindeby wind farm. *Journal of Wind Engineering and Industrial Aerodynamics*, *62*(2-3), 191-211.

Barthelmie, R., Courtney, M., Lange, B., Nielsen, M., & Sempreviva, A. (1999, March). Offshore wind resources at Danish measurement sites. In *Proceedings of european wind energy conference* (p. 1101-1104). Nice, France.

Barthelmie, R., Folkerts, L., Larsen, G., Rados, K., Pryor, S., Frandsen, S., et al. (2006, July). Comparison of wake model simulations with offshore wind turbine wake profiles measured by sodar. *Journal of Atmospheric and Oceanic Technology*, *23*(7), 888-901.

Barthelmie, R., Frandsen, S., Réthoré, P., & Jensen, L. (2007, December). Analysis of atmopsheric impacts on the development of wind turbine wakes at the Nysted wind farm. In *Proceedings of the european offshore wind conference and exhibition.* Berlin, Germany.

Barthelmie, R., Hansen, K., Frandsen, S., Rathmann, O., Schepers, J., Schlez, W., et al. (2009, July). Modelling and measuring flow and wind turbine wakes in large wind farms offshore. *Wind Energy*, *12*(5), 431-444.

Barthelmie, R., Hansen, K., & Pryor, S. (2011, July). Meteorological controls on wind turbine wakes. In *Proceedings of 13th international conference on wind engineering.* Amsterdam, The Netherlands.

Barthelmie, R., Hansen, O., Enevoldsen, K., Højstrup, J., Frandsen, S., Pryor, S., et al. (2005, May). Ten years of meteorological measurements for offshore wind farms. *Journal of Solar Energy Engineering*, *127*(2), 170-176.

Barthelmie, R., & Jensen, L. (2010, September). Evaluation of wind farm efficiency and wind turbine wakes at the Nysted offshore wind farm. *Wind Energy*, *13*(6), 573-586.

Barthelmie, R., Larsen, G., Pryor, S., Jørgensen, H., Bergström, H., Schlez, W., et al. (2004, July). ENDOW (Efficient Development of Offshore Wind Farms): Modelling wake and boundary layer interactions. *Wind Energy*, *7*(3), 225-245.

Barthelmie, R., Pryor, S., Frandsen, S., Hansen, K., Schepers, J., Rados, K., et al. (2010, August). Quantifying the impact of wind turbine wakes on power output at offshore wind farms. *Journal of Atmospheric and Oceanic Technology*, *27*(8), 1302-1317.

Campbell Scientific. (1999, June). *107, 108 and 105T temperature probes.*

Eecen, P., Wagenaar, J., & Bot, E. (2011, June). Offshore wind farms: losses and turbulence in wakes. modeling and validation. In *Proceedings of gotland wake conference* (p. 48-53). Visby, Sweden.

Elliot, D., & Cadogan, J. (1990, September). Effects of wind shear and turbulence on wind turbine power curves. In *European community wind energy conference and exhibition.* Madrid, Spain.

Frandsen, S., & Madsen, P. (2003, April). Spatially average of turbulence intensity inside

large wind turbine arrays. In *European seminar on offshore wind energy in the mediterranean and other european seas.* Naples, Italy.

Google Earth. (2012, February).

Grachev, A., & Fairall, C. (1997, April). Dependence of the Monin-Obukhov stability parameter on the bulk Richardson number over the ocean. *Journal of Applied Meteorology*, *36*(4), 406-414.

Hansen, K., Barthelmie, R., Jensen, L., & Sommer, A. (2012, January). The impact of turbulence intensity and atmospheric stability on power deficits due to wind turbine wakes at Horns Rev wind farm. *Wind Energy*, *15*(1), 183-196.

Jensen, N. (1983, November). *A note on wind generator interaction* (Tech. Rep. No. Risø-M-2411). Roskilde, Denmark: Risø National Laboratory.

Katic, I., & Højstrup, J. (1986, October). A simple model for cluster efficiency. In *Proceedings of european wind energy association conference and exhibition* (p. 407-409). Rome, Italy.

Kouwenhoven, H. (2007, October). *User manual data files meteorological mast NoordzeeWind* (2.0 ed.).

Lange, B., Johnson, H., Larsen, S., Højstrup, J., Kofoed-Hansen, H., & Yelland, M. (2004, June). On detection of a wave age dependency for the sea surface roughness. *Journal of Physical Oceanography*, *34*(6), 1441-1458.

Lange, B., Larsen, S., Højstrup, J., & Barthelmie, R. (2004a, September). Importance of thermal effects and sea surface roughness for offshore wind resource assessment. *Journal of Wind Engineering and Industrial Aerodynamics*, *92*(11), 959-988.

Lange, B., Larsen, S., Højstrup, J., & Barthelmie, R. (2004b, September). The influence of thermal effects on the wind speed profile of the coastal marine boundary layer. *Boundary-Layer Meteorology*, *112*(3), 587-617.

Lange, B., Waldl, H.-P., Guerrero, A., Heinemann, D., & Barthelmie, R. (2003, January-March). Modelling of offshore wind turbine wakes with the wind farm program FLaP. *Wind Energy*, *6*(1), 87-104.

Manwell, J., McGowan, J., & Rogers, A. (2009). *Wind energy explained: theory, design and application* (2nd ed.). United Kingdom: John Wiley & Sons Ltd.

Méchali, M., Barthelmie, R., Frandsen, S., Jensen, L., & Réthoré, P. (2006, February-March). Wake effects at Horns Rev and their influence on energy production. In *Proceedings of the european wind energy conference and exhibition.* Athens, Greece.

Motta, M., Barthelmie, R., & Vølund, P. (2005, April/June). The influence of non-logarithmic wind speed profiles on potential power output at Danish offshore sites. *Wind Energy*, *8*(2), 219-236.

Nielsen Nissen, J. (2008). *On the application of a numerical model to simulate the coastal boundary layer.* Unpublished doctoral dissertation, University of Copenhagen.

Nielsen Nissen, J. (2012). *Personal correspondence.*

Rados, K., Larsen, G., Barthelmie, R., Schlez, W., Lange, B., Schepers, J., et al. (2001, September). Comparison of wake models with data for offshore windfarms. *Wind Engineering*, *25*(5), 271-280.

Rohatgi, J., & Barbezier, G. (1999, January-April). Wind turbulence and atmospheric stability - their effect on wind turbine output. *Renewable Energy*, *16*(1-4), 908-911.

Sathe, A. (2009, December). *Project site data - OWEZ data analysis* (Tech. Rep. No. 2004-012). We@Sea.

Sathe, A., & Bierbooms, W. (2007, June). Influence of different wind profiles due to

varying atmospheric stability on the fatigue life of wind turbines. In *Journal of physics conference series* (Vols. 75, article 012056). Lyngby, Denmark.

Sathe, A., Gryning, S.-E., & Peña, A. (2011, February). Comparison of the atmospheric stability and wind profiles at two wind farm sites over a long marine fetch in the North Sea. *Wind Energy*, *DOI: 10.1002/we.456*.

Schluessel, P., Emery, W., Grassl, H., & Mammen, T. (1990, August). On the bulk-skin temperature difference and its impact on satellite remote sensing of sea surface temperature. *Journal of Geophysical Research*, *95*(C8), 13341-13356.

Sørensen, T., Thøgersen, M. L., & Nielsen, P. (2008, February). *Adapting and calibration of existing wake models to meet the conditions inside offshore wind farms* (Tech. Rep.). Aalborg, Denmark: EMD International A/S.

Stull, R. (1988). *An introduction to boundary layer meteorology.* Kluwer Academic Publishers.

Stull, R. (2000). *Meteorology for scientists and engineers* (2nd ed.). USA: Brooks/Cole Pacific Grove.

Sumner, J., & Masson, C. (2006, November). Influence of atmospheric stability on wind turbine power performance curves. *Journal of Solar Energy Engineering*, *128*, 531-538.

Thøgersen, M. L. (2011, January). WindPRO / PARK - Introduction to wind turbine wake modelling and wake generated turbulence [Computer software manual]. Aalborg, Denmark.

Thomsen, K., & Sørensen, P. (1999, March). Fatigue loads for wind turbines operating in wakes. *Journal of Wind Engineering and Industrial Aerodynamics*, *80*(1-2), 121-136.

Troen, I., & Petersen, E. (1989). *European wind atlas.* Roskilde, Denmark: Risø National Laboratory.

Vector Instruments. (n.d.). *Low power A100L2 anemometer.*

Veldkamp, H. (2011-2012). *Personal correspondence.*

Vestas Wind Systems A/S. (n.d.). *Images.* Retrieved 29 September 2011, from http://www.vestas.com/en/media/images.aspx

Vestas Wind Systems A/S. (2011a). *Project description MTSC001 - Comparison of available park/wake models and the effect of atmospheric stability on the energy production.*

Vestas Wind Systems A/S. (2011b). *V164-7.0MW product brochure.* Retrieved 18 September 2011, from http://www.vestas.com/en/wind-power-plants/procurement/turbine-overview/v164-7.0mw-offshore.aspx#/vestas-univers

Vestas Wind Systems A/S. (2011c). *V80-2.0MW product brochure.* Retrieved 1 October 2011, from http://nozebra.ipapercms.dk/Vestas/Communication/Productbrochure/V80/V80UK/

Wharton, S., & Lundquist, J. (2010, February). *Atmosperic stability impacts on power curves of tall wind turbines - An analysis of a West Coast North American wind farm* (Tech. Rep. No. LLNL-TR-424425). USA: Lawrence Livermore National Laboratory.

Wharton, S., & Lundquist, J. (2011, April). Assessing atmospheric stability and its impacts on rotor-disk wind characteristics at an onshore wind farm. *Wind Energy*, *DOI: 10.1002/we.483*.

Wijk, A. van, Beljaars, A., Holtslag, A., & Turkenburg, W. (1990, April). Evaluation

of stability corrections in wind speed profiles over the north sea. *Journal of Wind Engineering and Industrial Aerodynamics*, *33*(3), 551-566.

Wind turbines – part 12-1: Power performance measurements of electricity producing wind turbines (2nd (committee draft) ed.) [Computer software manual]. (2011, November).

Zagar, M. (2011-2012). *Personal correspondence regarding VSU.*

Appendix A

Derivation of Jensen model for wind turbine wakes

The method of calculating the wake as applied in (amongst others) WindPRO is based on the model by Jensen (1983) and further developed by Katic and Højstrup (1986), and is one of the most parameterized forms. It is based on the balance of mass. The model will be introduced for a single wake, after which the combined effect of multiple wakes is considered.

A.1 Single wake

Assume that the wake is axi-symmetrical, such that it has a circular shape of diameter D_w and that it has a uniform wake velocity U_w. Furthermore, it is assumed that the wake expands linearly on either side with a factor k, called the wake decay constant (or wake expansion factor). Since it is assumed that the wake velocity is uniform for each downstream distance, a "top hat" wake wind speed profile results. The mass flow through the wake area will then be:

$$\dot{m}_w = \rho \frac{\pi}{4} D_w^2 U_w \tag{A.1}$$

where ρ is the air density.

Due to the wake expansion the rotor diameter D is smaller than the wake diameter D_w. The air just behind the rotor, but being a fully developed wake already, is assumed to have velocity U_r. Outside the rotor area, the air has free-stream velocity U. This is visualized in figure A.1. The mass flow through an equal disc area D_w at the rotor plane thus becomes:

$$\dot{m} = \rho \frac{\pi}{4} D^2 U_r + \rho \frac{\pi}{4} \left(D_w^2 - D^2 \right) U \tag{A.2}$$

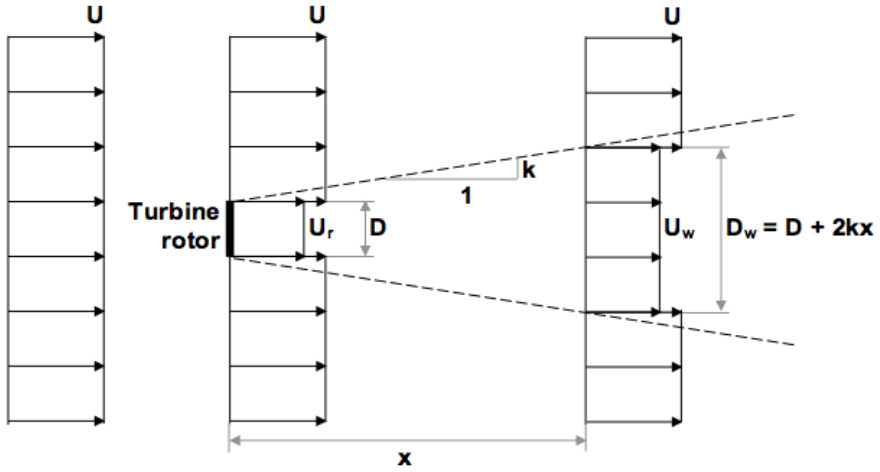

Figure A.1: Visualization of the "top hat" wake wind speed profile applied in the model by Jensen (after Thøgersen, 2011).

It is assumed that the air flows through a cylindrical control volume with the diameter equal to the wake diameter. Hence, it must hold that the mass flow through the wake diameter is conserved, such that:

$$\dot{m} = \dot{m}_w \tag{A.3}$$

Substituting the relations for the mass flow gives:

$$D^2 U_r + \left(D_w^2 - D^2\right) U = D_w^2 U_w \tag{A.4}$$

where similar terms have been removed. Rewriting this equation gives:

$$D^2 \left(U_r - U\right) + D_w^2 U = D_w^2 U_w \tag{A.5}$$

$$-D^2 \frac{U - U_r}{U} + D_w^2 = D_w^2 \frac{U_w}{U} \tag{A.6}$$

$$\frac{U_w}{U} = 1 - \left(\frac{D}{D_w}\right)^2 \frac{U - U_r}{U} \tag{A.7}$$

The wake diameter D_w at a downstream distance x can be expressed using the rotor diameter D and the wake decay constant k:

$$D_w = D + 2kx \tag{A.8}$$

Furthermore, the axial induction factor a is defined as usual, as the fractional decrease in wind velocity between the free-stream and the rotor plane (Manwell et al., 2009). In

a fully developed wake behind the rotor the flow velocity has decreased with twice the induction factor:

$$U_r = U\,(1 - 2a) \tag{A.9}$$

such that:

$$2a = \frac{U - U_r}{U} \tag{A.10}$$

Using the relations for D_w and $2a$, the ratio U_w/U can be rewritten as:

$$\frac{U_w}{U} = 1 - 2a\left(\frac{D}{D + 2kx}\right)^2 \tag{A.11}$$

The induction factor a can be written as a function of the thrust coefficient of the wind turbine:

$$C_T = 4a\,(1 - a) \tag{A.12}$$

which can be rewritten as:

$$(1 - 2a)^2 = 1 - C_T \tag{A.13}$$

and so:

$$2a = 1 - \sqrt{1 - C_T} \tag{A.14}$$

Hence, the ratio of wind speed in the wake and free-stream wind speed becomes:

$$\frac{U_w}{U} = 1 - \left(1 - \sqrt{1 - C_T}\right)\left(\frac{D}{D + 2kx}\right)^2 \tag{A.15}$$

and the wake velocity can thus be determined by:

$$U_w = U\left[1 - \left(1 - \sqrt{1 - C_T}\right)\left(\frac{D}{D + 2kx}\right)^2\right] \tag{A.16}$$

Alternatively, the dimensionless wake deficit is found by:

$$1 - \frac{U_w}{U} = \left(1 - \sqrt{1 - C_T}\right)\left(\frac{D}{D + 2kx}\right)^2 \tag{A.17}$$

Note that all parameters in the equation can be measured (U, C_T, D, x) or are known from empirical data (k). Hence, the wake velocity can be found.

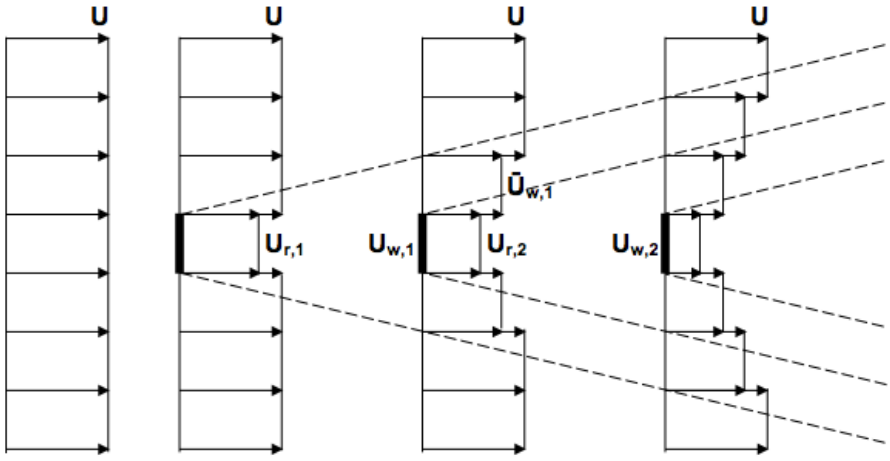

Figure A.2: Visualization of the Jensen wake model for multiple turbines in the wake of each other.

A.2 Multiple wakes

When a second turbine is operating in the wake of the first turbine, a combined wake effect will exist downstream of the second turbine. Using the wake velocity of the first turbine as the inflow velocity of the second turbine, a derivation of the wake velocity downstream of the second turbine can be made, analogous to that in the previous section.

The mass flow equilibrium can be set up as follows:

$$D^2 U_{r,2} + \left(D_w^2 - D^2\right) \overline{U}_{w,1} = D_w^2 U_{w,2} \tag{A.18}$$

where the subscript r denotes the velocity in the fully developed wake just behind a turbine. Subscript w denotes the wake velocity of a turbine, which at the same time is the inflow velocity of the next turbine. The numbers indicate the turbine number. The notation is illustrated in figure A.2.

According to Jensen (1983) the weighted velocity $\overline{U}_{w,1}$, being the "free-stream" velocity that passes along the second wind turbine, but still being in the (expanded) wake of the first turbine, is a small amount lower than the true free-stream wind speed U. Next to that, the difference with the free-stream wind speed decreases for increasing downstream distance from the wind turbine. Jensen states that assuming this velocity to be equal to the true free-stream wind speed U is therefore allowed. Additionally, it is stated that this will make sure that the power output of the row of turbines will not be underestimated. The equation then becomes:

$$D^2 U_{r,2} + \left(D_w^2 - D^2\right) U = D_w^2 U_{w,2} \tag{A.19}$$

Using the "free-stream" velocity before the second turbine, $U_{w,1}$, and the velocity just behind the rotor in the fully-developed wake, $U_{r,2}$, it can be stated that:

$$2a = \frac{U_{w,1} - U_{r,2}}{U_{w,1}} \tag{A.20}$$

where a is the axial induction factor. Rewriting gives:

$$U_{r,2} = (1-2a)\,U_{w,1} \tag{A.21}$$

Substituting in the mass flow equilibrium gives:

$$D^2\,(1-2a)\,U_{w,1} + \left(D_w^2 - D^2\right)U = D_w^2 U_{w,2} \tag{A.22}$$

which upon rewriting becomes:

$$D^2\left((1-2a)\,U_{w,1} - U\right) + D_w^2 U = D_w^2 U_{w,2} \tag{A.23}$$

$$-D^2\left(1-(1-2a)\,\frac{U_{w,1}}{U}\right) + D_w^2 = D_w^2\,\frac{U_{w,2}}{U} \tag{A.24}$$

$$\frac{U_{w,2}}{U} = 1 - \left(1-\left(1-\left(1-\sqrt{1-C_T}\right)\right)\frac{U_{w,1}}{U}\right)\left(\frac{D}{D+2kx}\right)^2 \tag{A.25}$$

where the relations for a and D_w as used in the previous section have been substituted. This can be simplified to:

$$\frac{U_{w,2}}{U} = 1 - \left(1-\sqrt{1-C_T}\,\frac{U_{w,1}}{U}\right)\left(\frac{D}{D+2kx}\right)^2 \tag{A.26}$$

Compared to the turbine operating in free-stream inflow as shown in equation A.15, for the turbine operating in the wake inflow the square root with the thrust coefficient is scaled with the wake velocity over the free-stream velocity.

For an arbitrary downstream turbine numbered i, this becomes:

$$\frac{U_{w,i}}{U} = 1 - \left(1-\sqrt{1-C_T}\,\frac{U_{w,i-1}}{U}\right)\left(\frac{D}{D+2kx}\right)^2 \tag{A.27}$$

The wake velocity behind turbine i can then be found as a result of the wake velocity behind an upstream turbine $i-1$. In this way, the direct influence of the upstream turbine is included. Similarly, other turbines further upstream influence the upstream turbine, and hence their effect is indirectly included as well.

A.3 Multiple wakes interacting

Although the model in the previous section works for a single row of turbines, it can not be applied to a wind farm. Katic and Højstrup (1986) extended the model by Jensen, and state that if the wakes from multiple turbines are interacting with each other, their combined effect needs to be taken into account. It is assumed that the momentum deficit in the interacting wake is equal to the sum of the momentum deficits in each wake at the

downstream position. This approach can be applied for wakes from a row of turbines, multiple rows of turbines or for partially overlapping wakes. This method is also applied in WindPRO (Thøgersen, 2011) and is explained as follows:

The most upstream turbine will give reduced wind speeds at the locations of the downstream turbines. Using these reduced wind speeds the wind speed deficits (with respect to the free-stream wind speed) at each downstream location can be determined. If a downstream turbine is in a partial wake, the wind speed deficit is multiplied by the ratio that the rotor is in this partial wake. Next, the square of the velocity deficits can be taken. At the next downstream location, the sum of the velocity deficits due to each of the upstream turbines is then set equal to the square of the velocity deficit at that location. From this deficit the wind speed upstream the respective turbine can be determined and using the Jensen model the wake wind speed behind this turbine can be calculated as well. The wind speed deficit of this turbine will then also be part of the turbines even further downstream, etc. Using this approach all wake influences on each turbine can be determined for each wind direction.

The momentum deficit is defined as the square of the difference between the free-stream wind speed and the wind speed in the wake (Lange, Waldl, Guerrero, Heinemann, & Barthelmie, 2003). This is valid, regarding that the cross-sectional area in the wake at the downstream position where the velocities are being determined has to be equal for all velocities, as the wakes overlap each other in that area, and that the air density at that position is the same for the individual and mixed wakes. If the inflow of a downstream turbine results from the interacting wakes of two turbines, and using the assumption regarding the momentum deficits, the momentum equation then becomes:

$$\frac{1}{2}\rho A\left(U - U_{w,mixed}\right)^2 = \frac{1}{2}\rho A\left(U - U_{w,1}\right)^2 + \frac{1}{2}\rho A\left(U - U_{w,2}\right)^2 \tag{A.28}$$

This equation can thus be simplified to:

$$\left(U - U_{w,mixed}\right)^2 = \left(U - U_{w,1}\right)^2 + \left(U - U_{w,2}\right)^2 \tag{A.29}$$

Rewriting gives the equation for the velocity in the mixed wake:

$$U_{w,mixed} = U - \sqrt{\left(U - U_{w,1}\right)^2 + \left(U - U_{w,2}\right)^2} \tag{A.30}$$

In general, for the wake inflow to a turbine n resulting from $n-1$ interacting wakes the inflow velocity becomes:

$$U_{w,mixed} = U - \sqrt{\sum_{i=1}^{n-1}\left(U - U_{w,i}\right)^2} \tag{A.31}$$

where $U_{w,i}$ is the wake velocity at turbine n due to turbine number i. The resulting mixed wake velocity and all the wake velocities as dictated by their corresponding turbine are determined at the same downstream location.

Katic and Højstrup (1986) states that using this method will result in an equilibrium level in the wake velocity after some downstream turbines. This is also observed in reality as can be seen in section 4.2.

Appendix B

Determining wind direction from multiple simultaneous observations

The metmast at OWEZ measures wind direction and wind speed at three positions at each height, using wind vanes and cup anemometers respectively. The three positions of the equipment are separated by 120 degrees, as shown in figure B.1. For each 10-minute period three simultaneous wind directions and wind speeds are measured.

B.1 Determining the true wind direction

Since the metmast disturbs the air flowing around it, some of the wind vanes (as well as the cup anemometers) may show a disturbed measurement value. Therefore, simply taking the average wind direction of all three wind vanes at the same height will most likely result in an incorrect wind direction. The following methods to determine the correct (undisturbed) wind direction are proposed:

1a Take the average of all three wind vanes.

1b Select two non-wake wind vanes using the average of all three wind vanes (of method 1a) as reference direction.

2 Select the two wind vanes of which the indicated values are the closest together.

3 Exclude the wind vanes that indicate wake operation.

A comparison is made to determine the wind direction at each height (21, 70 and 116 metres). The results per bin are shown in figure B.2. From the figure it can be seen that the results of methods 1b, 2 and 3 are similar. Method 1a clearly shows a different wind direction. The results of methods 1b and 3 are most similar to each other.

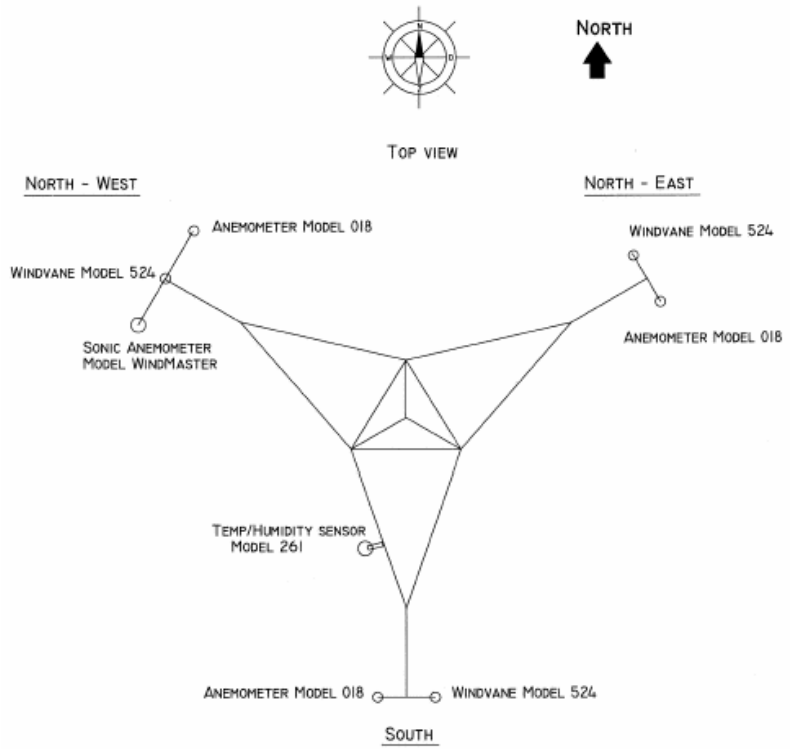

Figure B.1: Distribution of wind vanes and cup anemometers as occurring on the OWEZ metmast (here at 21 m) (Kouwenhoven, 2007).

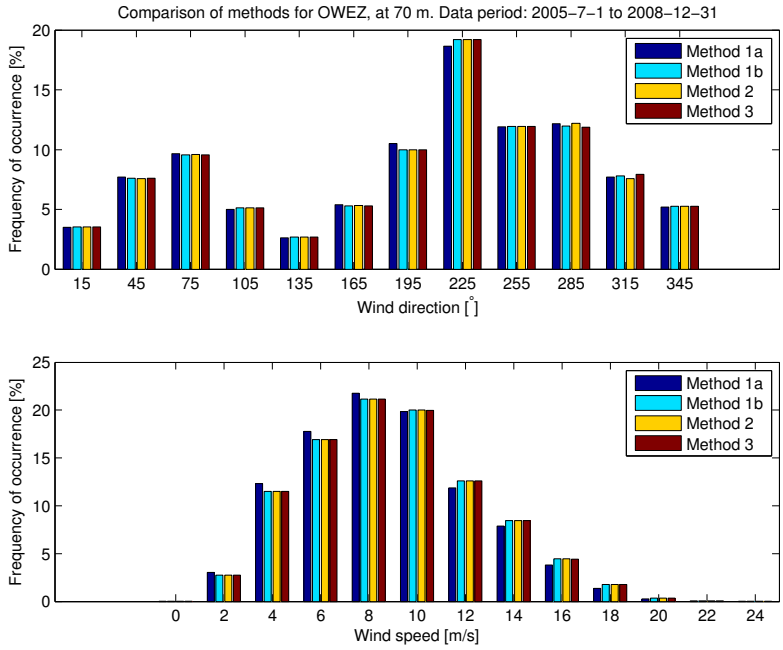

Figure B.2: Frequency of occurrence of the derived true wind direction using the different methods. Results are displayed as frequency of occurrence per $30°$ bin, at a measurement height of 70 m. The data is for OWEZ during the period 1 July 2005 to 30 November 2008.

B.1.1 Method 1a: Take the average of all wind vanes

Method 1a clearly shows a different wind direction distribution compared to the other methods, from which it is concluded that this method results in incorrect wind directions. This is as expected, as it includes the undisturbed as well as disturbed wind vanes.

B.1.2 Method 1b: Select two non-wake wind vanes

Method 1b uses the reference direction which is found using method 1a. Assuming that there is always a wind vane in the wake of the metmast, a choice can be made which two wind vanes should not be in the wake of the metmast by using the reference wind direction. For instance, if the wind is coming from the North (0°), then the Northwestern (NW) and Northeastern (NE) wind vanes are upstream of the metmast and hence not in its wake. However, using a reference direction that includes a measurement that is in the wake of the metmast means that the wind might not exactly come from the North. In case of a reference wind direction that, for example, is around 60° this might therefore result in the following problem. With the reference direction indicating 59° the Southern (S) sector would be counted as being in the wake, and the NW and NE sensors would be used to find the true wind direction. However, with the reference direction indicating 61° the NW sector would be counted as being in the wake, and the NE and S sensors would be used. Hence, the wrong decision might be made in selecting the wind vanes from which the true wind direction is determined.

B.1.3 Method 2: Select the two closest wind directions

Metod 2 selects the two wind vanes of which the indicated values are the closest together. In this case, another problem can be seen. With the wind coming from, for example, 0°, both the NW and NE sensors are are upstream of the metmast, and it might be assumed that they are both undisturbed. The S sensor is now in the wake of the metmast and hence most likely shows a disturbed measurement. Hence, the two closest readings of the wind vanes will be from the NW and NE sensors. Averaging their value will give a good indication of the true wind direction. Now assume the wind is coming from 180°. Sensors NW and NE now are both downstream of the metmast, while sensor S is now upstream of the mast and undisturbed. However, since sensors NW and NE are symmetrically spaced around the metmast (both at 120° from the wind direction), they again might indicate similar values for the wind direction. In this method there is no way of determining whether the two most similar readings are actually undisturbed. Hence, this method should not be used.

The problem occurring in method 2 might arise in method 1b as well. It was assumed that there is only one wind vane which is disturbed by the metmast, and so the true wind direction is determined from two wind vanes. However, when two wind vanes are disturbed, then the method might use one undisturbed sensor, but also one disturbed sensor. The assumption of having only one disturbed wind vane appears to be invalid.

A way to 'fix' this problem in method 1b could be to not divide the wind direction sector in 3 120° sectors of in which two wind vanes are used, but into 6 60° sectors in which

Table B.1: Rules used to determine whether a wind vane measurement is disturbed by the wake of the metmast at OWEZ.

Sensor	Wake sector	Undisturbed sector
NW	60° – 180°	0° – 60° and 180° – 360°
NE	180° – 300°	0° – 180° and 300° – 360°
S	300° – 360° and 0° – 60°	60° – 300°

Table B.2: Statistics of wind vane selection using method 3. The numbers indicate the percentage of cases in which the shown number of wind vanes is undisturbed and hence are used to determine the true wind direction. The data is for OWEZ during the period 1 July 2005 to 30 November 2008.

Measurement height	0 wind vanes	1 wind vane	2 wind vanes	3 wind vanes
21 m	0%	2.94%	96.99%	0.073%
70 m	0%	1.58%	97.76%	0.65%
116 m	0%	1.57%	98.01%	0.42%

either one or two sectors are being used. In case of two downstream wind vanes only the upstream wind vane can be selected, while in case of two upstream wind vanes these two can be selected both. However, the problem in selecting the proper one/two wind vane(s) from the reference direction in method 1b would still remain. For method 2 this solution can not be applied. The method becomes unusable when two wind vanes are disturbed.

B.1.4 Method 3: Exclude the wind vanes that indicate wake operation

It is hard to decide on a reference direction in method 1, and with the possibility of having either one or two disturbed measurements method 2 becomes inappropriate. The solution that is proposed, is as follows. Whenever a wind vane indicates that the wind is coming from the direction of the metmast, the value is discarded. The true wind direction is then found by taking the average of the remaining sensors. This is method 3. It is the method that is used throughout the analysis. Table B.1 shows the rules applied to determine whether a wind vane value is counted as undisturbed or not.

Another advantage of method 3 is that it is scalable. For instance, when a metmast has two instead of three measurements per height the method can still be applied. Also for a higher amount of wind vanes per height the method can be applied.

To get an insight in the results of this method the amount of included wind vanes are counted. The results are shown in table B.2. From the table it can be seen that most measurement periods indeed have two undisturbed wind vanes. However, in some cases two wind vanes are measuring disturbed wind and only one wind vane is selected. In a small amount of cases all wind vanes indicate an undisturbed measurement and all wind vanes are used. The opposite does not occur; never all measurement are disturbed so that 0 wind vanes are valid.

Table B.3: Rules used to determine whether a wind vane measurement is disturbed by the wake of the metmast at North Hoyle.

Sensor	Wake sector	Undisturbed sector
NE (wind direction)	180° – 270°	0° – 180° and 270° – 360°
SW (wind direction)	0° – 90°	90° – 360°
NW (wind speed)	90° – 180°	0° – 90° and 180° – 360°

B.2 Determining true wind speed and turbulence intensity

The wind speed is determined in a similar way as the wind direction. The undisturbed cup anemometers are selected based on the criteria of undisturbed wind vanes. Hence, if the NW and NE wind vane are used to determine the true wind direction, then the NW and NE cup anemometer are used too to find the true wind speed and turbulence intensity. Note that although the wind direction might not need to be determined that accurately, the wind speed needs to be known accurately in order to predict the power output.

B.3 Application to other metmasts

The same method can easily be applied to other metmasts.

At North Hoyle, at hub height (70 m) the measurements include 2 wind direction sensors (at Northeast and Southwest of the mast) and 1 wind speed sensor (at Northwest of the mast). A similar procedure can thus be applied to the wind direction, with the wake direction of the sensors as shown in table B.3. The wind speed is now in a different direction compared to the wind vanes. The newly determined true wind direction can then be applied to select only those wind speeds for which the metmast was not upstream the sensor (such that the sensor is not disturbed by the wake of the mast).

Since only the Northwest wind speed sensor is available at hub height at North Hoyle, the Southeast sector of measurements will drop out due to disturbed wind speed measurements. However, this sector would have been excluded from the filtered data anyway, as it coincides with the sector where the metmast is in the wake of the wind farm.

B.4 Observations from turbines

A second method that is used during the wake loss investigation in this study is to use the wind speed and wind direction as measured by the turbines. The 10-minute periods for which the wind is along the row direction and at 8.0 ± 0.5 m/s can be more accurately obtained from the turbines than from the measurements of the metmast. The metmast might be some distance away from the row and therefore not indicate the actual wind speed and wind direction that occurs at the row. This can result in using the wrong production data, i.e. using 10-minute periods for which the wind was not at the wanted wind speed or wind direction.

The turbine data is used as follows to determine the wake losses in this study. For the wanted row direction, the turbines to be investigated are selected. The wind speed and wind direction of the first turbine in each row is compared to the wanted wind direction sector and wind speed bin for each row of turbines. Per row of turbines the 10-minute periods that are in the wind direction sector and wind speed bin are then selected. The wake losses corresponding to these can then be obtained.

It should be noted that the wind direction of the turbines has been validated first, by checking against the wake losses occurring at the second turbine in the row. The row direction should be the wind direction with the largest wake loss. A possible offset in the wind direction measured by the turbines can then be corrected.

Appendix C

Validating sea surface temperature

In this chapter the sea surface temperature as measured by the metmast at the wind farms is compared with sea surface temperature data from the European Centre for Medium-Range Weather Forecasts (ECMWF). ECMWF has made a re-analysis of the global atmosphere from January 1979 to January 2012, called the ERA-Interim re-analysis. The data is available via the ECMWF data server: http://data-portal.ecmwf.int/data/d/interim_daily/.

The following approach is taken to find out if there is a temperature difference between the two sources. Similar timestamps between the two datasets are identified. Next the temperature difference at each similar timestamp is taken. Here ΔSST is defined as:

$$\Delta SST = seatemp_{ECMWF} - seatemp_{metmast} \tag{C.1}$$

From this an average temperature difference is found. If there exists a temperature difference between the two sources the sea surface temperature measured by the metmast can be corrected for that.

C.1 OWEZ

Data is used from 1 July 2005 to 30 November 2008 for OWEZ. Measurements from all directions are taken into account, as the sea surface temperature is not influenced by the wake of the wind farm. In Sathe et al. (2011) it is stated that there is a certain offset between the measured sea surface temperature by the metmast, which is actually 3.8 metres below mean sea level, and the sea surface temperature as obtained from the ERA-Interim re-analysis by ECMWF.

Sathe et al. found that the difference between the two data sources was -0.82 K, i.e. that the OWEZ sea surface temperatures had to be corrected by subtracting 0.82 K. The dataset used in this project is similar to that of Sathe et al., but due to different filtering the obtained temperature difference might be different.

Figure C.1: Locations of the ECMWF grid points (*Google Earth*, 2012).

Using the script obtained from Sathe et al. to analyse the ECMWF data it was found that it appears that Sathe et al. has used a grid point too far North from the metmast. The grid points of ECMWF are spaced by 1.5° in both longitude and latitude. The metmast at OWEZ is located at 52.6'N 4.4'E, which is close to the ECMWF point at 52.5'N 4.5'E. It appears however that Sathe et al. has used the ECMWF grid point at 54.0'N 4.5'E which is 155.8 km North of the metmast, hence the large difference in sea surface temperature offset. See the locations of the ECMWF grid points in figure C.1.

Using the ECMWF grid point at 52.5'N 4.5'E, which is the one closest to the metmast at 13.0 km, the temperature offset is only -0.14 K. The temperature and temperature difference at each timestamp are shown in figure C.2.

The temperature offset between the metmast measurements and the ECMWF re-analysis is small. Since the metmast is 13.0 km away from the ECMWF grid point and since the ECMWF dataset has a coarse grid, the metmast sea surface temperature is not adjusted for the offset with ECMWF.

In Sathe et al. (2011) it is stated that the temperature offset obtained is also resulting from comparison of the non-dimensional wind speed profiles which have a significant offset with the theoretical profiles without the correction. From the current study it is also found that without a correction the distribution of normalized wake losses of the different stability classes is not according to theory or earlier research as found in literature, suggesting a correction might still need to be applied to the measured sea surface temperature. The following reason for this is proposed. The sea surface temperature sensor at OWEZ is 3.8 metre below mean sea level. It is known that the water temperature is not the same

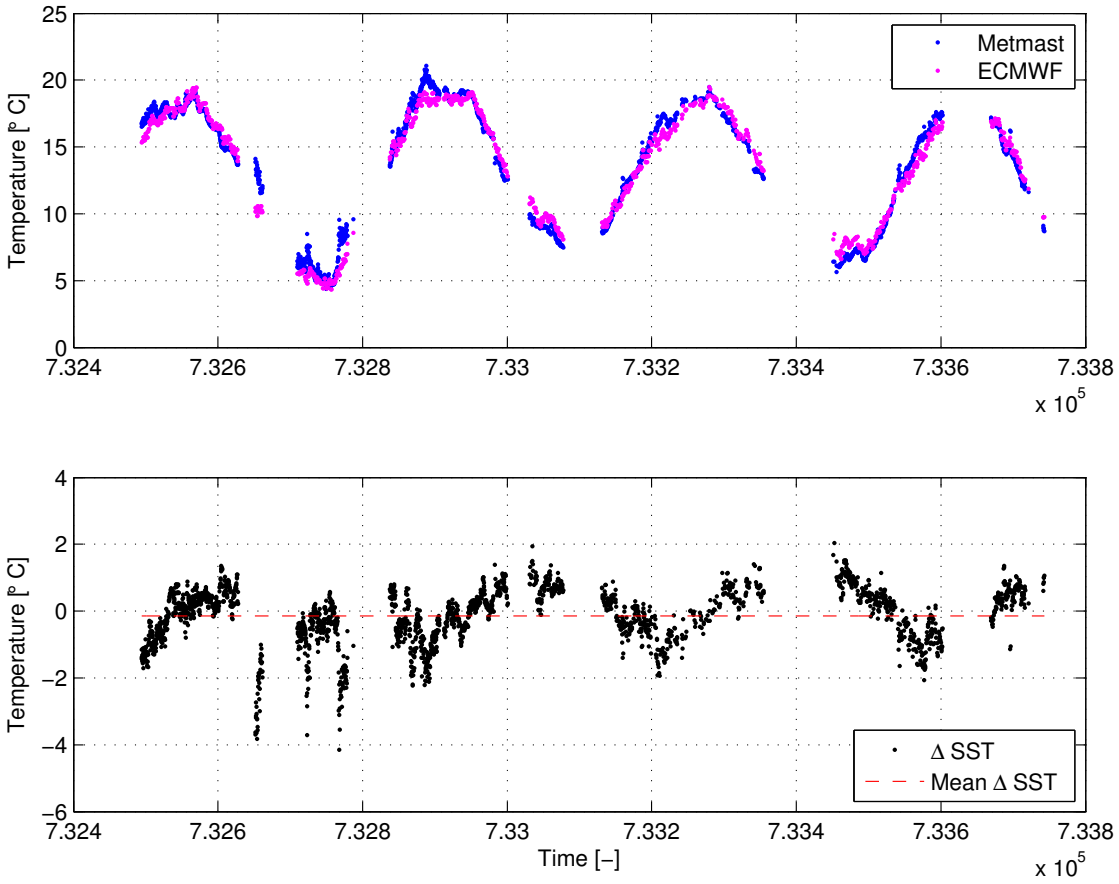

Figure C.2: Comparison of sea surface temperature at OWEZ, using metmast data and re-analysis data from ECMWF. The mean offset is found to be -0.753 K.

at the sea surface as at some metres below the sea surface (Schluessel et al., 1990), so it is expected that there is a certain offset in the sea surface temperature measurements. The offset due to this difference is unknown, and it might vary due to the variation of atmospheric conditions, time and water level as the metmast is fixed but the sea level is not. In Schluessel et al. (1990) it is stated that the difference between the bulk temperature, measured at more than one metre below the sea surface, and the sea surface temperature can range from -1.0 to 1.0 K with a mean difference in the order of tenths of degrees. Furthermore, in the current study there is a difference between the measured sea surface temperature and the air temperature at 2 m from the mesoscale data (which has a higher (3 x 3 km) resolution compared to the ECMWF grid), which should be close to the sea surface temperature. It is therefore proposed that a temperature correction should be applied to the sea surface temperature measured at OWEZ. Although the temperature difference found by Sathe et al. (2011) could not be recreated here, the wind speed profiles in Sathe et al. (2011) also confirm the temperature offset and are proven to be according to theory when using a correction of -0.82 K. A correction is therefore taken here in the order of -0.8 K.

An alternative for the metmast sea surface temperature measurement might be considered for future projects, for instance a floating buoy measuring the temperature at the air-sea interface.

C.2 North Hoyle

A similar analysis is performed for North Hoyle. Data is used from 14 September 2007 to 31 December 2011. Measurements from all directions are taken into account, as the sea surface temperature is not influence by the wake of the wind farm.

The North Hoyle metmast is located at 53.4'N -3.5'E. The neareast grid point is at 54.0'N -3.0'E as shown in figure C.1. The temperature and temperature difference at each timestamp are shown in figure C.3. A difference of -1.248 K is found. However, in this case the grid point is 74.4 km from the metmast and the geographic area surrounding the grid point is significantly different from that of the metmast (both are in a different coastal area). An alternative would be to average the ECMWF sea surface temperature using multiple grid points, but then the same problem of significant differences in geographic area occurs.

The results for North Hoyle are not corrected for the offset with ECMWF due to differences in location, but a temperature correction might still need to be applied. For North Hoyle no information was provided about the metmast. Except from the brands and types of installed sensors and the installed heights and directions for some of these as derived from the SCADA database no information is available. It is therefore unknown whether there might be offsets due to calibration or for instance due to the water depth of the sea surface temperature measurements. Hence, no correction of the sea surface temperature is applied.

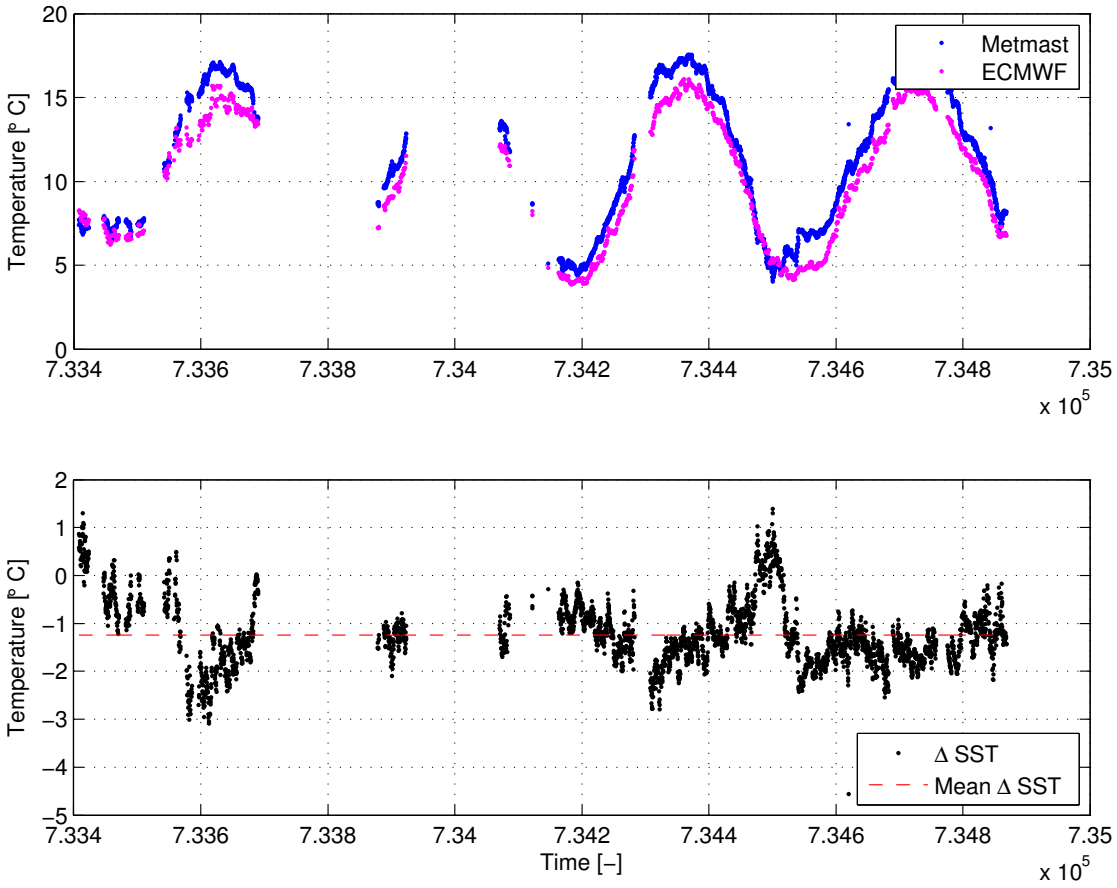

Figure C.3: Comparison of sea surface temperature at North Hoyle, using metmast data and re-analysis data from ECMWF. The mean offset is found to be -1.248 K.

Appendix D

Verifying stability methods

To ensure proper functioning of the calculations of Monin-Obukhov length to find the atmospheric stability, test cases are selected to verify the results. Of the wind farms investigated, OWEZ is the only park of which results of the atmospheric stability are available in literature. These are reported by Sathe (2009).

In Sathe (2009) various methods to investigate the stability are compared. Of the methods described, the gradient and bulk method are the ones that are considered in this project.

The stability classification applied is the common 5-bins distribution shown in table D.1.

Data is taken over the period 1 July 2005 to 31 December 2008. The wind speed (4-25 m/s) and wind direction (135°-315°) boundaries are taken the same as by Sathe (2009), and the filters applied to the data are the same. No stationarity filter has been applied to the data in this project though. As Sathe (2009) notes, it hardly shows any influence on the statistics of the atmospheric stability. The advantage of not applying the stationarity filter more data will remain for the later analyses.

The gradient method uses air temperature and wind speed at two measurement heights. The heights used by Sathe (2009) are 21 and 70 m. Both results are shown in D.1.

The bulk method uses air temperature and wind speed at one measurement height and the sea surface temperature. The wind speed at 0 m is zero. The height for the air measurements as used by Sathe (2009) is 21 m. The results are shown in D.2.

Table D.1: Monin-Obukhov length L [m] boundaries for stability classes as used by Sathe (2009).

Stability class	Boundaries
Very stable	$0 < L < 200$
Stable	$200 < L < 1000$
Neutral	$\|L\| > 1000$
Unstable	$-1000 < L < -200$
Very unstable	$-200 < L < 0$

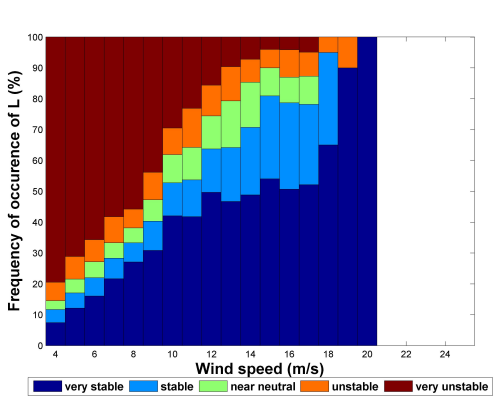

(a) Result by Sathe (2009)

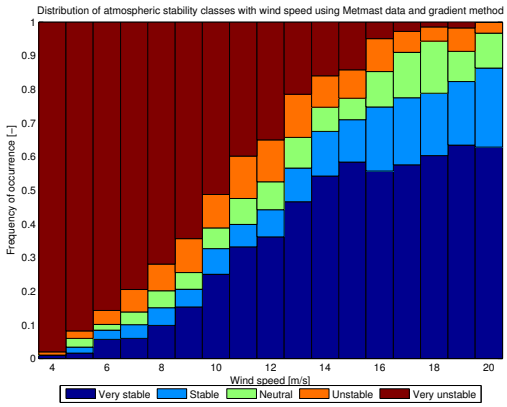

(b) Result in this project

Figure D.1: Verification of gradient method at OWEZ. a) Result by Sathe (2009), b) results in this project. Data period: 1 July 2005 to 30 November 2008.

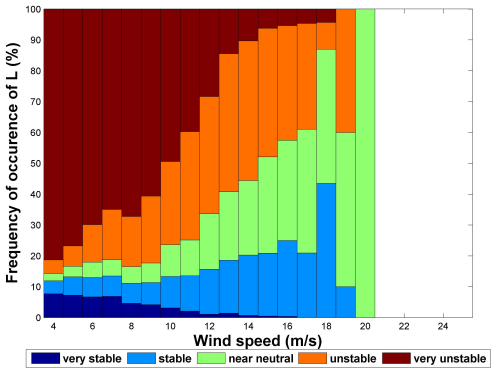

(a) Result by Sathe (2009)

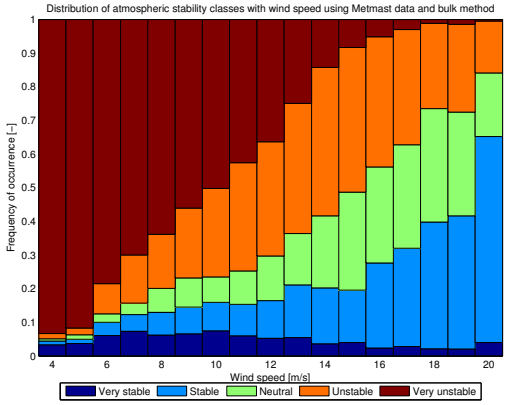

(b) Result in this project

Figure D.2: Verification of bulk method at OWEZ. a) Result by Sathe (2009), b) results in this project. Data period: 1 July 2005 to 30 November 2008.

The results from both methods are seen to be close to the ones as obtained by Sathe (2009), but some difference can be observed. Using the gradient method the results of Sathe (2009) show a lower amount of very unstable classes and a higher amount of unstable, neutral, stable and very stable conditions, especially at lower wind speeds, compared to the results in this project. The same is true for the bulk method.

A reason for the differences between the results of Sathe (2009) and the ones obtained here are likely to come from the input data, since both the gradient and bulk method show the same deviation. One reason of the difference could be that there is a slight difference in the applied filters and/or channels taken into consideration when filtering, resulting in a different filtered dataset.

More likely however, is that the difference results from the different method to obtain the wind direction and wind speed. Sathe (2009) determines the wind direction by selecting two sensors based on a reference direction which is the mean of the three wind vanes (i.e. method 1b as explained in appendix B). This means that there is still an uncertainty in the sensor selection due to including wake measurements in the determination of the reference direction. The determination of the wind speed as applied by Sathe (2009) uses the two cup anemometers indicating the wind speeds that are closest together. This however leaves the possibility that these two cup anemometers are both downstream of the metmast and are disturbed in a similar way. For example: when the wind is coming from the South, then the Northwest and Northeast sensor are both spaced at 120° from the wind direction and can thus indicate wind speeds which are disturbed in a similar way by the wake of the metmast. Hence, having two wind speed sensors that indicate a similar wind speed does not mean that this should be the true wind speed. The method applied in this project (selection of sensors based on excluding the disturbed sensors) tries to avoid these kinds of disturbances, which results in the possibility of different results. That the results are mainly different at low wind speeds makes sense, as the turbulent wake of the metmast has a higher impact on the wind direction and wind speed measurements at low wind speeds where the air is not as much forced to flow in a certain direction as at higher wind speeds. Cup anemometers have the tendency to respond faster to speed up than to speed down effects (Wharton & Lundquist, 2010). In turbulent conditions this means that the cup anemometers will have a tendency to overestimate the true mean wind speed. The selection of the two closest corresponding wind speed sensors as applied by Sathe (2009) might thus result in higher wind speeds than expected. This leads to a less unstable atmosphere. This can explain why there is a lower amount of very unstable classes and a higher amount of unstable, neutral, stable and very stable conditions at lower wind speeds in the results of Sathe (2009).

Overall it is concluded that the stability methods applied in this project seem to be working properly.

Appendix E

Correlation metmast and mesoscale data

Since the results regarding stability distribution and wake losses using metmast data or using mesoscale data are not in full correspondence it is interesting to know what causes the difference. In this appendix the correlation between the metmast and mesoscale measurements is investigated using data from North Hoyle. It is also investigated what input variable of the two dataset should have the highest correspondence due to its impact on the result of the stability analysis.

E.1 Correlation of input parameters

In this project atmospheric stability is calculated using the bulk method. The variables required for the calculation are the wind speed at hub height, ambient temperature at hub height and sea surface temperature. The correlation between the metmast and mesoscale data for these variables is shown in figures E.1, E.2 and E.3 respectively. Since the temperature gradient is determined from the temperatures and used in the analysis, figure E.4 shows the correlation for this quantity. The standards ("Wind turbines – Part 12-1: Power performance measurements of electricity producing wind turbines", 2011) state that to plot the wake losses wind speed normalization should be applied. To be able to do this, the ambient density is required. The correlation of this variable is therefore plotted in figure E.5.

Note that since only data with similar timestamps can be correlated with each other, and since metmast data is in 10-minute periods but mesoscale data is hourly, only a subset of both datasets can be used.

The correlations between the input parameters of metmast and mesoscale data as shown in the figures are summarized in table E.1. Both the ambient temperature and sea surface temperature have a high R^2, being 0.938 and 0.925 respectively. The temperature gradient only has a R^2 of 0.606 though.

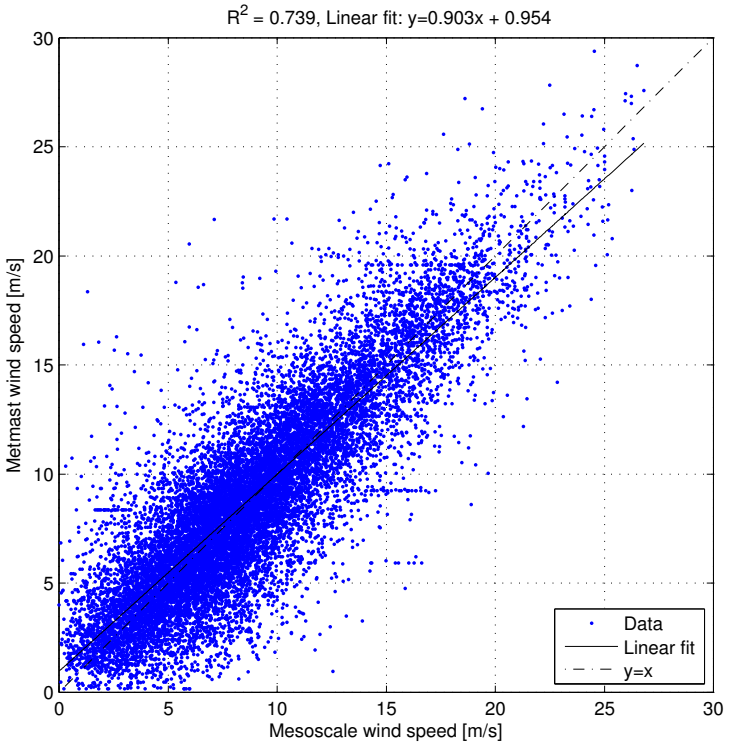

Figure E.1: Wind speed correlation between metmast and mesoscale data at North Hoyle.

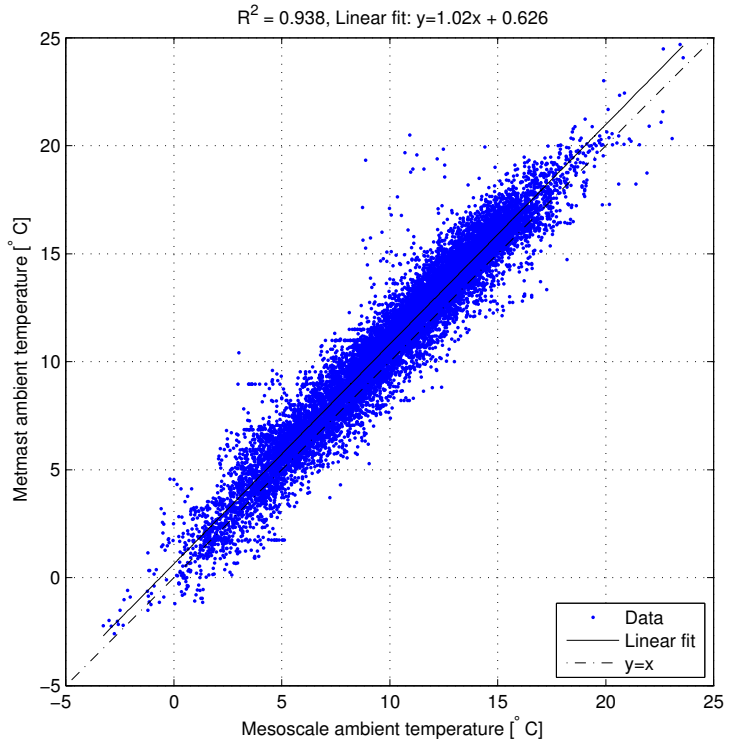

Figure E.2: Ambient temperature (at 70 m) correlation between metmast and mesoscale data at North Hoyle.

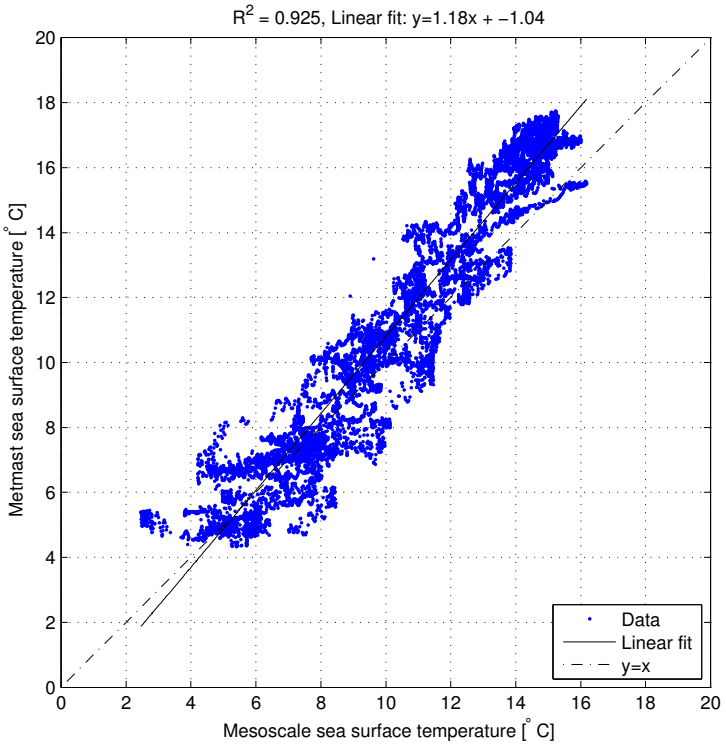

Figure E.3: Sea surface temperature correlation between metmast and mesoscale data at North Hoyle.

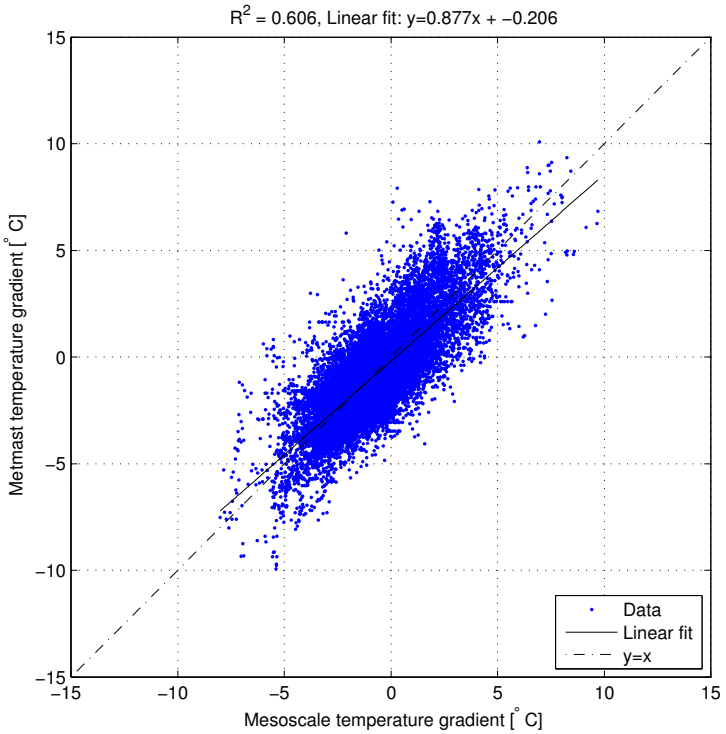

Figure E.4: Temperature gradient correlation between metmast and mesoscale data at North Hoyle.

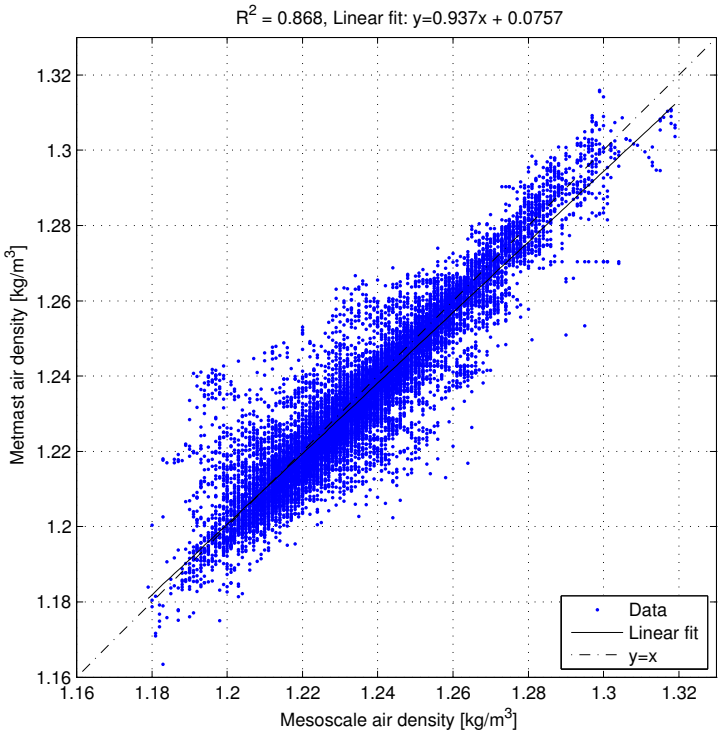

Figure E.5: Ambient density correlation between metmast and mesoscale data at North Hoyle.

Table E.1: Correlations between the input parameters of metmast and mesoscale data.

Parameter	R^2 [-]
Wind speed	0.739
Ambient temperature	0.938
Sea surface temperature	0.925
Temperature gradient	0.606
Ambient density	0.868

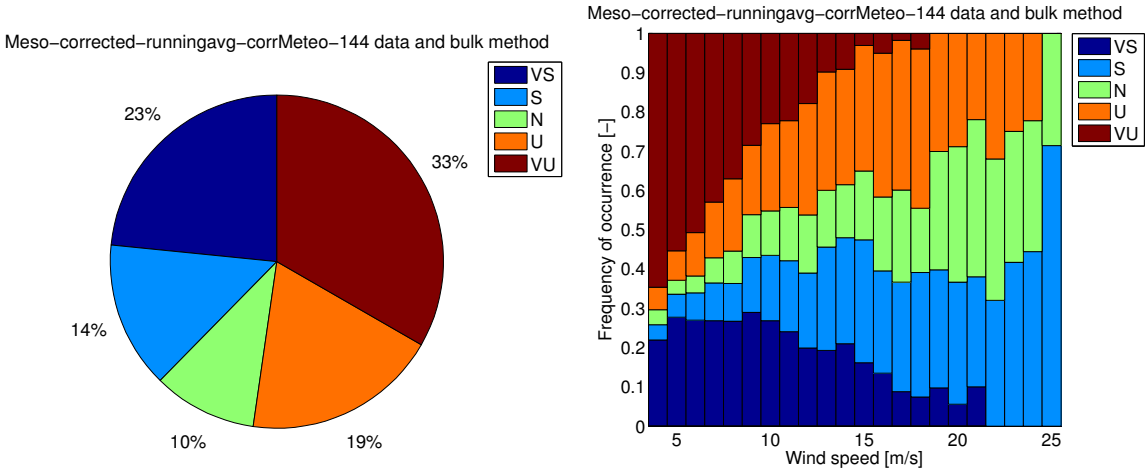

(a) In percentage

(b) Versus wind speed

Figure E.6: Distribution of stability classes at North Hoyle, using adapted mesoscale data. VS = very stable, S = stable, N = neutral, U = unstable, VU = very unstable. Data is taken over the period from 14 September 2007 to 31 December 2011. Wind directions 40° to 170° are excluded.

The equations shown in the top of the scatter plots show the best fit of the mesoscale data to the metmast data. A suggestion is made to use these equations to transform the mesoscale data to see whether the stability and wake loss results are closer to those of the metmast data than when using the unadapted mesoscale data. The data is adapted as follows:

$$Mesoscale_{adapted} = scaling \cdot Mesoscale_{unadapted} + offset \tag{E.1}$$

where the scaling and offset depend on the variable that is being adapted and can be found in the scatter plots.

E.2 Adapting mesoscale data

When the mesoscale wind speed, ambient temperature and sea surface temperature are adapted using the explained method, the stability distribution becomes as shown in figure E.6. The results are for those hourly mesoscale timestamps that also occur in the metmast timestamps. The same results using the unadapted data are shown in figure 4.12. It can be seen that the adapted results are closer to the results using metmast data (figure 4.8) than the unadapted mesoscale results are. Compared to the stability distribution of the unadapted mesoscale data, the adapted mesoscale data shows a higher number of very unstable cases, whereas there are less unstable, neutral and (very) stable cases occurring. Comparing these results with the metmast data in figure 4.8 it appears that the correction has brought the mesoscale data closer to the metmast data, and now only differ slightly.

To be able to plot the wake losses, the mesoscale ambient density is transformed according to the correspondence with the metmast data as well (since the wind speed of

the production data is normalized according to the standards). The wake losses for the various directions using the adapted mesoscale data become as shown in figures E.7b, E.8b and E.9b. These can be compared with the results of unadapted mesoscale data in figures E.7a, E.8a and E.9a respectively. The results using metmast data (and unadapted mesoscale data) are shown in figures 4.27, 4.28 and 4.29.

Figure E.7 shows the wake losses for a wind direction of 348.9°. Comparing the adapted mesoscale data with the wake losses of the unadapted mesoscale data no difference is visible for the very stable cases. The near-neutral case seems to have shifted to a higher wake loss, and a slightly lower wake loss can be seen for the very unstable case. This is in the direction of the metmast results (figure 4.27a), but there is still a difference between the very stable and near-neutral case wake losses using either adapted mesoscale data or metmast data.

For the 258.8° direction the results are shown in figure E.8. With respect to the unadapted mesoscale results, the near-neutral case of the adapted mesoscale data now shows a larger wake loss, whereas the very unstable case and slightly the very stable case show a smaller wake loss. The very unstable and near-neutral case wake losses seem to be further away from the metmast results (figure 4.28a), and the very unstable case does not show much improvement either.

The 282.5° wind direction is shown in figure E.9. A significant change can be seen comparing the results of the adapted mesoscale data with those of the unadapted mesoscale data. The near-neutral and very stable cases seem to have more or less changed places and the very unstable stability class shows a larger wake loss for the two most downstream turbines. The result is that the wake losses using adapted mesoscale data show almost the same results as the wake losses using metmast data in figure 4.29a.

Overall, for all three wind directions it can be said that adapting the mesoscale data gives varied results in comparing the wake losses with those using metmast data. In the first case the results are better, but there is still a big difference, in the second case the results seem to get worse and in the third case the results have improved significantly.

E.3 Correlation of stability parameters between different datasets

Transforming the mesoscale data gives varying success in getting wake losses closer to those using metmast data. However, the atmospheric stability distribution of the adapted mesoscale data appeared to be closer to the stability distribution of the metmast data. The input parameters to the bulk method show correlated scatter plots, so it is interesting to see how well the correlation of the stability parameter (Monin-Obukhov length L) is.

E.3.1 Mesoscale data

A scatter plot of metmast versus mesoscale data for the stability parameter is shown in figure E.10. The data points indicated in red designate those time instants where both metmast and mesoscale data indicates $|L| > 200$ (i.e. neutral).

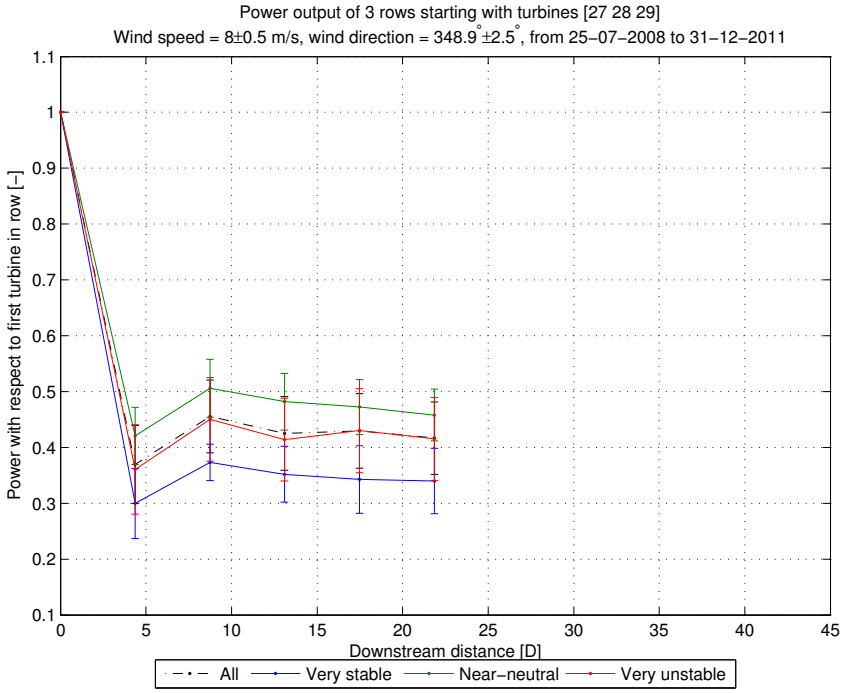

(a) Using unadapted mesoscale data

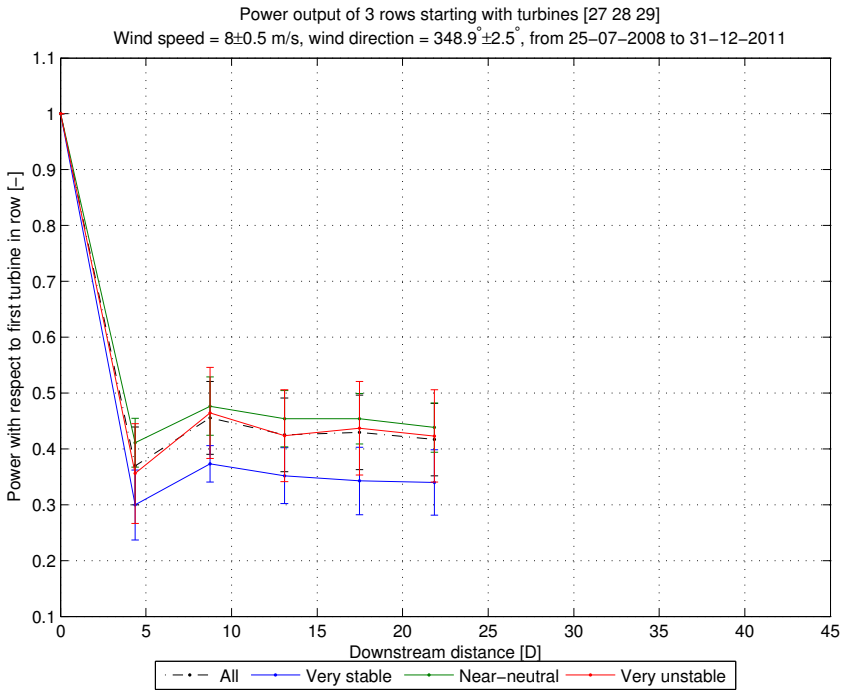

(b) Using adapted mesoscale data

Figure E.7: Wake losses at North Hoyle for winds coming from the $348.9° \pm 2.5°$ and wind speeds at 8.0 ± 0.5 m/s for various stability classes. a) using unadapted mesoscale data, b) using adapted mesoscale data. Wind speed and direction are taken as the average of the first turbine in the rows. Data is taken over the period from 11 June 2008 to 31 December 2011. The error bars represent one standard deviation (half above and half below the mean value).

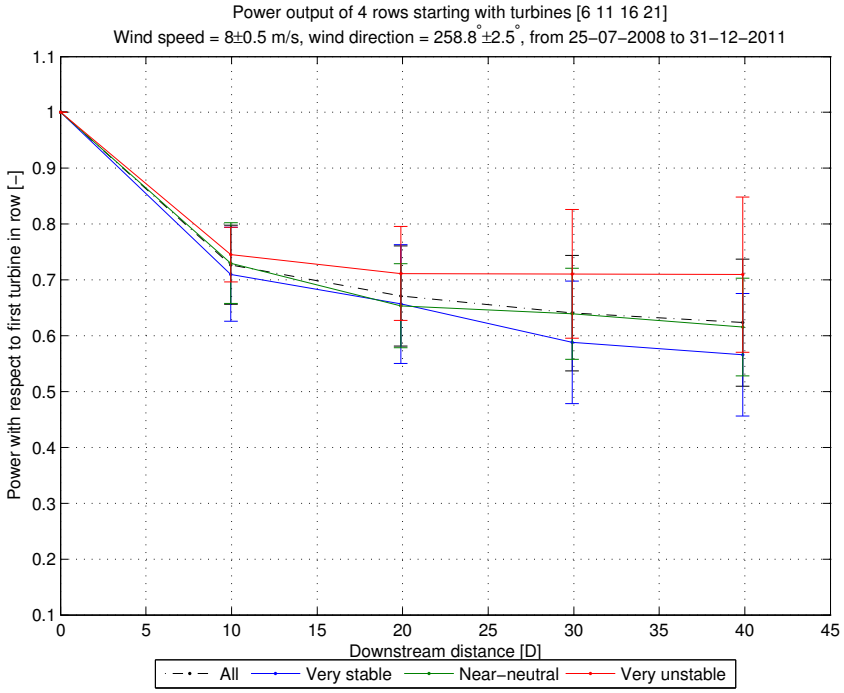

(a) Using unadapted mesoscale data

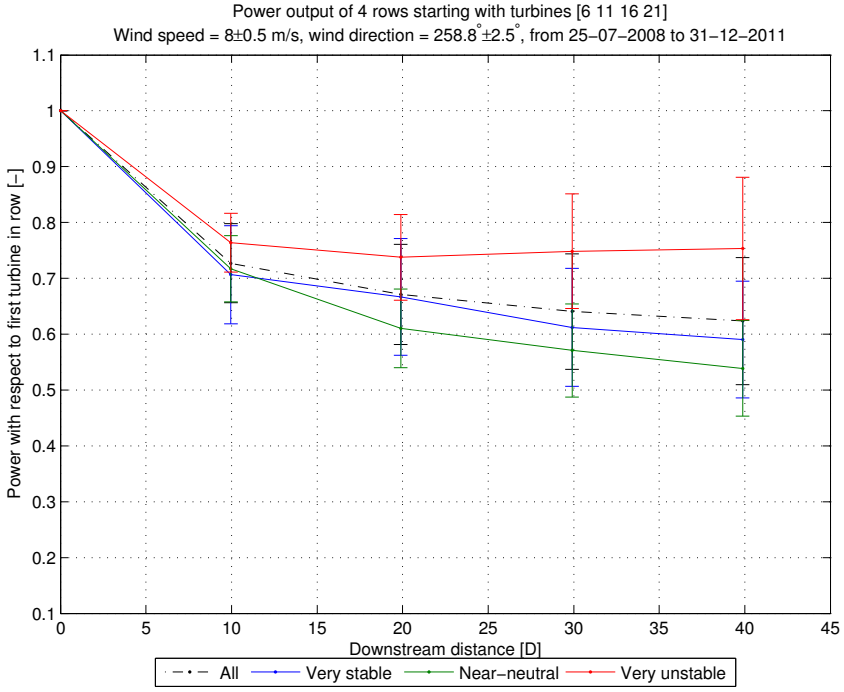

(b) Using adapted mesoscale data

Figure E.8: Wake losses at North Hoyle for winds coming from the $258.8° \pm 2.5°$ and wind speeds at 8.0 ± 0.5 m/s for various stability classes. a) using unadapted mesoscale data, b) using adapted mesoscale data. Wind speed and direction are taken as the average of the first turbine in the rows. Data is taken over the period from 11 June 2008 to 31 December 2011. The error bars represent one standard deviation (half above and half below the mean value).

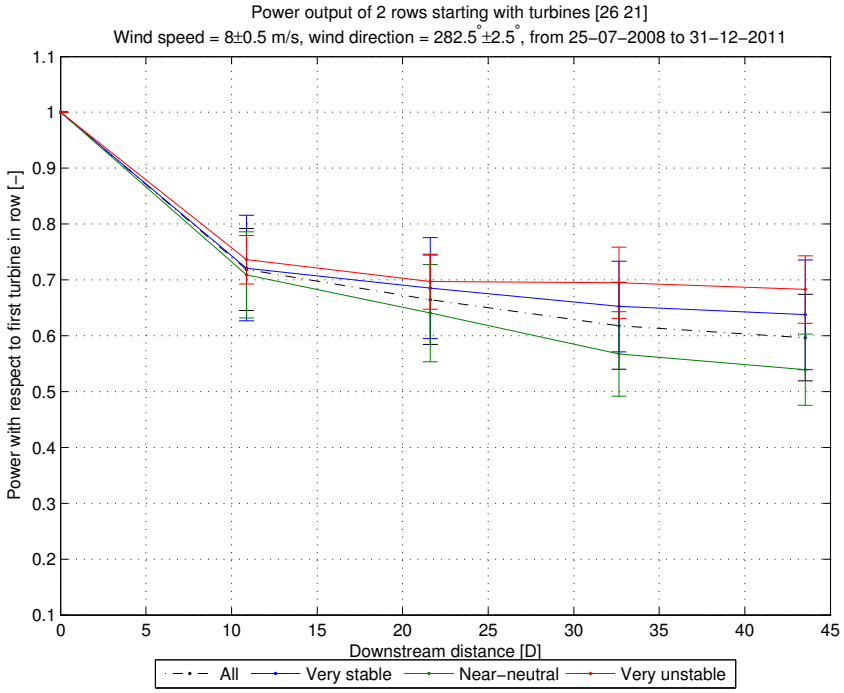

(a) Using unadapted mesoscale data

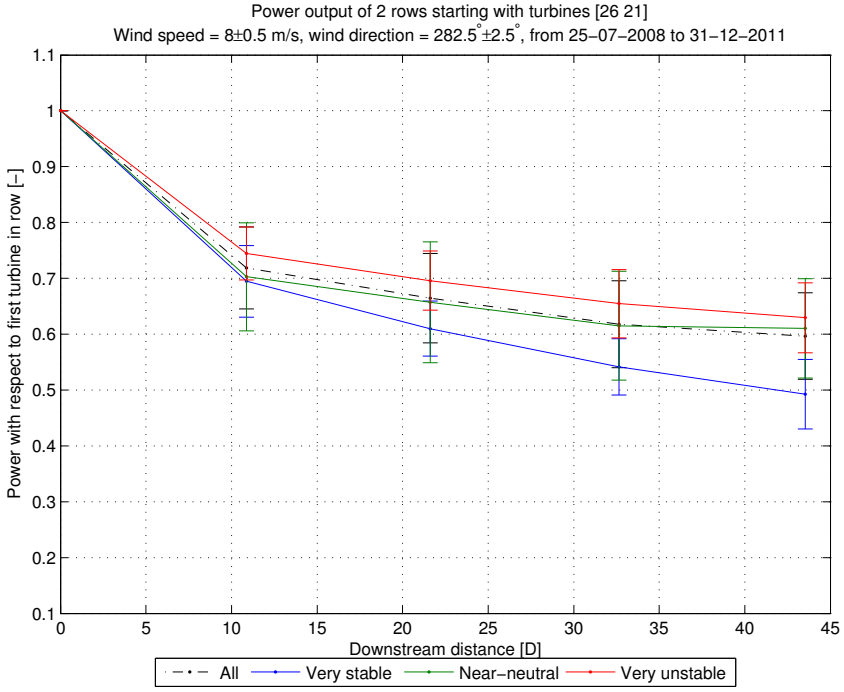

(b) Using adapted mesoscale data

Figure E.9: Wake losses at North Hoyle for winds coming from the $282.5° \pm 2.5°$ and wind speeds at 8.0 ± 0.5 m/s for various stability classes. a) using unadapted mesoscale data, b) using adapted mesoscale data. Wind speed and direction are taken as the average of the first turbine in the rows. Data is taken over the period from 11 June 2008 to 31 December 2011. The error bars represent one standard deviation (half above and half below the mean value).

It can be seen that the plot does not look like the plots of the other scatter clouds in appendix E.1, which are more shaped along the line $y = x$. The stability parameter seems to lay in a less correlated cloud. It also seems that the parameter is concentrated along the axes.

An alternative way of representing the stability is by using the dimensionless stability parameter $\zeta = z/L$ instead of the the Monin-Obukhov length L. The plot for ζ is shown in figure E.11a. It can be seen that in this plot the points are more distributed in the shape of a cloud along the $y = x$ direction than the L data points are. However, also in the plot of ζ it can be seen that there are data points located along the axes.

Note that where a lot of neutral data points are visible in the scatter plot of L, these points only form a small portion of the plot of ζ. This is because ζ uses the inverse of L.

Both the Monin-Obukhov length L and the dimensionless stability parameter ζ are determined using the Richardson number. The Richardson number is determined from the wind speed and temperature measurements (of which the scatter plots are shown in appendix E.1). Since the scatter plot of L, nor that of ζ looks like the well-correlated plots of the input signals, a scatter plot of the Richardson number is made and shown in figure E.11b. The Richardson scatter plot does show a cloud shape along the direction of $y = x$, and there appears to be a significant correlation between the metmast and mesoscale data.

The neutral cases are clearly visible as well. Because these cases have a $\zeta = z/L$ value close to zero the effect in the plot of L is that more data points are located along the axes. Small differences in the value of ζ (so in Richardson number) of the metmast and mesoscale stability when ζ is close to 0 can hence result in large differences in the value of L.

So:

- The plot of L does not show a cloud of data points aligned along $y = x$, since the metmast and mesoscale data do indeed not correspond to each other in each case.
- The fact that data points of L are located along the axes, and that they are not just laying in a completely uncorrelated cloud, is caused by Richardson numbers close to 0. A large spread in values occurs when L is determined from the Richardson number.

The large spread in Monin-Obukhov lengths of metmast and mesoscale data caused by Richardson numbers close to 0 becomes a cloud of data points when plotted on a log-log plot. This is shown in figure E.12, where the data are shown in separate log-log plots for positive and negative values. The equation for the Monin-Obukhov length shows no logarithms, but for illustrative purposes the log-log plot does show a cloud of data points between the Monin-Obukhov lengths of metmast and mesoscale data. The spread in data points remains, but the plots make it somewhat easier to see the size of the spread of the data points. The log-log plots also point out that there are some occurrences where metmast and mesoscale have opposite sign (i.e. opposite stability), although most occurrences have the same sign. The negative (i.e. unstable) data shows the most stretched data cloud, indicating correspondence between metmast and mesoscale data as well as the amount of atmospheric instability of the occurrences.

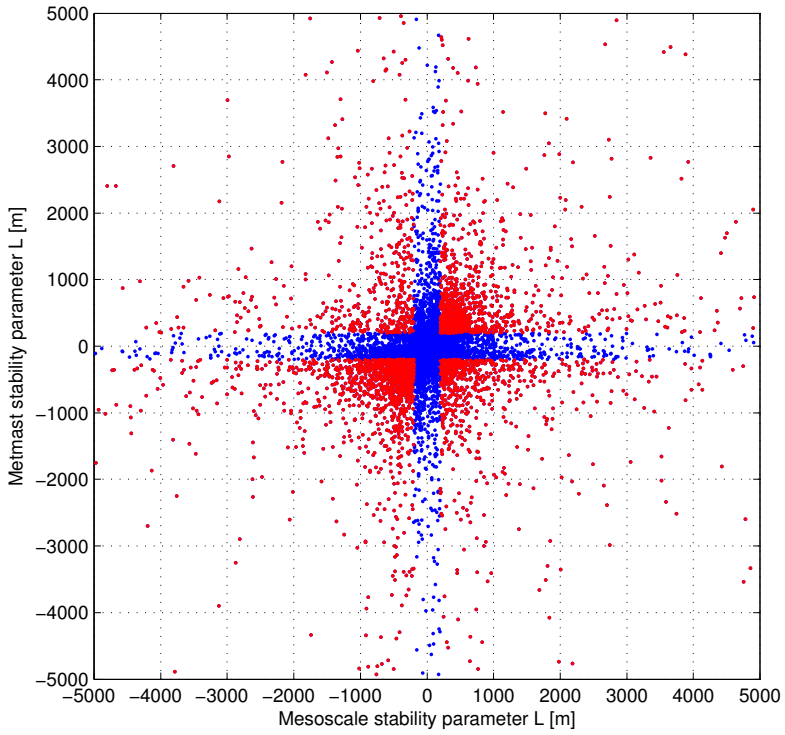

(a) Zoomed in

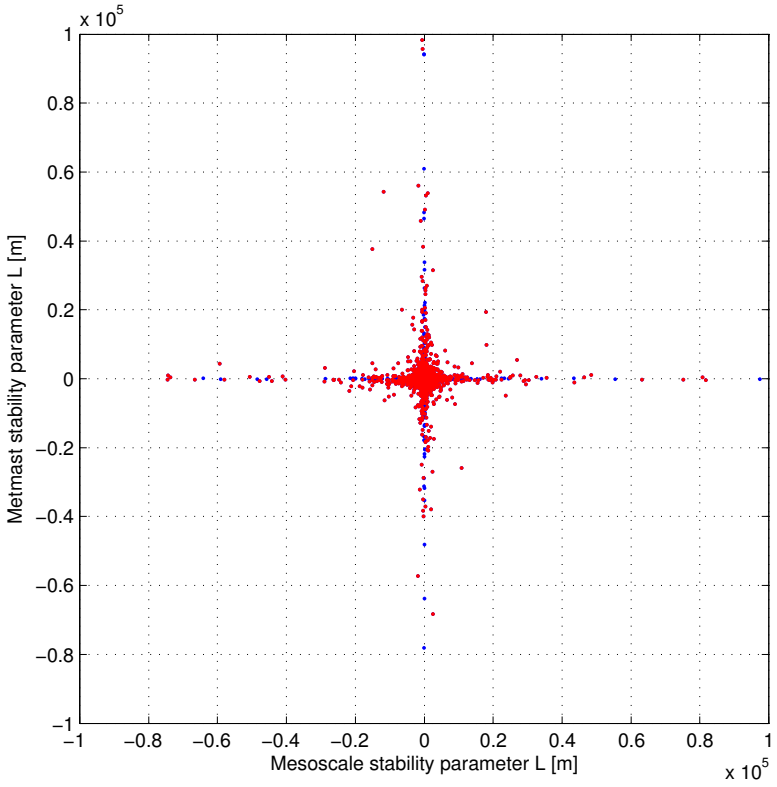

(b) Zoomed out

Figure E.10: Atmospheric stability correlation between metmast and mesoscale data at North Hoyle using Monin-Obukov length. The data points indicated in red designate those time instants where both metmast and mesoscale data indicates $|L| > 200$ (i.e. neutral).

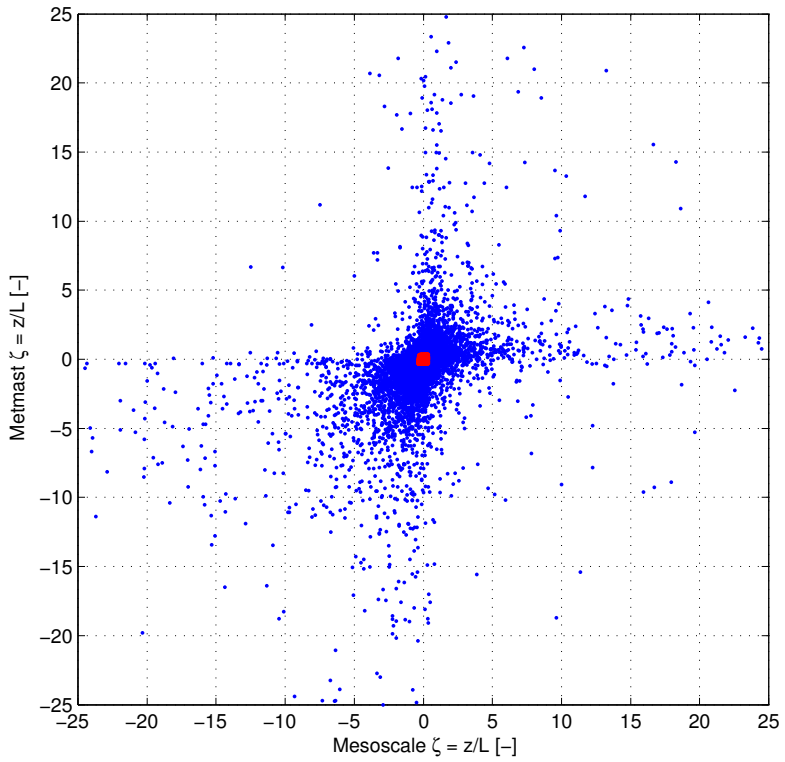

(a) ζ

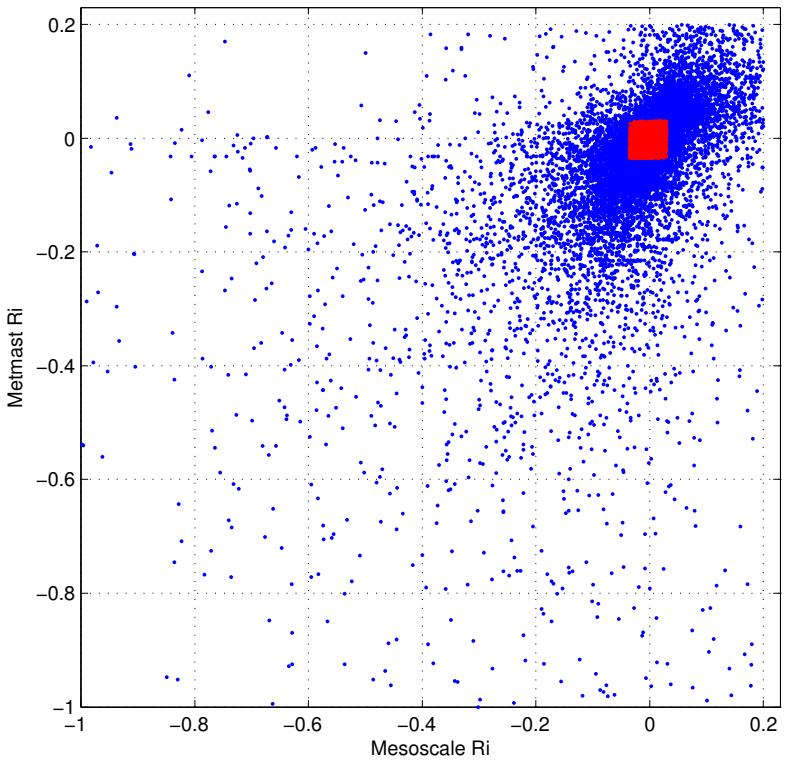

(b) Richardson number

Figure E.11: Atmospheric stability correlation between metmast and mesoscale data at North Hoyle using a) ζ and b) Richardson number. The data points indicated in red designate those time instants where both metmast and mesoscale data indicates $|L| > 200$ (i.e. neutral).

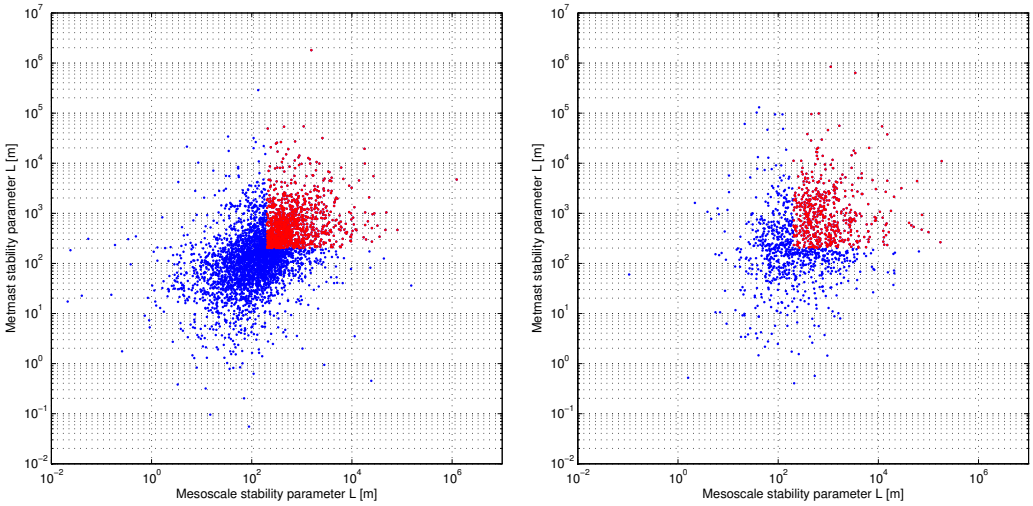

(a) Metmast: +, mesoscale: +

(b) Metmast: +, mesoscale: -

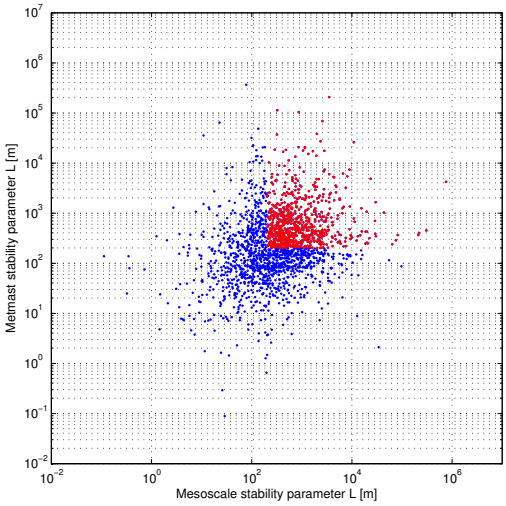

(c) Metmast: -, mesoscale: +

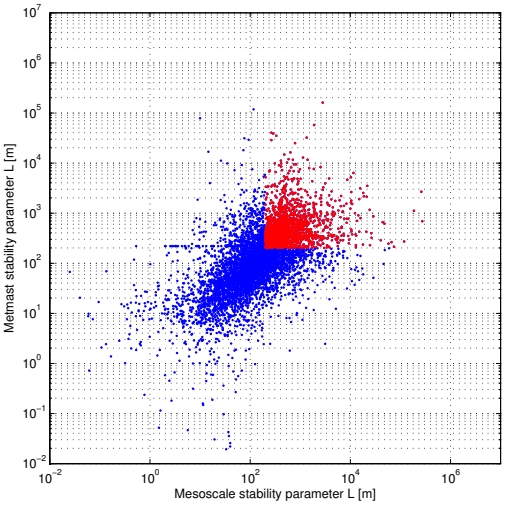

(d) Metmast: -, mesoscale: -

Figure E.12: Atmospheric stability correlation between metmast and mesoscale data at North Hoyle using Monin-Obukov length on a log-log plot. The data points indicated in red designate those time instants where both metmast and mesoscale data indicates $|L| > 200$ (i.e. neutral).

Table E.2: Correspondence of stability classes resulting from metmast and (unadapted) mesoscale data.

Metmast \ Mesoscale	Very stable	Stable	Neutral	Unstable	Very unstable	Sum
Very stable	13.1%	4.7%	1.2%	1.3%	1.5%	22%
Stable	3.7%	5.4%	2.4%	1.2%	1.2%	14%
Neutral	1.6%	2.2%	2.7%	2.5%	1.1%	10%
Unstable	1.5%	2.6%	3.6%	7.9%	3.9%	19%
Very unstable	3.0%	2.5%	2.4%	6.2%	20.6%	35%
Sum	23%	17%	12%	19%	28%	

To quantify the correspondence of the amount of occurrences per atmospheric stability class resulting from the two different data sets, the data is set out in a table. Table E.2 shows the results for the correspondence between metmast data and unadapted mesoscale data. For the time instants belonging to a certain stability class as indicated by the metmast data, the table shows the relative amount of occurrences per atmospheric stability class of the same time instants as indicated by the mesoscale data.

Ideally, only the diagonal entries should be non-zero, meaning that metmast and mesoscale data would always indicate the same stability class. However, it can be seen from the table that this is not the case. (Very) stable and (very) unstable cases seem to correlate well, whereas the neutral cases correlate less well.

For illustrative purposes another set of plots is created, now the values indicated in red designate those time instants where the metmast data indicates $|L| < 200$ (i.e. very (un)stable), but the mesoscale data indicates $|L| > 1000$ (i.e. neutral). See figures E.13, E.14a and E.14b.

From the plots it can be seen that a small spread in Richardson number and ζ value of the mesoscale data around 0 results in a large spread in the plot of L. The large spread of the Richardson number and ζ values of the metmast results in a small spread in the plot of L. The spread of the Richardson number for both metmast and mesoscale data, combined with the equation of the Monin-Obukhov length L, results in the special shape of the scatter plot where data points are aligned along the axes.

E.3.2 Adapted mesoscale data

In appendix E.1 a suggestion was made to adapt the mesoscale data according to its correlation with the metmast data. In the previous section the correlation of the stability parameter L was shown for metmast data and unadapted mesoscale data. Here, the adapted mesoscale data will be used, to see whether the correlation of the stability parameter with that of the metmast data improves.

The cloud of data points in the Richardson number plot, figure E.16b, seems to be a bit more narrow than for the unadapted mesoscale data. The spread in ζ values along the mesoscale axis in figure E.16a seems to be less. Also for the Monin-Obukhov length L in

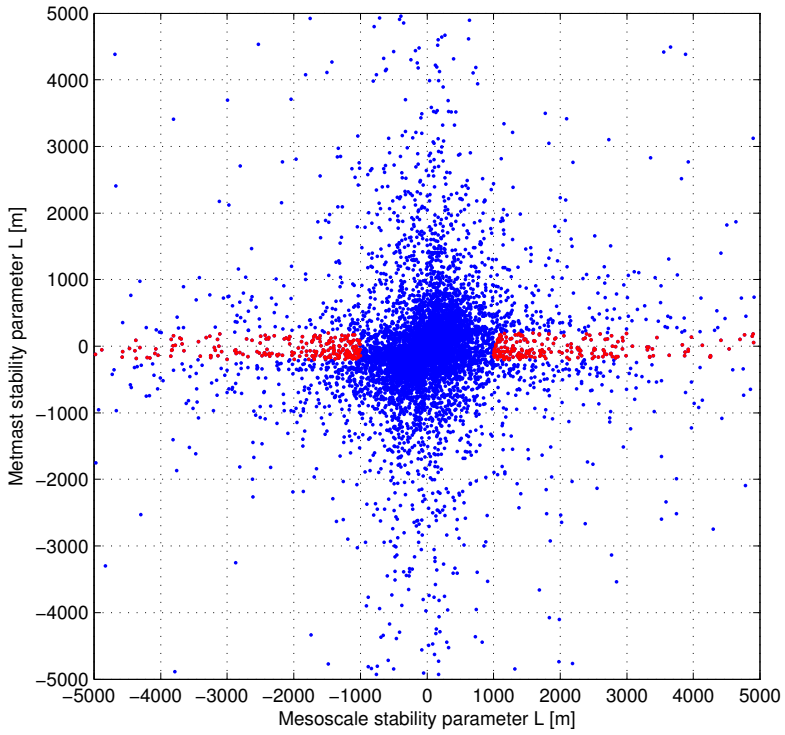

(a) Zoomed in

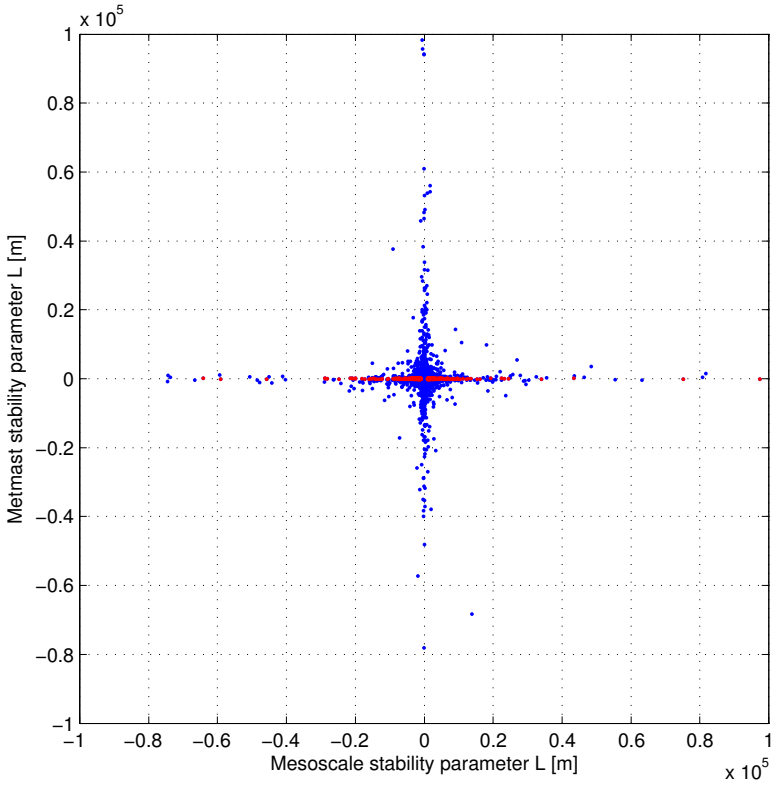

(b) Zoomed out

Figure E.13: Atmospheric stability correlation between metmast and mesoscale data at North Hoyle using Monin-Obukov length. The data points indicated in red designate those time instants where the metmast data indicates $|L| < 200$ (i.e. very (un)stable), but the mesoscale data indicates $|L| > 1000$ (i.e. neutral).

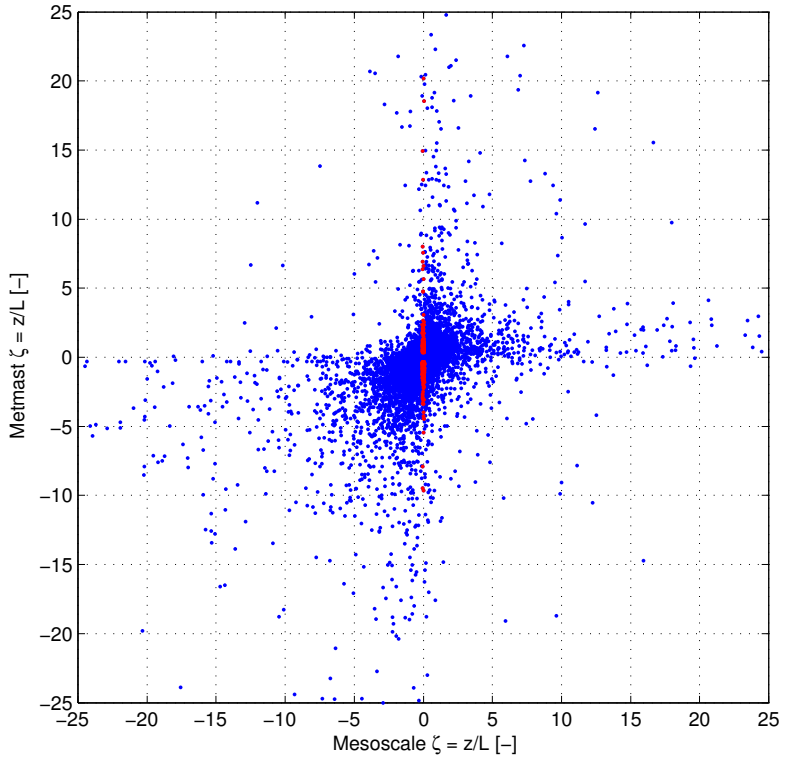

(a) ζ

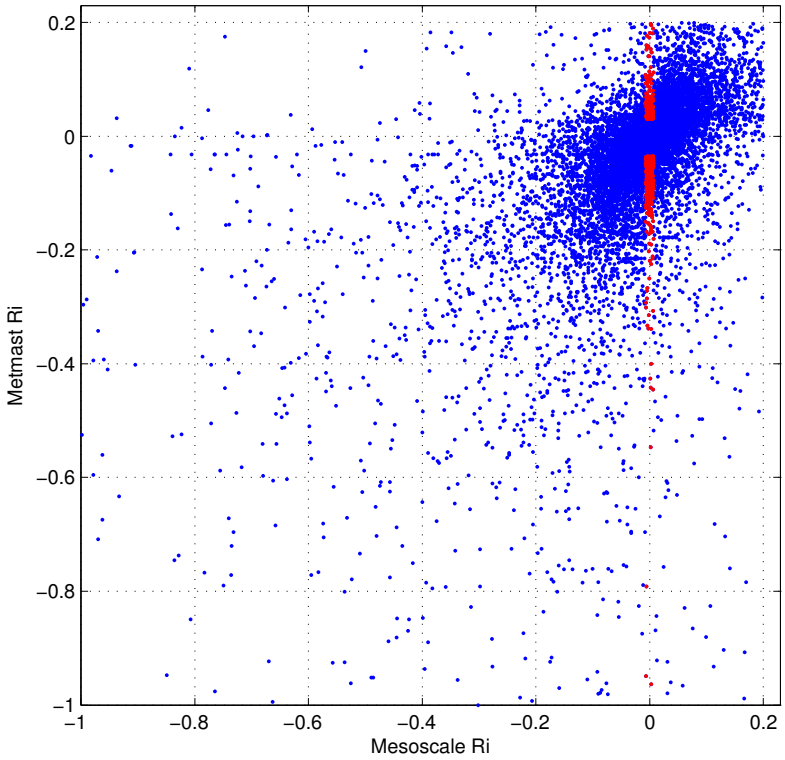

(b) Richardson number

Figure E.14: Atmospheric stability correlation between metmast and mesoscale data at North Hoyle using a) ζ and b) Richardson number. The data points indicated in red designate those time instants where the metmast data indicates $|L| < 200$ (i.e. very (un)stable), but the mesoscale data indicates $|L| > 1000$ (i.e. neutral).

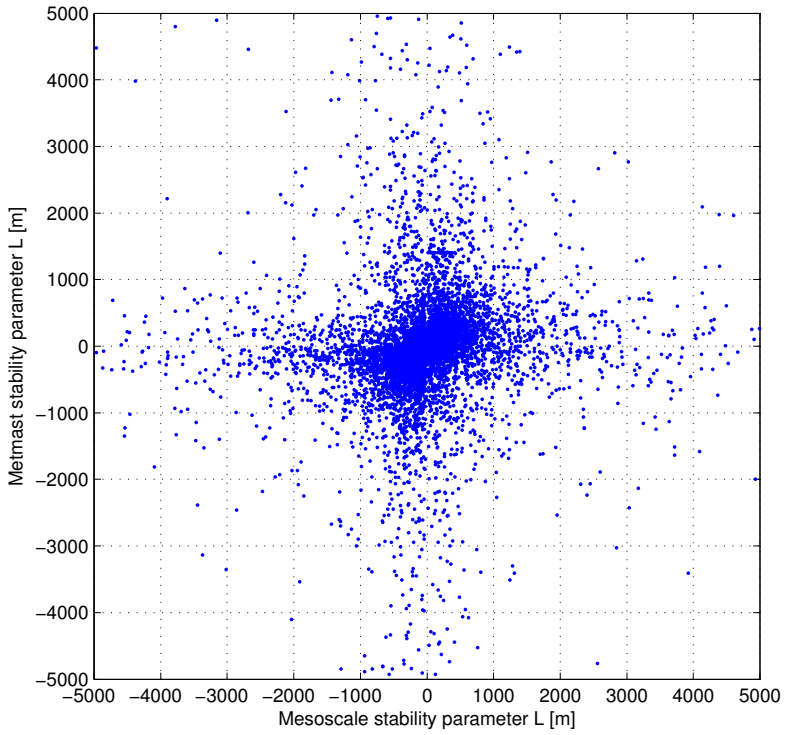

(a) Zoomed in

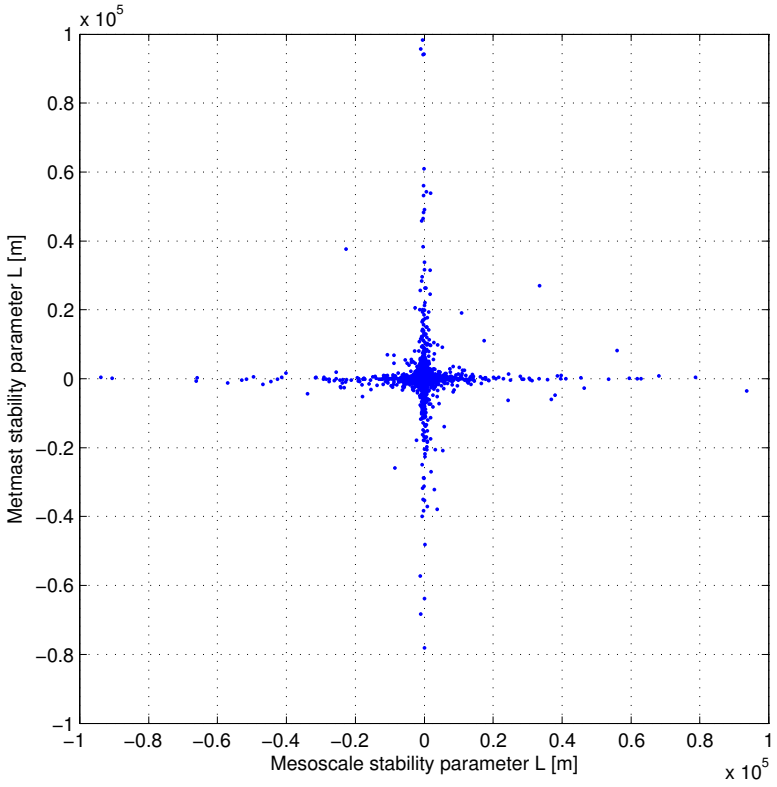

(b) Zoomed out

Figure E.15: Atmospheric stability correlation between metmast and adapted mesoscale data at North Hoyle using Monin-Obukov length.

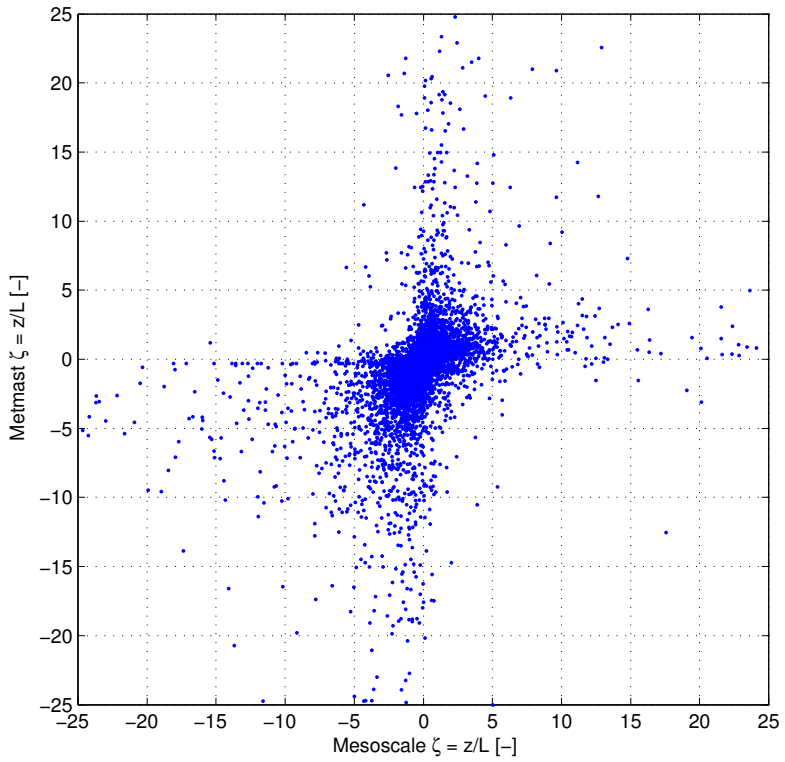

(a) ζ

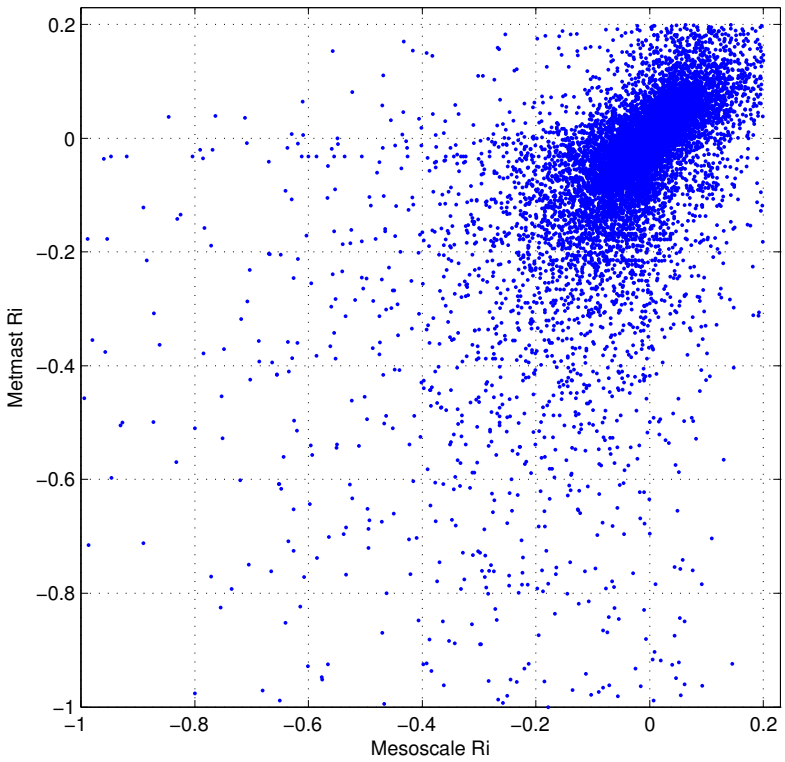

(b) Richardson number

Figure E.16: Atmospheric stability correlation between metmast and adapted mesoscale data at North Hoyle using ζ and Richardson number.

Table E.3: Correspondence of stability classes resulting from metmast and adapted mesoscale data.

Metmast \ Mesoscale	Very stable	Stable	Neutral	Unstable	Very unstable	Sum
Very stable	13.6%	4.2%	1.1%	1.2%	1.5%	22%
Stable	3.6%	5.1%	2.3%	1.3%	1.2%	14%
Neutral	1.1%	2.1%	2.4%	2.8%	1.1%	10%
Unstable	1.0%	1.6%	2.6%	8.3%	5.4%	19%
Very unstable	2.4%	1.6%	1.9%	5.8%	24.7%	36%
Sum	22%	15%	10%	19%	34%	

figure E.15 the cloud of data points seems to be a bit more narrow. Overall, there is no significant change visible though.

The table of correspondence of the different stability classes for the metmast data and adapted mesoscale data is shown in table E.3. The most significant changes occur in the occurrence of (very) unstable cases. This is as expected, as that was already found in figure E.6 where the stability distribution of the adapated mesoscale data is displayed. It can be seen that the metmast data agrees more with the adapted mesosale data than with the unadapted mesoscale data (in table E.2).

E.4 Sensitivity of stability analysis

In the previous section it was found that when the mesoscale data was adapted according to the linear fit of the metmast and mesoscale data, the agreement regarding atmospheric stability between the two datasets improved. The question arises which of the adapted variables has the largest impact on the comparison of the stability of the two datasets. In order to find out which variable has the highest influence, the following test is set up.

Three artificial variables are created, representing ambient wind speed at hub height, ambient temperature at hub height and sea surface temperature. Two sets of these variables are created: one representing the metmast and one representing the mesoscale data. Of each set, the two corresponding variables have the same standard deviation (so also the square thereof, the variance, is equal) and are related by a certain covariance. The values for this can be entered manually and will be varied in the analysis to find out what the effect is when the two datasets show a larger or smaller correlation for a certain variable. At this point it is worth mentioning that since the sea surface temperature and ambient temperature are also correlated to each other via the temperature gradient, these two variables cannot be randomly generated independent of each other, as that would mean their values would not be correlated. To avoid this problem, not the sea surface temperature, but the temperature gradient is randomly created. The sea surface temperature can then be derived by subtracting the temperature gradient from the ambient temperature. Now the sea surface temperature and the ambient temperature are correlated to each other. When all variables are created they are shifted such that their mean is similar to the mean of the metmast data (since the variables are created with a mean around zero).

Table E.4: Description of the different cases used to investigate the correlation between artifical metmast and mesoscale data.

Case	Description
1	All correlations are similar to those between the measured metmast and used mesoscale data (see also table E.1).
2	All parameters are highly correlated (0.99).
3-5	Investigate the impact of the different parameters by giving one parameter a lower correlation in each case, where in each case the same lower correlation (0.90) is used.
6-8	Investigate the impact of the different parameters by giving one parameter a lower correlation in each case, where the correlation as measured between the metmast and mesoscale data is used.

Table E.5: Correlation per variable between artifical metmast and mesoscale data. For a description of the cases, see table E.4.

Case	1	2	3	4	5	6	7	8
Wind speed	0.86	0.99	0.90	0.99	0.99	0.86	0.99	0.99
Ambient temperature	0.97	0.99	0.99	0.90	0.99	0.99	0.97	0.99
Temperature gradient	0.78	0.99	0.99	0.99	0.90	0.99	0.99	0.78

The correlation between the metmast and mesoscale data as measured, and for the cases used to create the artificial random variables that are used for testing, are shown in table E.5. Note that the square of the correlation is equal to the R^2-value shown in table E.1. Case 1 simply recreates the real data (similar to if two datasets would be used, one with the measured metmast and one with the used mesoscale data), whereas in case 2 all variables are created highly correlated (correlation of 0.99) between the two datasets (similar to using two datasets, both with almost the same metmast data). Cases 3-5 look at what happens when all variables are highly correlated, but one variable has a lower correlation (similar to using two datasets with almost the same metmast data, but one signal from one dataset is replaced by mesoscale data). In this case the one variable with disagreement between the two datasets is set to an equal correlation for all three cases (0.90). This way it can be investigated which of the variables has the highest impact on the disagreement between the stability distributions of the two datasets. Since for the real data the disagreement is not the same in each variable (see the correlations in case 1), cases 6-8 investigate which disagreement between the signals of the measured metmast and mesoscale data has the highest impact on the disagreement between their stability distributions. Again only one variable gets a lower correlation (as measured) while the other variables have a high correlation. The different cases are summarized in table E.4

The correlation of the articial data for case 1 is shown in figures E.17, E.18 and E.19 for the wind speed, ambient temperature and temperature gradient respectively. Note that it is very similar to the real data shown in figures E.1, E.2 and E.4 respectively. The correlation of Monin-Obukhov length is shown in figure E.20 and those of ζ and the Richardson number in figure E.21.

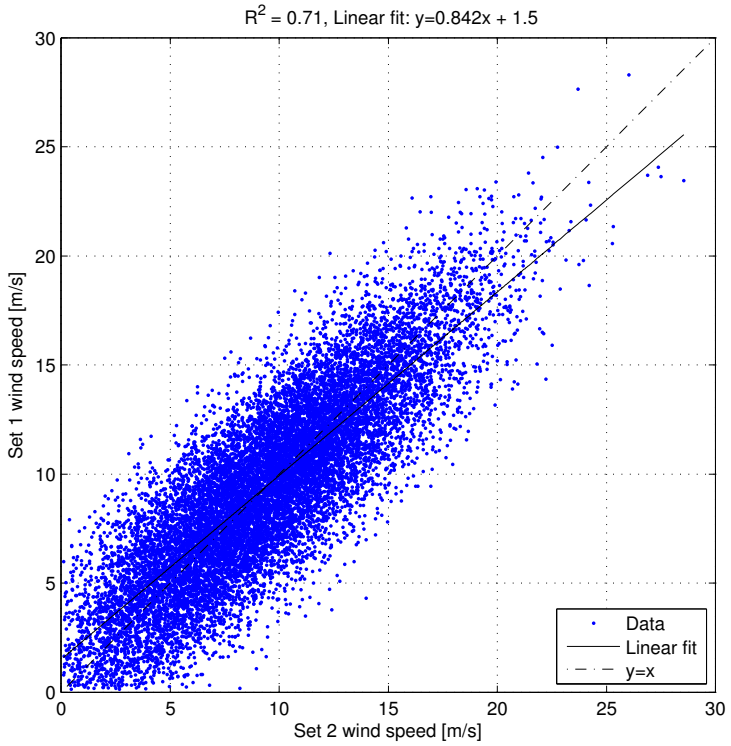

Figure E.17: Correlation between artificial metmast and mesoscale wind speed using correlation similar to real metmast data (case 1).

Similar plots are made for case 2, in which for all parameters the correlation between the two datasets is set to 0.99. These are shown in figures E.22, E.23 and E.24. The corresponding scatter plots of ζ and the Richardson number in figure E.26 clearly show a higher correlation compared to those of case 1. As a result, the scatter plot of the Monin-Obukhov length in figure E.25 also shows a higher agreement between the two datasets in case 2 as compared to case 1.

The stability of the artificial data is determined in the same way as for the real metmast and mesoscale data. The correspondence between the stability of the two datasets is then investigated as was done for the real data in section E.3. Since the artificial data is randomly generated, the stability for each case is determined 100 times. The different cases can then be compared.

To compare the different cases, the following comparison method is used. For each iteration a table of correspondence of the stability classes between the two datasets is created (such as those in table E.2 and E.3). Ideally, only the diagonal entries show a value and the off-diagonal entries are zero. As a measure for the error, the off-diagonal entries (and hence the disagreement between the two datasets) can either just be summed together, or the entries further away from the diagonal get a higher weight since they represent a larger disagreement. For example, if one of the datasets indicates stable, but the other dataset indicates unstable then that is a larger disagreement than if the second dataset would indicate neutral. Both methods are used here. The weights used to increase the contribution to the error of those entries that are further away from the diagonal are as

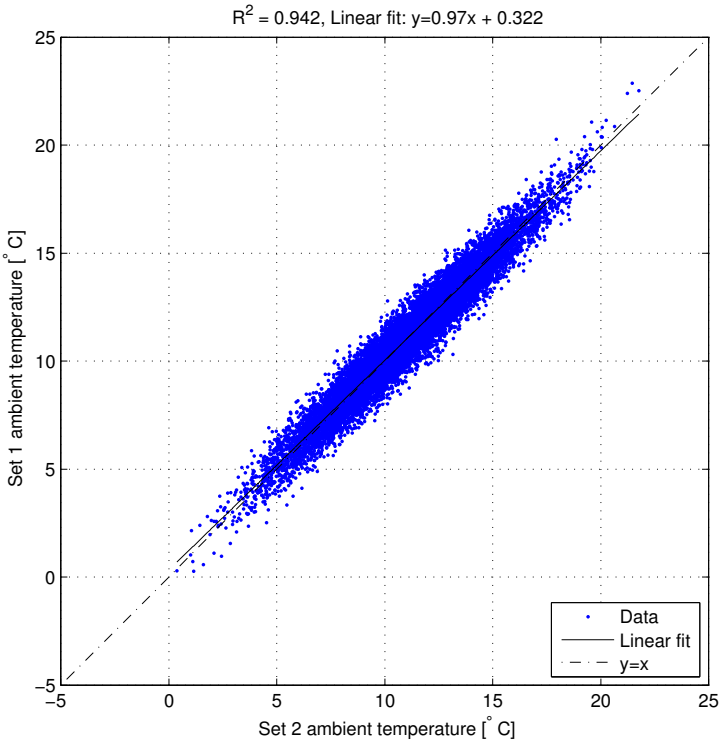

Figure E.18: Correlation between artificial metmast and mesoscale ambient temperature using correlation similar to real metmast data (case 1).

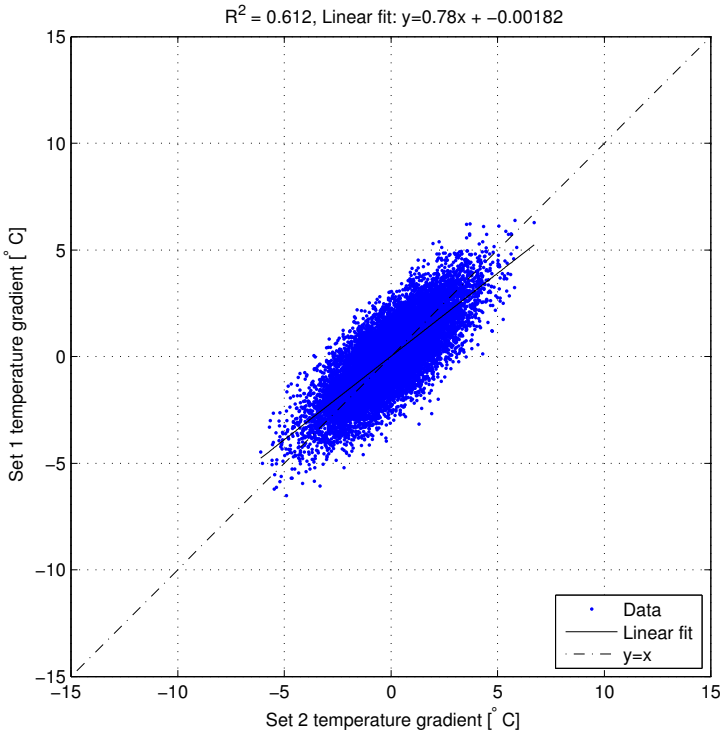

Figure E.19: Correlation between artificial metmast and mesoscale temperature gradient using correlation similar to real metmast data (case 1).

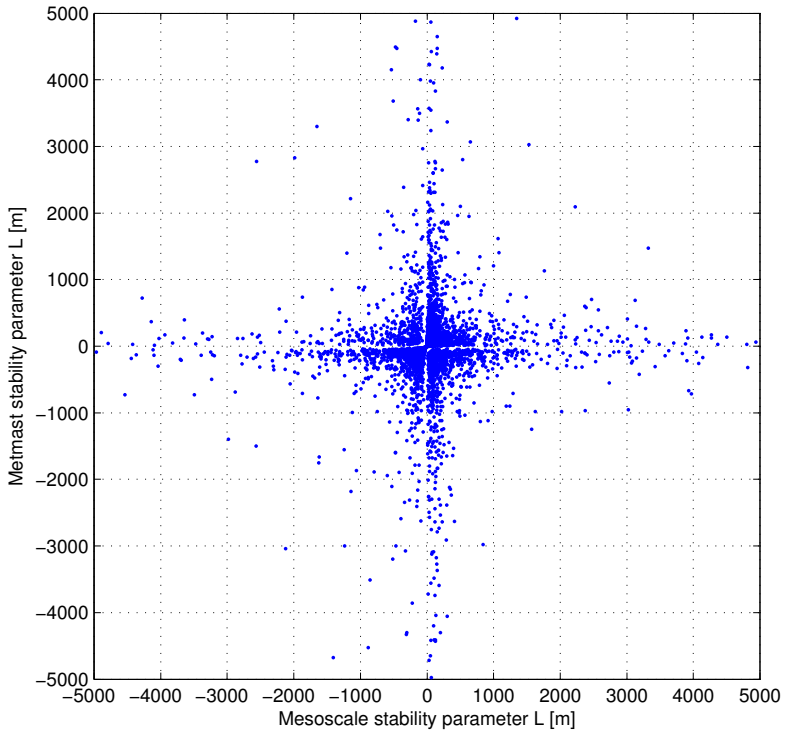

(a) Zoomed in

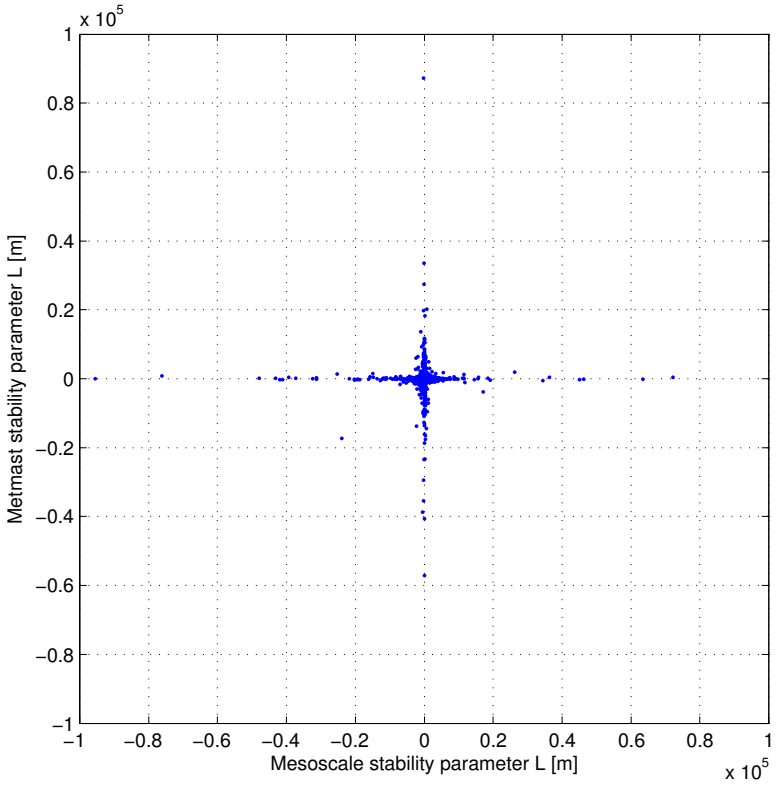

(b) Zoomed out

Figure E.20: Correlation between artificial metmast and mesoscale atmospheric stability using correlation similar to real metmast data (case 1).

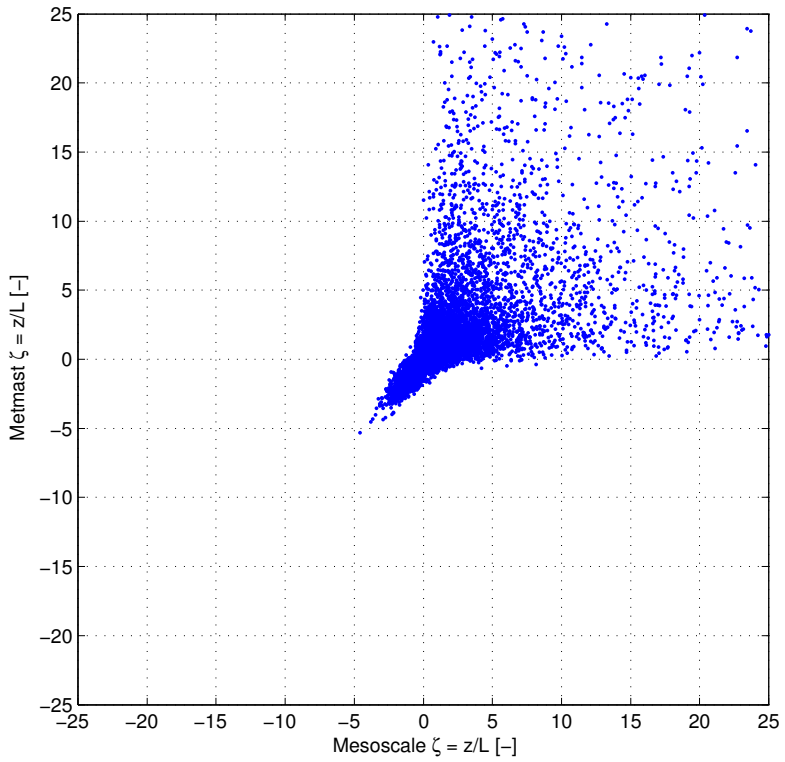

(a) ζ

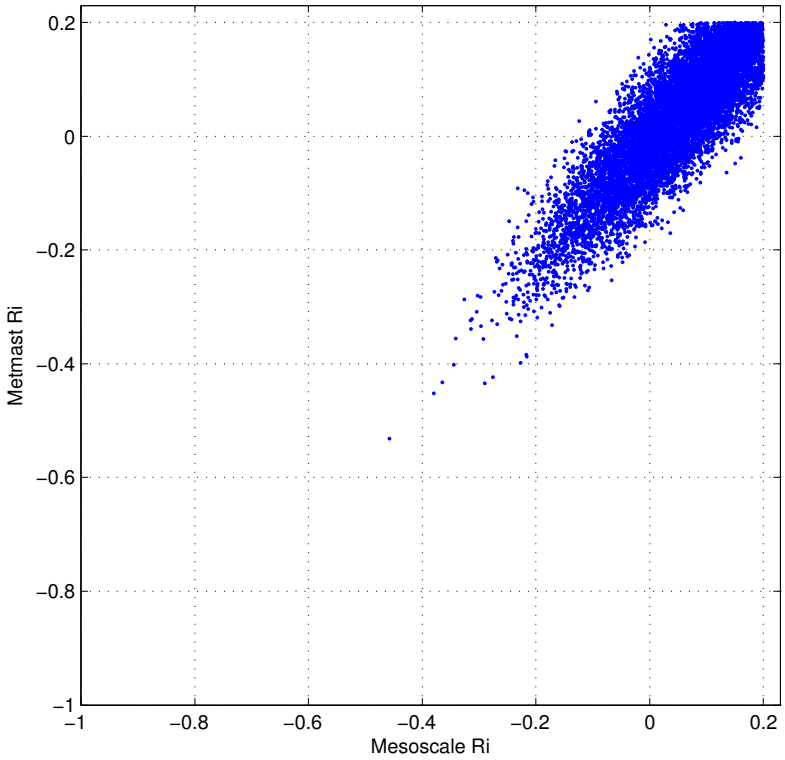

(b) Richardson number

Figure E.21: Correlation between artificial metmast and mesoscale a) ζ and b) Richardson number using correlation similar to real metmast data (case 1).

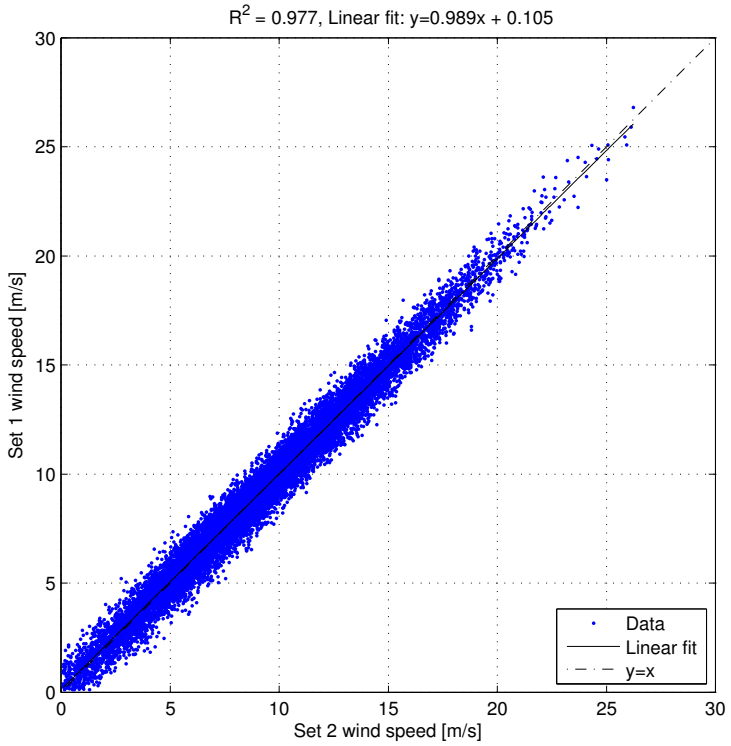

Figure E.22: Correlation between artificial metmast and mesoscale wind speed using high correlation (case 2).

shown in the following matrix:

$$M_{weighted} = \begin{bmatrix} 0 & 1 & 2 & 3 & 4 \\ 1 & 0 & 1 & 2 & 3 \\ 2 & 1 & 0 & 1 & 2 \\ 3 & 2 & 1 & 0 & 1 \\ 4 & 3 & 2 & 1 & 0 \end{bmatrix} \tag{E.2}$$

Basically, the numbers in the matrix represent the amount of stability classes that the values in a cell are away from the class that they ideally should be in, using the same order of very stable to very unstable as shown in table E.2 and E.3. Like in the two tables one of the two datasets that are compared is put along the vertical direction in the table, while the other dataset is put along the horizontal direction in the table and the entries in the tables correspond with the entries in the matrix. For example, when the dataset along the vertical direction indicates a stable measurement (row 4 in the matrix), but the dataset along the horizontal direction in the table indicates unstable (column 2 in the matrix), then the result of the data point of the second dataset is 2 classes away from that of first dataset. Hence, the matrix has a value of 2 at position $(4, 2)$. Due to similar reasoning entry $(2, 4)$ is 2 as well. The other entries are entered in a similar way.

The not-weighted sum simply has a 1 at all the places in the matrix, except at the

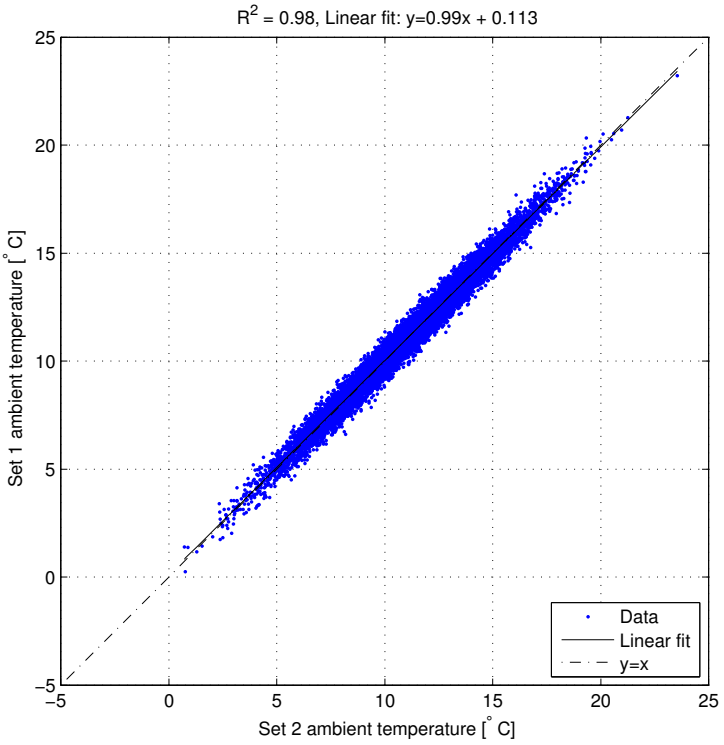

Figure E.23: Correlation between artificial metmast and mesoscale ambient temperature using high correlation (case 2).

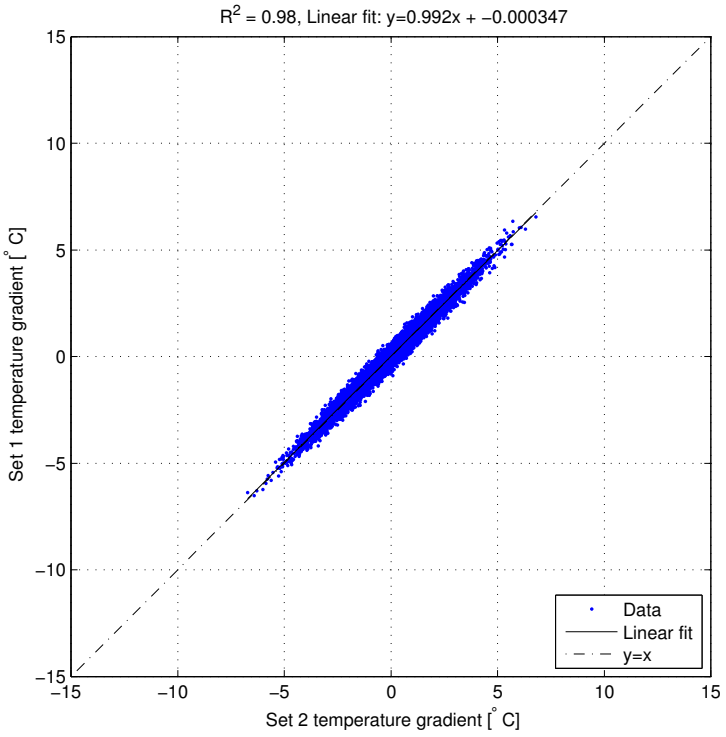

Figure E.24: Correlation between artificial metmast and mesoscale temperature gradient using high correlation (case 2).

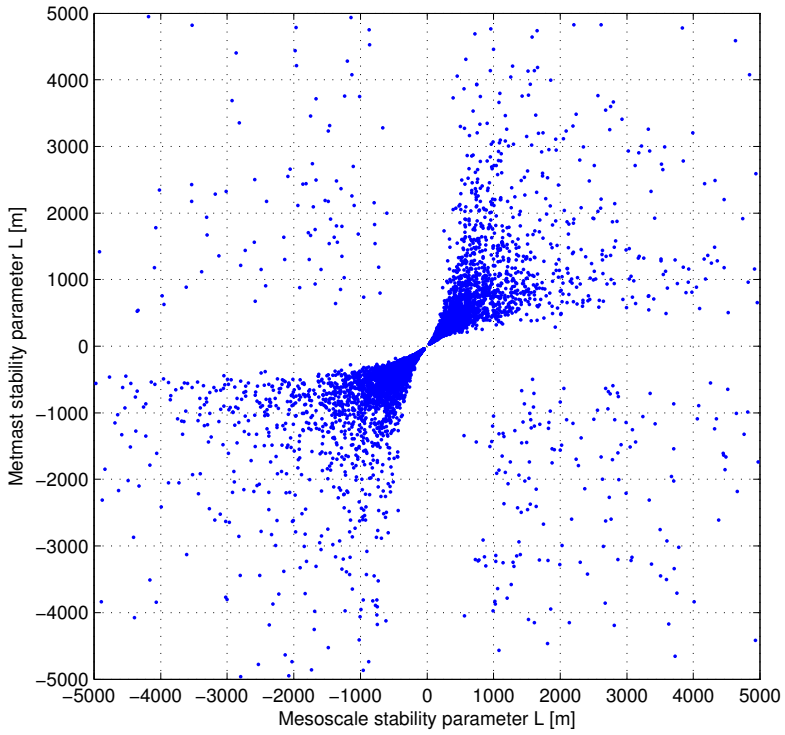

(a) Zoomed in

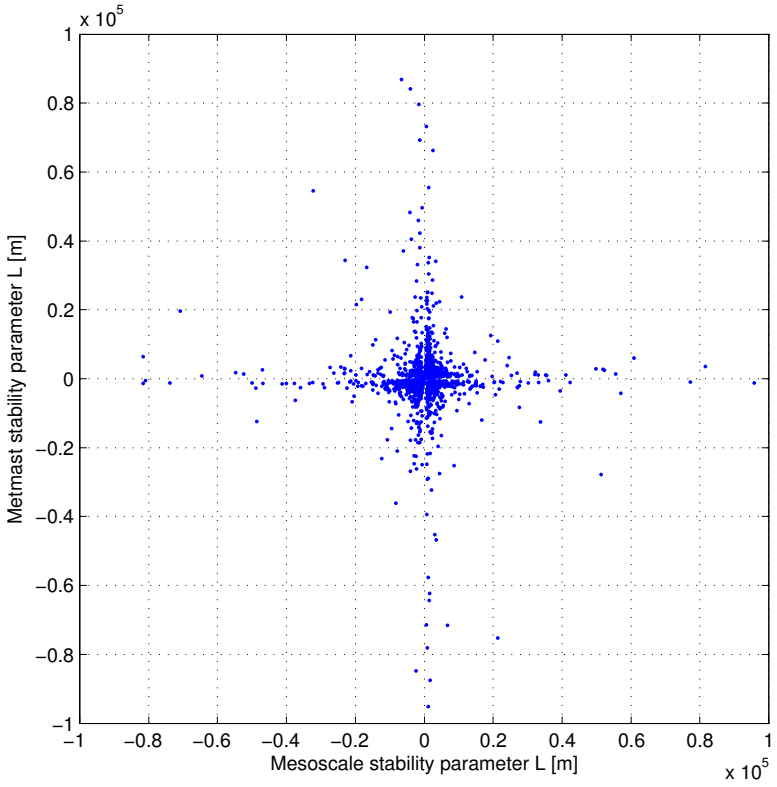

(b) Zoomed out

Figure E.25: Correlation between artificial metmast and mesoscale atmospheric stability using correlation similar to real metmast data (case 2).

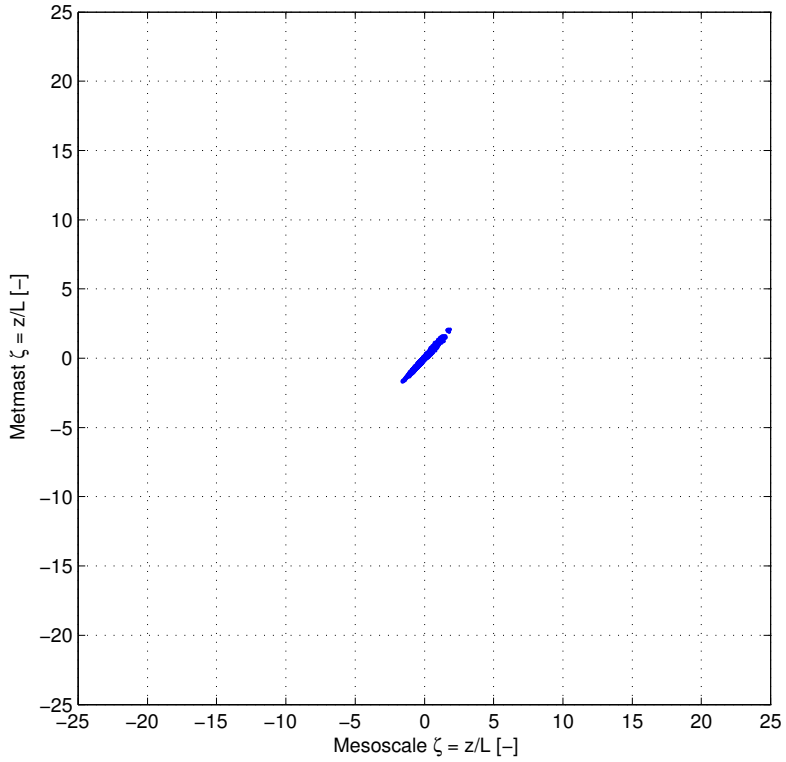

(a) ζ

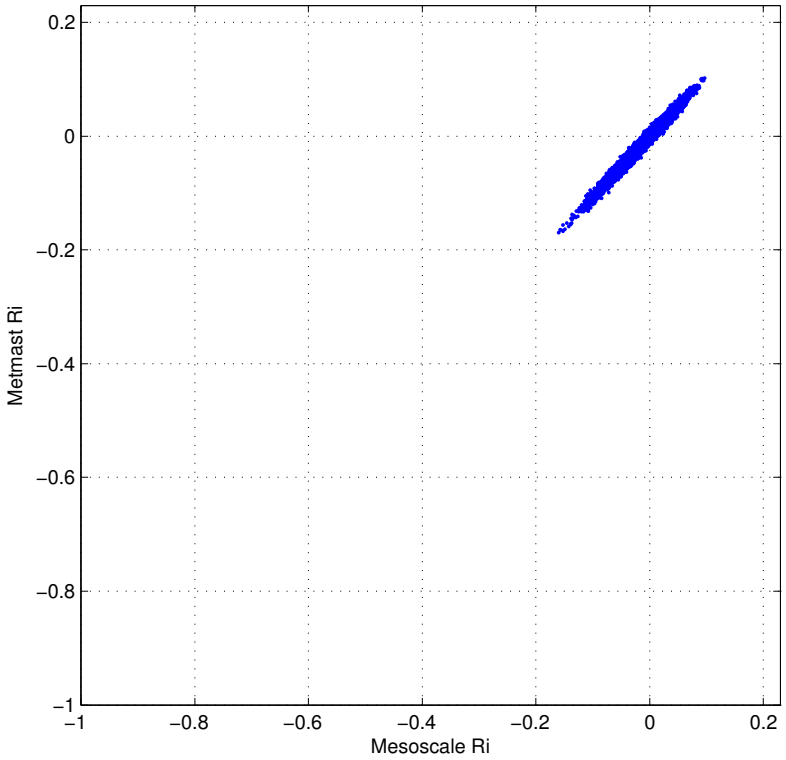

(b) Richardson number

Figure E.26: Correlation between artificial metmast and mesoscale a) ζ and b) Richardson number using correlation similar to real metmast data (case 2).

Table E.6: Sum and mean distance of the different correlation cases investigated. For a description of the cases, see table E.4

Case	1	2	3	4	5	6	7	8
Sum	31%	17%	21%	34%	22%	23%	24%	25%
Mean distance	0.56	0.24	0.29	0.62	0.35	0.33	0.39	0.42

diagonal:

$$M_{not-weighted} = \begin{bmatrix} 0 & 1 & 1 & 1 & 1 \\ 1 & 0 & 1 & 1 & 1 \\ 1 & 1 & 0 & 1 & 1 \\ 1 & 1 & 1 & 0 & 1 \\ 1 & 1 & 1 & 1 & 0 \end{bmatrix} \tag{E.3}$$

By dividing the weighted sum with 100%, the mean distance between the stability class of dataset 1 to that of dataset 2 is found. The non-weighted sum indicates the amount of disagreement between the two datasets, whereas the mean distance then indicates how many stability classes the erroneous data is on average lying away from the stability class where they are supposed to be in.

The results for each case for both the sum and the mean distance between the classes are shown in table E.6. As expected, from the table it can be seen that when the real data is recreated (case 1) the sum of the errors is the largest, and when all artificial signals are highly-correlated between the two datasets the sum of the errors is the smallest (case 2), although an error still remains. Comparing cases 3-5 it can be seen that the disagreement between the stability distributions is most sensitive to the ambient temperature. The ambient temperature influence is followed by that of the temperature gradient and that of the wind speed.

Cases 3-5 all investigate the same lower correlation (0.90) for one of the three variables. The real data however has varying sizes of the correlation for the different parameters. From cases 6-8 in the investigation it is found that for the real (measured) data, the disagreement between temperature gradient (case 8) has the highest impact on the disagreement of the stability distributions of the two datasets, closely followed by the ambient temperature. This is an interesting finding, since the impact of the temperature gradient was found to be lower than that of the ambient temperature when the correlation of all parameters is varied with the same value one by one (in cases 3-5). That the temperature gradient now seems to have a higher impact than the ambient temperature must be caused by the correlation of the temperature gradient (0.78) which is quite a bit lower than that of the ambient temperature (0.97). Apparently the correlation of the measured temperature gradient is that much worse compared to the measured ambient temperature and wind speed, that this variable now has the largest impact on the disagreement between the stability distribution of the two datasets.

Another thing can be seen from the table when looking at the mean distance values, which indicates how many stability classes the erroneous data is on average away from the stability class where they are supposed to be in. The error of case 5 is lower than that

of case 6 (22% versus 23%). The mean distance to the correct stability bin is however larger for case 5 than for case 6 (0.35 versus 0.33). This indicates that although in case 5 there is a smaller total error made, the data that lies in a different bin is on average laying further away from the bin where it is supposed to be in. The same can be seen when looking at the errors of cases 6-8. The errors are only 1% apart, but the differences between the mean distance to the correct bin are much larger. The temperature gradient not only causes the largest errors in the measured data, but also the errors that are on average the worst (i.e. the data lies away the furthest from where they are supposed to be).

Overall it can be said that the temperatures should be measured very accurately, as they have the highest impact on the stability classifications, either through the ambient temperature or through both the ambient temperature and sea surface temperature which make up the temperature gradient.

Appendix F

Sensitivity

In this chapter the sensitivity of the Monin-Obukhov length, wake losses and WindPRO simulations is investigated.

F.1 Sensitivity of Monin-Obukhov length to input parameters

The atmospheric stability is classified using the Monin-Obukhov length, which is found from the bulk Richardson number. In appendix E.4 it is found that the temperature gradient not only causes the largest errors in the measured data, but also the errors that are on average the worst (i.e. the data lies away the furthest from where they are supposed to be). Therefore an analysis is performed to see the sensitivity of the atmospheric stability to the size of the temperature gradient.

Assuming the ambient temperature equals $11.0°C$, which is equal to the average at North Hoyle, and for a wind speed of 8.0 m/s, which is equal to the wind speed used in the wake loss analysis, the influence of the temperature gradient can be found. Table F.1 shows the temperature gradient ranges for each stability class, where the temperature gradient is taken in steps of $0.1°C$.

From the table and noting that these calculations have been performed at an accuracy of 0.1° it can be seen that the neutral class occurs within a narrow range of temperature gradients of $-0.8°C \leq \Delta T \leq -0.6°C$, whereas the unstable and stable classes occur within a range of $-1.6°C \leq \Delta T \leq -0.9°C$ and $-0.5°C \leq \Delta T \leq 0.1°C$ respectively. The very stable and very unstable cases are about $1.9°C$ apart.

From the analysis it is clear that a small measurement error or offset in one of the temperatures can have a significant impact on the atmospheric stability found from the measurements. Taking the stable, neutral and unstable bins together as a near-neutral bin, as is done to plot the wake losses, gives a bin with a higher temperature gradient range which might compensate for the high sensitivity to changes in temperature gradient

Table F.1: Temperature gradient range per atmospheric stability class. Data is valid assuming an ambient temperature of $11.0°C$ and a wind speed of 8.0 m/s.

Stability class	Interval of temperature gradient
Very unstable	$\Delta T \leq -1.7°C$
Unstable	$-1.6°C \leq \Delta T \leq -0.9°C$
Neutral	$-0.8°C \leq \Delta T \leq -0.6°C$
Stable	$-0.5°C \leq \Delta T \leq 0.1°C$
Very stable	$\Delta T \geq 0.2°C$

of these bins separately. The size of the near-neutral bin is $0.1°C$ smaller than that for Horns Rev stated in Sørensen et al. (2008).

F.2 Sensitivity of wake losses to input parameters

In this section it is investigated what the impact of measurement errors is on the distribution of the wake losses over the different stability classes. During the investigation it was found that adding normally distributed random errors (noise) to the measurements has an insignificant effect on the atmospheric stability distribution and the average power per class in the wake loss investigation. Therefore the errors that are looked upon here are systematic errors. An example of this is a sensor with a measurement offset. The sensors that are of importance in determining the atmospheric stability are those of the wind speed, ambient temperature and sea surface temperature.

F.2.1 Sea surface temperature

The temperature sensors at North Hoyle have, in the applicable operating range, an accuracy of $\pm 0.1°C$ (Campbell Scientific, 1999). The effect of an error three times this size on the sea surface temperature and on the ambient temperature is investigated at North Hoyle. Figure F.1 shows the effect of a sea surface temperature offset of $+0.3°C$ and of $-0.3°C$. The wake losses without the added measurement error can be seen in figure 4.27a. When the sea surface temperature increases, the atmosphere will become more unstable. Power measurements that before belonged to the very stable case become more unstable and hence some may now fall in the near-neutral bin. The same might happen with near-neutral measurements changing to the very unstable bin. The opposite effect occurs when the sea surface temperature is decreased.

Figure F.1a indeed shows that the near-neutral line has a higher wake loss due to the added offset to the sea surface temperature, and the very unstable line has shifted somewhat down too (as it now contains some measurements that before belonged to the near-neutral bin). However, the very stable line has shifted up, indicating a smaller wake loss. This is against what is expected. Upon further investigation it is found that for this particular wind direction at North Hoyle the stable bin shows larger wake losses than the very stable bin. This is against what is expected also, and looking into the other two wind directions investigated at North Hoyle (with a larger spacing) shows that this effect only occurs at

this particular wind direction. It might be caused by the close spacing of the turbines, or there might be a temperature offset in the measurements: the stable measurements might actually be very stable in reality, such that a temperature offset should be subtracted from the sea surface temperature measurements to make all measurement more stable. This would lead to the measurements with the highest wake losses being in the very stable instead of in the stable class. It is interesting though that this effect is only visible for this particular wind direction. The result of adding the temperature offset as shown here is that only the very stable cases that are most stable (and for this particular case have a smaller wake loss) remain in the very stable bin. Hence, the very stable bin gets a smaller wake loss when the offset is added. This is only the case at this particular wind direction and for the other wind directions the effects are as expected (i.e. the lines all shift in the same direction depending on the temperature offset).

F.2.2 Ambient temperature

The ambient temperature occurs twice in the equation for the Richardson number (from which the Monin-Obukhov length is derived), namely once in the temperature difference and once as itself (see equation 2.13). This is as opposed to the sea surface temperature, which only occurs in the temperature difference. However, the graphs resulting for an offset to the ambient temperature (see figure F.2) are exactly the same as those for the sea surface temperature, i.e. a $+0.3°C$ offset in sea surface temperature corresponds to a $-0.3°C$ offset in ambient temperature and vice versa. From this it is clear that although the atmospheric stability also directly depends on the air temperature, it is the temperature difference that is more important for the atmospheric stability.

F.2.3 Wind speed

The third variable to which the atmospheric stability depends is the wind speed. The cup anemometers used at North Hoyle have, at a wind speed of 8 m/s, an accuracy of 0.1 m/s (Vector Instruments, n.d.). The effect of increasing the measured wind speed is that the measurement becomes more near-neutral (see figure 4.8b). Power measurements that before belonged to the very unstable case become more stable and hence some may now fall in the near-neutral bin. The same might happen with very stable measurements becoming more unstable. The result is that the measurements that were close to the near-neutral bin will shift to that bin while the more extreme stable and unstable measurements will remain in the very (un)stable bins. Hence, power output appears larger for the very unstable bin and smaller for the very stable bin, i.e. the wake losses appear smaller/larger respectively. The opposite effect occurs when the wind speed is decreased. Looking at figure F.3 it can be seen that when the wind speed is increased by 0.3 m/s (three times the accuracy of the sensor), the very stable bin gets a slightly higher power output. For this particular wind direction the very stable case responds counter intuitive, which has to do with the unexpected location of the wake losses in the stable bin as explained above. The very unstable bin does not change, which might result from the fact that no measurements are close enough to the near-neutral bin to change to that bin. When the wind speed is decreased by 0.3 m/s, the very unstable bin gets a lower power output (i.e. higher wake loss) as expected, since some power measurements that used to belong to the near-neutral

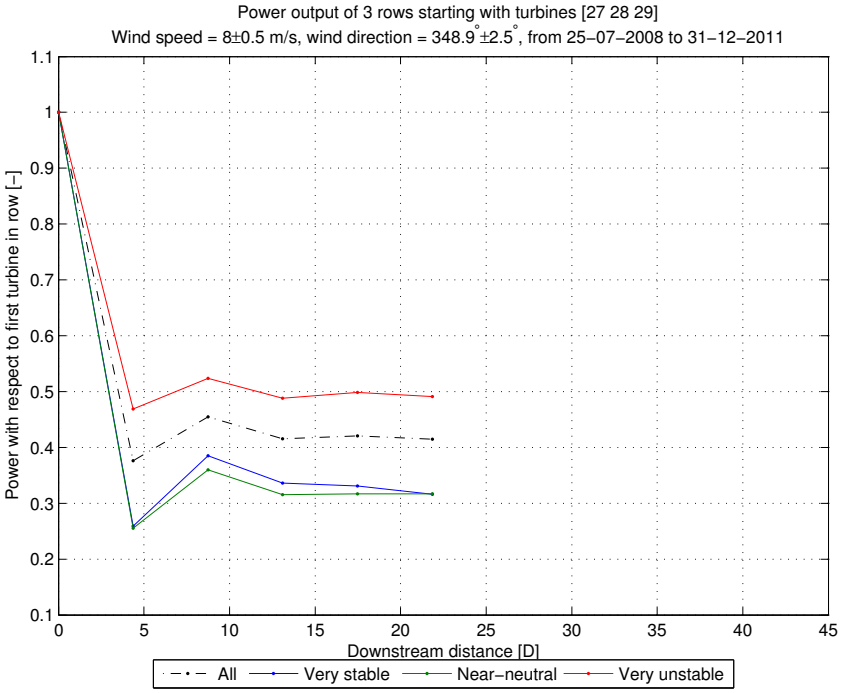

(a) Sea surface temperature offset of $+0.3°C$

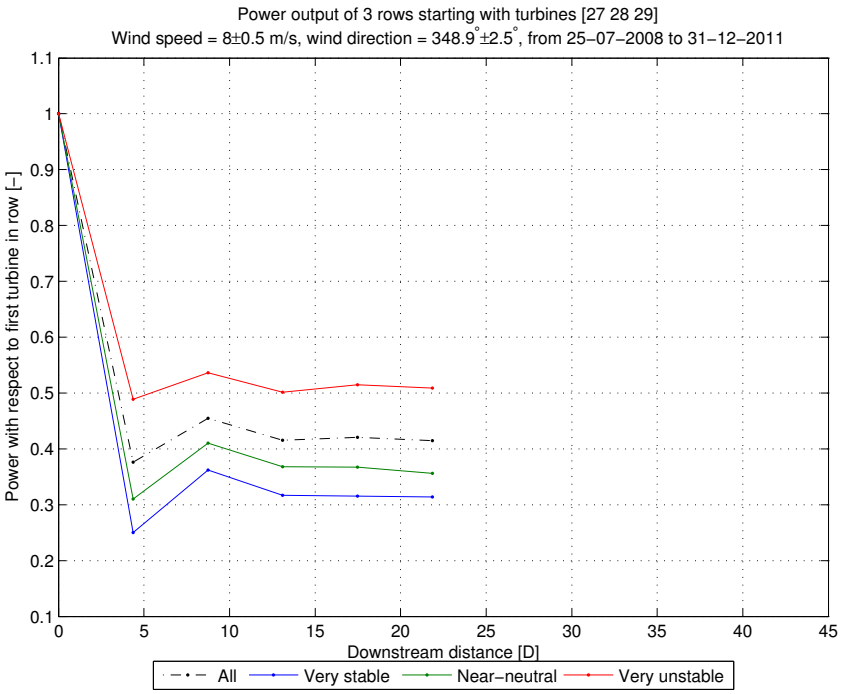

(b) Sea surface temperature offset of $-0.3°C$

Figure F.1: Sensitivity of wake losses at North Hoyle to offset in sea surface temperature measurement. Wind coming from $348.9° \pm 2.5°$ and wind speeds at 8.0 ± 0.5 m/s for various stability classes. a) sea surface temperature offset of $+0.3°C$, b) sea surface temperature offset of $-0.3°C$. Wind speed and direction are taken as the average of the first turbine in the rows. Data is taken over the period from 11 June 2008 to 31 December 2011.

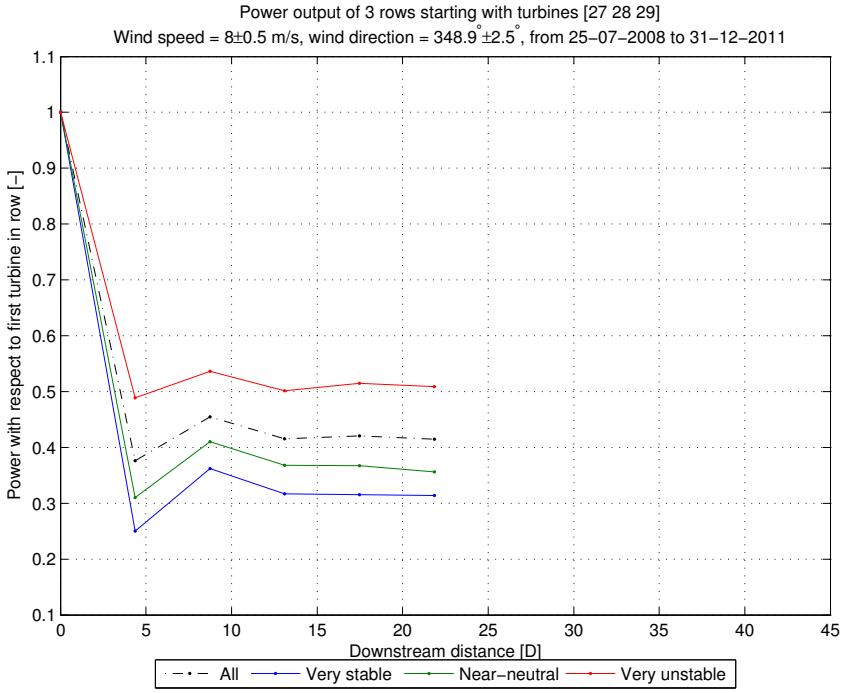

(a) Ambient temperature offset of $+0.3°C$

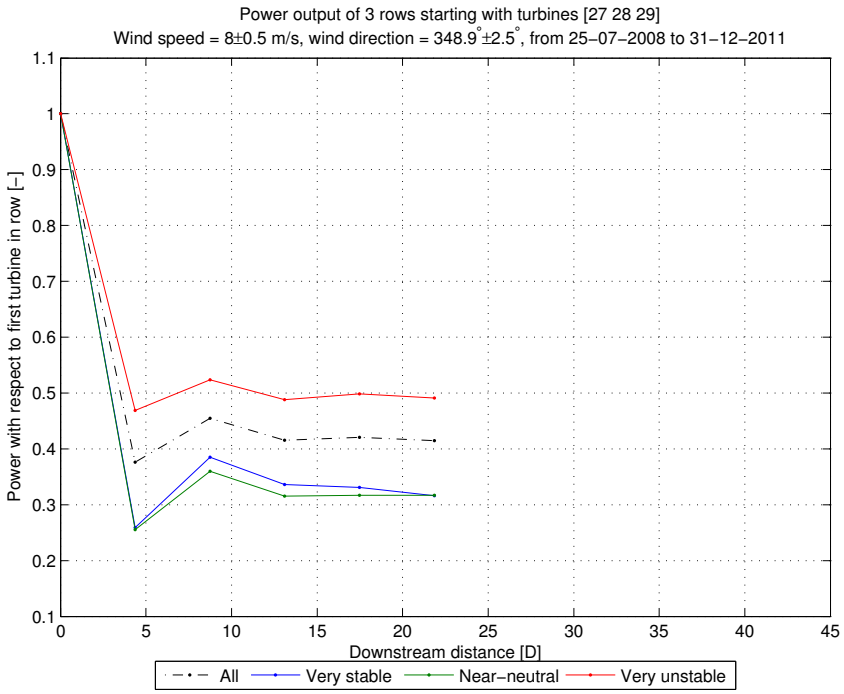

(b) Ambient temperature offset of $-0.3°C$

Figure F.2: Sensitivity of wake losses at North Hoyle to offset in ambient temperature measurement. Wind coming from $348.9° \pm 2.5°$ and wind speeds at 8.0 ± 0.5 m/s for various stability classes. a) ambient temperature offset of $+0.3°C$, b) ambient temperature offset of $-0.3°C$. Wind speed and direction are taken as the average of the first turbine in the rows. Data is taken over the period from 11 June 2008 to 31 December 2011.

bin also fall in the very unstable bin now. The very stable bin stays unchanged, indicating that there are no measurements changing to that bin from the near-neutral bin.

F.2.4 Conclusion

Comparing the influence of the temperature with that of the wind speed it can be seen that of the three parameters that are input to the equation for atmospheric stability, a measurement offset in the temperature difference has the highest impact. The effect of having a measurement error of the investigated size of three times the sensor accuracy is for all parameters limited to a few percent in indicated wake loss. Larger offsets are expected to give larger differences in wake loss.

F.3 Sensitivity of wake losses to WindPRO settings

In WindPRO the wind speed and wind direction bin size can be entered manually. For the simulations shown in the report, the wind direction bin size is 1° and the wind speed bin size is 1 m/s. WindPRO makes a frequency table of the imported wind data, with the number of cases for the combination of each wind speed and wind direction bin. WindPRO then models the power output of the wind farm for each combination of wind speed and wind direction bin. The frequency of occurrence of each bin is used to find a weighted average of all cases, which is the power output of the whole wind farm.

The question arises what the influence is of the wind direction bin size. Another question that arises is what the difference is between the results of the separate wind directions and how large the influence is of changing the wind speed. This is investigated for the wind direction case 258.8° at North Hoyle.

Figure F.4 shows the influence that the size of the wind direction sector has. When the modelled wind direction sector is increased, the average wake losses over the sector become smaller. This is as expected, since the wake losses are averaged over the whole sector and from literature it is known that the further away the wind direction is from the row direction, the smaller the wake losses (as can also be seen from measurements in figure 2.7). It can therefore be expected that when a larger wind sector is modelled, the wake losses resulting from this sector are smaller than for a more narrow wind sector, when centred around the row direction.

It is also possible to investigate the influence of the wind direction bin size entered in WindPRO. Since WindPRO internally integrates wind direction sectors in steps of 1° the bin size entered (e.g. 12 30° sectors) should not be a large influence to the simulation. For the cases investigated it is found that the park efficiency varies by a few tenths of percent when either taking 12 30° sectors or 360 1° sectors. However, the simulation time significantly increases and is about 8 times larger when 360 bins are modelled instead of 12.

When WindPRO simulates the wake losses over a wind direction sector, it computes the wake losses using 1° steps. Hence, using sectors of 1° the separate wind directions making up a certain larger sector can all be investigated. In figure F.5 the WindPRO simulations are shown for the separate 1° directions around the row direction. Since the wake sector

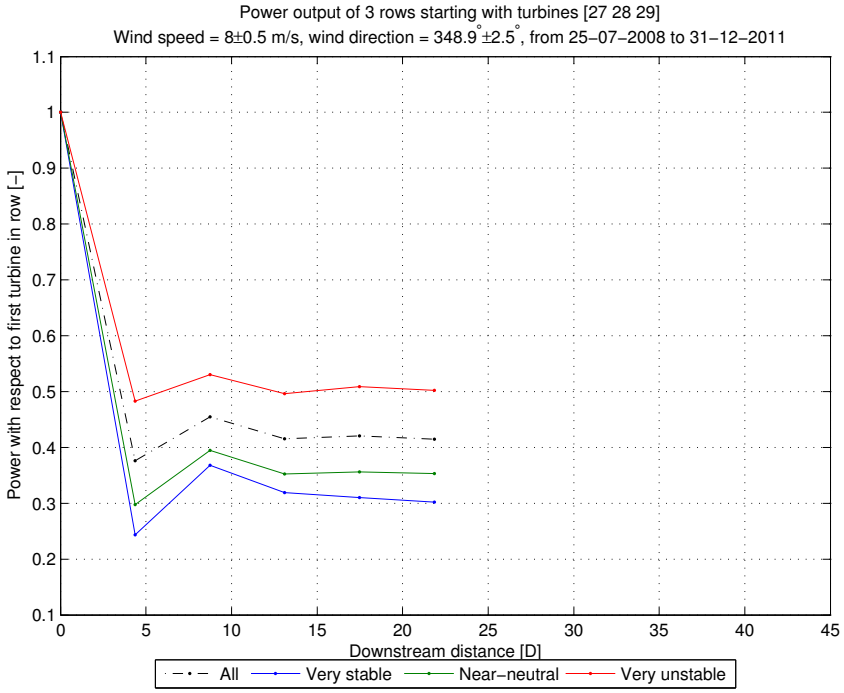

(a) Wind speed offset of +0.3 m/s

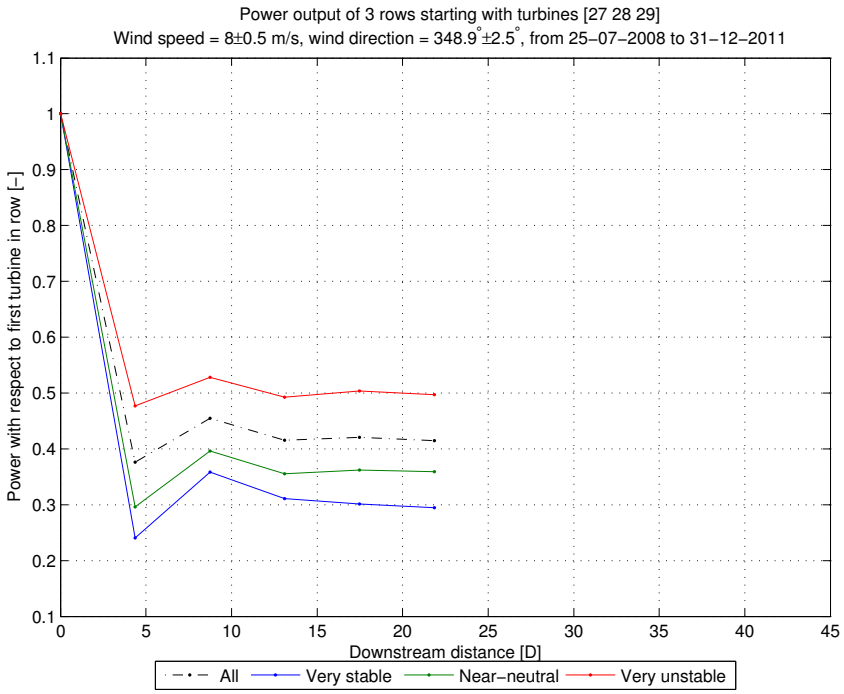

(b) Wind speed offset of −0.3 m/s

Figure F.3: Sensitivity of wake losses at North Hoyle to offset in wind speed measurement. Wind coming from $348.9° \pm 2.5°$ and wind speeds at 8.0 ± 0.5 m/s for various stability classes. a) wind speed offset of $+0.3$ m/s, b) wind speed offset of -0.3 m/s. Wind speed and direction are taken as the average of the first turbine in the rows. Data is taken over the period from 11 June 2008 to 31 December 2011.

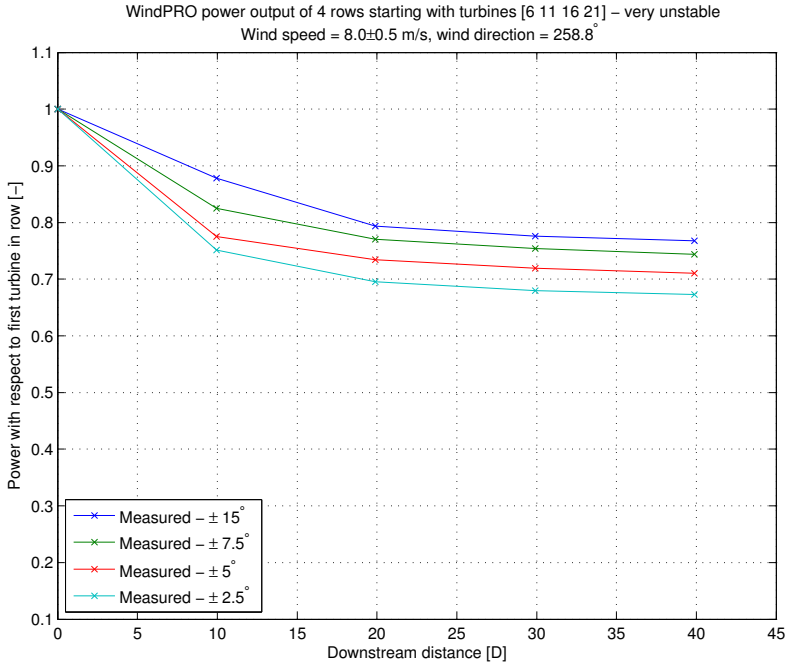

Figure F.4: Influence of wake sector size in WindPRO simulations. Simulated at wind speed 8.0 m/s and wind sectors centred at 259° at North Hoyle. Wake decay constant $k = 0.08$.

used in the analysis is ±2.5°, the measurements are from 256.3° to 261.3°, which is the reason that there are six different lines modelled. The point for the whole sector is a weighted average of the different lines in the sector, depending on their frequency of occurrence in the measurements.

The row direction of the turbines is 258.8° and in WindPRO this direction falls in the bin 258.5° – 259.5°. Firstly, it can be seen that this bin does not have the largest wake loss as expected, but that bin 259.5° – 260.5° has a slightly larger wake loss. Secondly, it can be seen that the power output increases faster (i.e. the wake losses decrease faster) when increasing the wind direction as compared to decreasing the wind direction. These are two observations that are unexpected. One would expect the row direction to have the largest wake losses, and that the wake losses would differ in a symmetric way around the row direction when changing the wind direction as the rows and columns in the wind farm are 90° to each other. It is unknown what causes these differences and it might have something to do with the way WindPRO models the wake losses. Correspondence with EMD/WindPRO has not resulted in an explanation for this.

In figure F.6 the effect of varying the wind speed can be seen. As expected, a higher wind speed results in a higher power output (i.e. smaller wake loss) and a smaller wind speed results in a lower power output (i.e. larger wake loss). The results differ about 1% and 2% for 7 and 9 m/s respectively when comparing to the result of 8 m/s. From correspondence with EMD/WindPRO it is found that WindPRO internally models the wind speeds in bins of 1 m/s. This means that if the result of for instance 7.5 m/s is wanted, the results for a simulation of 7.0 and 8.0 m/s have to be averaged manually.

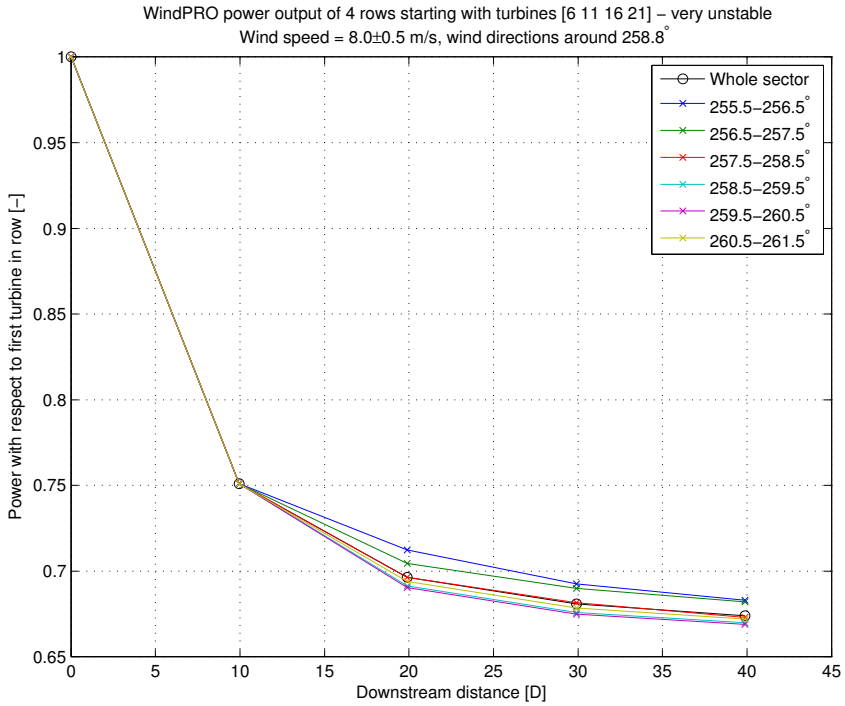

(a) Versus downstream distance

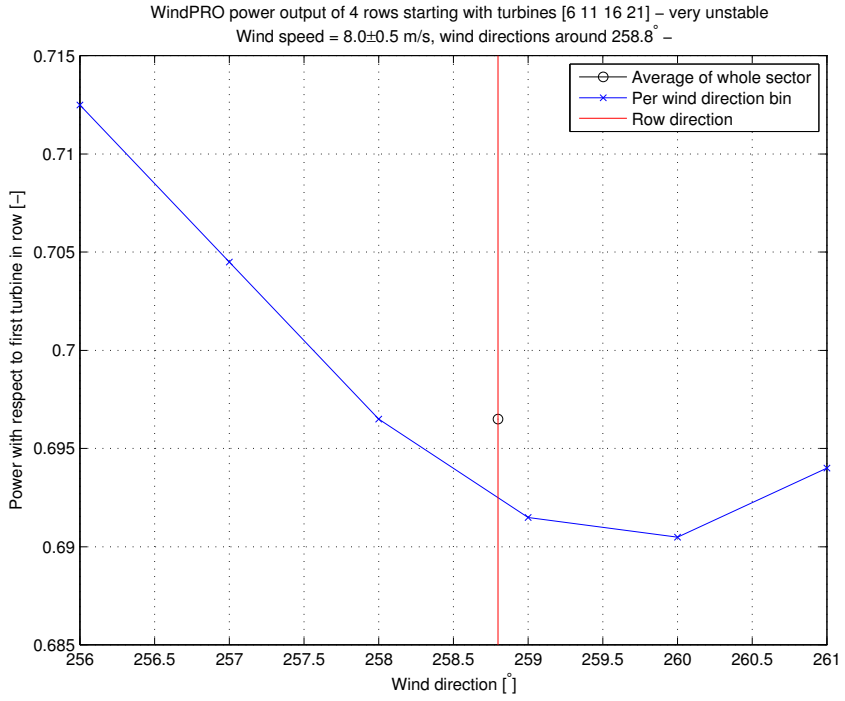

(b) Versus wind direction (at the third turbine, about $20D$)

Figure F.5: Influence of separate wind directions in WindPRO simulations. a) Versus downstream distance, b) versus wind direction (at the third turbine, about $20D$). Simulated at wind speed 8.0 m/s and wind directions around $259°$ at North Hoyle. Wake decay constant $k = 0.08$.

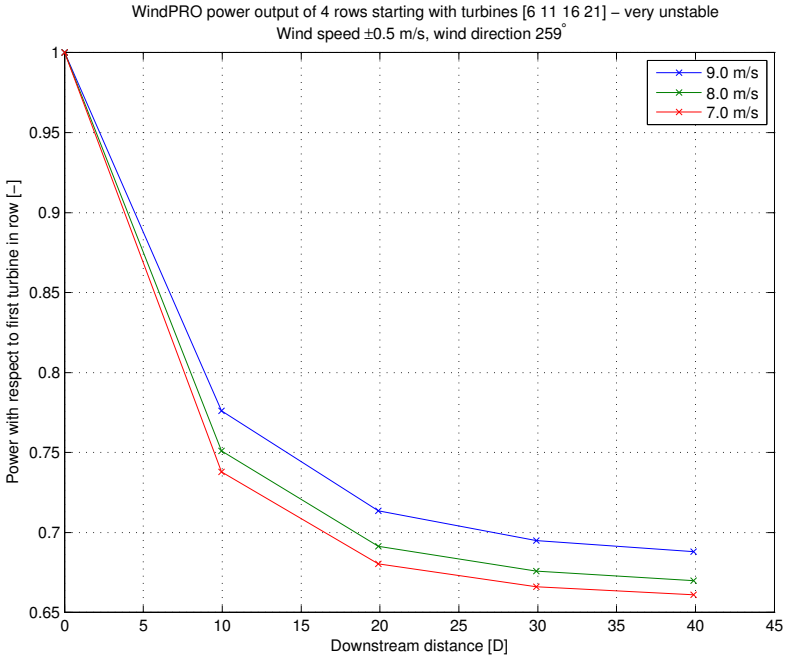

Figure F.6: Influence of varying wind speeds in WindPRO simulations. Simulated at varying wind speeds and wind direction $259° \pm 2.5°$ at North Hoyle. Wake decay constant $k = 0.08$.